MRC | Centre for Developmental and Biomedical Genetics

The University Of Sheffield.

Investigating the role of P2Y$_{12}$ in thrombosis, inflammation and infection in the zebrafish model

Rebecca Bright

Registration number: 100237904

A thesis submitted for the degree of

Doctor of Philosophy

At the University of Sheffield

Department of Cardiovascular Science

September 2014

Acknowledgements

I would like to thank both of my supervisors Dr Tim Chico and Professor Rob Storey for their advice and guidance over the course of my PhD and the Department of Cardiovascular Science for funding my scholarship. I would also like to thank Dr Stone Elworthy, Dr Rob Wilkinson and Dr Freek Van Eaden for their patience and advice throughout the process of generating ZFN and TALEN mutants.

I have really enjoyed my PhD, due to an interesting and varied topic and also a brilliant lab working environment. Many thanks to everyone in both the Chico and Bandmann labs for their invaluable scientific advice, support and laughs. This ensured that work was never a chore.

Finally I would like to thank my family and Andy for their unwavering encouragement and understanding.

Abstract

The $P2Y_{12}$ receptor is an important amplifier of thrombosis. $P2Y_{12}$ is activated by ADP, inducing release of α and dense granules from the platelet. α-granules contain a myriad of proteins including pro-inflammatory mediators involved in vascular inflammation. $P2Y_{12}$ antagonists are used in the treatment and prevention of arterial thrombosis and also reduce levels of inflammatory mediators, indicating that $P2Y_{12}$ may play a role in inflammation. α granules also release antimicrobial peptides suggesting that $P2Y_{12}$ may also be involved in resistance to infection.

Zebrafish embryos represent an excellent model to study thrombosis, inflammation and infection *in vivo*. Transgenic lines enable visualisation of leukocyte migration, whilst inoculation with pathogens enables modelling of resistance to infection. Temporary gene knockdown is achieved by injection of morpholino oligonucleotides and recent advances have enabled targeted mutation of specific gene loci.

This thesis describes my investigations into the role of $P2Y_{12}$ in thrombosis, inflammation and infection in these zebrafish models. I found that *p2y12* knockdown significantly reduced thrombus area in response to vessel injury. I also investigated the effect of knockdown of several platelet microRNAs on thrombosis. I found that knockdown of miR-223 significantly increased thrombus area after vessel injury, a novel finding which indicates a previously unsuspected role of miR-223 in thrombus formation. Leukocyte migration to sites of inflammation was examined in both control and *p2y12* morphants however I found no significant difference, suggesting $P2Y_{12}$ does not play a role in leukocyte migration in this model.

I investigated resistance to *S. aureus* infection and found a statistically significant reduction in survival of *p2y12* morphants. I generated a *p2y12* mutant which results in a frame shift proximal to the N-terminus, however I observed no effect on thrombosis or resistance to infection. This requires further investigation. My data shows that the function of $P2Y_{12}$ in thrombosis is conserved in the zebrafish and that $P2Y_{12}$ may play a role in resistance to *S. aureus* infection.

Table of Contents

Table of Figures

List of Tables

List of Abbreviations

AC	Adenylyl cyclase
ACS	Acute coronary syndrome
ADP	Adenosine diphosphate
AGM	Aorta-gonad-mesonephros
Akt	Protein kinase B
ApoE	Apolipoprotein E
ATP	Adenosine triphosphate
Bcc	*Burkholderia cenopacia*
BHI	Brain heart infusion
Bp	Base pair
CABG	Coronary artery bypass surgery
cAMP	cyclic AMP
CFU	Colony forming units
CRP	C reactive protein
CCR3	C-C chemokine receptor type 3
CCR4	C-C chemokine receptor type 4
CHT	Caudal haematopoietic tissue
CoDA ZFN	Context dependent assembly zinc finger nucleases
CPTP	Cylcopentyl-triazolo-pyrimidines
CTAP 3	Connective tissue activating protein 3
CYP-P450	Cytochrome P450
CXCR4	C-X-C Chemokine receptor 4
DEPC-H_2O	Diethyl pyrocarbonate treated H_2O
DMSO	Dimethyl-sulfoxide
DSB	Double strand break
FP-A	Prostaglandin F2α isoform A
FP-B	Prostaglandin F2α isoform B
GAPDH	Glyceraldehyde 3-phosphate dehydrogenase
gDNA	Genomic DNA
GFP	Green fluorescent protein

GPIIb/IIIa	Glycoprotein IIb/IIIa
GPVI	Glycoprotein VI
GTP	Guanosine 5’-triphosphate
Het	Heterozygote
Hom	Homozygote
Hpf	Hours post fertilisation
HPI	Hours post injury/infection
HSC	Haematopoietic stem cell
IHNV	Infectious hematopoietic necrosis virus
LDL	Low density lipoprotein
LPS	Lipopolysaccharide
MIP-1 α	Monocyte inflammatory protein
MCP-3	Monocyte chemotactic protein-3
MI	Myocardial infarction
MID	Multiplex identifier sequence
MiR	MicroRNA
MO	Morpholino oligonucleotide
Mpo	Myeloperoxidase
NHEJ	Non-homologous end joining
OCS	Open canalicular system
PAM	Prasugrel active metabolite
PAK4	p21 activating kinase
PBI	Posterior blood island
PBP	Platelet basic protein
PCI	Percutaneous coronary intervention
PDGF	Platelet derived growth factor
PF-4	Platelet factor 4
PI3-K	Phosphatidylinositol 3-kinase
PK	Platelet kinocidins
PKA	Protein kinase A
PKC	Protein kinase C
PLATO	Platelet inhibition and patient outcomes

PMPs	Platelet microbicidal proteins
PSGL-1	P-selectin glycoprotein ligand-1
RANTES	Regulated on activation, normal T cell expressed and secreted
RBI	Rostral blood island
ROS	Reactive oxygen species
Rpm	Revolutions per minute
RT	Room temperature
RT-PCR	Reverse transcriptase polymerase chain reaction
RVD	Repeat variable di-residue
SNP	Single nucleotide polymorphism
TALEN	Transcription activator-like effector nucleotides
TF	Tissue factor
TGF β	Transforming growth factor β
TP	Thromboxane-Prostanoid
TM	Transmembrane
TSA	Thrombus surface area
TTA	Time to attachment
TTO	Time to occlusion
TXA_2	Thromboxane A_2
UTR	Untranslated region
VASP	Vasodilator-stimulated phosphoprotein
VEGF	Vascular endothelial growth factor
VSMC	Vascular smooth muscle cell
vWF	Von Willebrand Factor
Wt	Wildtype

Chapter 1 : General Introduction

This thesis describes an investigation into the role of the $P2Y_{12}$ receptor in thrombosis, inflammation and infection using a novel zebrafish model.

The platelet plays a central role in primary haemostasis to maintain vessel integrity after injury. Platelets play a key role in atherothrombotic diseases. Anti-thrombotic drugs prevent further thrombotic events after myocardial infarction (MI) ((Mackman, 2008) for review) and since many of these target the $P2Y_{12}$ receptor, it is vital to understand the role of this receptor in physiological processes. My project seeks to validate the zebrafish model via the well characterised role of $P2Y_{12}$ in thrombosis, before investigating the indistinct role of the receptor in inflammation and response to infection. The zebrafish has been utilised for this investigation as it possesses many advantages over other *in vivo* models. This introduction will discuss some of the relevant literature relating to the $P2Y_{12}$ receptor with regards to platelet function, pharmacology and signalling pathways of the $P2Y_{12}$ receptor, in the context of thrombosis, inflammation and infection.

1.1 The platelet

Platelets are anucleate cell fragments, derived from the megakaryocyte and the second most abundant cell in the circulation. Platelets are vital to maintaining haemostasis and circulate for approximately 10 days before being cleared by macrophages (Harker, 1977). There are many different receptors expressed on the surface of platelets which are involved in adhesion, activation and aggregation. Alterations to endothelial surfaces caused by vessel damage or atherosclerotic plaques induce platelet activation, leading to platelet cytoskeletal remodelling to change shape from the spherical resting state to an activated state with extending lamellipodia and filopodia.

1.1.1 Thrombus Formation

Damage to endothelium, such as that by atherosclerotic plaque rupture, exposes von Willebrand factor (vWF) and collagen in the subendothelium of the vessel wall. Circulating platelets roll and tether to the vessel wall via binding of vWF to adhesion receptors glycoprotein (GP) Ib-IX-V and then adhere more firmly upon binding of collagen to receptors α2β1 and GP VI. Platelets then become activated via thrombin and release of adenosine diphosphate (ADP) from platelet dense granules, red blood cells and damaged endothelial cells (Mills et al., 1968, Hollopeter et al., 2001). ADP activates two ADP receptors on the surface of the platelet, $P2Y_1$ and $P2Y_{12}$; activation of both of these receptors is required for a full aggregation response (Daniel et al., 1998) (Jin and Kunapuli, 1998).

1.2 The $P2Y_{12}$ receptor

The $P2Y_{12}$ receptor is a G protein-coupled receptor (GPCR) which has been established as a key amplifier of platelet aggregation in response to vessel injury and platelet activation (Hollopeter et al., 2001). The $P2Y_{12}$ receptor is a seven trans membrane domain receptor coupled to the heterotrimeric guanosine 5'-triphosphate (GTP)-binding Gi protein. $P2Y_{12}$ is activated by binding of ADP and the more potent 2-methylthio-ADP (2-MesADP), it is activated to a lesser extent by ATP (Schmidt et al., 2013). Binding of these agonists activates the Gi protein coupled to the receptor, leading to inhibition of adenylyl cyclase (AC) activity and phosphatidylinositol 3-Kinase (PI3-K) activation (Geiger et al., 1999, Kunapuli et al., 2003). These mechanisms amplify and potentiate platelet aggregation initiated by thrombin, thromboxane A_2 (TXA_2) and $P2Y_1$ activation (Garcia et al., 2010, Jin et al., 2002, Li et al., 2003).

1.2.1 $P2Y_{12}$ activation

Platelet activation induces release of ADP from platelet dense granules, which activates $P2Y_{12}$ and, in a positive feedback mechanism, induces further dense granule release, thus amplifying the platelet aggregation response. $P2Y_{12}$ amplifies many processes involved with activation and aggregation of platelets, including release of dense granules and α granules, activation of the fibrinogen receptor

GPIIb/IIIa (αIIbß3) and generation of TXA_2 (Kauffenstein et al., 2001) . $P2Y_{12}$ sustains activation of GPIIb/IIIa to amplify and sustain platelet aggregation (Kauffenstein et al., 2001, Kamae et al., 2006). GPIIb/IIIa binds fibrinogen to enable cross-linking of fibrinogen between platelets, thus forming a stable thrombus. In addition, $P2Y_{12}$ activation amplifies platelet procoagulant activity with increased thrombin generation that not only activates platelets but also leads to formation of fibrin which forms a mesh to further stabilise thrombus (Dorsam et al., 2004). $P2Y_{12}$ is particularly important in enhancing thrombus formation at high shear such as in arterial thrombosis (Nergiz-Unal et al., 2010).

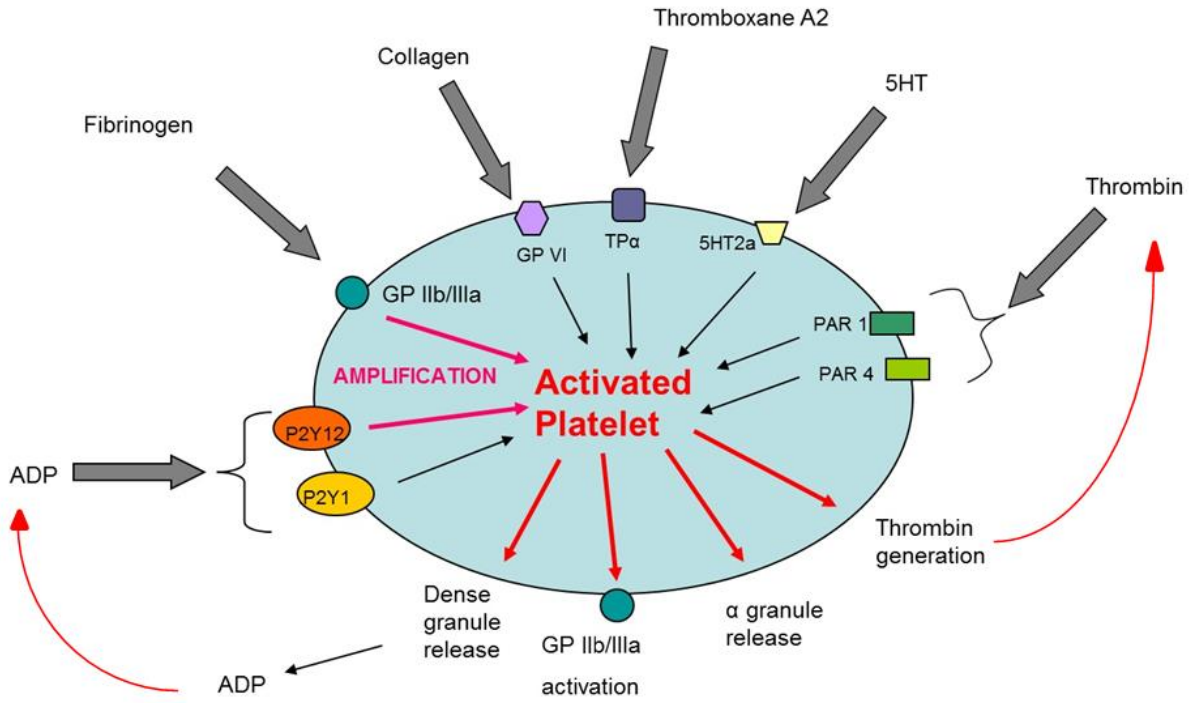

Figure 1.1 A schematic of the activated platelet.

The platelet is activated by a variety of agonists such as fibrinogen, collagen, TXA_2, 5HT, thrombin and ADP. The $P2Y_{12}$ receptor activation by released ADP induces a positive feedback mechanism to amplify platelet aggregation via dense granule release, GP IIb/IIIa activation and thrombin generation. Schematic adapted with permission from (Storey, 2006).

1.2.2 Intracellular signalling

$P2Y_{12}$ signalling activates the intracellular coupled G protein inducing a conformational change that uncouples subunits of the Gi protein. The $P2Y_{12}$ linked Gi protein has 3 subunits; αi, β and γ subunits, with β and γ forming a complex. The αi subunit is involved in the inhibition of AC, which under normal conditions synthesises cAMP from ATP. Therefore the inhibition of AC reduces levels of cAMP, leading to a reduction in phosphorylation of the vasodilator-stimulated phosphoprotein (VASP) by protein kinase A (PKA), which sustains platelet aggregation (Geiger et al., 1999).

The β and γ subunits dimerise to form a complex that dissociates from the αi subunit upon activation of the receptor. This dimer activates PI3K, which results in activation of both Akt and the small GTPase Rap1b (**Figure 1.2**) (Li et al., 2003, Woulfe et al., 2002). These interactions are involved in granule secretion and activation of GPIIb/IIIa which amplifies the platelet aggregation response (Fontana et al., 2003, Quinton et al., 2004). $P2Y_{12}$ signalling potentiates generation of the secondary mediator TXA_2 from arachidonic acid, to promote activation and recruitment of platelets to the site of aggregation via interaction with the thromboxane-prostanoid (TP) receptor.

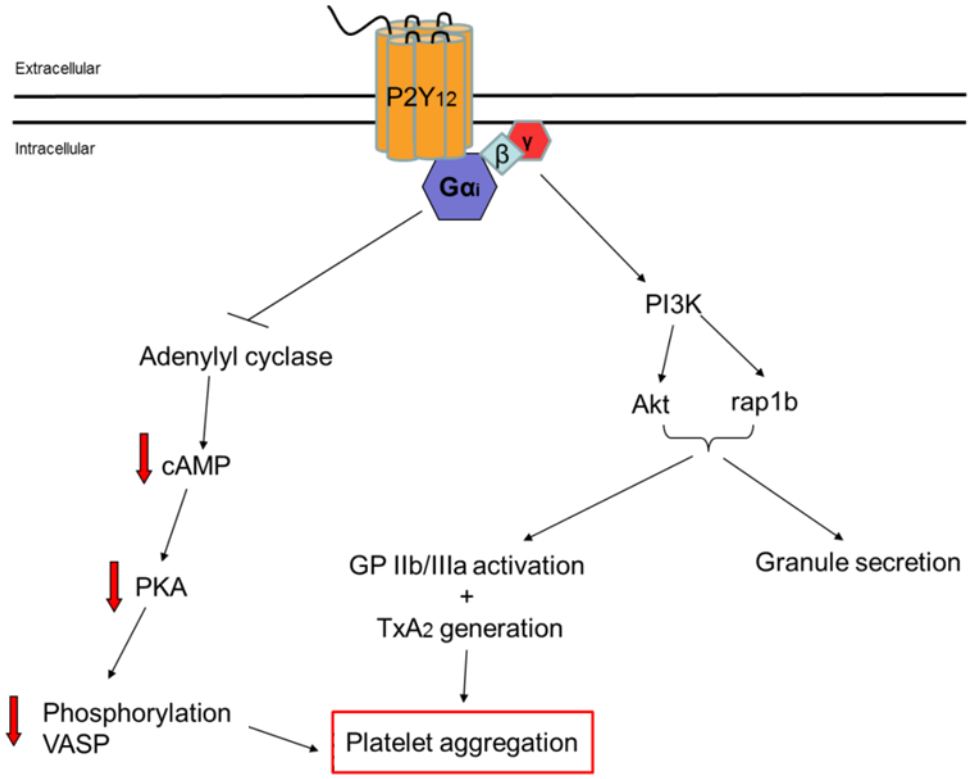

Figure 1.2 Intracellular pathways of the P2Y12 receptor.

Intracellular pathways involved in amplification of platelet aggregation following P2Y12 receptor activation. Uncoupling of the Gi linked protein subunits α and the βγ complex induces two distinct pathways; the inhibition of adenylyl cyclase leading to a reduction of phosphorylated vasodilator-stimulated phosphoprotein resulting in platelet aggregation. Also the activation of PI3K, leading to granule secretion and GP IIb/IIa acitivation, resulting in platelet aggregation. Figure adapted, with permission, from (Angiolillo et al., 2008).

1.2.3 Ligand interactions

ADP binds to $P2Y_{12}$ at the binding pocket in the extracellular portion of the receptor, between transmembrane (TM) regions 3, 5, 6 and 7 (Schmidt et al., 2013). The extracellular loop (EL) 2 is believed to be important in recognition of the ligand. In the human $P2Y_{12}$ receptor, Y^{105}, E^{188}, R^{256}, Y^{259} and K^{280} are proposed as important residues involved in ligand interaction, with K^{280} particularly important for ligand binding pocket function (Hoffmann et al., 2008, Schmidt et al., 2013, Ignatovica et al., 2012). These residues are highlighted by red circles in **Figure 1.3**. The DRY motif in the second intracellular loop is highly conserved in GPCRs and is important for intracellular trafficking, G protein interaction and localisation of $P2Y_{12}$ (highlighted by a red box in **Figure 1.3**)(Patel et al., 2014, Nygaard et al., 2009).

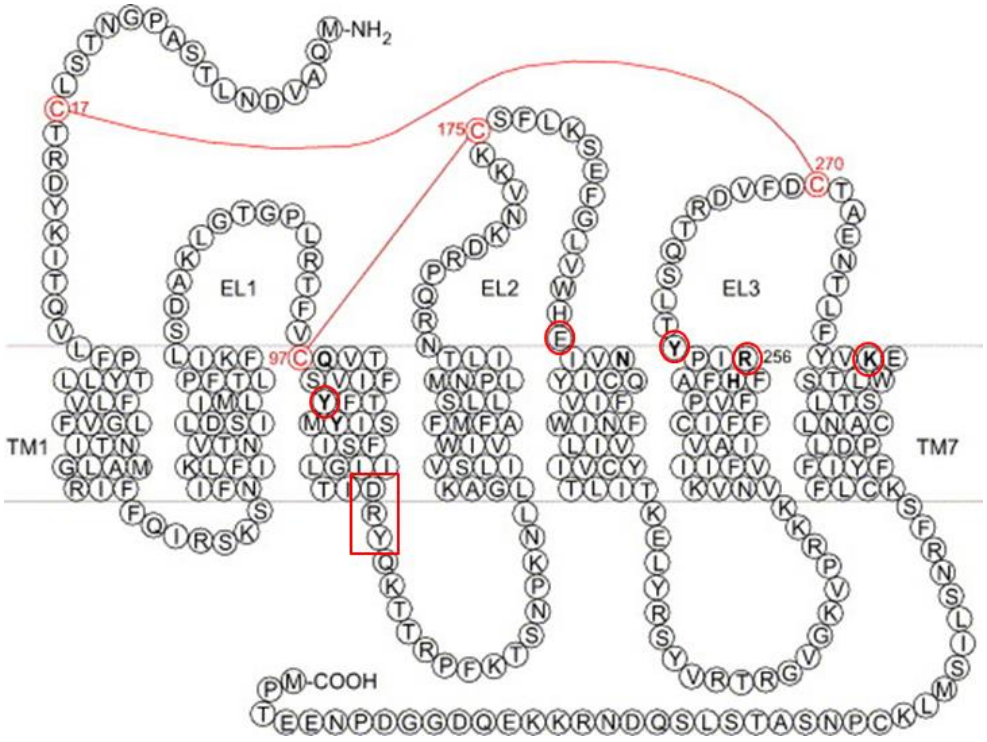

Figure 1.3 Predicted structure of the human P2Y$_{12}$ receptor.

A predicted structure for the human P2Y$_{12}$ receptor with the following key residues highlighted with red circles; Y^{105}, E^{188}, R^{256}, Y^{259} and K^{280} and the red box highlights the DRY motif. Disulphide bonds are shown in pink between Cys^{17} and Cys^{270} and Cys^{97} and Cys^{175} . Figure adapted from (von Kügelgen, 2006) with permission.

1.2.3 $P2Y_{12}$ expression

$P2Y_{12}$ is predominantly expressed on platelets, however it is also present in vascular smooth muscle cells (VSMC), microglia and macrophages (Hollopeter et al., 2001, Haynes et al., 2006, Wihlborg et al., 2004, Sasaki et al., 2003, Kronlage et al., 2010). There is some contention as to whether $P2Y_{12}$ is expressed on leukocytes other than macrophages (Diehl et al., 2010).

1.3 Platelet degranulation

Activated platelets release over 300 different proteins, contained within three different organelles: α granules, dense granules and lysosomes (Coppinger et al., 2004). Platelet degranulation is vital for a full thrombotic response, particularly in response to low agonist concentrations (Li et al., 2010). Degranulation occurs when there is fusion between the secretory vesicle and the plasma membrane, releasing granular contents. Activation of $P2Y_{12}$ by ADP contributes to the degranulation of dense granules, α granules and lysosomes from the platelet by amplifying intracellular responses initiated through activation of various receptors such as thrombin, TXA_2 and $P2Y_1$ (Hechler et al., 1998, Quinton et al., 2004).

1.3.1 α granules

α granules constitute the foremost secretory organelle, comprising the majority of different proteins released from the platelet. They contain factors involved in thrombosis, inflammation and immunity, including fibrinogen, vWF, platelet factor 4 and P-selectin (CD 62P) (Coppinger et al., 2004). α granules contain a heterogeneous population of proteins ranging from coagulation factors and pro-inflammatory mediators to antimicrobial peptides. These distinct populations of different factors often have contrary effects. It is suggested that pro-angiogenic factors such as vascular endothelial growth factor (VEGF) are contained within a separate population of α granules to anti-angiogenic factors such as Endostatin, with differential release depending on activation of receptors PAR1 or PAR4 respectively (Italiano et al., 2008, Sehgal and Storrie, 2007). vWF and fibrinogen are also segregated into distinct populations of α granules, whilst P-selectin is distributed throughout both populations. α granule subsets are proposed to consist

of spherical (comprising the majority) and tubular (not present in every platelet), containing different factors which can be differentially released (van Nispen tot Pannerden et al., 2010). For example, spherical α granules contain vWF and β-thromboglobulin which are not present in tubular α granules (van Nispen tot Pannerden et al., 2010) . It is however unclear as to the mechanism of differential release; whether this is due to activation of different receptors or due to different packaging of proteins such as vWF and fibrinogen within the α granule (Sehgal and Storrie, 2007). Activation of $P2Y_{12}$ regulates the small G protein Rap1b, which is particularly important in degranulation of α granules (Lova et al., 2002). This is demonstrated by $P2Y_{12}$ receptor antagonism reducing release of P-selectin from α granules and decreasing the subsequent expression on the platelet surface (Quinton et al., 2004).

1.3.2 Dense granules

Dense granules contain calcium ions and small molecules that contribute to the further activation of platelets including ADP, ATP and 5HT (Tranzer et al., 1966, Mills et al., 1968). Dense granule release is induced by several agonists such as collagen, TXA_2 and thrombin. Upon degranulation, released ADP forms a positive feedback mechanism to amplify the aggregation response through further activation of the $P2Y_{12}$ receptor and, to a lesser extent, $P2Y_1$ (Hechler and Gachet, 2011).

Table 1.1 A selection of peptides released from α granules.

A variety of peptides are released from α granules upon degranulation, a selection of these are shown in the table below, along with references. These peptides are involved in many different processes including coagulation, angiogenesis, adhesion, chemotaxis and microbial defence.

	Peptides released	**Reference**
Coagulation factors	Fibrinogen Factor V Thrombospondin	(Gerrard et al., 1980) (Vicic et al., 1980) (George, 1978)
Pro-angiogenic	VEGF	(Wartiovaara et al., 1998)
Anti- angiogenic	Endostatin	(Ma et al., 2001)
Pro- Inflammatory	PDGF P-Selectin CD40 ligand (CD 154)	(Witte et al., 1978) (Stenberg et al., 1985) (Kamykowski et al., 2011)
Adhesive ligands	vWF	(Cramer et al., 1985)
Platelet microbicidal proteins	Platelet Basic Protein (PBP) PF-4 RANTES (CCL5) IL-8 (CXCL8) CTAP 3	(Holt et al., 1986) (Senior et al., 1983) (Klinger et al., 1995) (Schaufelberger et al., 1994) (Castor et al., 1983)
Chemokines	Neutrophil Activating Protein 2 (CXCL7) RANTES (CCL5) β-Thromboglobulin Growth Regulating Oncogene-α (GRO- α)(CXCL1) PF-4 (CXCL4) Monocyte Inflammatory Protein (MIP-1 α) Monocyte Chemotactic Protein-3 (MCP-3)	(Piccardoni et al., 1996) (Klinger et al., 1995) (Gerrard et al., 1980) (Oquendo et al., 1989) (Klinger et al., 1995) (Power et al., 1995)
Cytokine	TGF β	(Assoian and Sporn, 1986)
Proteolysis	Vitronectin	(Seiffert and Schleef, 1996)

1.4 Platelet and leukocyte interaction

P-selectin (CD 62P) is an adhesion receptor which is translocated to the surface of activated platelets from α granules upon degranulation. P-selectin is a key releasate from α granules and is a marker of platelet activation (Stenberg et al., 1985). P-selectin, once expressed on the surface of activated platelets binds to its ligand P-selectin glycoprotein ligand-1 (PSGL-1) which is present on monocytes, neutrophils and endothelial cells, as shown in **Figure 1.3**. P-selectin enables platelets to roll on and adhere to activated endothelium and form platelet-leukocyte conjugates. Platelets are able to bind to monocytes, neutrophils and lymphocytes, leading to leukocyte activation and subsequent cytokine production, phagocytosis and release of neutrophil lysosomal enzymes (von Hundelshausen and Weber, 2007, Storey et al., 2002). This interaction between the platelet and the monocyte also induces production of tissue factor (TF) which further activates the coagulation cascade (Celi et al., 1994, Lindmark et al., 2000).

CD40 ligand (CD154) is an immunomodulating ligand that is translocated from α granules to the platelet surface as shown in **Figure 1.4**. CD40 ligand binds to the CD40 receptor expressed on monocytes, macrophages and endothelial cells. This interaction induces the expression of TF on the monocytes surface and endothelial cells to release chemokines to recruit leukocytes (Lindmark et al., 2000, Henn et al., 1998, Mach et al., 1997). Leukocytes, such as neutrophils and monocytes, adhere via these receptors to activated platelets in thrombi, and can contribute to thrombin generation for further fibrin deposition (Palabrica et al., 1992, Kirchhofer et al., 1997).

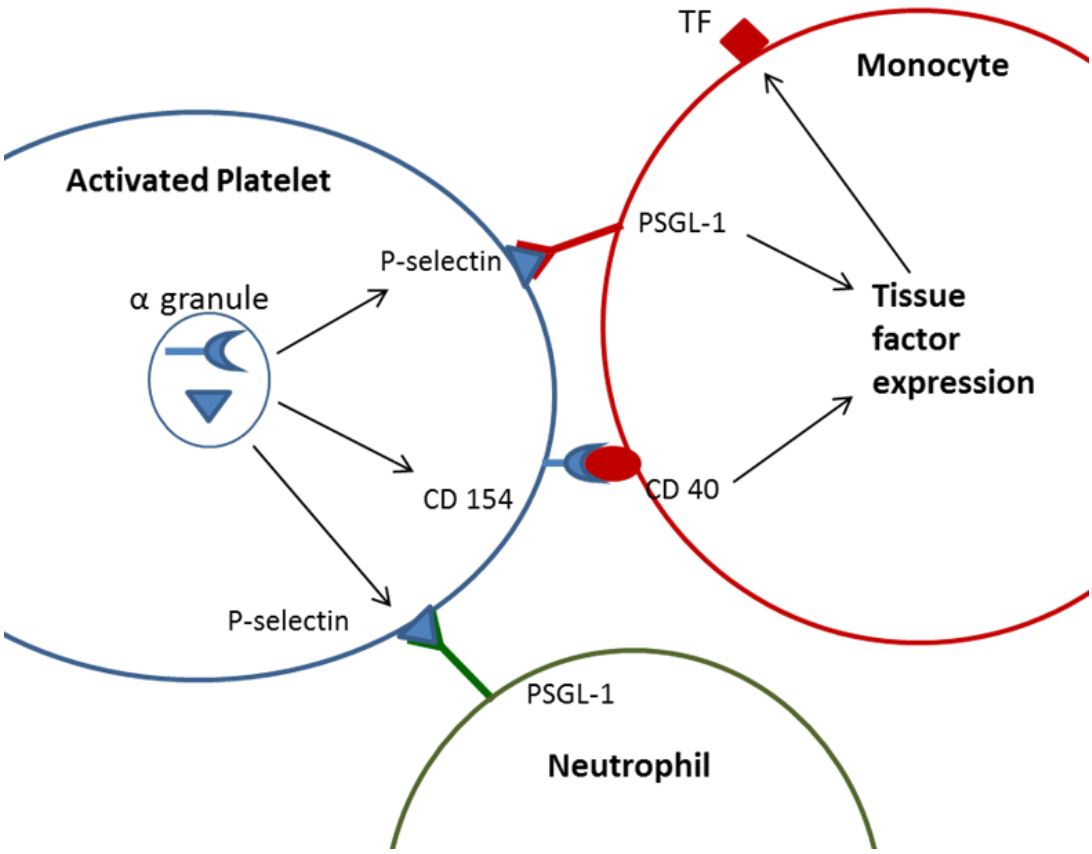

Figure 1.4 Schematic of platelet leukocyte interactions.

The activated platelet interacts with monocytes via P-selectin and CD154 expressed on the cells surface. These peptides are released from α granules and are translocated to the cell surface where they interact with the ligand and receptor respectively. The monocyte binds to P-selectin via its ligand PSGL-1 and CD154 via its receptor CD40. This interaction induces tissue factor expression on the surface of the monocyte. The platelet also interacts with neutrophils via binding of P-selectin to its ligand PSGL-1.

1.5 $P2Y_{12}$ antagonists

There are several different classes of $P2Y_{12}$ antagonists with variable mechanisms of action. The irreversibly binding thienopyridine class requires conversion to active metabolites for effect, which extends the time to onset of action. As thienopyridines irreversibly antagonise the receptor, they also have an increased time to offset of action, as this is dependent on the lifespan of the platelet which in humans is 7-10 days (Harker, 1977). Reversibly-binding antagonists have a shorter offset of action which can be beneficial in the pre-surgical situation. The new generation of cyclopentyl-triazolo-pyrimidines (CPTP) antagonists bind non-competitively and require no conversion to active metabolite, therefore have a quicker onset of action.

1.5.1 Clopidogrel

The thienopyridine clopidogrel is an irreversibly-binding $P2Y_{12}$ antagonist which requires hepatic conversion to its active thiol metabolite via the hepatic cytochrome P450 (CYP) enzymes, particularly CYP3A4 and CYP2C19 isoenzymes (Savi et al., 1994, Clarke and Waskell, 2003, Hulot et al., 2006). The active metabolite interacts with extracellular cysteine residues on the receptor to form a disulphide bridge with the extracellular target residue cysteine 97 to irreversibly interfere with ADP binding (Ding et al., 2003, Savi et al., 2006). Functional $P2Y_{12}$ oligomers are associated with cell membrane lipid rafts; when active metabolite binds $P2Y_{12}$, it dissociates these into dimers and monomers which become partitioned out of the lipid raft and thus disrupts ligand binding (Savi et al., 2006). Clopidogrel has been shown to induce a variable response between patients, partly due to genetic polymorphisms in the hepatic cytochrome enzymes, which impact upon conversion of the pro-drug to the active metabolite. It has been shown that up to 30% of Caucasians have a loss-of-function polymorphism in the CYP2C19 gene which reduces the pharmacodynamic effect of clopidogrel (O'Connor et al., 2011).

1.5.2 Prasugrel

Prasugrel is a thienopyridine irreversibly-acting prodrug which is rapidly converted to its active metabolite via cytochrome isoenzymes, particularly CYP3A4/5 and CYP2B6 as well as CYP2C9 and CYP2C19 in a manner which is unaffected by polymorphic mutations in CYP2C9 or CYP2C19 (Brandt et al., 2007). It has a similar mechanism of action to clopidogrel in which the active metabolite forms a disulphide bond with the receptor, preventing agonist binding (Algaier et al., 2008). Prasugrel induces greater and more consistent inhibition of $P2Y_{12}$ than clopidogrel, but incurs increased risk of bleeding which, when combined with a slow offset time, highlighting the disadvantages of thienopyridines (Wiviott et al., 2007) .

1.5.3 Cangrelor

Cangrelor is an ATP analogue which is directly acting and rapidly reversible. It binds to $P2Y_{12}$ competitively with a short half-life of approximately 5 minutes, requiring intravenous administration (Storey et al., 2001). As a result, cangrelor has a quick onset and offset mode of action.

1.5.4 Ticagrelor

Ticagrelor is a CPTP antagonist which reversibly and non-competitively binds $P2Y_{12}$ at a site distinct from the ADP binding site. This allosteric binding prevents conformational change of the receptor to activate the Gi protein, therefore preventing signal transduction caused by binding of ADP (van Giezen, 2008). Ticagrelor has rapid onset and offset with levels of inhibition directly correlating to the plasma concentration of drug (Gurbel et al., 2009). Ticagrelor induces a greater and more consistent inhibition than thienopyridines (van Giezen et al., 2009). Side effects of ticagrelor include dyspnoea and increased incidence of bradyarrhythmia both of which are proposed to be due to prevention of adenosine reuptake into red blood cells leading to an excess of extracellular adenosine (Gurbel et al., 2009, Cannon et al., 2007, Scirica et al., 2011). This area requires further investigation in order to determine the effects of ticagrelor on systems other than the $P2Y_{12}$ receptor.

1.6 $P2Y_{12}$ antagonism in thrombosis

Remijn et al. (2002) compared blood from a patient deficient in $P2Y_{12}$ to blood samples from healthy volunteers either without treatment or after treatment with cangrelor. Both $P2Y_{12}$ deficient and cangrelor treated samples showed reduced platelet adhesion to fibrinogen and the formation of smaller thrombi on collagen under conditions of flow (Remijn et al., 2002). The $P2Y_{12}$ receptor has also been studied in several animal models, establishing differing techniques to elucidate the $P2Y_{12}$ receptors' involvement in thrombosis following vessel injury. Van Gestel et al. (2003) injured the mesenteric arterioles of rabbits by vessel wall puncture which were exposed to $P2Y_{12}$ antagonists clopidogrel and cangrelor (formerly AR-C69931MX) to study their effect on thrombosis. This investigation found that antagonism of $P2Y_{12}$ reduces the size of thrombus by decreasing platelet adhesion to fibrinogen without effecting thrombus stability (van Gestel et al., 2003). The most common animal model for studying $P2Y_{12}$ is the $P2Y_{12}$ knockout mouse (*$P2Y_{12}$ -/-*) which has been utilised to investigate thrombotic response to vessel injury such as induced by ferric chloride ($FeCl_3$), femoral wire and laser irradiation technique (Foster et al., 2001) (Andre et al., 2003, Evans et al., 2009, Patil et al., 2010). *$P2Y_{12}$ -/-* mice have an increased bleeding time in response to amputation of the tail tip, with a reduced sensitivity to thrombin and collagen (Foster et al., 2001). In contrast to the Van Gestel investigation, Andre et al (2003) used the *$P2Y_{12}$ -/-* mouse after $FeCl_3$ injury to study stabilisation of thrombi and found that *$P2Y_{12}$ -/-* mice appeared to show increased embolization of thrombi when compared to wildtype, indicating that thrombi forming in the *$P2Y_{12}$ -/-* mice were more unstable than those in wildtypes (Andre et al., 2003). However *$P2Y_{12}$ -/+* mice do not appear to have altered thrombosis response compared to wildtype (Andre et al., 2003). Treatment with ticagrelor mirrors the response in the *$P2Y_{12}$ -/-* mouse with reduced thrombus formation after laser-induced vessel injury of arterioles in the cremaster muscle (Patil et al., 2010). Platelets are believed to be an important contributor to restenosis after percutaneous coronary intervention (PCI), leading to the role of $P2Y_{12}$ to be investigated in neointima formation after vessel injury (Patil et al., 2010). Our group found that $P2Y_{12}$ knockout or antagonism of $P2Y_{12}$ reduces

neointima formation after vessel injury when compared to wildtype mice, indicating that the early thrombosis response after vessel injury is a vital stage in the development of neointima (Evans et al., 2009).

There are several techniques utilising different mechanisms of vessel injury to induce thrombosis. $FeCl_3$ induces oxidative damage to the vessel when applied externally to the artery and thus diffuses through the wall to damage the vessel and expose its basement membrane to flowing blood (Kurz et al., 1990, Eckly et al., 2011). This mechanism for vessel damage is sufficient to induce thrombosis however there is little exposure of the internal elastic lamina, media or adventitia, which may affect the interactions for example of collagen with GPVI (Eckly et al., 2011). Femoral wire injury involves damaging the vessel wall via a guide wire passed within the femoral artery, resulting in a denudation of the wall and subsequent thrombosis (Roque et al., 2000). Wire injury is reported to be a weaker stimulus for thrombosis when compared to $FeCl_3$ injury (Evans et al., 2009). Laser irradiation of the vessel wall, such as in the mouse ear, induces heat damage which enables a non-invasive mechanism for damage of the vessel endothelium sufficiently to generate thrombosis (Rosen et al., 2001). This technique has also been utilised to monitor thrombus formation in the cremaster muscle of the mouse, which requires invasive surgery to open the cremaster, allowing the developing thrombus to be visualised *in vivo* (Patil et al., 2010). We have selected this laser irradiation technique for initiation of thrombosis in the zebrafish model, which enables *in vivo* visualisation of thrombus development, as above, in addition to a range of fluorescently labelled transgenic lines and an increased throughput, in comparison to the mouse.

1.7 $P2Y_{12}$ mutations and the effect on thrombosis

Several mutations in human *P2RY12* have been documented, with effects ranging from impaired ADP binding, reduced $P2Y_{12}$ activation after ADP binding or reduced cell surface expression. Cattaneo et al. (2003) observed a compound heterozygote for two different allelic mutations, R256Q and R265W, which resulted in a bleeding phenotype with reduced $P2Y_{12}$ activation and G_i signalling but without impaired ADP binding or cell surface expression (Cattaneo et al., 2003). Fontana et al. (2009)

showed haploinsufficiency of *P2RY12* in an individual heterozygous for a 378delC mutation, resulting in a frame shift and truncation of *P2RY12* downstream of the third transmembrane domain (Fontana et al., 2009, Conley 2001). This patient showed a mild platelet dysfunction including abnormal platelet aggregation, slight deficiency in [^{33}P]2MeS-ADP binding sites and a secretion defect (Cattaneo et al., 2000). Daly et al. (2009) investigated a patient with impaired ligand binding after a substitution mutation of K174E in *P2RY12*, a mutation which affects the second extracellular loop of $P2Y_{12}$ (Daly et al., 2009). In addition to this mutation, this patient also had mild type 1 von Willibrand disease and a *VWF* defect, resulting in a bleeding tendency (Daly et al., 2009). Patel et. el (2014) studied a patient homozygous for R122C substitution within the highly conserved DRY motif of *P2RY12* whom showed reduced ADP-stimulated platelet aggregation and a reduction in $P2Y_{12}$ cell surface expression with a high proportion of $P2Y_{12}$ located intracellularly (Patel et al., 2014). This patient also had a polymorphism in *F2 R* resulting in a reduced expression of PAR-1 and reduced aggregation in response to PAR-1 activating peptide (Patel et al., 2014).

In other species, a naturally occurring deletion of serine 173 (173Sdel) in *P2Y12* was detected in the Greater Swiss Mountain Dog, resulting in excessive post-operative bleeding (Boudreaux and Martin, 2011). Considerable work has been undertaken on the *$P2Y_{12}$ -/-* mouse (Foster et al., 2001), however the *$P2Y_{12}$ -/+* mouse does not appear to have altered thrombosis response, therefore there does not appear to be the same haploinsufficiency of mouse *P2Y12* compared to human *P2RY12* (Andre et al., 2003).

1.8 $P2Y_{12}$ antagonism in inflammation

$P2Y_{12}$ activation plays a role in inflammation through the amplification of α and dense granule release. α granules contain a myriad of factors (**Table 1.1**), some of which are required for inflammation, such as the chemoattraction of leukocytes via chemokines and pro-inflammatory mediators (Steinhubl et al., 2007). $P2Y_{12}$ is proposed to work in conjunction with $P2Y_2$ and A_3 adenosine receptors to amplify chemotactic response of macrophages (Kronlage et al., 2010). $P2Y_{12}$ may play an important role in inflammation. Treatment of acute coronary syndrome (ACS)

patients with $P2Y_{12}$ antagonists reduces inflammatory markers such as P-selectin, C reactive protein (CRP) and CD40L, therefore reducing platelet-leukocyte aggregation (Steinhubl et al., 2007). As $P2Y_{12}$ is important in the release of α granules from the activated platelet, antagonism of this receptor reduces granule release. P-selectin and CD40L are both proposed to be important in development of atherosclerotic plaques. Recent work by our group has shown that it is vessel wall $P2Y_{12}$ rather than platelet $P2Y_{12}$ which plays a role in early development of atheroma (West et al., 2014).

As previously discussed, ticagrelor is a $P2Y_{12}$ antagonist which also blocks reuptake of adenosine. There are 4 cell surface adenosine receptors; A_1, A_{2A}, A_{2B} and A_3. These receptors are present on a variety of different cell types including smooth muscle, endothelial cells, macrophages, and platelets. Adenosine is produced by the break-down of ATP, and is proposed to have both anti and pro inflammatory effects depending on which adenosine receptor is activated. Activation of A_1 and A_3 receptors, which are both linked to the Gi protein, increases neutrophil chemotaxis, adhesion to endothelium and phagocytosis (Cronstein et al., 1992) (Chen et al., 2006). Kronlage et al. (2010) propose that A_3 signalling complements purinergic receptor signalling from $P2Y_2$ and $P2Y_{12}$ to amplify chemotactic signalling of macrophages (Kronlage et al., 2010). A_{2A} is linked to the Gs protein, and A_{2B} is linked to both the Gs and Gq proteins; activation of these receptors inhibits neutrophil and macrophage degranulation (Nakav et al., 2008) (Fredholm, 2007). Therefore there is a differential effect of adenosine on inflammatory processes, dependent upon which receptors are activated. This emphasises that the role of excess adenosine in inflammation during ticagrelor treatment requires further investigation.

1.9 $P2Y_{12}$ in infection

Platelets play a role in host defence against bacterial, viral, protozoan and fungal infections. Circulating platelets are the first cells to respond to chemotactic signals and accumulate at sites of vascular injury and infection (Yeaman and Bayer, 1999). Activated platelets are capable of internalising pathogens such as bacteria or viruses, into the open canalicular system (OCS) (Youssefian et al., 2002).

Degranulation of α granules releases many antimicrobial proteins, chemokines and cytokines involved in killing pathogens and recruiting leukocytes to sites of infection (**Table 1.1**). $P2Y_{12}$ is an important activator of intracellular pathways required for α granule degranulation and therefore may play a role in the platelet response to infection.

1.9.1 Antimicrobial peptides

Antimicrobial peptides can directly interact with pathogens via surface receptors enabling the internalisation of pathogens. Many antimicrobial peptides have been identified, some of which act as chemokines, cytokines or directly to destroy the pathogen such as thrombocydins or kinocidins, termed platelet microbicidal proteins (PMPs) or platelet kinocidins (PK). Examples of antimicrobial peptides contained within platelets are demonstrated in **Table 1.1,** for example PF-4 is a kinocidin (Yeaman et al., 2007, Tang et al., 2002). These peptides are specialised to function in the acidic pH associated with inflammatory conditions thus contributing to host defence against invading pathogens (Tang et al., 2002). Platelets express chemokine receptors, such as CXCR4, CCR1, CCR3 and CCR4, and are capable of autocrine and paracrine signalling (Boehlen and Clemetson, 2001).

1.9.2 $P2Y_{12}$ antagonism and infection

A previous study has suggested that antagonism of the $P2Y_{12}$ receptor may increase risk of post-operative infection after coronary artery bypass graft (CABG) surgery, although it is unclear whether $P2Y_{12}$ antagonism itself or dual therapy with both aspirin and clopidogrel increased risk (Blasco-Colmenares et al., 2009). It would be interesting to investigate the effect of dual therapy with other combinations of $P2Y_{12}$ antagonists or a non- $P2Y_{12}$ antagonist, since this effect may be due to a decrease in anti-microbial peptide release or instances of reoperation (perhaps due to bleeding complications) associated with anti-platelet treatment (Blasco-Colmenares et al., 2009). In the PLATO study, patients treated with ticagrelor showed a reduced rate of mortality and infection compared to those treated with clopidogrel (Varenhorst et al., 2012, Storey et al., 2013). Post hoc analysis has suggested that partly this may be due to differential effects of the drugs on

susceptibility to pulmonary infection and its complications (Storey et al., 2013). These results have caused some controversy as to the reliability of the trial, for example Serebrauny (2011) criticised the perceived high death rates documented in PLATO, suggesting these were higher than previous ACS trials and the inclusion of an alive patient initially reported as dead (Serebruany, 2011). However this suggestion was rebutted by both Ohman and Roe (2011) and Wallentin et al. (2011) who defended the results of the trial stating that all the data was correctly interpreted (Ohman and Roe, 2011) (Wallentin et al., 2011). Although unconfirmed, there are several plausible reasons for a differential effect of $P2Y_{12}$ antagonists on susceptibility to infection. These drugs have different mechanisms of action, with ticagrelor binding $P2Y_{12}$ at a distinct site away from the ADP binding pocket and also preventing adenosine re-uptake. Therefore it is possible that it is this excess of adenosine which is contributing to the potential protective effects of ticagrelor compared to clopidogrel.

Staphylococcus aureus infection is known to induce the release of PMP and kinocidins from the platelet (Trier et al., 2008). Treatment of rabbit platelets with $P2X_1$ antagonist and cangrelor inhibited staphylocidal response via a reduction in levels of platelet microbicidal proteins and kinocidins (Trier et al., 2008). Therefore, $P2X_1$ and $P2Y_{12}$ positive feedback systems are proposed to mediate the release of microbicidal proteins and kinocidins (Trier et al., 2008). This emphasises the important role $P2Y_{12}$ plays in peptide release from α granules. $P2Y_{12}$ receptor involvement in defence against malarial parasites has been investigated and it was found that the $P2Y_1$ receptor, rather than $P2Y_{12}$, mediates defence against this type of infection (McMorran et al., 2009).

This represents an area which requires further investigation to ascertain the role of $P2Y_{12}$ activation and α granule release in defence against parasite, bacterial, viral and fungal infections. $P2Y_{12}$ antagonists are widely used clinically therefore it is vital to fully elucidate the effects of $P2Y_{12}$ antagonism on resistance to infection.

1.10 The use of zebrafish to model thrombosis, inflammation and infection response

1.10.1 Zebrafish background

The zebrafish *(Danio rerio)* is a small tropical freshwater fish originating in India, Bhutan and Pakistan, which grows up to 4cm in length. The zebrafish possesses many advantages, including low maintenance costs and a short generation time with high fecundity: each female produces approximately 200-300 embryos per week from 3 months of age, enabling high-throughput investigations requiring large animal numbers, such as mutagenesis screens. The zebrafish has a fully functioning circulation by approximately 25 hours post fertilisation (hpf), however the embryo is able to obtain enough oxygen via diffusion in the first few days of development so that circulation is not required (Rombough, 2002). This enables the investigation of some embryonically lethal malformations or interventions which would be impossible in other models. Zebrafish embryos are optically transparent, enabling easy visualisation of cardiac function and blood circulation, via low powered light microscopy. This represents a considerable advantage for use of the zebrafish, as although visualisation of circulation is possible in the mouse model, the zebrafish model enables use of a variety of fluorescently labelled transgenic lines, and ease of genetic manipulation enable high throughput investigations of inflammatory and infective responses, which are limited in current mammalian models.

1.10.2 Genetic manipulation of zebrafish

The zebrafish genome has been fully sequenced, facilitating reverse genetic studies of gain-of-function and loss-of-function of candidate genes, via overexpression or knockdown. Gene overexpression is possible via injection of synthesised mRNA into 1-2 cell stage embryos. Gene knockdown can be achieved by injecting 1-2 cell stage embryos with a synthetic antisense morpholino oligonucleotide (MO), which binds complimentarily to the sense strand of the mRNA to prevent translation, therefore inducing targeted knockdown for several days post fertilisation (dpf). Both these techniques have been widely used to investigate the function of specific genes. Recently, newer methods have been developed enabling targeted stable mutation

of genes of interest. Two examples of these are: context dependent assembly (CoDA) zinc finger nuclease (ZFN) and transcription activator-like effector nucleotides (TALENs), which induce a targeted cleavage of specific gene loci so that a subsequent mutation occurs via erroneous nonhomologous end joining (NHEJ)(Mussolino et al., 2011, Sander et al., 2011). I will discuss these more fully in Chapter 5, in which I exploit these to generate a stable *p2y12* mutant zebrafish line.

Transgenesis has allowed generation of many transgenic lines expressing fluorescent reporter proteins or other constructs under the control of gene promoters to induce cell type specific expression. This allows identification and tracking of fluorescently labelled cells. **Table 2.1** summarises some examples of transgenic lines relevant to my research.

Approximately 70% of human protein coding genes possess at least one zebrafish orthologue (Howe et al., 2013). This relatively high degree of conservation determines a great similarity to mammals in many different systems such as cardiovascular, digestive and nervous systems. The zebrafish ancestry has undergone a genome duplication leading to several transcript variants of some genes (Amores et al., 1998).

Zebrafish have increasingly been utilised for small molecule screens due to their suitability for high-throughput investigations. Drug treatment can be achieved via addition of the pharmaceutical agent to the media. Zebrafish can withstand low concentrations of dimethyl-sulfoxide (DMSO), therefore this is often utilised for dissolving hydrophobic drugs. In zebrafish embryos, agents are primarily taken up through the skin (Rombough, 2002).

1.10.3 Limitations of zebrafish models

There are some disadvantages of the zebrafish as a model. There are currently few antibodies raised against zebrafish proteins, restricting the use of western blotting for the detection of proteins, unless there is sufficient cross-reactivity with existing antibodies, which is rare. The adaptive immune system of the zebrafish develops approximately 4-6 weeks post fertilisation and has been suggested to be less evolved than the innate system (Lam et al., 2004). However this delay in development of the adaptive immune system could represent an advantage for studying the innate system in isolation (Sullivan and Kim, 2008). The presence of one or more transcript variants, due to the zebrafish genome duplication event, can complicate the functional assessment of genes after knockdown (Amores et al., 1998). The genetic divergence between mammals and zebrafish limits the investigation of some genes which do not possess a zebrafish orthologue. There are also obvious anatomical differences between mammalian models and zebrafish such as an absence of lungs and a lack of heart septation.

The zebrafish nevertheless represents a useful model for investigation of many diseases and signalling pathways, particularly when used in conjunction with other animal models, to explore physiological processes for which the zebrafish offers a simplified model.

1.10.4 Zebrafish *p2y12*

p2y12 is expressed on microglia where it is involved in the detection of purinergic signals required to induce chemotaxis to sites of central nervous system (CNS) injury (Haynes et al., 2006). *p2y12* has been investigated in the zebrafish with regards to its function in microglial cells (Sieger et al., 2012). Sieger et al. (2012) generated a p2y12::P2Y12-GFP transgenic by the fusion of GFP to the C' terminus of *p2y12*. This transgenic was used to visualise microglial migration to sites of injury in the optic tectum *in vivo*. Two different translation-blocking *p2y12* morpholinos were used; P2Y12mo and P2Y12mo2 (See **Table 2.3)**. Injection of these morpholinos blocked microglial response to injury and reduced expression of P2Y12-GFP (Sieger et al., 2012). It is important to note that this work was published during the course

of my project and that this study did not investigate the role of platelet $P2Y_{12}$ in thrombosis, inflammation or infection.

1.10.5 Zebrafish haematopoiesis

Haematopoiesis in the zebrafish occurs in 2 waves; the primitive wave and the definitive wave. The primitive wave occurs before 24 hpf and originates in the posterior lateral mesoderm (PLM), which later becomes the intermediate cell mass (ICM) and is the site of erthryopoiesis, and the anterior lateral mesoderm (ALM), which later becomes the rostral blood island (RBI) and is the site of myelopoiesis (Davidson et al., 2003, Bennett et al., 2001, Detrich et al., 1995). A transient wave of haematopoiesis, generating erythromyeloid progenitors (EMP), occurs at approximately 24 hpf, at the start of circulation, in the posterior blood island (PBI) (Bertrand et al., 2007). The definitive wave originates in the aorta-gonad mesonephros (AGM) region located in the ventral region of the dorsal aorta, which was previously the ICM and which is where haematopoietic stem cells (HSC) are produced (Murayama et al., 2006). By 36 hpf the PBI becomes the caudal haematopoietic tissue (CHT), the site of definitive erythropoiesis and myelopoiesis (Jin et al., 2009, Galloway et al., 2005). HSC's from the AGM seed the thymus for lymphopoeisis and the kidney for further generation of HSCs and definitive haematopoeisis in the larval stage (Murayama et al., 2006, Kissa et al., 2008).

1.10.6 Zebrafish thrombocytes

Thrombocytes are the nucleated equivalent of human platelets, found in non-mammalian vertebrates. 6% of the blood cell population comprises of thrombocytes, which first appear in circulation at approximately 36 hpf (Jagadeeswaran et al., 1999). Thrombocytes possess many key platelet receptors such as $P2Y_1$, GP IIb/IIIa and GP Ib (Jagadeeswaran et al., 1999, Gregory and Jagadeeswaran, 2002). Thrombocytes have been shown to be activated by agonists such as ADP, arachidonic acid, ristocetin and collagen, consequently they are able to adhere, secrete, phagocytose and form aggregates with filopodia-like projections upon activation (Gregory and Jagadeeswaran, 2002, Tournoij et al., 2010). Zebrafish thrombocytes are also able to secrete ATP upon activation by collagen and

arachidonic acid (Jagadeeswaran et al., 1999). Gregory and Jagadeeswaran (2002) labelled zebrafish thrombocytes with the thrombocyte-specific lipophilic dye DiI-C18 in whole blood samples, of which 4 µl were obtained from an adult fish. DiI-C18 only labelled 50% of the thrombocytes, prompting investigation as to why the entire population of thrombocytes were not labelled with this method (Gregory and Jagadeeswaran, 2002). It is proposed that DiI distinguishes two different populations of thrombocytes; rapidly activated young thrombocytes that initiate thrombosis, which are DiI+, and less active DiI- mature thrombocytes (Thattaliyath et al., 2005). Treatment with the $P2Y_1$ receptor antagonist adenosine-3',5-bisphosphate (A3P5P) inhibited thrombocyte activation in response to ADP, establishing the presence of this receptor, however there was no investigation into $P2Y_{12}$ presence on thrombocytes (Gregory and Jagadeeswaran, 2002).

Zebrafish possess orthologues of many key proteins involved in thrombocyte aggregation including P-selectin, CD154 and vWF (Sun et al., 2010) (Gong et al., 2009, Carrillo et al., 2010). Zebrafish homology to mammalian P-selectin and CD41 is 39% and 40% respectively (Sun et al., 2010, Lin et al., 2005). However, zebrafish lack the collagen receptor GPVI (Hughes et al., 2012). Conservation of these proteins supports the use of zebrafish as a model for investigation into functions and processes of the platelet. A transgenic line with green fluorescent protein (GFP) reporter expressed under the control of the CD41 promoter (CD41:GFP), the α subunit of GP IIb, was generated to visualise thrombocytes *in vivo* (Lin et al., 2005). This transgenic labels haematopoietic stem cells (HSC) in a GFP^{low} level of fluorescence and thrombocytes in a GFP^{high} level of fluorescence (Lin et al., 2005). The HSC identity of GFP^{low} cells has been confirmed by reconstitution of the haematopoietic lineage from GFP^{low} cells transplanted into irradiated adult fish (Ma et al., 2011). GFP positive cells appear at 33-35 hpf between the posterior cardinal vein and the dorsal aorta in an area of mesenchyme similar to the mammalian aorta/gonad/mesonephros region (AGM). These then migrate via the axial vein to the thymus and caudal haematopoietic tissue (CHT) and enter circulation at approximately 48 hpf (Kissa et al., 2008). By 5 dpf the site of thrombopoiesis moves from the CHT to the kidney (Lin et al., 2005)

1.10.7 Using zebrafish to model thrombosis

The most common method for investigation of thrombosis in zebrafish uses targeted laser irradiation to injure vessel endothelium, sufficient to induce thrombosis (Gregory et al., 2002). This was developed to enable quantification of time to occlusion (TTO) of the vessel, time to attachment (TTA) of the first cell to the damaged endothelium and time to dissolution (TTD) of the thrombus (Gregory et al., 2002, Jagadeeswaran, 2005). The developing thrombus can be imaged *in vivo* and O'Connor et al (2009) introduced a method for measurement of thrombus surface area (TSA) by the use of ImageJ software, enabling quantification of thrombus area (O'Connor et al., 2009). Since development of this method, it has been utilised to ascertain the effect of antisense MO knockdown of proteins or receptors involved in aggregation. Knockdown of prothrombin resulted in a prolonged TTO upon vessel injury showing similarities with the prothrombin -/- mouse (Day et al., 2004). Knockdown of PKCα and PKCβ resulted in attenuated thrombus formation, determined by quantification of TSA, recapitulating the phenotypes observed in the PKCα -/- mouse (Williams et al., 2011). **Table 1.2** summarises the previously published studies of thrombosis using the zebrafish.

Table 1.2 Summary of thrombosis studies using the zebrafish.

Many genes have been investigated by knockdown and laser induced thrombosis in the zebrafish model. The effect of gene knockdown on thrombus formation can be quantified using; time to attachment (TTA), time to occlusion (TTO) and thrombus surface area (TSA). This table shows the genes investigated, the function of the gene, the location of vessel injury and the effect of gene knockdown on the thrombosis response. (N.S non-significant, ↓ decrease, ↑ increase, TM transmembrane.)

Gene	**Function of gene**	**Anatomical location of injury**	**Phenotype of gene knockdown**	**Reference**
Factor VII Factor VIIi	Coagulation factor	Caudal vein	↑ TTO ↓ TTO	(Gregory et al., 2002)
Prothrombin	Coagulation factor II	Caudal vein	↑ TTO	(Day et al., 2004)
GPIIb FVIII ANTXR2 BAMBI DCBLD2 ESAM LRRC32	Platelet receptor Coagulation factor Platelet TM protein Platelet TM protein Platelet TM protein Platelet TM protein Platelet TM protein	Dorsal aorta	TTA N.S, ↓ TSA TTA N.S, ↓TSA TTA N.S , TSA N.S ↑ TTA, ↓ TSA TTA N.S, ↑ TSA TTA N.S, ↑ TSA ↑ TTA, ↓ TSA	(O'Connor et al., 2009)
PKCα PKCβ	Platelet kinase	Ventral wall dorsal aorta	↑ TTA, ↓ TSA TTA N.S, ↓ TSA	(Williams et al., 2011)

1.10.8 Using zebrafish to model inflammation

The zebrafish immune system is highly conserved and comprises both innate and adaptive immune systems. The adaptive system, as mentioned, develops later, but does still possess antigen-presenting cells, T and B cells (Neely et al., 2002). The innate system consists of neutrophils, macrophages and eosinophils, with eosinophils appearing at 5 dpf (Lieschke et al., 2001).

Neutrophils are the most abundant circulating leukocyte and the first inflammatory cell to respond to injury (Lieschke and Trede, 2009). They travel to sites of damaged tissue via chemotaxis then degranulate to release enzymes such as myeloperoxidase (MPO) and also produce reactive oxygen species (ROS). Neutrophils are also capable of limited phagocytosis of debris or pathogens and their removal by either apoptosis or retrograde chemotaxis contributes to inflammation resolution (Mathias et al., 2009, Renshaw et al., 2006). Lieschke et al. (2001) identified the neutrophil specific gene myeloperoxidase (*mpo also* referred to as *mpx*) coding for the granulocytic protein myeloperoxidase (Lieschke et al., 2001). Expression of this gene is first detected at 18 hpf in the posterior intermediate cell mass (ICM), these *mpo* positive cells then migrate to the anterior yolk sac by 20 hpf, and reach the circulation by approximately 24 hpf (Lieschke et al., 2001, Bennett et al., 2001).

Tail fin injury by transection or needle injury has become established as a model for tissue injury sufficient to induce an inflammatory response (Lieschke et al., 2001, Renshaw et al., 2006, Mathias et al., 2006). Renshaw et al. (2006) generated the MPO:GFP transgenic with expression of the GFP reporter under the control of the *mpo* promoter, enabling live tracking of neutrophils *in vivo* (Renshaw et al., 2006). Mathias et al. (2006) also generated a zMPO:GFP transgenic and utilised this line to investigate neutrophil response to needle induced ventral tail fin injury and resolution of inflammation. It was noted that neutrophils underwent bidirectional chemotaxis from the vasculature both towards the site of injury and resolved inflammation upon retrograde migration returning to the vasculature (Mathias et

al., 2006). Both of these injury methods induced a peak in neutrophil numbers at the site of injury at 6 hours post injury (hpi) and resolution by 24 hpi.

The primary function of the macrophage is to phagocytose debris, dead cells and infective pathogens. Macrophages are slower to respond to and migrate towards sites of tissue damage than neutrophils. They remain at sites of injury longer than neutrophils, resolving inflammation and enabling tissue regeneration (Ellett et al., 2011, Li et al., 2012b). Macrophages originate from dorsally derived blood progenitors in the rostral blood island (RBI) and first appear in the yolk sac at approximately 24 hpf before migrating to the circulation (Herbomel et al., 1999, Warga et al., 2009). There are two key markers used to identify macrophages; colony stimulating factor 1 receptor (*CSFR1*) expressed on macrophages and xanthophores (skin pigmentation cells) and *mpeg1* (macrophage expressed gene 1) expressed specifically on macrophages (Gray et al., 2011, Ellett et al., 2011). Macrophages can be visualised in a *CSFR1*:Gal4;UAS:mCherry-nt (*fms:nfsB.mCherry*) transgenic line where the *CSFR1* promoter (*fms*) is used to drive Gal4 expression which in turn activates the UAS promoter to drive expression of a mCherry-nitroreductase fusion protein, thus labelling macrophages with mCherry (Gray et al., 2011). This was crossed to the *mpo*:GFP transgenic to produce a double transgenic (*fmsgal4;*UNM*;mpo*GFP) enabling tracking of both macrophages and neutrophils (Gray et al., 2011). This transgenic was utilised in the tail transection model of inflammation to assess migration of both neutrophils and macrophages to the site of inflammation. Macrophage numbers at the site of tail transection continue to increase until 48 hours post injury (Gray et al., 2011).

1.10.9 Using zebrafish to model the response to infection

Zebrafish are a useful model for studying the response to pathogenic infection. Due to the later development of the adaptive immune system, these studies have primarily investigated the response of the innate immune system. Zebrafish have been infected with various pathogens to investigate the host response including *Escherichia coli, Streptococcus* and *Burkholderia cenopacia* (Neely et al., 2002, Vergunst et al., 2010). A systemic or localised infection can be specified by

intravascular injection or intramuscular injection (Benard et al., 2012). Inoculation with fluorescently labelled bacteria, such as Ds-Red expressing *Salmonella typhimurium* or GFP expressing *Staphylococcus aureus,* enabled tracking of infective pathogens and monitoring phagocytosis by macrophages (van der Sar et al., 2003, Prajsnar et al., 2008, Colucci-Guyon et al., 2011). Van de Sar et al. (2003) utilised DsRed-expressing *Salmonella typhimurium* to enable visualisation of pathogen phagocytosis by macrophages (van der Sar et al., 2003). Although most bacteria were lysed, some were able to further divide, eventually killing the macrophage (van der Sar et al., 2003). Vergunst et al. (2010) utilised both DsRed and GFP expressing *Burkholderia cenopacia (Bcc)* to visualise the interaction of this pathogen with both neutrophils and macrophages. This showed that *Bcc* was able to survive phagocytosis by macrophages and replicate to create an intramacrophage niche, enabling further dissemination of infection (Vergunst et al., 2010). Prajsnar et al. (2008) inoculated embryos with GFP expressing *S. aureus*, which was taken up into both neutrophils and macrophages in control fish but remained free in circulation in fish with depleted myeloid cells (Prajsnar et al., 2008). This highlights the importance of myeloid cells in internalizing pathogens and maintaining the immune response.

Zebrafish response to bacterial derived proteins has been studied utilising chemoattractants such as; *E. coli, Pseudomonas aeruginosa* and *Salmonella enterica* derived lipopolysaccharide (LPS) and N-formyl-methionyl-leucyl-phenylalanine (fMLP) (Medearis et al., 1968, Marasco et al., 1984, Novoa et al., 2009, Taylor, 2010, Elks et al., 2011). Novoa et al. (2009) bathed 2 dpf embryos in both *E. coli* and *P. aeruginosa* derived LPS in order to assess tolerance to LPS after previous exposures. Varying concentrations of LPS were utilised ranging from 5 to 150 μg/ml for *E. coli* derived and 5 to 100 μg/ml of *P. aeruginosa* derived LPS and it was found that previous exposure to LPS increased tolerance upon a second exposure (Novoa et al., 2009). Taylor (2010) assessed neutrophil migration to sites of tail fin injury in 4 to 6 dpf embryos after bathing them in *E. coli* derived LPS at a concentration of 1 to 10 μg/ml. It was found that LPS exposure increased neutrophil numbers at the site of tail fin injury (Taylor, 2010). Elks et al. (2011) exposed 2-3 dpf embryos to 100 nM

fMLP after tail fin transection, finding that the neutrophil chemoattractant fMLP, increased speed of neutrophil migration and reduced meandering of movement towards injury (Elks et al., 2011, Marasco et al., 1984).

The zebrafish immune response to viral infections has been modelled via intravascular introduction of infectious haematopoietic necrosis virus (IHNV) (Ludwig et al., 2011). This was shown to disrupt vessel integrity of the endothelium, particularly in veins (Ludwig et al., 2011).

Fungal infection has been modelled in the zebrafish by infection with *Candida albicans* via injection into the hindbrain or yolk of 30 hpf embryos, whereupon the yeast form changes to the hyphal form within 34 hours post infection (hpi) (Chao et al., 2010). Brothers et al (2011) found that *C. albicans,* which was injected into the hindbrain, replicated and disseminated throughout the embryo, overwhelming half of the population of injected fish within 48 hpi (Brothers et al., 2011). This developing infection was visualised via the use of GFP or yCherry expressing *C. albicans* (Brothers et al., 2011).

These studies demonstrate the advantages of the zebrafish for modelling infection, particularly when coupled with the use of transgenic lines. Tracking and assessing pathogen and leukocyte behaviour and interactions are not currently possible in other animal *in vivo* models, for example the mouse, rat or rabbit, which have previously been utilised in the investigation of $P2Y_{12}$. Therefore the establishment of the zebrafish for modelling the response to infection offers an opportunity to investigate the role of $P2Y_{12}$ in these processes.

1.11 Platelet MicroRNAs

MicroRNAs (miRNAs or miRs) are short non coding RNAs, approximately 21-25 nucleotides long, which post-transcriptionally regulate gene function. MicroRNAs bind to the 3'UTR (untranslated) region of mRNA and repress translation via binding at low complementarity, or target mRNA for degradation via binding with high complementarity, therefore subsequently silencing gene expression (Bartel, 2004). Platelets contain a large number of miRNAs involved in many different processes including platelet activation, granule exocytosis, angiogenesis and platelet

aggregation (Nagalla et al., 2011, Urbich et al., 2008). A cluster of miRNAs highly expressed in platelets have been identified via microarray screening to be implicated in MI; miR-21, miR-24, miR-126, miR-223 and miR-197 (Zampetaki et al., 2012).

MiR-24 regulates apoptosis and angiogenesis and is expressed in endothelial cells and cardiomyocytes (Fiedler et al., 2011, Qian et al., 2011). MiR-24 has differential regulative effects depending on the cellular expression. Endothelial expression of miR-24 is increased in hypoxic conditions, such as after MI. Overexpression of miR-24 induces apoptosis in endothelial cells whereas antagonism reduces apoptosis (Fiedler et al., 2011). MiR-24 has been previously investigated in zebrafish: Fiedler et al. (2011) injected zebrafish embryos with miR-24 precursors to overexpress miR-24, which induced abnormal vascular development and blood accumulation. Knockdown of the miR-24 targets PAK4 and GATA2, a method to mimic miR-24 overexpression, resulted in a similar phenotype (Fiedler et al., 2011). In cardiomyocytes, miR-24 regulates the pro-apoptotic protein Bim and expression decreases in ischaemic conditions such as the border zone of the left ventricle after MI, thus exacerbating apoptosis (Qian et al., 2011).

MiR-223 is a myeloid specific miRNA which regulates myeloid differentiation and may regulate maturation (Johnnidis et al., 2008, Fazi et al., 2005). In the Bruneck study, miR-223 was inversely associated with risk of MI (Zampetaki et al., 2012). There is a miRNA-223 binding site in the 3' UTR of the *P2RY12* mRNA, indicating miR-223 may regulate P2y12 protein expression (Landry et al., 2009). Recent work by Leierseder et. al (2013) in the miR-223 null mouse showed that there is no significant effect on platelet activation, aggregation and bleeding time although there was a modest reduction in platelet production (Leierseder et al., 2013). However using miRNA prediction databases there is currently no prediction of a miR-223 binding site in mouse *P2Y12*, www.mirBase.org, therefore these results are consistent with a lack of miR-223 regulation of *P2Y12* in the mouse. There is no literature regarding miR-233 regulation of *p2y12* in the zebrafish, with prediction software also not currently predicting a binding site for miR-223 in *p2y12*. It is possible that *P2RY12* may be regulated by other miRNAs as four more miRNA

binding sites that are predicted in the mRNA 3' UTR; miR-21, miR-221, let-7i and let-7g (Landry et al., 2009).

MiR-126 is expressed in endothelial cells and is associated with Vascular Endothelial Growth Factor (VEGF) signalling, angiogenesis and vascular integrity (Wang et al., 2008, Fish et al., 2008). MiR-126 was positively associated with risk of MI (Zampetaki et al., 2012). Knockdown of this miRNA in the zebrafish affects vascular integrity inducing haemorrhaging and also ectopic vessel branching from inter segmental vessels (Fish et al., 2008, Nicoli et al., 2010). MiR-126 regulates *c-myb* which negatively regulates megakaryocytopoiesis, therefore promoting the thrombocyte cell fate. Previous studies showed that knockdown of miR-126 reduced numbers of thrombocytes and increased erythrocytes numbers (Grabher et al., 2011).

Platelet miRNAs miR-223 and miR-126 expression is sensitive to anti platelet therapy, with reduced expression upon treatment with prasugrel (Willeit et al., 2013). Therefore platelet miRNAs have been suggested as biomarkers for platelet activation. Further investigation is required to assess the role of platelet miRNAs in a number of different processes such as aggregation and vascular inflammation.

1.12 Aims

The role of the P2Y**12** receptor in thrombosis is well proven in various model systems. However little is currently known about the role of P2Y**12** on the innate immune response and on response to infection, although clinical data suggests that P2Y**12** antagonism may influence the risk of infection in humans. In addition, much remains to be understood about the regulation of platelet responses, particularly the role of platelet microRNAs.

The aims of my work were therefore to;

- Characterize the role of P2Y12 in thrombosis in the zebrafish
- Assess the effect of morpholino antisense mediated knockdown of platelet miRNAs on thrombus formation *in vivo* in the zebrafish
- Investigate the role of P2Y12 on leukocyte migration in the zebrafish
- Investigate the role of P2Y12 in the response to infection in the zebrafish

1.13 Hypothesis

I hypothesised that knockdown of the P2Y12 receptor in the zebrafish would reduce thrombus formation after vessel injury. I also hypothesised that knockdown of P2Y12 would impair inflammatory response to injury and resistance to infection, due to a reduced release of pro-inflammatory mediators and antimicrobial peptides from thrombocyte α granules.

Chapter 2 : Materials and methods

2.1 Materials

All plastic ware was obtained from Starlab, Milton Keynes, UK, except for 90 mm petri dishes which were obtained from Sterilin, Newport, UK. All enzymes and enzyme buffers were, unless otherwise stated, obtained from New England BioLabs, Ipswich, USA. All reagents used in the *in situ* hybridization protocol, unless otherwise stated, were obtained from Sigma-Aldrich, Gillingham, UK. Distilled, deionized and ultra filtered water (MQ H_2O) was obtained from Millipore, MA, USA. MS222 (PharmaQ, Hampshire, UK) was obtained by the aquaria staff and pH adjusted to pH 7. LPS was obtained from Alexis Biochemistry, serotype R515, pH 7. Adenosine was obtained from Sigma-Aldrich (Gillingham, UK) with a molecular weight of 267.24 g/mol. Prasugrel active metabolite (molecular weight 497.57) was obtained from SiChem, Bremen, Germany. Ticagrelor (molecular weight 522.57) was obtained from Sequoia Research Chemicals, Pangbourne, Berkshire, UK.

2.2 Zebrafish husbandry

2.2.1 Home office regulations

Zebrafish were maintained according to Home Office regulations, under the licence number 40/3434 held by Dr TJA Chico and my personal licence number 10235. Zebrafish were raised in the Centre for Developmental Biomedical Genetics (CDBG) and fed Artemia (ZMSystems, Hampshire, UK) by the aquaria staff. Zebrafish were maintained with a light: dark cycle of 14:10 hours.

2.2.2 Embryo collection

Breeding tanks were placed in adult fish tanks the night before embryos were required. Breeding tanks consisted of an opaque plastic tub with a wire mesh separator containing marbles which encourage breeding, the mesh separator allows embryos to pass into the collection tub and prevent the fish from consuming them. Embryos were collected with the use of a tea strainer the following morning and were then incubated at 28°C with 40 embryos per petri dish containing E3

media (2.8 g 5 mM NaCl,0.48g 0.33mM $CaCl_2$, 0.127g 0.17 mM KCl, 0.817g 0.33 mM $MgSO_4$ in distilled H_2O with 150 µl 0.01% Methylene Blue). Embryos which were not used for investigations were incubated for a maximum duration of 5.2 dpf at which point they were anaesthetised with MS222 (PharmaQ, Hampshire, UK) and destroyed with bleach. Pair mating of individual fish was utilised for the generation of embryos from specific fish, such as for screening of F0 mutants and crossing of founders. This consisted of an individual pair mating tank with an insert enabling embryos to pass through and a separator to keep the male and female separated. Removal of the separator enables the fish to mate and generate embryos at a required time.

2.2.3 Fin clipping

Adult fish were anaesthetised in 4.2% MS222 in system water for approximately 45 seconds, the latter 1/3rd of the tail was transected with scissors and forceps used to transfer the fin clip to an individually labelled 0.2 ml tube. Fish were then deposited into a correspondingly labelled tank and fin clip gDNA extracted with Red Extract, in order to screen for mutations.

2.2.4 Zebrafish lines used

Table 2.1 lists the various transgenic zebrafish lines used in this thesis. The CD41:GFP line was a kind gift from Dr Martin Gering, University of Nottingham, Queens Medical Centre, UK. The p2y12::P2Y12-GFP line was a kind gift from Dr Francesca Peri, EMBL Heidelberg, Germany. *Nacre* were used for assessment of thrombosis response as the lack of pigmentation facilitated imaging of the forming thrombus (Lister et al., 1999) . London wild type (LWT) were utilised for the assessment of resistance to infection. For the generation of mutant lines, ZFN and TALEN RNA was injected into the ABWT background.

Table 2.1 Summary of fluorescent transgenic lines.

A list of some frequently used transgenic lines, relevant to this thesis, including the gene and promoter driving the fluorescent reporter, alongside references.

Transgenic line	**Gene and promoter**	**Reference**
CD41:GFP	GFP driven by thrombocyte receptor GPIIb	(Lin et al., 2005)
*Fli1:*GFP	GFP driven by endothelial cell marker	(Lawson and Weinstein, 2002)
fmsgal4;UNM;mpoGFP	mCherry driven by *CSFR1* promoter for macrophages and GFP by neutrophil specific *mpo* promoter	(Gray et al., 2011)
Gata1:DsRed	DsRed driven by erythroid specific transcription factor	(Traver et al., 2003)
*mpeg1:*GFP	GFP driven by macrophage specific *mpeg1*	(Ellett et al., 2011)
MPO:GFP	GFP driven by neutrophil specific *mpo* promoter	(Renshaw et al., 2006)
zMPO:GFP	GFP driven by neutrophil specific *mpo* promoter	(Mathias et al., 2006)
p2y12::P2Y12-GFP	C- terminus *p2y12* fused to GFP	(Sieger et al., 2012)

2.3 General zebrafish methods

2.3.1 Morpholino injections

Morpholinos (MO) were custom made by GeneTools (www.gene-tools.com) and diluted to 1 mM with MQ H_2O. The optimum concentration for each morpholino was titrated in order to minimise non-specific toxicity. MOs were diluted to the final concentration in MQ H_2O and 100% Phenolred (Sigma-Aldrich, Gillingham, UK). The volume of morpholino injected was quantified by injection onto mineral oil on a graticule prior to embryo injection. The morpholino was injected into the yolk of 1-2 cell stage embryos using pulled microcapillary needles and a micromanipulator. **Table 2.2** shows the list of MOs used in this thesis. **Table 2.3** shows a list of previously published MOs relevant to this thesis.

Table 2.2 Morpholinos used in this thesis.

This table lists the morpholinos used in this thesis, including names, sequences, quantities injected and the mode of action of the morpholino. The amount of standard control morpholino was matched corresponding to the amount of active morpholino injected.

Morpholino	**Sequence 5'-3'**	**Amount injected (ng)**	**Mechanism of action**
Standard control	CCTCTTACCTCAGTTACAATTTATA	Corresponding amount to active morpholino	No biological activity
$P2Y_{12}$	AGCTGAGCTGCGTTGTTTGCTCCAT	1.2	Translation blocking
P2Y12mo2	GGACTTCATTACTTCACCCAGCAGG	0.3 nl of 0.3 mM	Translation blocking (Sieger et al., 2012)
miR-126	TGCATTATTACTCACGGTACGAGTT	4.22	Targets miR guide strand
miR-223	GGGTATTTGACAAACTGACACCCCT	3.49	Targets miR guide strand
miR-24	ACCTGTTCCTGCTGAACTGAGCCAG	4.22	Targets mature miR

Table 2.3 Previously published morpholinos relevant to the work in this thesis.

This table lists the morpholino names, sequences, quantities injected and the relevant references. Both $P2Y_{12}$ morpholinos listed are ATG blocking, and the miR-126 morpholino is a multi blocker morpholino, enabling the blocking of several different stages of miRNA maturation.

Morpholino	**Sequence 5'-3'**	**Amount injected (ng)**	**Reference**
P2Y12-mo P2Y12-mo2	AGCTGCGTTGTTTGCTCCATTGAT GGACTTCATTACTTCACCCAGCAGG	0.3mM, unlisted volume	(Sieger et al., 2012)
miR-126	TGCATTATTACTCACGGTACGAGTTTGAGTC	4-8 7-20	(Fish et al., 2008, Nicoli et al., 2010)

2.3.2 Mounting

For laser injury, 3 dpf fish were anaesthetised with 4.2% MS222 (Sigma-Aldrich, Gillingham, UK) in E3 and immobilised for imaging, mounted laterally in 1% low melting point (LMP) (VWR, Lutterworth, UK) agarose on a square coverslip (Menzel-Gläser, Braunschweig, Germany). This was inverted onto mounting slide with a rectangular aperture containing E3. For confocal imaging of inflammatory response, embryos were mounted on a circular cover slip (Menzel-Gläser, Braunschweig, Germany) with 1% LMP agarose, which was allowed to set before more agarose was added. Once the agarose had set, the coverslip was sealed with petroleum jelly to a small petri dish with a pre-lathed circular hole in the middle. The embryos were subsequently immersed in E3 in order to prevent dehydration of the agarose. For imaging of microglia, 3 dpf embryos were mounted in 1% LMP agarose with the dorsal aspect of the head closest to the coverslip. These were then inverted on to a slide with a viewing chamber and sealed with nail varnish for imaging at x40 magnification.

2.3.3 Image capture of microglia

An Olympus LV 1000 with x40 (oil immersion) magnification was utilised to image GFP fluorescence in the 3 dpf p2y12::P2Y12-GFP transgenic embryos. Prior to imaging, 24 hpf embryos had been exposed to 0.002% Phenylthiourea (PTU)(Sigma-Aldrich, Gillingham, UK) in E3 to prevent melanisation, to aid visualisation of the brain. Z slices were taken at 1.5 µm intervals ranging over approximately 40 µm and stacked in ImageJ.

2.3.4 Image capture of thrombocytes

3 dpf embryos of either CD41:GFP or p2y12::P2Y12-GFP transgenic background were mounted laterally in LMP and imaged using x10 or x20 magnification on a Perkin Elmer (Cambridge, UK) UltraVIEW Vox spinning disk microscope with Volocity software. Z slices were taken every 0.5 µm over a range of 50 µm. These slices were then stacked in Volocity.

2.3.5 Laser injury

An Olympus IX2-UCB inverted microscope with a Micropoint (Andor, Belfast, UK) N_2 pulsed laser through 440 nm coumarin dye was utilised. A mirrored slide was utilised to assess the position and size of the ablation site. 6 pulses of laser at medium power with the attenuator plate at half way, were directed to the ventral wall of the dorsal aorta at somite 17, opposite the cloaca, at a magnification of x20. The extent of vessel injury was controlled for by visually assessing the ablation of endothelium.

2.3.6 Image capture of thrombosis

I captured images with Video Savant software via the use of a Basler high speed camera. Videos were recorded for 10 minutes after laser injury, with a frame delay of 90. Thrombus area was monitored every 15 seconds for the first 2 minutes, then every minute from 2 minutes until 10 minutes post injury (see **Table 2.4**).

2.3.7 Thrombosis image analysis

Approximately 6 frames of recording for each time point were exported and saved as a sequence in TIFF format. These image sequences were then analysed using ImageJ software, in which the free draw properties of this software were used to draw around the thrombus and calculate the thrombus area in pixels. Thrombus area for each time-point was plotted on a graph in GraphPad Prism6 and the area under the curve was utilised as the final result representing total thrombus area.

Table 2.4 Selection of frames for thrombus development analysis.

Thrombus area was analysed after laser injury every 15 seconds for the first 2 minutes, then every minute until 10 minutes. Images were recorded at approximately 10 frames per second. For each time point listed below, 6 frames were exported for thrombus area analysis in ImageJ.

Time point (seconds)	Frame selection for export
0	0
15	150-156
30	300-306
45	450-456
60	601-607
75	751-756
90	901-907
105	1052-1058
120	1202-1208
180	1803-1809
240	2404-2410
300	3006-3012
360	3607-3613
420	4208-4214
480	4809-4815
540	5410-5416
600	6012-6018

2.3.8 Tail fin transection

3 dpf *fmsgal4;UNM;mpoGFP* embryos were anaesthetised with 4.2% MS222 (Sigma-Aldrich, Gillingham, UK) in E3 and placed on a strip of parcel tape on a petri dish lid. All excess media was removed and a scalpel blade (Swann-Morton) was utilised to transect the tail fin by a smooth rolling motion of of the blade, at the site of pigmentation distal to the gap in pigmentation seen at the position of the loop in circulation. This site of transection does not damage the blood vessel in the tail. The embryos were then immersed in E3 media and allowed to recover for approximately 30 minutes before being placed individually into wells in a 24 well plate containing 500 µl of E3 with the addition of 50 µl of MS222. Fluorescent macrophages and neutrophils were visualised at x20 magnification on an Olympus IX2-UCB inverted microscope. Macrophage and neutrophil numbers were counted within the region of interest at 1, 4 and 8 hours post injury. The region of interest consisted of the site of fin transection to the loop in circulation, a region of approximately 100 µm.

2.3.9 Ventral tail fin incision

3 dpf *fmsgal4;UNM;mpoGFP* embryos were anaesthetised with 4.2% MS222 (Sigma-Aldrich, Gillingham, UK) in E3, and placed on a strip of parcel tape on a petri dish lid. All excess media was removed and an incision of approximately 20 µm was made into the ventral tail fin opposite the gap in pigmentation, using a 5 mm micro scalpel. The fish were allowed to recover in E3 media before being anaesthetised and mounted in for spinning disk confocal imaging as per section **2.3.2**. Images were captured using x10 magnification on a Perkin Elmer (Cambridge, UK) UltraVIEW Vox spinning disk microscope with Volocity software. Z slices were obtained at 1, 4, 8 and 12 hours post injury. The z slices were taken approximately 2 µm slices over a range of 60 µm, these slices were combined to form a stacked image. For macrophage and neutrophil analysis, Z slices were stacked into an extended focus view and a circle with a diameter of 200 pixels centred at the site of injury. The number of macrophages and neutrophils were counted within this region of interest at each time point imaged.

2.3.10 Vessel injury for assessment of inflammation response

3 dpf *fmsgal4;UNM;mpoGFP* embryos were anaesthetised with 4.2% MS222 (Sigma-Aldrich, Gillingham, UK) in E3 and mounted laterally in 1% low melting point agarose on a slide. Several fish were mounted on one slide and 30 pulses of laser at medium power were directed to the circulatory loop in the tail. Each embryo was deposited to a single well in a 24 well plate containing 500 µl of E3 with the addition of 50 µl of MS222. Macrophages and neutrophils were visualised and numbers were counted within the region of interest at 1 hour, 4 hour and 8 hour post injury. The region of interest consisted of 200 µm; 100 µm either side of the site of injury.

2.4 Embryo exposure methods

2.4.1 Ticagrelor

Ticagrelor was diluted from a stock concentration of 2500 µM in 100% dimethyl-sulfoxide (DMSO) (Sigma-Aldrich, Gillingham, UK) to 20 µM and 25 µM in E3 (without methylene blue). 55 hpf *nacre* embryos were exposed to final concentrations of 20 µM and 25 µM ticagrelor and incubated overnight at 28°C. A control group was incubated with corresponding concentrations of DMSO in E3 without methylene blue, to control for any possible effect of DMSO. 3 dpf embryos were then laser injured and the thrombosis response quantified as in section **2.3.5**.

2.4.2 Prasugrel active metabolite (PAM)

Prasugrel active metabolite stock concentration of 10 mg/ml (20 mmol/L) in 100% DMSO was diluted to 20 µM and 50 µM. Control solutions of E3 containing corresponding concentrations of DMSO were used control for DMSO effect. 3 dpf *Nacre* embryos were exposed to either control solutions or solutions containing PAM approximately 1 hour before laser injury, as per section **2.3.5**.

2.4.3 Adenosine exposure after tail fin transection

7 mg of adenosine (Sigma-Aldrich, Gillingham, UK) was dissolved in 2 ml system water to give a stock concentration of 13 mM. This stock was then serial diluted in system water to 100 nM and 10 nM. System water alone was used as a control. 3

dpf *fmsgal4;*UNM;*mpo*GFP embryos were anaesthetised and the tail fin transected as discussed in section **2.3.8**. These embryos were then placed in individual wells of a 24 well plate and 500 µl of either control, 10 nM or 100 nM adenosine solution was added to the embryos. Leukocytes were visualised as in **2.3.8** and macrophage and neutrophil counts were assessed over a time course of 8 hours.

2.4.4 LPS exposure after tail fin transection

Tail fin transection was conducted as documented in **2.3.8**. Embryos were placed in individual wells of a 12 well plate and 500 µl of an *E. coli* derived LPS (serotype R515 Alexis Biochemistry) solution or E3 control was added to each well. LPS was diluted to a final concentration of 1 µg/ml of LPS in E3 media (without methylene blue). Macrophages and neutrophils were visualised as in **2.3.8** and numbers were monitored over 8 hours.

2.4.5 fMLP exposure after tail fin transection

Tail fin transection was conducted as documented in 2.3.8, with a sterile scalpel blade briefly immersed in f-met-leu-phe (fMLP) 20 nM. These embryos were placed in individual wells of a 12 well plate with 500 µl E3 (without methylene blue). Tail fins of the control embryos were transected with a sterile scalpel blade and were then transferred to individual wells with 500 µl E3 (without methylene blue). Macrophages and neutrophils were visualised as in 2.3.8 and numbers were monitored over 8 hours.

2.4.6 *Staphylococcus aureus* preparation and injection

The *S. aureus* for injection was prepared from a stock of SH1000 strain which was stored at -80°C contained on small beads. One bead was removed and spread on a brain heart infusion (BHI) LB plate overnight at 37°C. One colony from this plate was used to inoculate 10 ml BHI LB broth which was then incubated overnight at 37°C 250 rpm. 500 µl of culture was added to 50 ml BHI LB broth, shaken at 250 rpm and incubated at 37°C for 2 hours. The optical density of the bacterial culture was determined via spectrophotometry (Beckman Coulter, High Wycombe, UK), using a blank with 1 ml LB media and another cuvette with 900 µl media plus 100 µl bacterial solution. Wavelength was set to 600 nm and calibrated to the blank media

sample. The OD value of the bacterial sample was then analysed. 40 ml of the bacterial solution was centrifuged at 4,500 g for 10 minutes at 4°C. The OD value was used to calculate the volume of sterile PBS to resuspend the pellet in, such that the OD_{600} was equivalent to 1. The bacterial concentration was assessed by serial dilutions plated on BHI LB agar plates. SH1000 samples were stored at -80°C, for a maximum of 2 months, and were defrosted and vortexed before use.

10 µl of bacterial suspension was loaded into a microinjection needle. For injection, embryos were anaesthetised in 0.02% MS222 and immobilised in 3% methylcellulose on a slide. Bacterial suspension was microinjected onto a graticule and adjusted to a volume of 1 nl. 1 nl was injected directly into the circulation of 30 hpf embryos at the point of the yolk sac circulation valley (duct of Cuvier). A PBS control was taken after the completion of injection of each slide, with 4nl injected into 1 ml of sterile PBS. Any embryos which were damaged or bleeding were removed and the remaining embryos immersed in E3 media. These embryos were then transferred to individual wells of a 96 well plate. For the PBS control experiment, 10 µl of sterile PBS was loaded into a microinjection needle and 1 nl injected directly into 30 hpf embryos as above. Following injection 4 nl of PBS solution was injected into 1 ml of sterile PBS. 3 x 10 µl of each slide PBS control was plated onto BHI LB agar plates and incubated overnight at 37°C. Mean CFU counts were determined the following morning for each slide and were recorded. Each *S. aureus* injection needle was used for a maximum of 1 hour, after which point bacterial aggregates were prone to block the needle and increase the CFU count per 1 nl injection. Embryo survival was monitored over the time course of approximately 90 hours post infection (hpi), and mortality was recorded at each time point. These results were then plotted on a Kaplan-Meier plot. Care was taken to quantify the CFU of each injection in order to establish a matched CFU count between control and *p2y12* morphants to enable a suitable range of bacterial load between experiments for comparison. This range in CFU counts incorporates a certain amount of variation between experiments due to technical challenges of precise injection directly into the circulation and blockage of the microinjector needle by bacterial aggregates at the needle tip.

After injection of *p2y12*^{sh340} mutants, gDNA of embryos was extracted using Red Extract protocol within 12 hours after death. Following completion of this experiment, a PCR and test digest was used to genotype the embryos and correlate this genotype to survival.

2.5 Molecular methods

2.5.1 Primer design

All primers were designed in Primer3 software (http://frodo.wi.mit.edu/primer3/) using the Ensembl cDNA sequence for *p2y12*. The online genomic database (www.ensembl.org) was searched and the following gene sequence (ENSDARG00000069945) which had previously been annotated as the $P2Y_{12}$ receptor-like (Zv9), was utilised. A list of all primers used in this thesis is shown in **Table 2.6.**

2.5.2 RNA extraction

Approximately 20 embryos at the desired time point were collected into a 1.5 ml tube and all excess E3 media removed. 100 µl DEPC-treated H_2O was added to wash the embryos. This H_2O was then removed and 250 µl TRIzol (Life Technologies, Paisley, UK) reagent was added and the embryos homogenized with a 23 gauge needle. This solution was incubated at room temperature for 5 minutes then 50 µl of chloroform was added and mixed by inversion. This was then incubated at RT for 3 minutes then centrifuged for 15 minutes at 4°C and 16.3 g. The top layer of supernatant was removed (~ 100 µl) and transferred to a new tube. 85 µl of isopropanol was added and inverted to mix. This was incubated at RT for 10 minutes then centrifuged at 16.3 g for 15 minutes at 4°C. The supernatant was poured off to leave a pellet, to which 250 µl 75% ethanol was added, this was briefly vortexed then centrifuged at 16.3 g for 10 minutes at 4°C. The supernatant was then removed from the pellet and the pellet was allowed to air dry for 2-3 minutes at RT. This RNA pellet was then resuspended in 15 µl DEPC-H_2O and stored at -80°C. RNA was used to produce cDNA via a reverse transcriptase (RT) reaction using the Verso (Thermo Scientific, UK) kit.

2.5.3 PCR protocols

Several different polymerase chain reaction (PCR) protocols were used, as documented in **Table 2.5**. For each 10 µl PCR reaction I added approximately 600 ng of cDNA per reaction tube, diluted to 1 µl with MQ H_2O, 5 µl Biomix (Bioline, London, UK), 1 µl forward primer, 1 µl reverse primer and 2 µl MQ H_2O. The annealing temperature was optimised for each primer set using a gradient PCR reaction.

Table 2.5 PCR parameters used in this thesis.

Below are the PCR parameters used within this thesis, including general PCR conditions which were utilised for the majority of PCR reactions, also included are specific conditions utilised in the process of Zinc Finger Nuclease (ZFN) generation of mutants.

	Segment	Number of cycles	Temperature	Duration
General PCR conditions	1	1	95°C	3 minutes
	2	31	95°C	30 seconds
	3		50-65°C	30 seconds
	4		72°C	1 minute
	5	1	72°C	5 minutes
	6	1	10°C	hold
ZFN cycle conditions	1		95°C	2 minutes
	2	19	95°C	20 seconds
	3		50°C	20 seconds
	4		72°C	5 minutes
	5		72°C	3 minutes
	6		10°C	hold
ZFN colony PCR conditions	1	1	94°C	2 minutes
	2	29	94°C	20 seconds
	3		60°C (reducing 0.2°C each cycle)	20 seconds
	4		72°C	45 seconds
	5	1	72°C	3 minutes
	6	1	10°C	hold
ZFN titanium PCR conditions	1	1	98°C	30 seconds
	2	14 or 34	98°C	10 seconds
	3		55°C	15 seconds
	4		72°C	5 seconds
	5	1	72°C	5 minutes
	6	1	10°C	hold
Phusion High Fidelity conditions	1	1	98°C	30 seconds
	2	35	98°C	10 seconds
	3		66°C	30 seconds
	4		72°C	20 seconds
	5	1	72°C	10 minutes

Table 2.6 Primers used in this thesis.

A list of all primers used in this thesis, including names, sequence and the purpose for the primers.

Primer	Sequence 5'-3'	Purpose
P2Y12 1st half left	CTTCACCCAGCAGGACTCAT	Sequencing *p2y12*
P2Y12 1st half right	CTCTACAAGTCGTACGCCCG	
P2Y12 2nd half left	ACCCCAAACGTCTACTGCAC	
P2Y12 2nd half right	AAACACTGGGGCTTGTTCTG	
P2Y12 F4	AGCTCAGCTTCTCCAACAGC	P2Y12 probe generation
P2Y12 R3	GCACAGAATTGAGGGAGGAC	
LCS2	GAAAAGTTCCGCATGCAAAT	CoDA ZFN mutagenesis
goodRCS2	CACCTAAAAACCCACCTGAG	
LseqCS2	TGCAGGATCTGCCACCAT	
RseqCS2	TCCTTGATCCACCCAAATGT	
LseqFok	GCCAGAAATTCCACTCAGGA	
RseqFok	CCCCCTGAACCTGAAACATA	
SP7 left 1	CAGCAAATCCCACTTCATCA	
SP7 right 1	GTAGACGTTTGGGGTTGGTG	
SP5 left 1	GTTGGCCGTGTTTTTCATTT	
SP5 right 1	AGCACAGAATTGAGGGAGGA	
A titanium	CGTATCGCCTCCCTCGCGCCATCAG	
B titanium	CTATGCGCCTTGCCAGCCCGCTCAG	
TAL_R2	GGCGACGAGGTGGTCGTTGG	TALEN mutagenesis
SeqTALEN_5-1	CATCGCGCAATGCACTGAC	
Bam Left 3	GCGTCTCCAACAGTTCATCC	
Bam Right 2	AAGGGGAATGTGAGGGTCAT	
Forward P2Y12 ultramer with EcoRI	ATAACGGTGGAGGAATTCATGGAACAGACC ACACAACTCAGCTTCTCCAACAGCAGC	*p2y12* mRNA synthesis
Reverse P2Y12 Primer with XbaI	GGAGTCAGTGTCTAGAGTCATGTCAGTGCG TTTCCCTGT	

2.5.4 RNA injection

RNA was stored at -80°C and defrosted on ice before injection. Needles were prepared in sterile conditions and 2 µl of RNA loaded into the needle. RNA volume was calibrated using a graticule and was then injected into 1 cell stage wildtype embryos, either into the yolk or directly into the cell.

2.5.5 DNA sequencing

DNA sequencing was conducted at the Core Genomic Facility at the University of Sheffield, UK. DNA samples were submitted at approximate concentrations of 50 ng/µl and primers were submitted at approximate concentrations of 1 pmol/µl. DNA sequencing chromatograms were analysed using FinchTV software.

2.5.6 *p2y12* mRNA synthesis

mRNA was synthesised using alternate codons to those targeted by the *p2y12* morpholino, but which coded for the same amino acids. The changing of codons at the morpholino target ensured that the synthesised mRNA would be less likely to bind the morpholino directly, therefore would not interfere with the interaction of the morpholino with the native *p2y12.* Specific primers were designed for this process; an ultramer forward primer with the altered codons and EcoRI restriction site, and a reverse primer matching the C terminus sequence, with an XbaI site included (shown in **Table 2.6**). A Phusion (New England BioLabs, Ipswich, USA) reaction was used with 234 ng DNA template (3.5 µl), 29.5 µl MQ H_2O, 10 µl 5x Phusion HF buffer, 2 µl 5mM dNTPs, 2.5 µl Forward $P2Y_{12}$ primer with EcoRI site, 2.5 µl Reverse primer with XbaI site, 0.5 µl Phusion DNA polymerase, under the conditions shown in **Table 2.5**. This reaction was run in duplicate and combined to form 100 µl, the PCR product was assessed on a 2% gel, and purified in a QIAquick PCR purification column, as per manual instructions (Qiagen, Manchester, UK), and eluted into a volume of 50 µl.

The vector pCS2 was utilised, 5µg was digested at 37 °C for 2 hours, in the following reaction; 28.6 µl pCS2 vector, 2 µl EcoRI-HF, 2 µl XbaI, 5 µl 10x Cut smart buffer (New England Biolabs, Ipswich, USA), 13 µl MQ H_2O. This reaction was then treated with 2.5 µl shrimp alkaline phosphatase (SAP, New England Biolabs, Ipswich, USA)

and incubated for a further 30 minutes, then inactivated at 65°C for 5 minutes. 1.98 µg of $P2Y_{12}$ template for insert was digested at 37 °C for 2 hours in the following reaction; 33 µl template, 2 µl EcoRI-HF, 2 µl XbaI, 5 µl 10x Cut smart buffer, then purified using a QIAquick PCR purification column (Qiagen, Manchester, UK), and eluted with MQ H_2O into a volume of 30 µl. The vector and insert were ligated together at a 3:1 molar ratio at room temperature for 5 minutes in the following reaction; 97 ng/µl vector, 42 ng/µl insert, 8.4 µl MQ H_2O, 10 µl 2x ligation buffer, 1 µl Quick T4 DNA ligase (New England Biolabs, Ipswich, USA). A ligation control containing vector without insert, controlled for self -ligation of the vector. 2 µl of each reaction was transformed into 25 µl NEB 10 beta competent cells and transformed as per manual instructions. 70 µl transformed cells were streaked on carbenicillin LB agar (50 µg/ml in 35% LB agar) plates and incubated at 37°C overnight. 1 colony was picked and grown overnight in 100 ml LB broth containing ampicillin, for Nucleobond midi prep (Macherey-Nagel, Germany), as per manual instructions. The correct insertion of template was assessed by digestion of the midi-prep for 1 hour at 37 °C in the following reaction; 0.5 µl midi-prep, 1 µl EcoRI-HF, 1 µl XbaI, 2 µl 10x Cut smart buffer and 15.5 µl MQ H_2O, and gel electrophoresis to confirm the correct band size of insert. To further confirm the correct insert, the 0.5 µl midi-prep was incubated at 37 °C for an hour, with 1 µl NotI, 1 µl XhoI and 7.5 µl buffer 3.1. 5 µg of midi-prep was linearised in a digest with 3 µl NotI, 5 µl 10x Cut smart buffer and 39.4 µl MQ H_2O, and incubated for 2 hours at 37 °C. Complete linearisation was assessed by gel electrophoresis, then the reaction was purified using the QIAquick PCR purification column, as per manual instructions. 3 reactions of SP6mMessage mMachine kit were run in triplicate, with 600 ng of purified linearised plasmid added to each reaction; 6 µl plasmid, 10 µl 2x NTP/CAP, 2 µl 10x reaction buffer and 2 µl enzyme mix, incubated for 2 hours at 37 °C. 1 µl TURBO DNase was added, and incubated for a further 15 minutes, then all 3 reactions combined and purified and by phenol:chloroform extraction as per manual instructions, and eluted into 20 µl MQ H_2O, ready for injection.

2.5.7 Whole mount *in situ* hybridization *p2y12* probe manufacture

Primers were designed towards *p2y12* to produce a PCR product of 800-1200 base pairs these were P2Y12 F4 and P2Y12 R3, with PCR conditions as per **Table 2.5**, with an annealing temperature of 60°C. This PCR product was purified using Mini Elute PCR purification kit (Qiagen, Manchester, UK), and quantified using a nanodrop spectrophotometer (Beckman Coulter, High Wycombe, UK) then stored at -20 °C. 4µl of the purified PCR product was incubated for 30 minutes at room temperature with 1 µl of TOPO vector (Invitrogen, Paisley, UK) and 1 µl of salt solution (4:1 ratio with MQ H_2O). 100 µl of competent cells (Invitrogen, Paisley, UK) were defrosted on ice and 5 µl of transformed TOPO vector was added and incubated on ice for 30 minutes. These cells were transformed using heat shock by incubation for 2 minutes at 42 °C in a water bath then 2 minutes on ice. 900 µl of SOC was added to the transformed cells and incubated for 1 hour at 37°C, shaken at 225 rpm. 30 µl of 0.1M IPTG and 30 µl XGAL (20 µg/µl) was added to LB agar plates, then 100 µl of the transformed cells were plated and incubated at 37°C overnight.

These plates were incubated at 4°C for 1 hour for a blue reaction to develop in colonies without the correct insertion and leaving the colonies with the correct insertion white. A colony PCR was run on several of the white colonies, by dabbing a pipette tip onto the colony, and inoculating the PCR master-mix, then finally into a Falcon containing 3ml of LB culture, including a blank as a control. This LB culture was incubated overnight at 37°C. The PCR master-mix contained forward and reverse primers for M13 as per the TOPO kit (Invitrogen). This PCR product was run on a 1% agarose gel to check if the sequence has been inserted. 500 µl of this culture was aliquotted into a 1 ml 100% glycerol and stored at -80°C. For linerisation of the probe the remainder of the culture was purified via a MiniPrep kit (Qiagen, Manchester, UK), and quantified by nanodrop spectrophotometry. Some of the purified culture was sequenced and then checked against the genetic sequence of interest via BLAST. Specific cleavage enzymes were selected according to their restriction sites in order to ensure they would not cut the PCR product sequence.

For the antisense probe, 5 µg of the purified plasmid was used- 15 µl was digested with 2.5 µl of HIND3 enzyme, 5 µl of NEB2 buffer and 27.5 µl of MQ H_2O, by incubation at 37°C for 2 hours. An undigested control was run alongside, omitting the plasmid. 4 µl of these products were run on a 1% agarose gel with 1 µl loading buffer (Bioline), to check the plasmid had been linearised. 0.5 µl of 25mg/ml Proteinase K and 2.5 µl SDS 10% was added to the linearised plasmid and incubated at 37°C for 30 minutes. This plasmid was purified using the MinElute kit (Qiagen, Manchester, UK), and quantified by nanodrop spectrophotometry.

In order to transcribe the antisense probe, 1050 ng of cut plasmid was incubated for 2 hours at 37°C with 2 µl of buffer, 1 µl RNAase inhibitor, T7 Polymerase, 6 µl MQ H_2O and 2 µl DIG RNA labelling kit. After 2 hours, 2 µl of DNAase I (BioLabs) was added to destroy the plasmid this was incubated for a further 30 minutes at 37°C, then run on a 1% agarose gel, to check for a smeared band. 10 µl of ammonium acetate 7.5 M and 60 µl 100% ethanol both of which ice cold, were added and inverted to purify the probe. The probe was centrifuged at 16.3 g for 15 minutes at 4°C. The supernatant was poured off and the pellet washed with 100 µl of 70% ethanol and re-spun at 16.3 g for 5 minutes. Supernatant was poured off and the remaining pellet was air dried for 3 minutes before being resuspended in 30 µl MQH_2O and 70 µl formamide. This probe was then stored at -80°C.

2.6 Histochemical methods

2.6.1 Whole mount *in situ* hybridization

Whole mount *in situ* was performed as per Thisse et al. (1993) protocol (Thisse et al., 1993). 24 hpf embryos were exposed to PTU and then fixed at desired time points 24-72 hpf, in 4% paraformaldehyde made in 1x PBS (1 PBS tablet (Sigma-Aldrich, Gillingham, UK) in 200 ml MQ H_2O). The fixed fish were stored in 100% methanol, at -20°C with approximately 20 embryos per 1.5 ml eppendorf. These embryos were re-hydrated by successive 5 minute incubations with 500 µl methanol and PBT (0.1% TWEEN-20 in 1x PBS) per eppendorf; 75% methanol and 25% 1x PBT, then 50% methanol and 50% 1x PBT, followed by 25% methanol and 75% 1xPBT and finally washed 4 times with 100% 1x PBT. The fixed embryos were

then permeabilized by incubation at RT with 10µg/ml of proteinase K ((Roche)in PBT) for varying times according to level of development; 1 dpf embryos for 8 minutes, 2 dpf for 20 minutes and 3 dpf for 60 minutes. Embryos were then re-fixed with 4% PFA (in PBS) for 20 minutes at RT followed by 4 washes in PBT for 5 minutes each. Embryos were then pre-hybrized in 250 µl of pre-heated hybridization mix A (50% formamide, 5x SSC, Heparin (50 ml of 50mg/ml), TWEEN-20 0.1%, tRNA (500 µg/ml), citric acid in MQ H_2O 50ml pH 6) for 3 hours at 68°C. This hybridization mix was replaced with 100 µl of 98 µl hybridization mix A and 2 µl of RNA probe and incubated at 68°C overnight.

The hybridization mix containing the probe was removed and stored at -20°C for further *in situs*. The embryos were washed with successive 15 minute incubations with hybridization mix B (50% formamide, 5x SSC, TWEEN-20 0.1%, citric acid in MQ H_2O 50ml pH 6) with 2x SCC (NaCl 17.53g, citric acid trisodium salt 8.82g in 1 L MQ H_2O at pH 7) at 68°C. First; 75% Hybridization mix B and 25% 2x SSC, then 50% Hyb B and 50% 2xSSC, followed by 25% Hyb B and 75% 2x SSC. The embryos were then washed with pre-warmed 2xSSC for 15 minutes at 68°C, then 2 washes of pre-warmed 0.2x SSC at 68°C for 30 minutes each. The fixed embryos were then washed in successive 10 minute incubations at RT of 0.2x SSC and 1xPBT. The first wash with 75% 0.2x SSC and 25% 1xPBT, then 50% 0.2x SSC and 50% 1x PBT, followed by 25% 0.2x SSC and 75% 1x PBT. Finally the embryos were incubated for 10 minutes with 100% 1xPBT at RT. The embryos were then incubated with 500 µl of blocking buffer (2mg/ml bovine serum alubumin (BSA) (Sigma-Aldrich, Gillingham, UK), 2% sheep serum in 1x PBT) at RT for 3 hours. This was replaced with blocking buffer containing 1:5000 dilution of Anti-DIG antibody, and incubated at 4°C overnight.

This blocking buffer and antibody was removed and the embryos were washed 6 times with 1x PBT in 15 minute incubations, whilst protected from light. Embryos were equilibrated with 3x 5 minute washes with NTMT buffer (0.1M Tris HCL pH 9.5, 50 mM $MgCl_2$, 0.1M NaCl, 0.1% TWEEN-20 in MQ H_2O). 1 ml staining solution (0.35% 5-Brono-4-chloro-3-indolyl-phosphate (BCIP), 0.45% NBT (Sigma-Aldrich, Gillingham, UK) in blocking buffer) was added per well and protected from light.

Embryos were monitored every 15 minutes to check for staining. Once staining had occurred it was stopped by removing the staining solution and washing 3 times in 1xPBT for 5 minutes each wash. Background staining was removed by methanol clearing; 5 minutes with 50% 1xPBT/50% Methanol, 30 minutes in 100% methanol, followed by 5 minutes in 50% 1xPBT/50% methanol. Embryos were then washed 3 times in 1xPBT for 5 minutes each wash and fixed in 500 µl 4% PFA in PBS for 20 minutes at RT. The PFA was washed off in 3 successive washes of 1xPBT of 5 minutes each step. The embryos were then added to glycerol for storage purposes, first 25% glycerol for 10 minutes, then 50% glycerol for 10 minutes followed by 75% and stored at 4°C.

2.7 Zebrafish mutagenesis methods

2.7.1 ZFN mutagenesis protocol

Target regions for ZFN mutagenesis were chosen using the Ensembl cDNA sequence for *p2y12* and the software on http://zifit.partners.org/ZiFiT/ChoiceMenu.aspx. IDT ultramers at a concentration of 4 nmole were ordered corresponding to F1 and F2F3 for both left and right subunits for each ZFN. This ultramer is specific to the *p2y12* sequence and have the zinc finger sequences as 5' extensions which are added to the generic backbone. The following generic plasmid backbones were used; LtalpidCS2 and RtalpidCS2 suitable for ZFN with 5-6bp spacers and CS2 7aL and CS2 7aR for the 7bp spacer ZFN. Each plasmid was linearised individually with Age1 enzyme, in the following reaction; 1 µl 259 ng/µl plasmid, 34 µl water, 5 µl 10x NEB buffer 1 and 1 µl Age1. This reaction was mixed and incubated at 37°C for 1 hour, then cleaned using Qiaquick PCR kit and eluted into 50 µl. The linearised plasmid was amplified with the following primers; LCS2 and goodRCS2 (see **Table 2.6**). 1 µl linearized plasmid, 14 µl water, 4 µl 5x Herculase buffer, 0.5 µl 10mM dNTPs, 0.5 µl LCS2 primer, 0.5 µl goodRCS2 primers, 0.4 µl Herculase II. This was added to a thermocycler under the conditions shown in section ZFN cycle conditions in **Table 2.5**. 1 µl Dpn1 was then added and incubated at 37°C for 1 hour. This amplicon was purified from a 0.8 % seakem agarose gel with a Qiaquick gel extraction kit, and eluted into 200 µl. This forms the generic backbone to which specific zinc fingers can be added. Ultramer primers were designed specifically for

the *p2y12* sequence with 5' extensions of the zinc finger motifs, enabling the addition of these motifs to the amplicon backbone. These ultramers were termed F1 for the first ZF motif and the second and third motifs were both added to the F2F3 ultramer.

2.7.2 Addition of zinc fingers to the generic backbones

The left and right monomers for each ZFN were assembled individually using the different generic backbone amplicons produced from the above reactions. These reactions were assembled on ice; 1 µl generic backbone amplicon (e.g left or right), 14 µl water, 4 µl 5x Herculase II buffer, 0.5 µl 10 mM dNTPs, 0.5 µl µM F1 primer, 0.5 µl µM F2F3 primers and 0.4 µl Herculase II. This was cycled on the above ZFN cycle program. 2 µl of PCR product was run on a 0.8% seakem agarose gel electrophoresis and check for a 5069bp band. A Qiaquick PCR clean up kit (including the HCl step) was used to purify the product and it was eluted into 44 µl.

This product was then digested with Age1 enzyme, by assembling 44 µl PCR product, 34 µl water, 5 µl 10X NEB buffer1 and 1 µl Age1 and incubating it at 37°C for 1 hour. The product was purified with a Qiaquick PCR clean up kit (including the HCl step) and eluted into 50 µl. 10 µl of this product was run on a 0.8% gel electrophoresis to check for a 5059bp band. This PCR product DNA fragment was ligated to create a circular plasmid with the following reaction; 2 µl of the Age1 cut eluted product, 2.5 µl 2xNEB quick ligase buffer and 0.5 µl NEB quick ligase incubated at room temperature for 5 minutes. This reaction was transformed into NEB 10 beta competent cells, the 50 µl aliquot of cells were divided into 12.5 µl each tube, 1 µl of reaction was added to the cells and incubated on ice for 30 minutes. These cells were heat shocked at exactly 42°C for 30 seconds, then placed immediately on ice for 5 minutes. 250 µl of room temperature SOC was added to each tube and incubated at 250 rpm at 37°C for 1 hour. 50 µl of each reaction was streaked on carbenicillin LB agar (50 µg/ml in 35% LB agar) plates and incubated at 37°C overnight.

8 colonies were selected for each plate and a colony PCR using the following primers was performed; LseqCS2 and RseqCS2 (see **Table 2.6**). The RT-reaction was

as follows; 9 µl water, 10 µl reddymix, 1 µl 10 µM LseqCS2 and 1 µl 10 µM RseqCS2, with PCR conditions as shown in the ZFN colony PCR section of **Table 2.5.** Each PCR tube was inoculated with a different colony. 5 µl of the PCR products were run on a 1.5% agarose gel and a product of 602bp was assessed. 6 colonies were sequenced using the LseqCS2 and RseqCS2 primers, to check for correct insertion of ZF motifs. The FokI nuclease domain of one of these clones with the correct sequence was further checked by PCR (705bp product) and sequencing with FokI primers; LseqFok and RseqFok (see **Table 2.6**). Upon confirmation of the correct FokI nuclease domain, a midi prep (Qiagen, Manchester, UK high speed midi kit) was prepared from this colony by inoculating 50 ml LB broth (20% LB agar broth) containing carbenicillin.

2.7.3 Preparation of ZFN mRNA for injection

Both the left and right ZFN plasmids were linearised individually in the following reaction; 6 µg (left/right) ZFN SC2 plasmid, 30 µl 10x NEB buffer 3, 3 µl 10 mg/ml BSA NEB, 2.5 µl Not1 and water to a total volume of 300 µl. This reaction was incubated at 37°C for 2 hours. 1 µl of the linearised product was run on a 0.8% gel electrophoresis alongside 1 µl unlinearised product, to check for complete linearization. The Not1 digested reaction was then purified with a Qiaquick PCR clean up kit and eluted into 30 µl of MQ water and concentration quantified by spectrophotometry. mRNA was synthesised using Ambion SP6 mMessageMachine kit, with the following reaction; 3 µl 400 ng/µl DNA, 5 µl NTP CAP mix, 1 µl 10x buffer and 1 µl enzyme mix. This reaction was mixed then incubated at 37°C for 2 hours. 1 µl of this reaction was aliquotted out for testing and 1 µl of DNAase turbo was added to the 10 µl reaction and incubated for a further 20 minutes. 1 µl of synthesised mRNA without DNAase treatment was run on a 0.8% gel electrophoresis alongside 1 µl of DNAase treated mRNA to test for DNA contamination. This DNAase treated mRNA reaction was purified using Qiagen RNeasy MinElute kit (Qiagen, Manchester, UK) and eluted into 14 µl MQ water. 1 µl for each left and right was quantified with spectrophotometry and then the mRNA was immediately stored at -80°C. Equal ng of left and right mRNA was mixed

together and injected into 1 cell stage wildtype embryos at 0.5, 1 and 1.5 nl. Gel loading tips were used to load 3 µl of mRNA into the needle for injection.

2.7.4 Screening for ZFN mutations

454 deep sequencing was used for the screening of mutations in the F1 progeny of F0 injected fish. Deep sequencing sequences many different amplicons which have been pooled together. 6 F0 fish were in-crossed and the F1 offspring were pooled and genomic DNA extracted, these F0 fish were then placed in a separate tank and a specific multiplex identifier sequence (MID) primer was assigned to the gDNA samples from this tank. The assignment of specific barcoded primers enabled sequences to be assigned back to a tank. Therefore if a mutation was present in samples with a particular MID sequence, this could be tracked to a tank of 6 fish which would then need sequencing individually to identify a founder. During PCR amplification often the primers are not fully amplified, therefore some nucleotides can be missing from the end of the primers. For 454 sequencing to be effective, full length amplicons are required, therefore titanium primers were used, which are added as 5' extensions to the gene specific primers and prevent them from being truncated (see **Table 2.6**). An MID was added between the titanium primer and the gene specific primer to enable identification.

gDNA was extracted from pooled embryos from 1 tank containing 6 fish. Approximately 60 embryos per pair at 72 hpf were added to a 1.5 ml tube on ice and all excess media removed. 700 µl of embryo digestion buffer was added (10 mM Tris-HCL pH 8, 1mM EDTA, 0.3% Tween 20 and 0.3% NP40). The embryos plus this buffer were heated to 98°C for 10 minutes, then 30 µl 25mg/ml proteinase K (Roche) was added on ice. The samples were then incubated at 55°C for 3 hours, then 98°C for 10 minutes. 450 µl of lysate was added to 250 µl 7.5 M ammonium acetate, and spun at room temperature at 13,000 g for 5 minutes. The supernatant was removed and added to 700 µl isopropanol and centrifuged at 16.3 g at 4°C for 30 minutes. The supernatant was removed and discarded and the pellet washed with 70% ethanol, then spun at room temperature for 5 minutes, the ethanol was then removed and the pellet allowed to air dry for 1 minute. This pellet was then

resuspended in 100 µl MQ water. gDNA samples from each pair in a tank were combined to form a pool of gDNA from 1 tank. This gDNA was then amplified with primers with specific MID sequence in a first PCR reaction and a second PCR with titanium primers alone extends and re-amplifies the amplicon to ensure the amplicon is of full length. For the first PCR reaction the following was assembled on ice; 1 µl of x20 diluted gDNA sample form one tank, 14 µl MQ water, 4 µl 5x phusion high fidelity (HF) buffer, 0.4 µl 10mM dNTPs, 1 µl left (MID) primer 10 µM, 1 µl right (MID) primer 10 µM and 0.2 µl phusion enzyme. This reaction was run with the PCR conditions shown in **Table 2.5**, section ZFN titanium primer PCR conditions, for 34 cycles. 5 µl of this product was run on a 2% gel electrophoresis. The remaining 15 µl of product was purified using a Qiaquick PCR clean up kit (with HCl step) and eluted into 300 µl MQ water. This product was then re-amplified with titanium primers alone; 1 µl eluted PCR product, 14 µl MQ water, 4 µl 5x phusion HF buffer, 0.4 µl 10mM dNTPs, 1 µl 10 µM a titanium primer, 1 µl 10 µM b titanium primer and 0.2 µl phusion enzyme. This was cycled using the same program as listed in the ZFN titanium PCR section of **Table 2.5,** but for only 14 cycles. This reaction was purified and eluted into 30 µl MQ H_2O. 2 µl of this reaction was run on a 2% gel electrophoresis to check for the 223bp band. These amplicons each with individual MID sequences were then combined into 1 sample and submitted for 454 deep sequencing.

2.7.5 TALEN mutagenesis protocol

The following TALEN mutagenesis protocol is based on the protocol from Cermak et al. (2011) and modified by Stone Elworthy (CDBG, University of Sheffield) (Cermak et al., 2011). A TALEN target site was chosen using the software available at https://boglab.plp.iastate.edu/node/add/talen and inputting the *p2y12* sequence obtained from Ensembl. The parameters were changed to 15-21bp spacer and to be flanked by Ts, so that the final repeat variable di-residue (RVD) is NG. The minimum spacer length was 15 and maximum was 21. The minimum array length was set to 15 and a maximum array length was set to 21. Boxes with the following were un-ticked; 'Require C, G or T at position (not A)', 'percent composition', 'do not allow sites to end in a G' and 'require A, C or G at position 1 (not a T)'. Ticked was 'require

a T at position N'. A TALEN site was chosen which contained a 15bp spacer region and 15 RVD left subunit and 15 RVD right subunit. The target site within the spacer region had a BamHI restriction enzyme recognition site.

2.7.6 TALEN RVD assembly

Each subunit was first assembled as two halves, an A and a B for both the left and right subunit. The A and B parts were added together along with the final RVD upon addition to the destination vector. Constituent plasmids combined to form the A and B parts. Part A was combined into the pFusA plasmid with the first 10 RVDs and B containing the other RVDs minus the last RVD, into the pFusB plasmid. As the array lengths are variable, there are several B plasmids available, depending on the number of RVDs in the array. The final RVD is not added at the first golden gate reaction stage so the RVD number in the B part is one less than the full complement, therefore pFusB4 was utilised. Each RVD corresponds to a plasmid labelled with a well number from the original plate, a list of these plasmids can be found at: http://www.addgene.org/TALeffector/goldengate/voytas/Plate1/ . All plasmids were defrosted on ice, then gently mixed and pulse spun. Each of the four golden gate reactions were prepared separately in 0.2 ml tubes on ice.

Part A contained; 1 µl on each RVD plasmid at a 100 ng/ µl, 1 µl pFusA at 100 ng/ µl, 4 µl H_2O, 2 µl T4 ligase buffer (NEB), 2 µl T4 ligase (NEB), 1 µl Bsa1 (NEB).

Part B contained; 1 µl on each RVD plasmid at a 100 ng/ µl, 1 µl appropriate pFusB plasmid at 150 ng/ µl, 2 µl 10x T4 DNA ligase buffer (NEB), 2 µl T4 ligase (NEB), 1 µl Bsa1 (NEB).

Each reaction was gently mixed and placed in a TALEN cycling program without the Hot-lid option, of 10x (37°C/ 5 minutes + 16°C/ 10 minutes) + 50°C/ 5 minutes + 80°C/ 5 minutes. After completion of this cycling, 0.3 µl of 25mM rATP and 1 µl plasmid safe nuclease was added, the reaction was gently mixed and incubated at 37°C for 1 hour. Each golden gate reaction was transformed into NEB10Beta competent cells. 50 µl of cells were thawed and carefully divided into 4 x 2 ml tubes with 12.5 µl each, on ice. 1 µl of reaction was added to each tube and incubated on ice for 30 minutes. These cells were then heat shocked at exactly 42° for 30

seconds, then placed immediately back on ice for 5 minutes. 250 µl of room temperature SOC was added to each tube and then placed horizontally on a shaker at 250 rpm at 37°C for 1 hour. 50 µl of each reaction was streaked on warmed LB agar (35% LB agar) selection plates containing spectinomycin (50 µg/ml) Xgal (20 mg/ml) and incubated overnight at 37°C. 3 well separated white colonies were picked for each reaction, and grown at 250 rpm overnight at 37°C in 6 ml of LB medium (20% LB broth) containing spectinomycin in a 25 ml universal with a loose lid.

The universal tubes containing the overnight culture were spun down for 30 minutes at 4°C at 16.3 g. The supernatant was then poured off and the pellet purified by QIAprep miniprep kit on 1 of the 3 LB cultures per unit, following the Qiagen protocol and eluting the DNA in 50 µl MQ H_2O.

The A and B part for each plasmid was then checked by an NheI XbaI digest. The mastermix used contained 22 µl H_2O, 5 µl NEB2 buffer, 0.5 µl 10mg/ml BSA, 1 µl NheI and 2 µl XbaI, on ice. 6 µl of the mastermix was transferred to 4 µl of mini prep in a 0.2 ml tube and incubated at 37°C for 1 hour. 2 µl of 5x loading dye (Bioline) was added and the reaction was run on a 1.1% seakem agarose gel alongside 5 µl, 2 µl and 1 µl loadings of 5 x diluted NEB 2log DNA ladder. Band sizes were checked against the expected sizes of 266bp, 2132bp and 500 bp-1100 bp depending on the number of RVDs. The band intensities were used to approximate the plasmid concentration, such that at least 150 ng of plasmid will be added to the 2nd golden gate reaction.

The 2nd golden gate reaction combines the A and B part of each subunit, along with the final RVD which corresponds to the well labelled E4. The mastermix for each subunit was; 5 µl H_2O, 4 µl A miniprep, 4 µl B miniprep, 1 µl 150ng/ µl plasmid E4, 1 µl 75 ng/ µl pCAGT7TALEN, 2 µl 10x T4 ligase buffer (NEB), 2 µl T4 DNA ligase (NEB), 1 µl Esp3I. This reaction was gently mixed and cycled in the same TALEN incubation cycle as above. Each golden gate reaction was then transformed in NEB10Beta competent cells in which the 50 µl of cells were carefully separated into 2 tubes each with 25 µl, and 2 µl of reaction was added. This reaction transformed as above

and 50 µl of the transformation was streaked onto pre-warmed carbenillin Xgal LB agar plates. The plates were grown overnight at 37°C and one well separated white colony was picked for each subunit. This was then grown up overnight in 100 ml of LB carbenicillin (50 µg/ml) media in a baffled flask at 250 rpm and 37°C. A NucleoBond midi prep (Macherey-Nagel, Germany) was used for purification of each culture, following the instruction booklet, with the final precipitation in 6 individual 1.5 ml eppendorf tubes per plasmid culture. The tubes were spun at 4°C at 16.3 g for 30 minutes, after which the supernatant was removed and the pellet was washed with 1 ml 70% ethanol. The tubes were spun again, then all excess ethanol was removed and the pellets were air dried for 1 minute on the bench top. Each tube was resuspended in 20 µl H_2O and vortexed, the 6 individual tubes were then pooled for each plasmid to give a 120 µl final volume per by spectrophotometry (A260 Beckman Coulter, High Wycombe, UK). 20 µl of 100 ng/ µl of each preparation was sent for sequencing with the following primers: TAL_R2 and SeqTALEN_5-1 (see **Table 2.6**). These sequences were checked alongside the predicted sequences for each construct, utilising the combination of sequence fragments for each RVD and the sequence of the plasmid backbone for each FusB. These array sequences were then inserted into the pCAGT7TAL backbone sequence.

Each plasmid was tested with a BamHI and XbaI digest to check for the correct insertion of RVDs into the plasmid. Each digest should give bands between 4346bp and 3669bp, depending on the number of RVDs. For each plasmid the following was assembled on ice; 7 µl H2), 1.5 µl 100ng/ µl DNA, 1 µl 10x NEB3 buffer, 0.1 µl 100x BSA, 0.5 µl BamHI, 0.5 µl XbaI. This reaction was gently mixed and incubated for 1 hour at 37 °C. The digested samples were then run on a 0.7% seakem agarose gel, alongside 5 µl, 2 µl and 1 µl of 5x diluted NEB 1kb DNA ladder.

The left and right pCAGT7TAL constructs were then linearised with NotI, with the following reaction; 6 µg L construct, 6 µg R construct, 30 µl 10x NEB3 buffer, 3 µl 10 mg/ml BSA, 2.5 µl NotI and made up to a total volume of 300 µl with H_2O. This reaction was gently mixed then incubated at 37 °C for 1 hour. It was then purified using 2 QIAquick PCR clean up columns (Qiagen, Manchester, UK) and eluted with H_2O, with the eluent of the first tube used to elute the 2^{nd}, so that the total eluent

volume was 30 µl. 1 µl of NotI linearization was added to 15% ficol with loading dye and 6 µl, 3 µl and 1 µl of this was loaded on the same 0.7% gel as the BamHI and XbaI digest above. The relative intensities of the NotI bands were used to quantify the concentration of the linearised plasmid.

2.7.7 Preparation of TALEN mRNA for injection

mRNA for injection was prepared from the NotI linearised plasmid using an Epicenter T7 MessageMax ARCA kit. The following reaction was prepared on ice; 5.5 µl 400 ng/ µl DNA, 2 µl 10x Buffer, 8 µl NTP CAP mix, 2 µl 100mM DTT, 0.5 µl scriptguard, 2 µl enzyme mix. This was gently mixed and incubated at 37 °C for 3 minutes. 1 µl of DNAase was then added and mixed gently before being incubated for a further 15 minutes at 37°C. This reaction was purified using a Qiagen RNA MinElute column, following the kit instructions, and then eluted into 14 µl of H_2O. 0.5 µl of the eluent was added to 1 µl 5x loading dye and 4.5 µl H_2O and run on a 0.7% seakem agarose gel. After confirmation of a band with no DNA contamination, the RNA was stored at -80°C.

RNA was microinjected into 1 cell stage embryos with 3 nl injected into the yolk and 1 nl injected directly into the cell. 24 hpf embryos were inspected for signs of toxicity such as small heads or delayed development and the optimised dose was termed sufficient to induce a minority of embryos (approximately 30%) with toxic phenotype. The somatic mutation rate induced by the TALEN RNA was assessed via gDNA extraction of 6 individual 72 hpf embryos injected with TALEN RNA and between 2-4 uninjected controls. The gDNA was amplified by PCR with specific primers designed to incorporate the target site and produce a product of 220bp. Digestion of the PCR product with the restriction enzyme BamHI was used to test for somatic mutations. A full cleavage of the product indicated that there was no mutation to the target site, whereas a partial cleavage of the product indicated that there was a mutation to the target region. The following protocol was used for gDNA extraction from individual embryos; single dechorionated embryos were added to a 0.2 ml tube on ice and all excess media removed. 50 µl of embryo digestion buffer was added. The embryo plus this buffer were heated to 98°C for 10

minutes, then 4 µl 25mg/ml proteinase K (Roche) was added on ice. The samples were then incubated at 55°C for 3 hours, then 98°C for 10 minutes, then added to 100 µl of H_2O. This lysate was spun at 4°C for 30 minutes and the supernatant was utilised for PCR reaction.

For amplification of the gDNA, an annealing temperature of 61°C was used, with standard PCR conditions as shown in **Table 2.5**. A 10 µl reaction was prepared for each sample comprising of 5 µl 2x Biomix Red, 1 µl 10 µM forward primer, 1 µl 10 µM reverse primer, 2 µl H_2O and the addition of 1 µl gDNA. For each PCR reaction 2 µl of a control sample was removed to be used as an undigested control. 1 µl of BamHI enzyme was added to each tube and incubated for 3 hours at 37°C. 9 µl of this digestion reaction was then run on a 2% gel alongside 5 µl of low molecular weight ladder (NEB). The presence of an undigested band in the TALEN mRNA injected gDNA indicated that a mutation was present and the remaining embryos from this RNA injection were raised.

2.7.8 Screening for TALEN mutations

Potential founder fish were screened for mutation via in-crossing a male and female fish from the F0 injected groups. gDNA from the F1 embryos of this in-cross was extracted at 72 hpf by the pooling of 3 embryos per tube and the above screening PCR and enzyme digest was utilised to screen for mutations in the target site. When a partial digest was present, the male and female from that pair were out-crossed to wildtypes, so the founder could be identified via the screening of these embryos. F1 gDNA of 24 embryos was extracted using Red Extract kit (Sigma-Aldrich, Gillingham, UK) using the following protocol; 3x 72 hpf embryos were added to each of 8x 0.2 ml tubes and all excess media was removed. 25 µl of extraction solution and 6.25 µl of tissue solution were added to each tubes and vortexed. The samples were incubated at room temperature for 15 minutes then vortexed. The tubes were incubated at 95°C for 3 minutes then allowed to cool, and finally 25 µl of neutralization solution was added. 1 µl of gDNA from each of the 8 pools of embryos was added to a 10 µl PCR reaction. 1 µl of BamHI was added to the PCR product and incubate for 3 hours at 37°C, the digested product was then run on a 2

% gel to screen for mutations. gDNA from 8 individual embryos were screened for the out-cross of potential founders. This enabled the sequencing of gDNA from an individual F1 embryo carrier of the mutation. From this sequencing 2 mutations were determined; *p2y12*^{sh338} with a 6bp deletion and *p2y12*^{sh340} with a 10bp deletion. F1 embryos from these out-crosses to *nacre* were raised.

The adult F1 fish were fin clipped to identify carriers for the above mutations (section **2.2.3**). The above screening PCR and digest were run for each fin clip enabling the identification of heterozygotes for each mutation. Non carriers for the mutations were culled.

2.8 Statistical analysis methods

2.8.1 Experimental design

Experimental design within this thesis was approached with the initial consideration that each individual embryo represents an experimental unit. This is consistent with the Home Office licence held by Dr Tim Chico and my personal licence. In order to adhere to the 3 Rs, ("Replacement, Reduction and Refinement") with particular consideration to "Reduction", the fewest possible animals were utilised for each experiment (Russell, 1959). To test reproducibility of results, the majority of experiments were repeated on 3 separate occasions, representing 3 experimental replicates. Where there are replicates of 3 or more, I have included statistical analysis of the data. Where data represents a single experiment or 2 experimental replicates, I have presented the data but not statistically analysed it.

I was blinded in all experiments involving MO, drug exposure and embryo inoculation with *S. aureus.* For experiments with *p2y12*^{sh338} or *p2y12*^{sh340} I phenotyped the embryos subsequent to data generation and analysis. This approach ensured I generated unbiased data.

2.8.2 Data handling

Pseudoreplication is briefly defined as using inferential statistics to test replicates which are not statistically independent (Hurlbert, 1984). Therefore in order to avoid this, results of 3 or more experiments have been handled in 2 different ways. The

first approach combined each experimental replicate into a single mean, for example 3 mean values from 3 experimental replicates, this is shown as a column plot. The second approach considered each embryo (from all experimental replicates) as a separate experiment, for example 30 values if 10 embryos were utilised per experiment with 3 replicates, this is shown as a scatter plot. The first approach reduces the statistical power of the data as it is a comparison of 3 values as opposed to 30. To my knowledge the second approach is commonly used to analyse animal model data, with each embryo representing a single experimental unit, as each procedure for each embryo is an independent event and this enables a thorough statistical analysis without using statistics to generate a mean of a mean. I sought independent advice from a statistician located in the Mathematics and Statistics department, for statistical analysis of my data. Data in all graphs are shown as mean ± standard error of the mean (SEM).

There are some possible genetic similarities between the embryos used per experiment as they are generated from the same tank containing approximately 30 adults. However in all experiments requiring setting up of pairs, embryos from each pair were pooled to ensure a mix of genetic variance. In experiments with embryos obtained from marbling, this pooling of embryos occurred naturally.

2.8.3 Statistical tests used in this thesis

Several different statistical tests were used depending on the data type. Data presented considering all embryos as independent experiments (ie n=30), was subjected to a D'Agostino & Pearson omnibus test for Gaussian distribution. In cases where 2 groups were assessed and data was not normally distributed, or a mix of both, a Mann Whitney test was used, for example in the area under the curve data. For analysis of data representing the mean of each experimental replicate (ie n=3) there were often too few data values to obtain a normality assessment, in which case, a non-parametric test was used, for example a Mann Whitney.

A contingency table with a Fishers exact statistical test was used for the comparison of percentage thrombus formation in control and *p2y12* morphants. For the

comparisons of macrophage and neutrophil numbers over a time course, with 3 or more replicates, numbers were plotted against time and shown as mean ± SEM. A test for multiple comparison was utilised, such as a 2way ANOVA with Sidak's multiple comparison test for 2 groups or Tukey's post test for more than 2 groups. Embryo survival after inoculation with *S. aureus* was plotted on a Kaplan-Meier survival plot and analysed with a Mantel-Cox test.

Chapter 3 : The role of P2Y12 in thrombosis in the zebrafish

P2Y12 is an important amplifier of thrombosis, and drugs that antagonise P2Y12 are frequently used as treatments for atherothrombotic diseases (for review (Mackman, 2008)). It is, therefore, vital to fully understand the roles of P2Y12 and further investigate the mechanisms by which these drugs work. The effect of P2Y12 receptor knockout and antagonism has previously been studied in several animal models, primarily the mouse, in which P2Y12 knockout or antagonism reduces thrombus formation and increases bleeding times (Foster et al., 2001, Andre et al., 2003). P2Y12 has not previously been investigated in the zebrafish in terms of thrombosis. Therefore, it was necessary to first confirm the *p2y12* genetic sequence and expression pattern before investigating the effect of gene knockdown. This chapter will show results of *p2y12* expression studies in zebrafish embryos and the effect of knockdown and antagonism of P2Y12 on thrombosis. It was important to assess the thrombosis response after *p2y12* knockdown in order to validate the use of the model for further investigations into inflammation and infective responses. This chapter will also discuss work investigating the role of platelet microRNAs in thrombus formation after vessel injury.

3.1 Results

3.1.1 Is P2Y12 expressed in the zebrafish?

3.1.1.1 Zebrafish P2Y12 homology

I first sought to establish similarities between the zebrafish *p2y12* and human *P2RY12*, to determine whether the zebrafish would be a viable model for investigation of the P2Y12 receptor. *p2y12* is currently uncharacterized and no details are available on www.ncbi.nlm.nih.gov regarding this gene in zebrafish. However, a predicted *p2y12* sequence is available at www.ensembl.org described as p2Y purinoceptor 12-like with the Ensembl identification of

ENSDARG00000069945, at the locus of CU571333.2-201 and the transcript identification of ENSDART00000102224.

I used ClustalW alignment software to compare the protein sequences of human, mouse, rat and zebrafish P2y12. Conservation of residues would indicate which elements of the protein are functionally important. There is 52% identity and 76% similarity between zebrafish and human P2y12 protein sequence, with many key residues involved in ligand binding and activation conserved in the zebrafish. Highlighted in yellow are the conserved residues that are known to be vital for ligand binding: Y105, E188, R256, Y259 and K280 (Schmidt et al., 2013, Ignatovica et al., 2012, Hoffmann et al., 2008) (**Figure 3.1 A**). There is a partial conservation of the DRY motif, highlighted by the red box, which is known to play an important role in trafficking and G protein interaction (Nygaard et al., 2009). There are several differences between these orthologues, particularly the number of exons; zebrafish *p2y12* has one exon, human has three and the mouse has four.

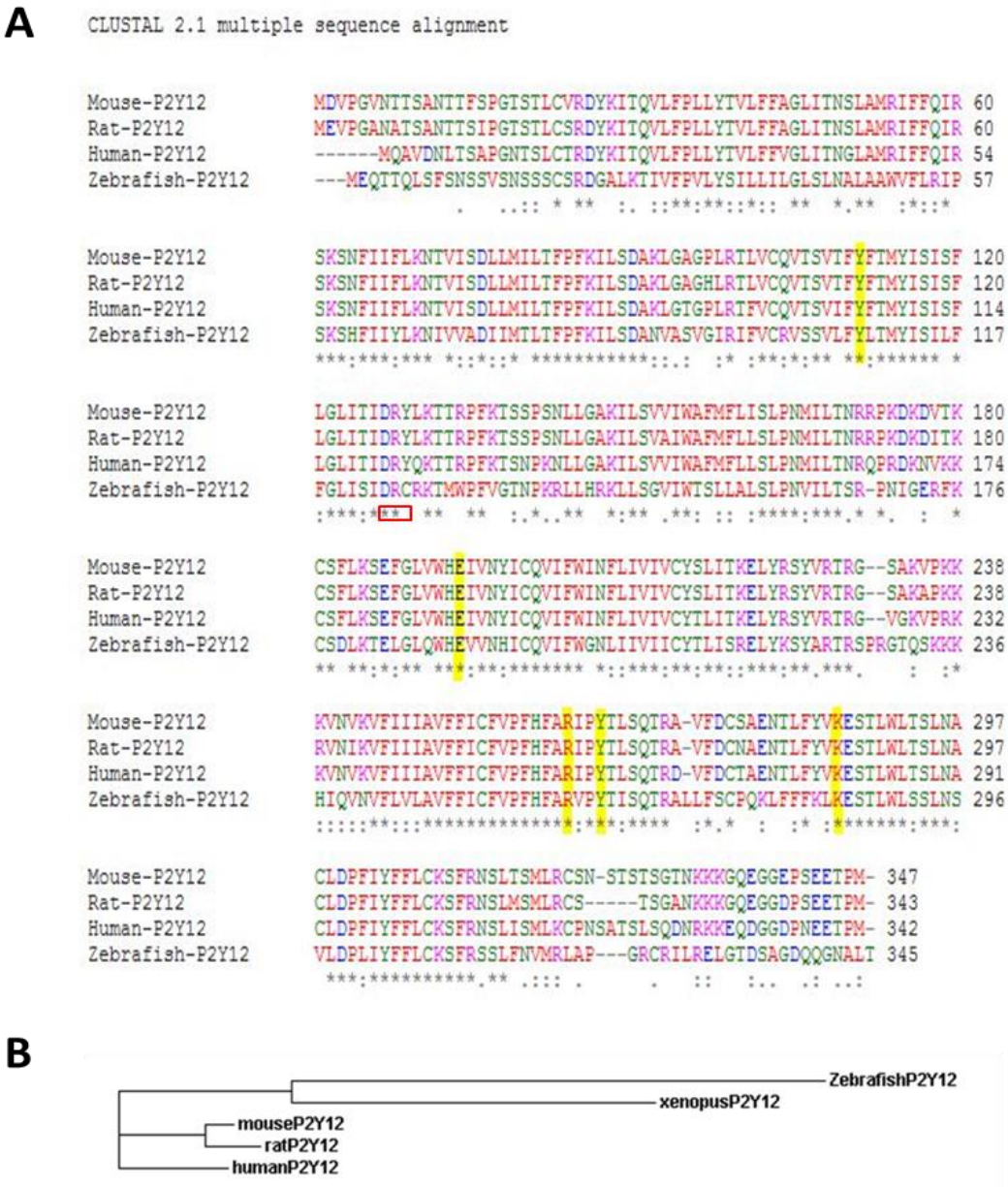

Figure 3.1 Alignment and phylogenetic analysis of P2y12 protein sequence.

A shows the alignment of human, mouse, rat and zebrafish protein sequence, [*] represent identical residues, [:] represents conserved substitution and [.] represents semi-conserved residues. The colours correspond to the physicochemical properties of the residues; Red is for small hydrophobic, Blue is for acidic, Magenta is for Basic-H and Green is for hydroxyl, sulfhydryl, amine or G. Highlighted in yellow are the conserved residues which are known to be vital for ligand binding: Y105, E188, R256, Y259 and K280 (Schmidt et al., 2013, Ignatovica et al., 2012, Hoffmann et al., 2008). The red box shows the partial conservation of the DRY motif in zebrafish. **B** shows a phylogenetic tree showing the evolutionary relationship of human, rat, mouse, zebrafish and xenopus P2Y$_{12}$ sequences.

3.1.1.2 *p2y12* expression in the developing zebrafish embryo

It was necessary to determine the time course for *p2y12* expression in the developing embryo to ascertain whether it would be suitable for knockdown. MOs induce transient knockdown which lasts approximately 3 days from injection at the 1 cell stage; therefore to assess the effect of knockdown, it must be expressed at these early time points. This was investigated by RT-PCR utilising primers (highlighted red), designed to the cDNA sequence for zebrafish *p2y12* from the Ensembl predicted sequence **(Figure 3.2 A)**. RNA was extracted from 1 dpf to 5 dpf embryos. **Figure 3.2 B** shows that *p2y12* is expressed in the developing zebrafish embryo from 1 dpf onwards and **C** shows a control for Glyceraldehyde 3-phosphate dehydrogenase (GAPDH), an enzyme which catalyses glycolysis of glucose, which is known to be expressed at these time points and acted as my control.

3.1.1.3 Zebrafish *p2y12* sequence

To confirm the zebrafish *p2y12* gene sequence, two pairs of primers were designed to the span the whole gene, from the predicted *p2y12* sequence on Ensembl. The first primer pair started at the 5' untranslated region (UTR) to base pair 671 and the second pair starting at 429 through to the 3'-UTR. Individual wildtype embryo cDNA was utilised for the PCR reaction with these primer pairs (**Figure 3.3**). This PCR product was sequenced, finding seven single nucleotide polymorphisms (SNPs), however these SNPs did not change the protein sequence (**Table 3.1**).

A

cttcacccagcaggactcatcaATGGAGCAAACAACGCAGCTCAGCTTCTCCAACAGCAGCGT
CTCCAACAGTTCATCCTGTTCTCGAGACGGCGCTCTGAAAACCATCGTCTTCCCCGTCC
TCTACTCCATCCTCCTCATCCTGGGATTATCCCTGAACGCTCTGGCGGCTTGGGTTTTCC
TCCGGATCCCCAGCAAATCCCACTTCATCATCTACCTGAAGAACATCGTGGTGGCCGAC
ATCATCATGACCCTCACATTCCCCTTTAAAATATTATCCGATGCCAATGTAGCGTCCGTGG
GCATCCGCATTTTTGTGTGCCGCGTGTCCTCCGTGCTCTTCTACCTCACCATGTACATCA
GCATCCTGTTCTTCGGTTTGATCAGCATCGATCGCTGCAGAAAAACCATGTGGCCGTTC
GTAGGCACCAACCCCAAACGTCTACTGCACAGAAAACTGCTTTCGGGAGTCATCTGGA
CGTCTCTCCTGGCTCTTTCGCTCCCAAATGTAATCCTGACCAGTCGTCCGAATATTGGAG
AGCGCTTCAAATGCAGCGATCTCAAAACTGAGCTCGGACTGCAGTGGCATGAGGTGG
TCAATCATATATGCCAGGTCATCTTTTGGGGAAACCTTATAATCGTGATCATATGCTACAC
GCTTATTTCCAGAGAGCTCTACAAGTCGTACGCCCGCACGAGGTCTCCGCGTGGGACG
CAAAGCAAGAAGAAACACATCCAGGTTAATGTGTTCCTGGTGTTGGCCGTGTTTTTCA
TTTGTTTTGTGCCGTTTCACTTCGCGCGAGTGCCCTACACCATCAGCCAGACGCGCGCC
CTCCTGTTCAGCTGCCCGCAGAAGCTGTTTTTCTTCAAGCTGAAGGAGAGCACGCTGT
GGCTGTCCTCCCTCAATTCTGTGCTGGATCCGCTCATCTACTTCTTCCTCTGCAAGTCCTT
CAGGTCGTCGCTGTTTAATGTGATGCGATTGGCTCCGGGACGCTGCAGGATCCTGAGG
GAGCTCGGGACAGATTCGGCCGGCGATCAACAGGGAAACGCACTGACATGAtggacaa
aacacggacacacacatgggaaaaacactggggcttgttctgtaaacatgcaatt

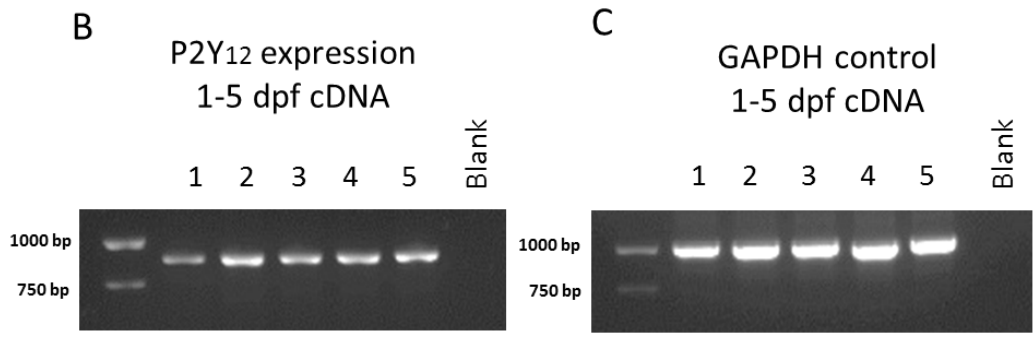

Figure 3.2 Expression of P2Y12 and GAPDH control in 1 dpf to 5 dpf zebrafish embryos.

The cDNA sequence of the zebrafish *p2y12* is shown in **A**, with primers highlighted in red and the start codon underlined. The untranslated (UTR) sequences both up and downstream of the cDNA sequence are in lower case. **B** shows expression of P2Y12 in wildtype zebrafish embryos from 1 dpf to 5 dpf. The final channel is a blank sample, which is a negative for cDNA. **C** shows expression of the GAPDH control primer pair, with a blank sample negative for cDNA in the final channel.

cttcacccagcaggactcatcaATGGAGCAAACAACGCAGCTCAGCTTCTCCAACAGCAGCGT
CTCCAACAGTTCATCCTGTTCTCGAGACGGCGCTCTGAAAACCATCGTCTTCCCCGTCC
TCTACTCCATCCTCCTCATCCTGGGATTATCCCTGAACGCTCTGGCGGCTTGGGTTTTCC
TCCGGATCCCCAGCAAATCCCACTTCATCATCTACCTGAAGAACATCGTGGTGGCCGAC
ATCATCATGACCCTCACATTCCCCTTTAAAATATTATCCGATGCCAATGTAGCGTCCGTGG
GCATCCGCATTTTTGTGTGCCGCGTGTCCTCCGTGCTCTTCTACCTCACCATGTACATCA
GCATCCTGTTCTTCGGTTTGATCAGCATCGATCGCTGCAGAAAAACCATGTGGCCGTTC
GTAGGCACCAACCCCAAACGTCTACTGCACAGAAAACTGCTTTCGGGAGTCATCTGGA
CGTCTCTCCTGGCTCTTTCGCTCCCAAATGTAATCCTGACCAGTCGTCCGAATATTGGAG
AGCGCTTCAAATGCAGCGATCTCAAAACTGAGCTCGGACTGCAGTGGCATGAGGTGG
TCAATCATATATGCCAGGTCATCTTTTGGGGAAACCTTATAATCGTGATCATATGCTACAC
GCTTATTTCCAGAGAGCTCTACAAGTCGTACGCCCGCACGAGGTCTCCGCGTGGGACG
CAAAGCAAGAAGAAACACATCCAGGTTAATGTGTTCCTGGTGTTGGCCGTGTTTTTCA
TTTGTTTTGTGCCGTTTCACTTCGCGCGAGTGCCCTACACCATCAGCCAGACGCGCGCC
CTCCTGTTCAGCTGCCCGCAGAAGCTGTTTTTCTTCAAGCTGAAGGAGAGCACGCTGT
GGCTGTCCTCCCTCAATTCTGTGCTGGATCCGCTCATCTACTTCTTCCTCTGCAAGTCCTT
CAGGTCGTCGCTGTTTAATGTGATGCGATTGGCTCCGGGACGCTGCAGGATCCTGAGG
GAGCTCGGGACAGATTCGGCCGGCGATCAACAGGGAAACGCACTGACATGAtggacaa
aacacggacacacacatgggaaaaacactggggcttgttctgtaaacatgcaatt

Figure 3.3 Zebrafish *p2y12* sequence.

Underlined is the sequence targeted by the ATG MO designed for this thesis. Highlighted are primer sites for sequencing the gene; purple shows the primer pair for the 1st half of the gene ranging from the 5' untranslated (lower case) region to 671bp. Blue shows the primer pair for the 2nd half of the gene ranging from 429bp to the 3' untranslated region.

Table 3.1: SNPs found by sequencing zebrafish *p2y12*.

Several SNPs were found after sequencing *p2y12*. The position is shown along with the base change, these SNPs do not change the protein sequence.

SNP position	Base change
132	C>T
181	C>T
495	G>A
560	A>G
756	T>C
768	T>C
879	C>T

3.1.1.4 Tissue distribution of *p2y12* expression

A *p2y12* specific antisense riboprobe was generated to bind to the *p2y12* mRNA in the zebrafish embryo, enabling spatial assessment of *p2y12* expression. I utilised whole mount *in situ* hybridisation (WISH) to determine the *p2y12* expression pattern at 24 hpf, 32 hpf, 48 hpf and 72 hpf. A sense riboprobe was used as a control. **Figure 3.4** shows that there is little staining with the sense probe, however staining can be clearly seen in the antisense probe at 24 hpf, 32 hpf, 48 hpf and 72 hpf. This staining is evident in haematopoietic regions at 24 hpf, 32 hpf, 48 hpf and 72 hpf. Staining for *p2y12* can be seen at 24 hpf in the intermediate cell mass (ICM) a site of the primitive wave of haematopoiesis (Lin et al., 2005). By 32 hpf there is staining in the ICM and in the posterior blood island (PBI), consistent with the location of thrombocytes before they enter circulation. These sites are areas of definitive haematopoiesis; the ventral region of the dorsal aorta is also known as aorta-gonad mesonephros (AGM) region and the PBI becomes the caudal haematopoietic tissue (CHT) after 36 hpf (Chen and Zon, 2009). By 48 hpf, staining is present in the AGM (previously the ICM) and the CHT (previously PBI). There is also increased staining in the dorsal aorta and caudal vein, indicating that *p2y12* expressing cells are in circulation rather than exclusively at sites of haematopoiesis. At 72 hpf there is reduced staining in the CHT however there are some cells stained corresponding to the kidney, which is a site of definitive haematopoiesis. The decrease in staining at 72 hpf may be due to a reduction in static thrombocytes residing in the tissues as they migrate to and enter the circulation. The presence of staining in the ventral dorsal aorta region and the PBI corresponds to the origins of thrombocytes, erythrocytes and neutrophils. Jagadeeswaran et al. (1999) showed that thrombocytes appear in circulation at approximately 36 hpf, however Warga et al. (2009) propose that they can be discerned as early as 24 hpf along the ICM (Jagadeeswaran et al., 1999, Warga et al., 2009). It was important to establish the identity of the *p2y12* stained cells, as *P2RY12* is not only expressed on thrombocytes but also vascular smooth muscle, macrophages and an as yet unknown leukocyte population identified in humans, by Diehl et al. (2010). It was, however, possible to exclude vascular smooth muscle from this investigation as this

is not present in zebrafish embryos prior to 72 hpf (Santoro et al., 2009). Macrophages are present in the ICM and PBI by 30 hpf, so it was important to distinguish between the *p2y12* stained cells as either thrombocytes, leukocytes or a combination of both (Bennett et al., 2001, Bertrand et al., 2007). I used a probe for *L-plastin* which is specific for macrophages and early neutrophils (**Figure 3.5**) to compare expression patterning to *p2y12*, to assess whether *p2y12 w*as expressed on macrophages. If the *p2y12 in situ* was detecting expression on macrophages, it might be expected that there would be a comparable level of staining between *p2y12* and *L-plastin in situs*. However the *in situ* for *L-plastin* showed considerably more staining at 48 and 72 hpf when compared to the *p2y12 in situ*, indicating that more cells express *L-plastin,* at these time points, than *p2y12*. This does not exclude the possibility of a population of macrophages expressing *p2y12*, as it is possible the increased staining with the *L-plastin* probe may be accounted for by early neutrophils. However, as the *p2y12* expression pattern corresponds to sites of haematopoiesis and reduces by 72 hpf, it is likely that the majority of *p2y12* expressing cells are thrombocytes and their precursors.

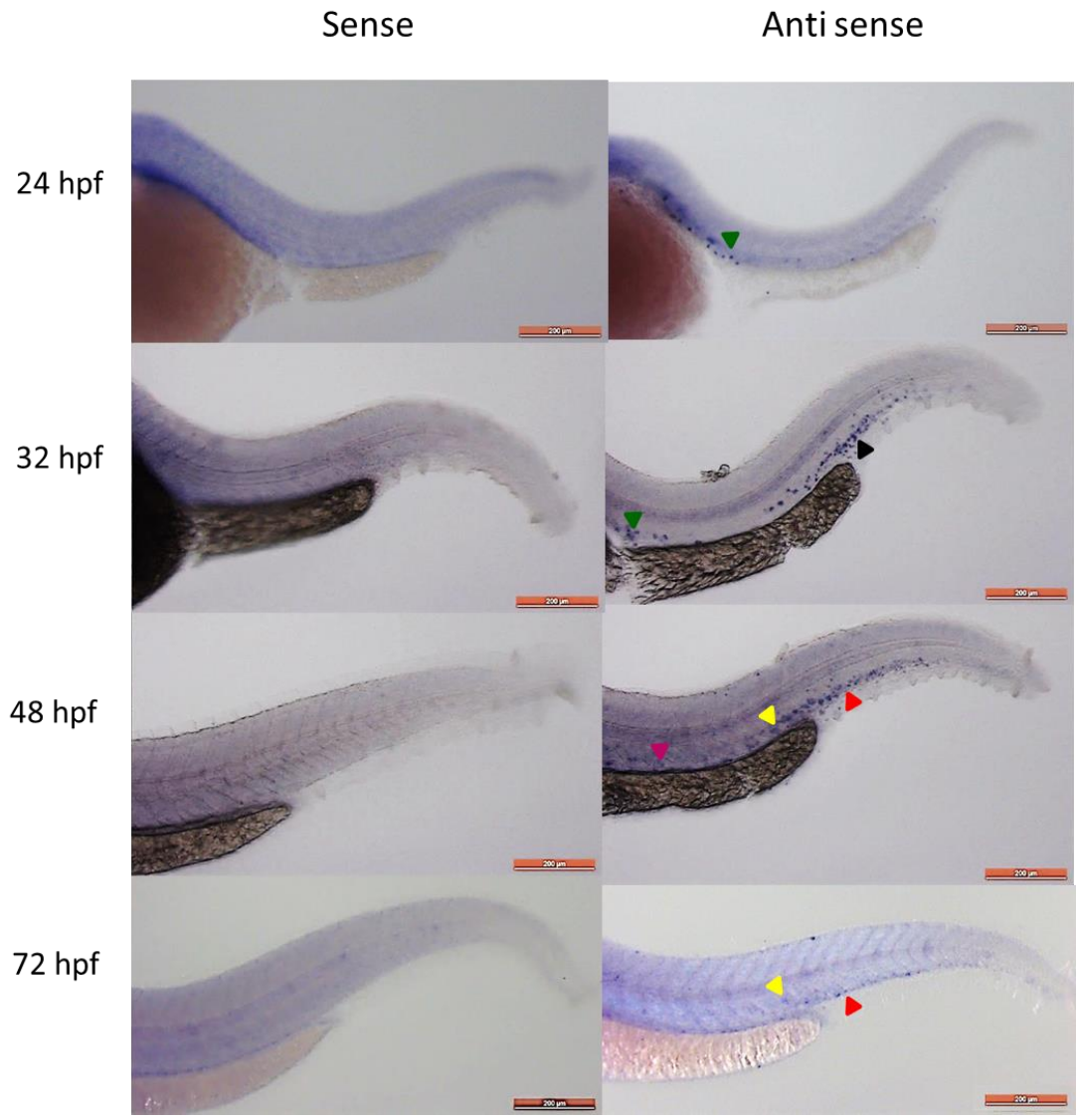

Figure 3.4 *p2y12* expression patterning in 24 hpf, 32 hpf, 48 hpf and 72 hpf embryos.

p2y12 is expressed in haematopoietic regions in the mid trunk and tail in the anti-sense column. Staining for *p2y12* is evident in the intermediate cell mass (ICM) highlighted by the green arrow head and posterior blood island (PBI) highlighted by the black arrow head in the 24 hpf and 32 hpf embryos. At 48 hpf staining is present in the aorta-gonad-mesonephros (AGM, shown by the purple arrow head) and caudal haematopoietic tissue (CHT shown by the red arrow head) with some staining also in the caudal vein and the dorsal aorta (yellow arrow head). At 72 hpf there is reduced staining in the AGM however there is still staining present in the CHT, dorsal aorta and caudal vein. Scale bars indicate 200 µm.

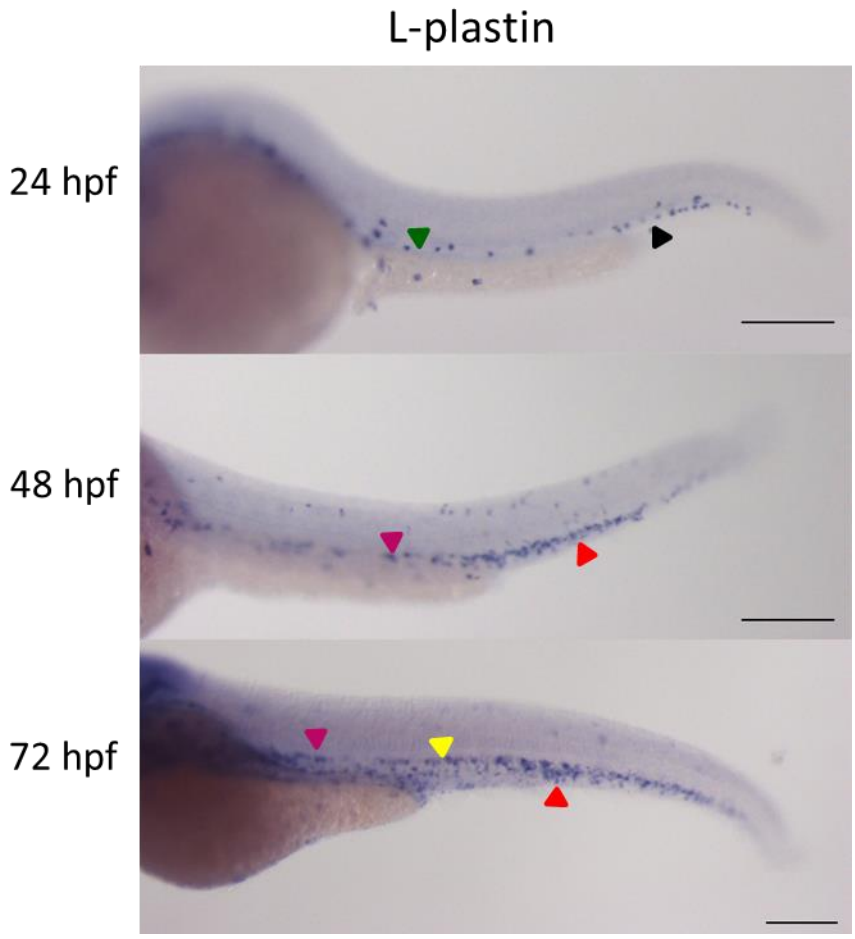

Figure 3.5 Expression patterning of *L-plastin* marker for leukocytes.

Expression patterning for *L-plastin*, staining is evident at 24 hpf in the intermediate cell mass (ICM, shown by the green arrow head) and posterior blood island (PBI, shown by the black arrow head). At 48 hpf in the aorta-gonad-mesonephros (AGM, shown by the purple arrow head) and caudal haematopoietic tissue (CHT, shown by the red arrow head). At 72 hpf there is considerable staining in the CHT and in the dorsal aorta (yellow arrow head). Scale bars indicate 200 µm.

3.1.2 Knockdown of zebrafish *p2y12*

3.1.2.1 Knockdown of *p2y12* does not affect gross morphology

The predicted zebrafish *p2y12* gene is a single exon, preventing the use of a splice modifying MO. Therefore, I utilised an ATG start site MO designed for this work, which prevents translation of mRNA to protein via sterically blocking the translation initiation complex. The concentration of MO was optimised such that only a minority of embryos showed signs of non-specific toxicity such as small heads, cardiac oedema and delayed development, as documented in **Table 3.2**. 1.2 ng was selected as a suitable amount of morpholino to be injected and **Figure 3.6** shows 3 dpf embryos injected with 1.2 ng of control MO (termed control morphant) and *p2y12* MO (termed *p2y12* morphant). There were no gross morphological differences between control and *p2y12* morphants. It was necessary to assess whether *p2y12* knockdown affected vessel development which could impede assessment of thrombus formation. **Figure 3.7** shows 3 dpf control and *p2y12* morphants in the *Fli1*:GFP transgenic background, in which endothelial cells express GFP. There was no significant difference between vascular anatomy in control and *p2y12* morphant groups, indicating that *p2y12* knockdown did not affect vascular development. This enabled subsequent testing of the role of $P2Y_{12}$ in thrombosis.

Table 3.2 The optimisation of *p2y12* morpholino amount for injection.

The amount of *p2y12* morpholino for knockdown was optimised to an amount which caused a toxic phenotype in only a minority of embryos. This table shows the amount of morpholino injected (ng) and percentages of embryos with toxic phenotypes, such as small head, delayed development or cardiac oedema. This table also includes the percentage of viable embryos – embryos deemed suitable for experimental use, with no non-specific toxic phenotype.

Amount of *p2y12* morpholino (ng)	**Percentage embryos with toxic effects (%)**	**Percentage viable embryos (%)**	**Volume injected (nl)**	**Number of embryos injected**
4.2	100	0	1	68
2.1	28	72	0.5	65
1.2	17	83	0.5	66
1.0	21	79	0.5	30

Figure 3.6 Gross morphology of 3 dpf control and *p2y12* morphants.

3 dpf control and *p2y12* morphants embryos are shown, in the wildtype background.There apears to be no significant difference in gross morphology between control and *p2y12* morphants. The scale bar represents 1 mm.

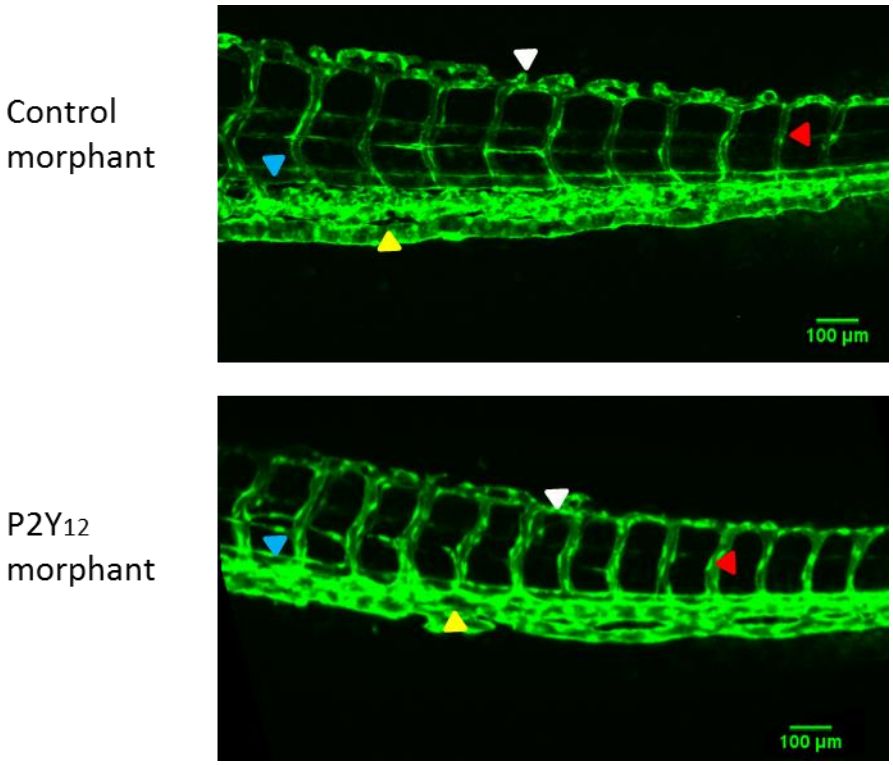

Figure 3.7 Vascular morphology of 3 dpf control and *p2y12* morphants in *Fli1*:GFP.

This transgenic has vascular endothelial cells expressing GFP, there appears to be no significant difference in vasculature between control and *p2y12* morphants. White arrow head shows dorsal longitudinal anastomotic vessel, red show intersegmental vessels, yellow shows caudal veins and blue shows dorsal aortas. Scale bar represents 100 µm.

3.1.2.2 The effect of *p2y12* knockdown on thrombocyte number

I attempted to ascertain whether there was a difference in thrombocyte number between the *p2y12* morphant and control morphant groups, as this could impact upon thrombus development. A CD41:GFP transgenic was utilised in which haematopoietic stem cells (HSC) express a low level of GFP (GFP^{low}) and thrombocytes express a high level of GFP (GFP^{high}) (Lin et al., 2005). The caudal haematopoietic region (CHT) of 3 dpf control and *p2y12* morphants was imaged, and the number of GFP^{high} cells was quantified. **Figure 3.8** shows preliminary data obtained from this single experiment. There appeared to be no difference in thrombocyte number between *p2y12* morphants and control morphants, from this single experiment, however as the experiment was not repeated, no statistical test was performed.

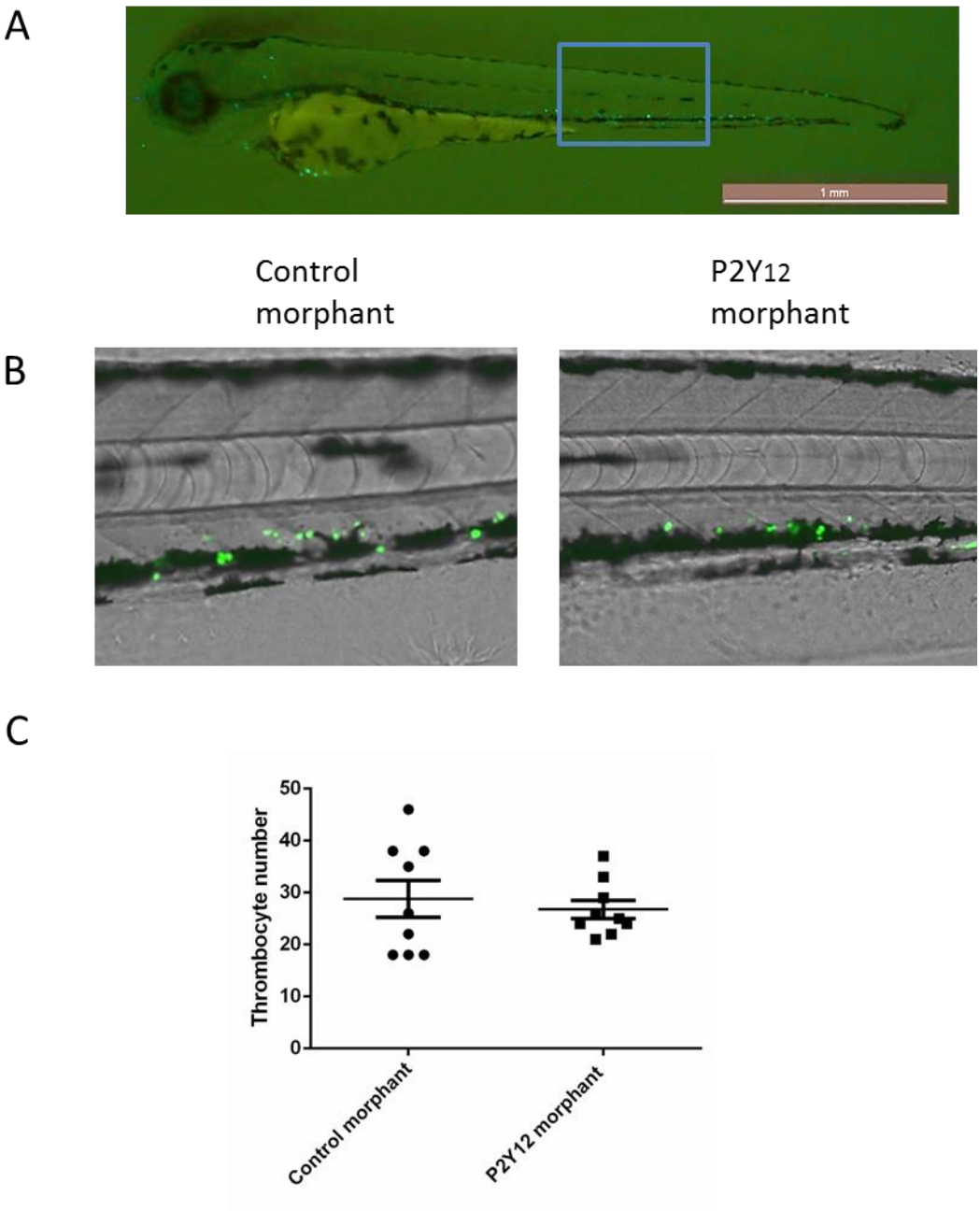

Figure 3.8 GFP positive thrombocytes in 3 dpf CD41:GFP embryos.

A shows a 3 dpf CD41:GFP embryo, the blue box highlights the region of interest. **B** shows the overlay of bright field and GFP+ thrombocytes in both control and P2Y12 morphant 3 dpf embryos. **C** shows a scatter graph of the number of CD41:GFP positive thrombocytes in the caudal haematopoietic region of both control and *p2y12* morphant fish, with each individual embryo represented. Data shown are mean ± SEM, with 9 embryos in each group. These data represent a single experiment therefore no statistical test was used.

3.1.2.3 The effect of *p2y12* knockdown on P2y12 protein expression in the p2y12::P2Y12-GFP transgenic.

Sieger et al. (2012) generated a p2y12::P2Y12-GFP transgenic in which GFP is fused to the C-terminus of *p2y12* driven under the native *p2y12* promoter. Sieger et al. (2012) demonstrated that after injection with a *p2y12* ATG MO, GFP fluorescence in microglia was significantly reduced (Sieger et al., 2012). I obtained this transgenic and injected my *p2y12* ATG morpholino which was virtually identical to the first of two *p2y12* morpholinos (P2Y12-mo) utilised by Sieger et al. (2012) (**see Table 2.3**). I imaged the dorsal region of the head of 3 dpf control and *p2y12* morphants and found an apparent reduction in GFP fluorescence and fewer branched microglia present in the *p2y12* morphants. However fluorescence was not quantified therefore this represents preliminary data indicating that my MO may reduce, if not completely prevent, protein translation (**Figure 3.9**).

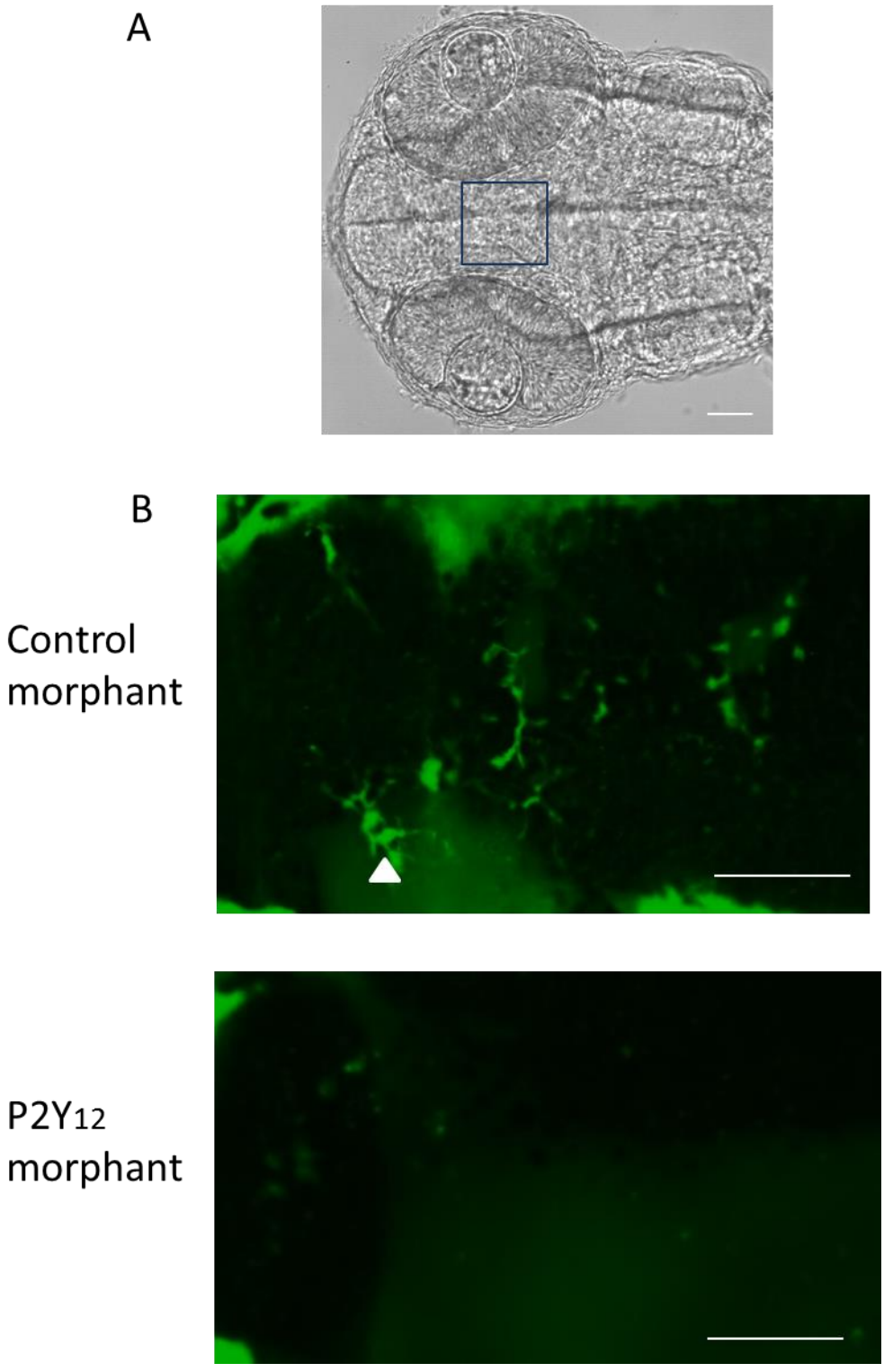

Figure 3.9 Dorsal view of zebrafish brain in p2y12::P2Y12-GFP.

A shows the dorsal view of the head of a 3 dpf embryo, the region of interest has been highlighted by a blue box. **B** shows both control and *p2y12* morphants, branched microglia in the control morphant are evident in the control morphant only (highlighted by an arrow head). Scale bars represent 50 µm.

3.1.2.4 The effect of *p2y12* knockdown on thrombocytes in the p2y12::P2Y12-GFP transgenic.

I found that that knockdown of *p2y12* appeared to reduce fluorescence of microglia in the p2y12::P2Y12-GFP transgenic, but did not appear to affect thrombocyte numbers in the CD41:GFP transgenic. I then investigated whether the fluorescence of GFP positive thrombocytes were affected by *p2y12* knockdown. **Figure 3.10** shows a wildtype 3 dpf embryo in **A**, and in **B** the caudal haematopoietic region (CHT) of 3 dpf control and *p2y12* morphants. GFP positive cells are visible in the CHT region of control morphants, there appears to be fewer GFP positive cells in the CHT of the *p2y12* morphants. The low fluorescence of this transgenic determined a relatively long exposure time, which was too long for the imaging of individual GFP positive cells within the circulation. Therefore, in these images, the dorsal aorta and caudal vein appear outlined by blurred GFP, due to circulating GFP positive cells within the vessel. Due to this low fluorescence, the thrombocyte fluorescence was not quantified, therefore this is preliminary data representative of a single experiment, without quantification. There appears to be reduced fluorescence in the CHT of the *p2y12* morphant which might suggest a possible reduction in translation of P2y12 protein, however this would require further experimentation to confirm.

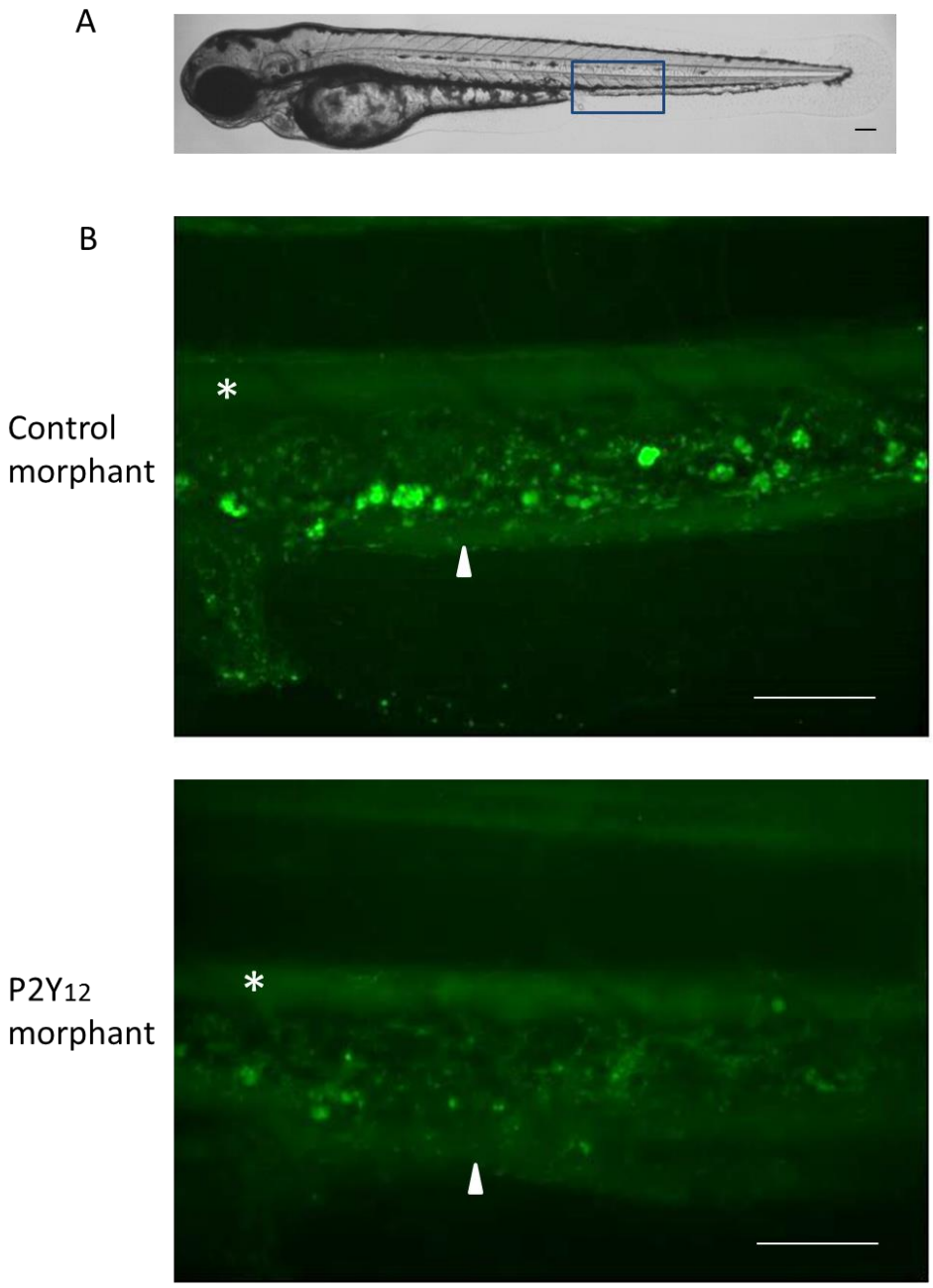

Figure 3.10 The caudal haematopoietic tissue (CHT) region of control and *p2y12* morphant 3 dpf p2y12::P2Y12-GFP embryos.

A wildtype 3 dpf embryo is shown in **A**, with the region of interest highlighted by a blue box. **B** shows both control and *p2y12* morphants in the p2y12::P2Y12-GFP transgenic line. The asterisk highlights the dorsal aorta and the arrow head highlights the caudal vein, with the CHT region between these vessels. Scale bars represent 50 μm.

3.1.2.5 The effect of *p2y12* knockdown on thrombosis in zebrafish embryos

Knockout of the $P2Y_{12}$ receptor in mice significantly reduces thrombus formation after vessel injury (Foster et al., 2001, Andre et al., 2003). Therefore, I hypothesised that knockdown of *p2y12* in the zebrafish would similarly reduce thrombosis after vessel injury. To investigate this, I used a laser to injure vessel endothelium and induce thrombosis. The ventral wall of the dorsal aorta, at the position opposite the cloaca, was selected as an easily identified location to induce arterial thrombosis. Our lab has previously established that this technique is sufficient to ablate the endothelium (Quaife and Chico, 2012). Thrombosis was induced by laser injury and thrombus area quantified over time using ImageJ software. **Figure 3.11** shows examples of a developing thrombus in two different transgenic backgrounds; CD41:GFP and CD41:GFP;*Gata1*:Dsred (a movie of **B** is available on the attached DVD). Both $P2Y_1$ and $P2Y_{12}$ are required to produce a full aggregation response to ADP in humans (Jin and Kunapuli, 1998). $P2Y_1$, alongside other receptors, instigate thrombus formation, whereas $P2Y_{12}$ amplifies and sustains this initial platelet activation response (Daniel et al., 1998). I observed thrombosis for 10 minutes, in order to observe both initial thrombus development and, importantly, the amplification of thrombosis which is driven by the $P2Y_{12}$ receptor, subsequent to this.

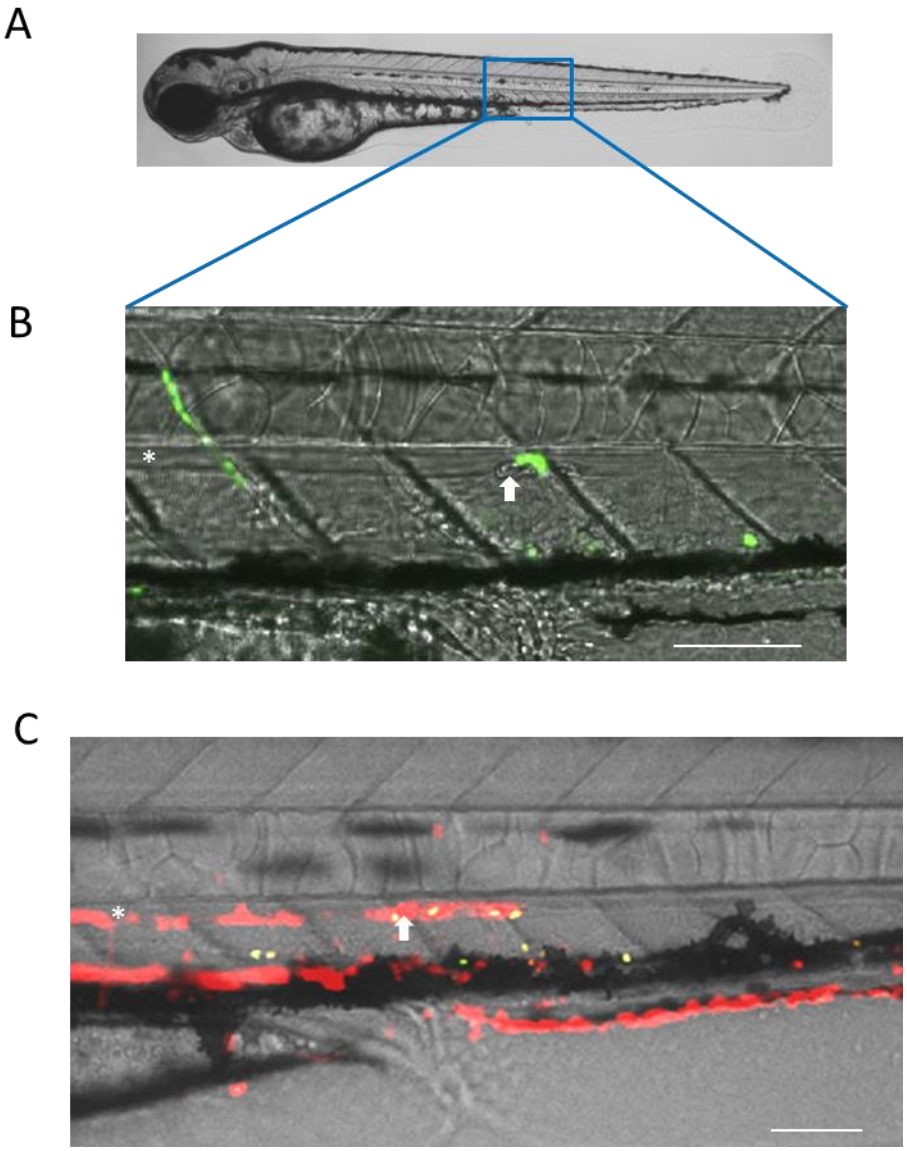

Figure 3.11 Thrombus development after vessel injury.

A wildtype 3 dpf embryo is shown in **A** with a blue box highlighting the region of **B** and **C**. **B** shows a thrombus in the CD41:GFP background, the arrow indicates the site of laser induced injury on the ventral wall of the dorsal aorta, the asterisk indicates the dorsal aorta. The thrombus can be seen in brightfield, with thrombocytes in green fluorescence, (a movie of this thrombus development is available on the attached DVD). **C** shows a thrombus in the CD41:GFP;Gata1:dsRed background, with erythrocytes in the thrombus fluorescing red and thrombocytes, shown as yellow, fluorescing green. Scale bars represent 100 µm.

Figure 3.12 shows the time course of thrombus development in 3 dpf control MO injected CD41:GFP;*Gata1*:Dsred transgenic embryos. In this transgenic, thrombocytes express GFP and erythrocytes express red fluorescent protein DsRed. **A** shows a bright field image of the region of interest, and **B** shows development of thrombus over 10 minutes. The thrombus occluded the vessel and blocked blood flow to the tail by 2 minutes after vessel injury, and subsequently embolised by approximately 8 minutes, enabling blood to flow past the site of injury and reach the tail. The composition of the thrombus can be seen to consist of both Dsred+ erythrocytes and GFP+ thrombocytes. A movie of this time course can be seen on the attached DVD.

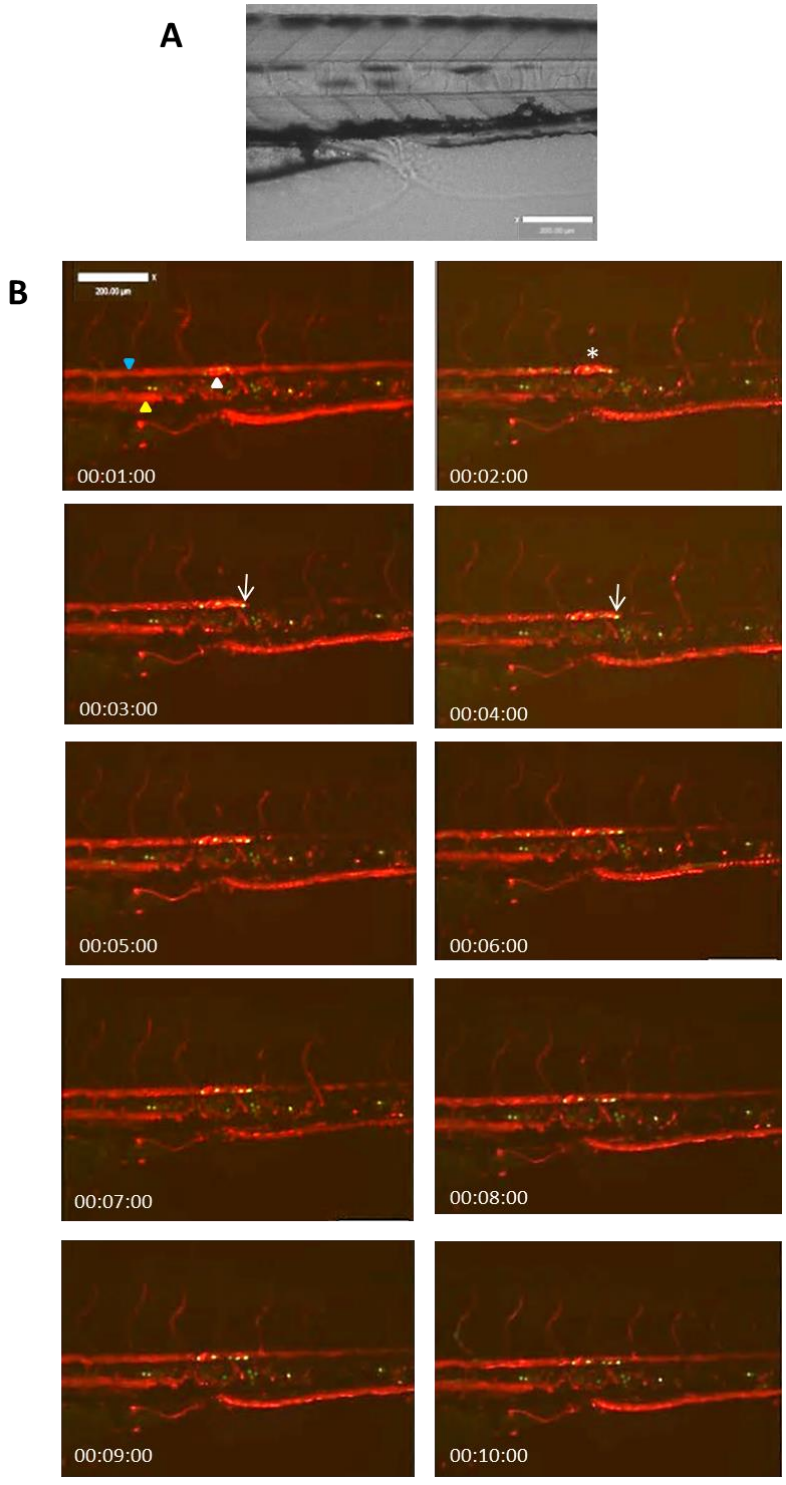

Figure 3.12 Thrombosis in CD41:GFP;Gata1:DsRed 3 dpf embryos.

A shows a bright field image of the mid trunk region of a 3 dpf embryo. **B** shows thrombus development over 10 minutes after laser induced injury. The white arrow head indicates the site of laser injury. The vessel fully occludes after 2 minutes and embolises after approximately 8 minutes. CD41:GFP labelled thrombocytes are evident at the site of thrombus highlighted by a white arrow. The yellow arrow head indicates the caudal vein, the blue indicates the dorsal aorta and the white asterisk indicates the occluding thrombus.

3.1.2.6 *p2y12* knockdown significantly reduces thrombosis

Control and *p2y12* morphants, in groups of 4-6, underwent laser induced injury to the ventral wall of the dorsal aorta and the thrombus area was quantified over ten minutes. This was repeated on four different days. **Figure 3.13 A** shows a plot of thrombus area over ten minutes after injury, where each embryo has been considered as a separate experiment (control n=21 and *p2y12* morphants n=20). **Figure 3.13 B** shows a statistically significant reduction in the mean area under the curve of *p2y12* morphants compared to control when analysed by combining each experimental replicate into a single mean (n=4 p=0.02). **C** shows a statistically significant reduction in thrombus area in *p2y12* morphants with each embryo representing a separate experiment (control n= 21 and *p2y12* morphants n=20, $p<0.0001$). **Figure 3.14** shows a significant reduction in thrombi development in *p2y12* compared to control morphants, with 77% of *p2y12* morphants forming thrombi compared to 100% of control morphants. These results are consistent with the reduction in thrombosis seen in the *P2Y$_{12}$ -/-* mouse (Foster et al., 2001).

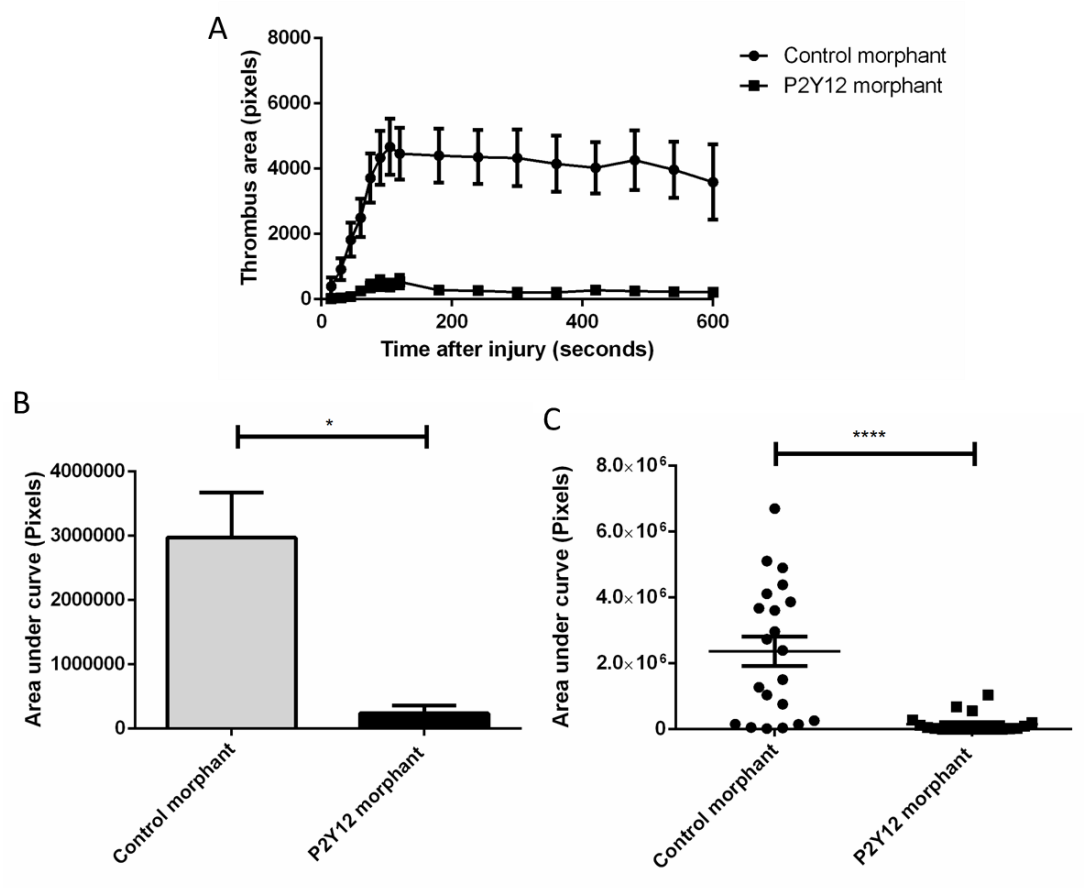

Figure 3.13 The effect of *p2y12* knockdown on arterial thrombosis.

Groups of 4-6 *p2y12* morphant or control embryos underwent laser induced aortic injury and thrombus area was quantified over 10 mins. Four replicate experiments were performed on different days. **A** shows a plot of thrombus area over 10 minutes following laser induced aortic injury, where every embryo has been considered as a separate experiment (n=21 control and n=20 *p2y12* morphants). **B** shows the mean area under the curve in *p2y12* morphants or controls where data has been analysed by combining each experimental replicate into a single mean (n=4, p=0.02). **C** shows a scatter graph with each individual embryo represented as an experimental unit ($p<0.0001$). A Mann Whitney test was applied for analysis of both **B** and **C**, data is presented as mean ± SEM.

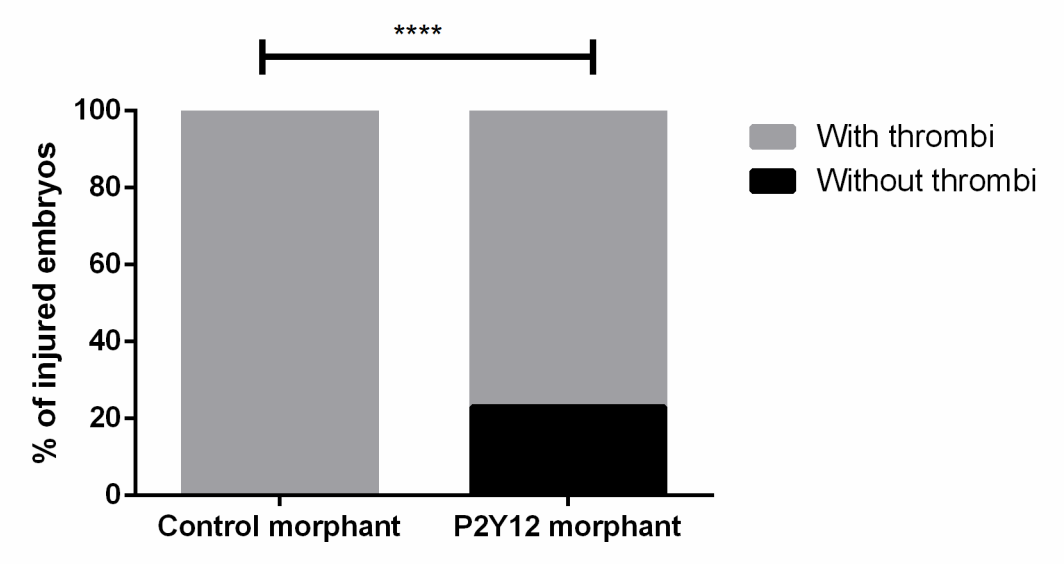

Figure 3.14 The effect of *p2y12* knockdown on arterial thrombi formation.

Groups of 4-6 *p2y12* morphant or control embryos underwent laser induced aortic injury and embryos were observed to determine whether or not a visible thrombus was generated. Four replicate experiments were performed on different days, and data from each replicate was combined into a single mean (ie n=4). Fishers exact test was used for analysis $P<0.001$.

3.1.2.7 Does *p2y12* knockdown, by the published P2Y12-mo2, affect thrombus formation?

In order to assess whether the previous data showing a significant reduction in thrombus area after *p2y12* knockdown was a specific phenotype rather than a potentially non-specific effect of the *p2y12* morpholino, I obtained the published P2Y12-mo2 morpholino (Sieger et al., 2012). This morpholino, as shown in **Figure 3.15 A,** targets the 5' UTR region of *p2y12* thus acting as a translation blocking morpholino. I injected the morpholino amount as documented by Sieger et al. (2012) and this resulted in no significant morphological differences in the P2Y12-mo2 morphants (**Figure 3.15 B**). I quantified the thrombosis response of groups of 6-7 control or P2Y12-mo2 morphants at 3 dpf, by laser induced aortic injury in three replicate experiments, performed on different days. **Figure 3.16 A** shows a plot of thrombus area over 10 minutes following injury, where every embryo has been considered as a separate experiment. There is a non-significant trend for reduced thrombus area in the P2Y12-mo2 morphants, when analysing the data by combining each experimental replicate into a single mean, as in **Figure 3.16 B** (n=3, p=0.1). However, I found that there was a statistically significant reduction in thrombus area in the P2Y12-mo2 morphant compared to control morphants, when considering each embryo as a single experimental unit in **Figure 3.16 B** ($p<0.0001$, control n=22 and P2Y12-mo2 morphants n=21).

A

tcatttcattatgcattctttcattcaggacttcattacttcacccagcaggactcatcaATGGAGCAAACAAC
GCAGCTCAGCTTCTCCAACAGCAGCGTCTCCAACAGTTCATCCTGTTCTCGAGACGGC
GCTCTGAAAACCATCGTCTTCCCCGTCCTCTACTCCATCCTCCTCATCCTGGGATTATCCC
TGAACGCTCTGGCGGCTTGGGTTTTCCTCCGGATCCCCAGCAAATCCCACTTCATCATCT
ACCTGAAGAACATCGTGGTGGCCGACATCATCATGACCCTCACATTCCCCTTTAAAATAT
TATCCGATGCCAATGTAGCGTCCGTGGGCATCCGCATTTTTGTGTGCCGCGTGTCCTCC
GTGCTCTTCTACCTCACCATGTACATCAGCATCCTGTTCTTCGGTTTGATCAGCATCGATC
GCTGCAGAAAAACCATGTGGCCGTTCGTAGGCACCAACCCCAAACGTCTACTGCACAG
AAAACTGCTTTCGGGAGTCATCTGGACGTCTCTCCTGGCTCTTTCGCTCCCAAATGTAA
TCCTGACCAGTCGTCCGAATATTGGAGAGCGCTTCAAATGCAGCGATCTCAAAACTGA
GCTCGGACTGCAGTGGCATGAGGTGGTCAATCATATATGCCAGGTCATCTTTTGGGGA
AACCTTATAATCGTGATCATATGCTACACGCTTATTTCCAGAGAGCTCTACAAGTCGTAC
GCCCGCACGAGGTCTCCGCGTGGGACGCAAAGCAAGAAGAAACACATCCAGGTTAAT
GTGTTCCTGGTGTTGGCCGTGTTTTTCATTTGTTTTGTGCCGTTTCACTTCGCGCGAGT
GCCCTACACCATCAGCCAGACGCGCGCCCTCCTGTTCAGCTGCCCGCAGAAGCTGTTT
TTCTTCAAGCTGAAGGAGAGCACGCTGTGGCTGTCCTCCCTCAATTCTGTGCTGGATCC
GCTCATCTACTTCTTCCTCTGCAAGTCCTTCAGGTCGTCGCTGTTTAATGTGATGCGATT
GGCTCCGGGACGCTGCAGGATCCTGAGGGAGCTCGGGACAGATTCGGCCGGCGATC
AACAGGGAAACGCACTGACATGAtggacaaaacacggacacacacatgggaaaaacactggggctt
gttctgtaaacatgcaatt

B

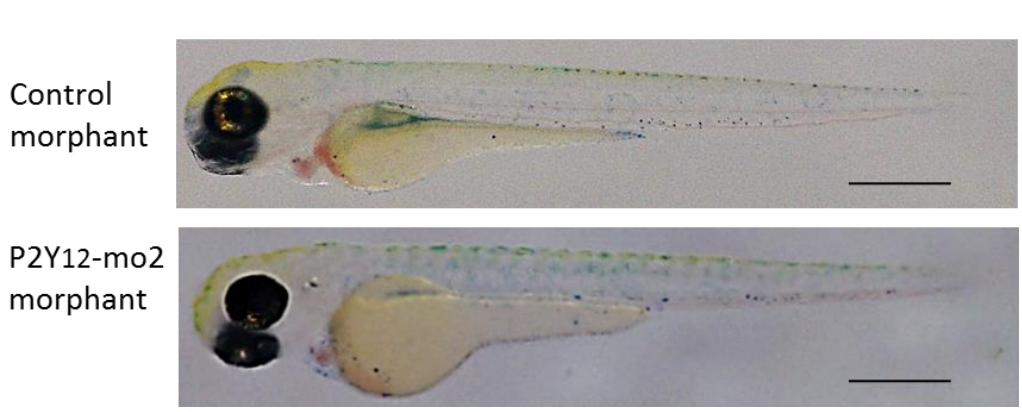

Figure 3.15 P2Y12-mo2 target and morphant morphology at 3 dpf.

A shows, highlighted in red, the target of the published P2Y12-mo2 within the 5' untranslated region of *p2y12* (Sieger et al., 2012). Underlined is the *p2y12* morpholino custom designed for my project. **B** shows the morphology of both control and P2Y12-mo2 morphant 3 dpf embryos in the *nacre* background, there appears to be no significant morphological difference. Scale bars represent 500 µm.

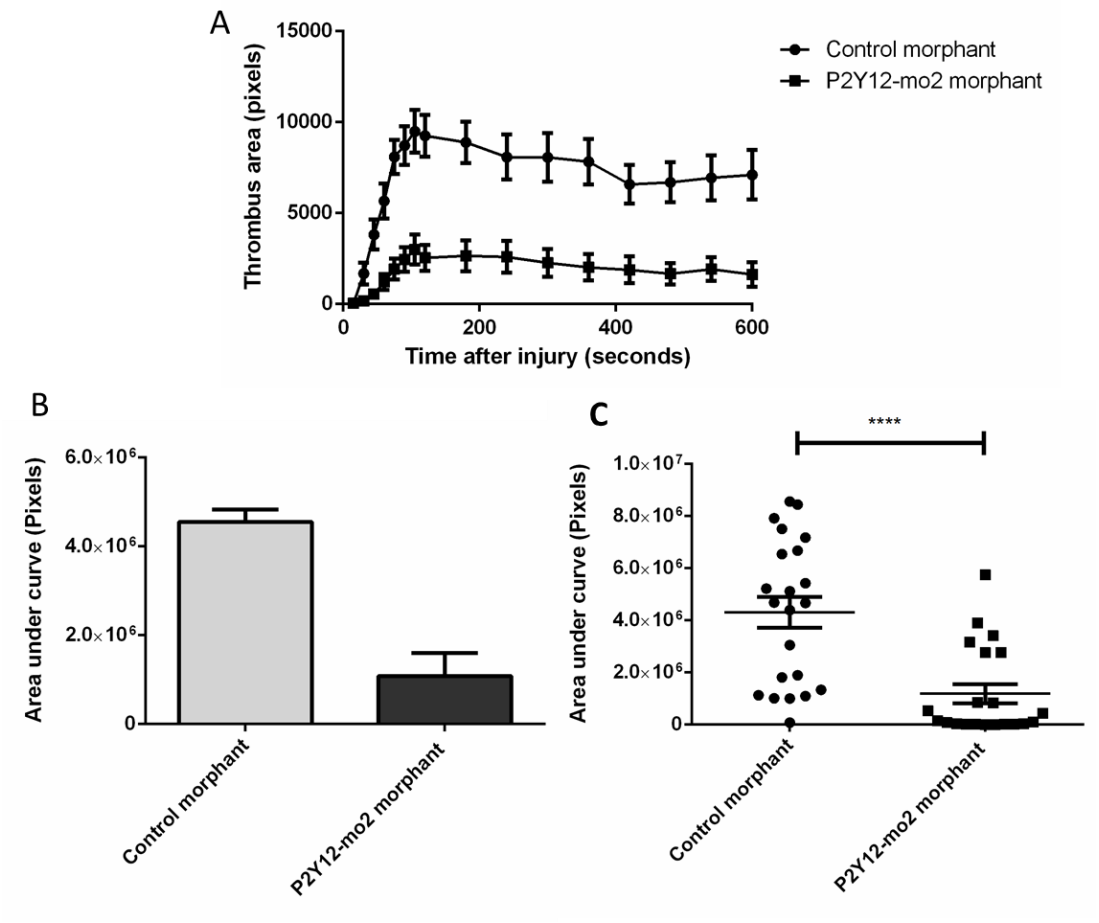

Figure 3.16 The effect of P2Y12-mo2 on thrombosis.

The published P2Y12-mo2 morpholino was utilised to knockdown *p2y12* (Sieger et al., 2012). The thrombotic response after laser induced injury of the aorta was assessed as in **Figure 3.13**. Groups of 6-7 P2Y12-mo2 morphant or control embryos underwent laser induced aortic injury and thrombus area was quantified over 10 mins. Three replicate experiments were performed on different days. **A** shows a plot of thrombus area over 10 minutes following laser induced aortic injury, where every embryo has been considered as a separate experiment (n=22 control and n=21 P2Y12-mo2 morphants). **B** shows the mean area under the curve in P2Y12-mo2 morphants or controls where data has been analysed by combining each experimental replicate into a single mean (n=3, p=0.1). **C** shows a scatter graph with each individual embryo represented as an experimental unit ($p<0.0001$). A Mann Whitney test was applied to both **B** and **C**, data is presented as mean ± SEM.

3.1.3 Investigating the specificicity of the *p2y12* morpholino effect

3.1.3.1 Investigation into possible cross-reacting P2Y$_{12}$ antibodies

One method for confirming that morpholino knockdown has reduced translation of RNA to protein, is by western blotting. This requires a specific antibody to the zebrafish peptide sequence. I investigated whether there would be suitable antibodies available for detection of P2y12 in the zebrafish. **Figure 3.17** shows an alignment of the human and zebrafish P2y12 peptide sequences, with the epitopes targeted by currently available antibodies highlighted. **Table 3.3** shows the details of these antibodies, including the currently known species cross reactivity. I found a relatively low sequence homology between human and zebrafish in the epitopes recognised by these antibodies. This precluded using western blotting to confirm protein knockdown.

Figure 3.17 P2Y12 antibody peptide targets

This shows a ClustalW alignment of human P2RY12 and zebrafish P2y12, highlighted are examples of peptide sequences targeted by commercially available P2Y12 antibodies. Highlighted in yellow is the antibody available from Alomone labs APR-012(Israel), red font underlined shows the antibody available from Sigma Aldrich, UK. Blue highlighting shows the antibody available from Alomone labs APR-020 (Israel), and purple shows the antibody available from Novus Biologicals, USA.

Table 3.3 Currently available P2Y12 antibody target sequences and their percentage identity.

Examples of antibody targets in the human *P2RY12* sequence is shown along with the zebrafish *p2y12* percentage identity of this target. Also included are details of the species reactivity and product information.

P2Y12 amino acid target in the human sequence	Percentage identity of target sequence between human and zebrafish (%)	Species tested in	Product information
(C)KTTRPFKTSNPKNLLGAK	55	Human, rat and mouse	Alomone Labs, Israel, #APR-012
YQKTTRPFKTS	36	Human	Sigma Aldrich, Gillingham, UK #6997
CTAENTLFYVKES	38	Human, rat and mouse	Alomone Labs, Israel, #APR-020
SLSQDNRKKEQDGGDPNEETPM	9	Human and primate	Novus Biologicals, USA NBP1-78249

3.1.3.2 Does overexpression of zebrafish *p2y12* mRNA rescue the effect of the *p2y12* morpholino on thrombosis?

In an attempt to assess the specificity of my custom designed *p2y12* ATG morpholino, I synthesised a *p2y12* mRNA construct to which the morpholino should not bind, but which would produce the correct $P2Y_{12}$ peptide. This was achieved by changing the codons in the sequence targeted by the morpholino to synonymous codons to which the MO was not complementary (**Figure 3.18**). In dose ranging optimisation studies, **Table 3.4**, I found that co-injection of 34.6 pg mRNA with 1.2ng of either a control or *p2y12* MO induced a 7% rate of abnormality (similar to injections with a control morpholino or uninjected embryos in other experiments). Bright field micrographs of 3 dpf embryos after co-injection of *p2y12* RNA with control or *p2y12* MO, are shown in **Figure 3.19**.

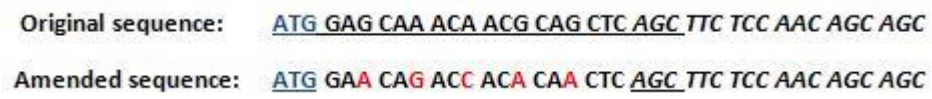

Figure 3.18 *p2y12* sequence with both the original sequence and the amended sequence with the morpholino target under lined.

The ATG start site of *p2y12* is shown in blue font, the morpholino target is underlined, and the primer target is in italics. I changed a nucleotide from each codon to ensure the same peptide was translated but that the morpholino should not bind.

Table 3.4 Optimisation of *p2y12* RNA amount for co-injection with *p2y12* morpholino.

The amount of RNA was optimised by co-injecting several different amounts of miss matched *p2y12* RNA along with 1.2 ng of either control or *p2y12* morpholino. The amount of RNA in picograms is shown, along with the percentage of embryos with toxic phenotype compared to percentage of viable embryos. 34.5 pg was selected as the highest amount of RNA which only resulted in a minority of embryos with a toxic phenotype, such as delayed development, cardiac oedema or small heads.

Amount of *p2y12* RNA injected (pg)	**Percentage of embryos with toxic phenotype (%)**		**Percentage of viable embryos (%)**		**Number of embryos injected**	
	Control mo	***p2y12* mo**	**Control mo**	***p2y12* mo**	**Control mo**	***p2y12* mo**
277	31	56	69	44	60	87
138.5	20	30	80	70	40	60
69.25	12	23	88	77	42	68
34.6	13	7	87	93	14	107

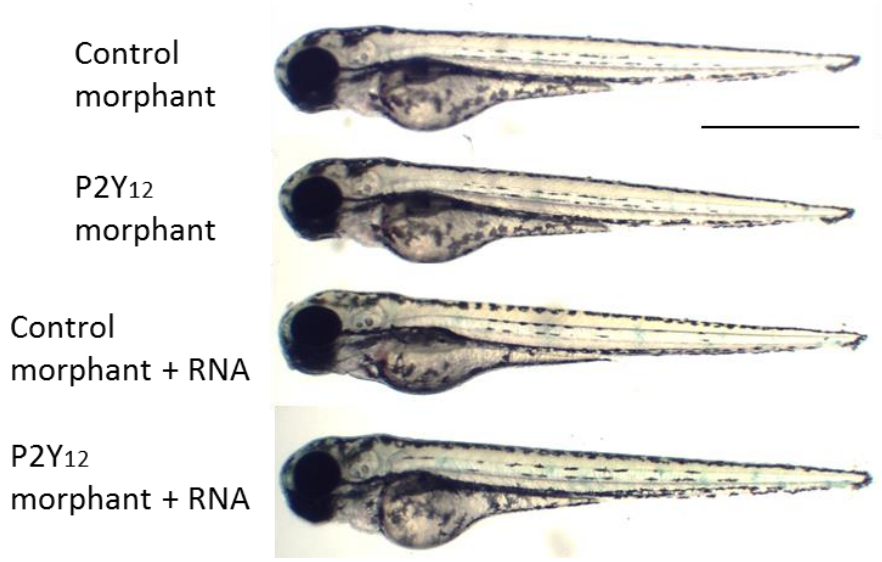

Figure 3.19 Gross morphology of 3 dpf embryos after injection of control morpholino with/without *p2y12* RNA and *p2y12* morpholino with/without RNA.

The gross morphology of control morphants, *p2y12* morphants, control morphants co-injected with *p2y12* RNA and *p2y12* morphants co-injected with *p2y12* RNA are shown at 3 dpf. There appears to be no significant dfference in gross morphology of embryos after *p2y12* RNA and morpholino co-injection. Scale bar represents 1 mm.

I then assessed the effect of mRNA injection on laser-induced thrombosis in 3 dpf embryos co-injected with *p2y12* or control morpholino. **Figure 3.20 A** shows the thrombus area plotted over 10 minutes, **B** shows the area under the curve of this data as means per replicate, and **C** shows the data from each individual embryo. Injection of *p2y12* mRNA into control morphants was associated with a non-significant reduction in thrombus after injury, compared with control morpholino alone. As expected, *p2y12* knockdown significantly reduced thrombosis. Co-injecting *p2y12* morphants with *p2y12* mRNA was associated with a slightly less pronounced reduction in thrombosis, with the result that there was no significant difference in thrombosis between control morphants and *p2y12* mRNA/*p2y12* MO injected embryos, although there remained a clear trend to a reduction in thrombosis. The *p2y12* mRNA was therefore unable to definitively rescue the morphant phenotype.

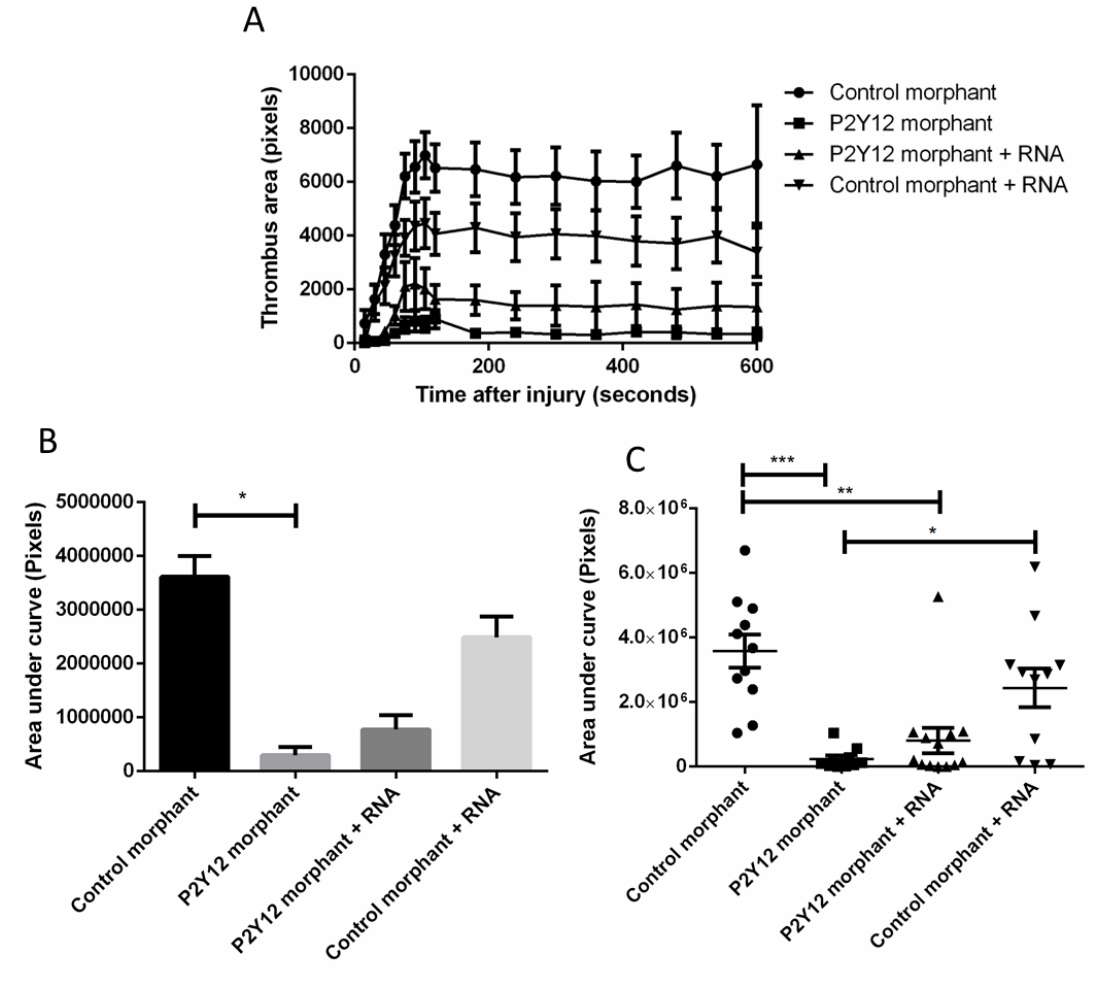

Figure 3.20 Thrombosis response in control and *p2y12* morphants with and without co-injection of *p2y12* RNA.

The thrombotic response after laser induced injury of the aorta was assessed as in **Figure 3.13**. Groups of 3-4 *p2y12* morphant or control embryos with or without co-injection with *p2y12* RNA, underwent laser induced aortic injury and thrombus area was quantified over 10 mins. Three replicate experiments were performed on different days. **A** shows a plot of thrombus area over 10 minutes following laser induced aortic injury, where every embryo has been considered as a separate experiment (n=11 control, n=10 *p2y12* morphants, n=11 control co-injected with *p2y12* RNA and n=13 *p2y12* morphants co-injected with *p2y12* RNA). **B** shows the mean area under the curve in *p2y12* morphants or controls where data has been analysed by combining each experimental replicate into a single mean (n=3) There is a significant reduction in thrombus area between control and *p2y12* morphants (* = mean rank difference 8.33). **C** shows a scatter graph with each individual embryo represented as an experimental unit. There is a significant reduction between control morphant and *p2y12* morphant (***= mean rank difference 23.21), control morphant and *p2y12* morphant with RNA (** = mean rank difference 18.4). There is a significant increase between *p2y12* morphant and control morphant with RNA (* = mean difference -15.49). A Kruskal-Wallis with Dunn's multiple comparison test was applied. These data and are presented as mean ± SEM.

3.1.4 Does treatment with P2Y$_{12}$ antagonists reduce thrombus formation?

Treatment of mice with ticagrelor reduces thrombus formation to a similar extent as seen in *P2Y$_{12}$ -/-* mice (Patil et al., 2010). I therefore investigated whether clinically used P2Y$_{12}$ antagonists have similar effects in the zebrafish model. 2 dpf embryos were incubated overnight with the reversible P2Y$_{12}$ antagonist ticagrelor and the effect on thrombosis was assessed. Preliminary data from this single experiment showed that exposure to 25 µM ticagrelor may reduce heart rate, however in this preliminary single experiment, no clear evidence of an effect on thrombus area was observed compared to controls (**Figure 3.21**). Ticagrelor has been shown to induce ventricular pauses in patients with acute coronary syndrome and so any effect on heart rate would be interesting and potentially relevant (Scirica et al., 2011). I therefore repeated this experiment with a lower concentration of ticagrelor (20 µM), which appeared to induce no difference in heart rate or thrombus area, between control and ticagrelor exposed embryos (**Figure 3.22**). These preliminary results suggest that treatment with ticagrelor at these concentrations has no significant effect on thrombus formation. The effect of 25 µM ticagrelor on heart rate indicates that the drug may have penetrated sufficiently to induce a physiological effect, though it is possible that this was insufficient to affect thrombosis. These data represent 1 and 2 experimental replicates respectively, therefore no statistical analysis was applied and they require replication before their results can be interpreted.

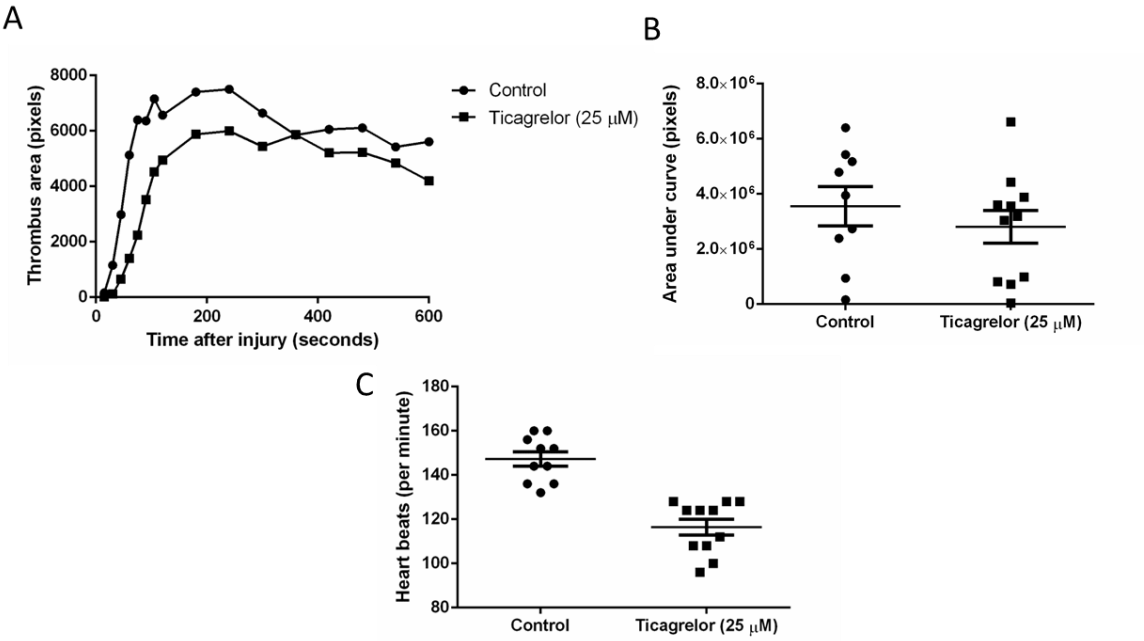

Figure 3.21 Effect of 25 μM ticagrelor on thrombus formation in 3 dpf embryos.

Groups of 10 control and 11 ticagrelor exposed embryos underwent laser induced aortic injury and thrombus area was quantified over 10 mins. **A** shows a plot of thrombus area over 10 minutes following laser induced aortic injury. **B** shows a scatter plot of the area under the curve of thrombus and **C** shows a scatter plot of heart rate in control and ticagrelor exposed embryos. This data represents a single experiment with out replication, with each embryo representing a single experimental unit. Therefore no statistical test was applied. Data is presented as mean ± SEM.

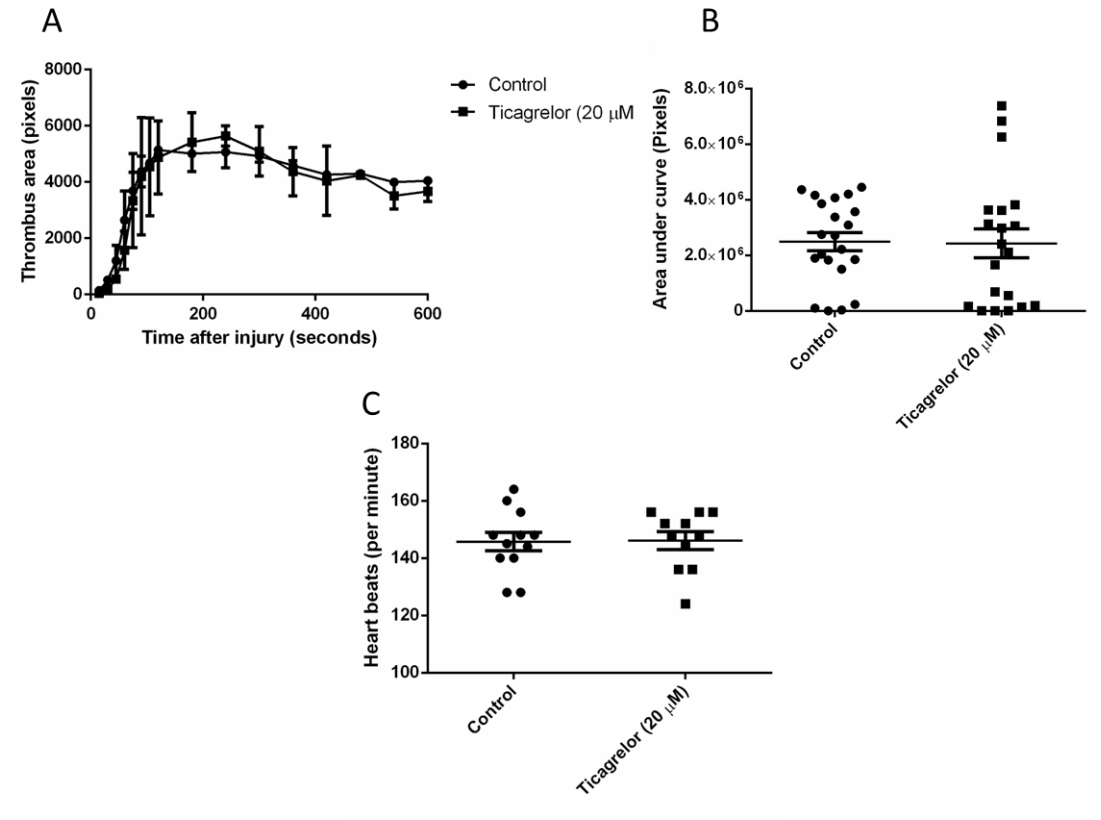

Figure 3.22 Effect of 20 µM ticagrelor on thrombus formation in 3 dpf embryos.

Groups of 10-11 control and ticagrelor exposed embryos underwent laser induced aortic injury and thrombus area was quantified over 10 mins. Two replicates were performed on different days (control n=21 and ticagrelor n=20). **A** shows a plot of thrombus area over 10 minutes following laser induced aortic injury. **B** shows a scatter plot of the area under the curve of thrombus and **C** shows a scatter plot of heart rate in control and ticagrelor exposed embryos. This data represents 2 independent experiments, with each embryo representing a single experimental unit. Therefore no statistical test was applied. Data is presented as mean ± SEM.

The irreversible $P2Y_{12}$ antagonist prasugrel usually requires activation by liver cytochrome isoenzymes to its active metabolite, prasugrel active metabolite (PAM). I therefore next investigated the effect of PAM on thrombosis. I treated 3 dpf embryos with 20 µM PAM, two hours before laser injury. **Figure 3.23 A** and **B** shows that there appears to be no difference in thrombosis between control groups and PAM treated groups. Increasing the concentration of PAM to 50 µM (**Figure 3.23 C and D**) also appeared to have no effect on thrombosis. These data are the result of single experiments respectively therefore no statistical analysis was applied to this data. Further experimentation would be required to identify if PAM affects thrombosis response in this model.

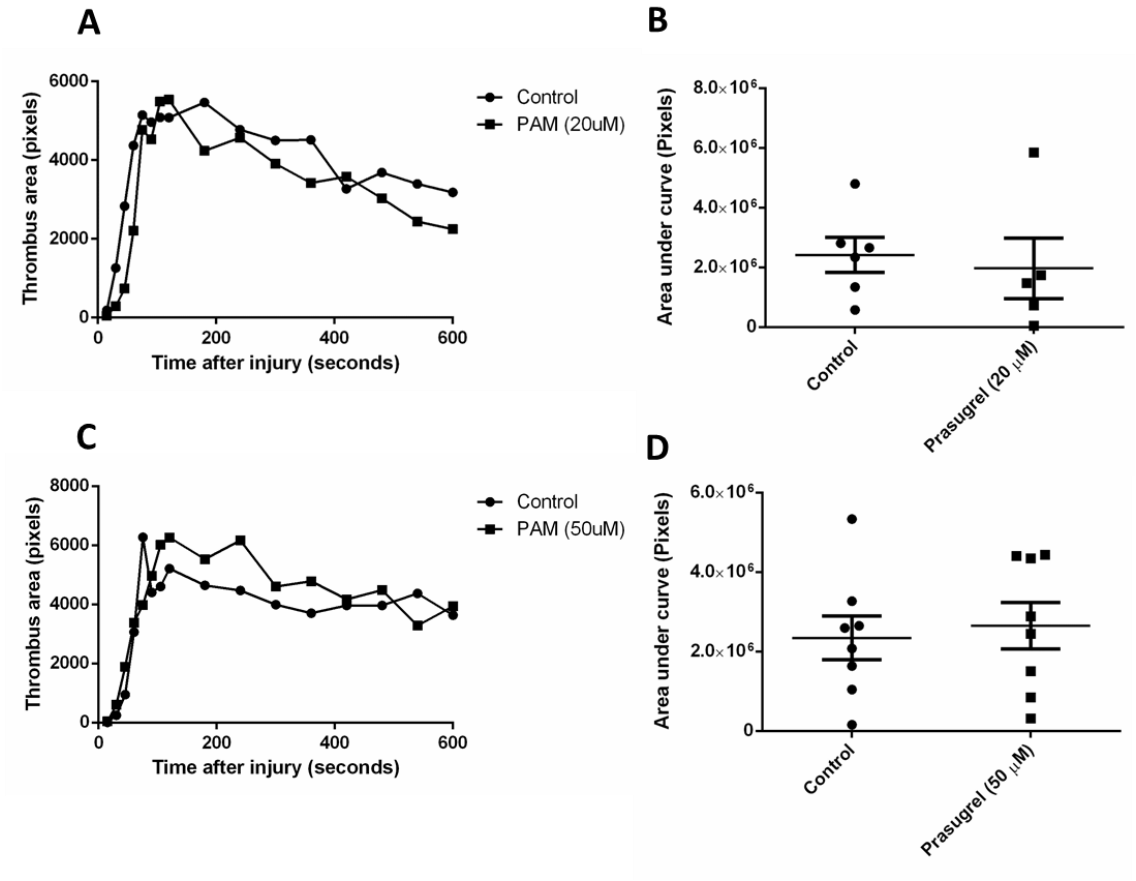

Figure 3.23 Effect of 20 µM and 50 µM prasugrel active metabolite (PAM) on thrombosis in 3 dpf embryos.

Groups of 5-8 control and PAM exposed embryos underwent laser induced aortic injury and thrombus area was quantified over 10 mins. 3 dpf embryos were exposed to PAM at 20 µM (**A** and **B**) and 50 µM (**C** and **D**). **A** and **C** shows plots of mean thrombus area against time over 10 minutes. Graphs **B** and **D** show scatter plots with each individual embryo represented as an independent experimental unit. Data presented as mean ± SEM. All graphs represent a single experimental replicate, with each embryo representing a single experimental unit, therefore no statistical test was applied.

3.1.5 Do platelet microRNAs play a role in thrombosis?

3.1.5.1 Selection of platelet miRNAs for investigation

A cluster of miRNAs which are highly expressed by platelets have been implicated in MI risk, however their functional involvement in thrombosis is unknown (Zampetaki et al., 2012). miR-24, miR-126 and miR-223 were selected from these differentially expressed miRNA species to investigate their roles in thrombosis. miR-223 has a predicted binding site in the 3' UTR region of *P2RY12* mRNA in humans, indicating a potential role for regulation of P2y12 protein expression (Landry et al., 2009). Both miR-223 and miR-126 levels are reduced after anti-platelet therapy, indicating a possible use as biomarkers for platelet activation. I therefore sought to investigate the previously undetermined roles of miR-223, miR-126 and miR-24 in thrombosis.

3.1.5.2 Knockdown of miR-24, miR-126 and miR-223 does not affect vascular development

Before assessing any effect on thrombosis, it was important to ascertain whether knockdown of these miRNAs affected vascular development. I therefore used MO induced knockdown of each miRNA in *Fli1:*GFP transgenic embryos and examined the vasculature at 3 dpf (**Figure 3.24).** I detected no abnormality in vascular development, such as aberrant branching or looping, in the miR morphants compared with controls.

Table 3.5 Optimisation of morpholino amounts for each miRNA morpholino

The dose response of each miRNA morpholino was optimised for injection. An appropriate amount was deemed sufficient to cause a toxic phenotype in only a minority of embryos. This table shows the amount of morpholino injected (ng) and percentages of embryos with toxic phenotypes, such as small head, delayed development or cardiac oedema. This table also includes the percentage of viable embryos – embryos deemed suitable for experimental use, with no non-specific toxic phenotype. The following amounts were selected: miR-223 3.49 ng, miR-126 4.22 ng and miR-24 2.1 ng.

Morpholino target	Amount of miR morpholino (ng)	Percentage embryos with toxic effects (%)	Percentage of viable embryos (%)	Volume injected (nl)	Number of embryos injected
miR223	6.98	64	36	1	30
	3.49	28	72	0.5	50
miR-126	7	73	27	1	40
	4.22	27	73	1	78
mir-24	4.21	96	4	1	40
	3.49	32	67	0.5	43
	2.1	28	72	0.5	40

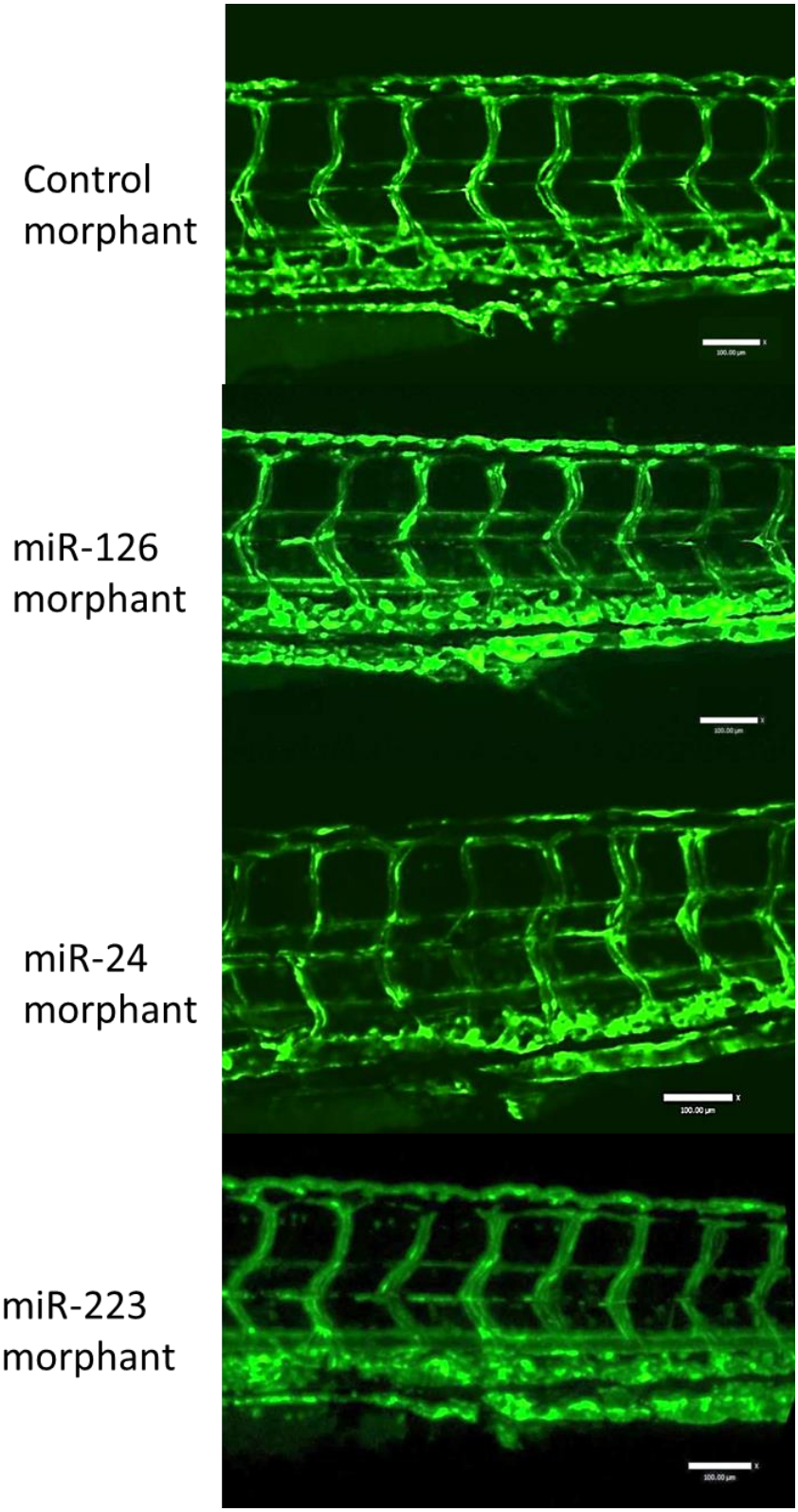

Figure 3.24 Vascular morphology in miR morphant 3 dpf *Fli1*:GFP embryos.

The vasculature of the trunk is shown for control, miR-126, miR-24 and miR-223 morphants at 3 dpf, in the *Fli1*:GFP genetic background. Scale bars represent 100 µm.

3.1.5.3 Knockdown of either miR-24 or miR-126 does not affect thrombosis

Figure 3.25 shows the effect of miR-24 knockdown on thrombus after laser injury. Three experimental replicates of n=9-10 embryos/group were performed. **Figure 3.25 A** shows the area of thrombus over 10 minutes following injury with each embryo considered as a single experiment (n=29-30/group). I analysed the area under the curve for the data shown in **Figure 3.25 A**, and expressed this as either the mean value per replicate experiment (n=3/group, **Figure 3.26 B**) or by individual embryo (n=30-31/group, **Figure 3.26 C**). No statistically significant differences between groups were detected by either approach.

Figure 3.26 shows the effect of miR-126 knockdown on thrombus after laser injury in the same assays, after three experimental replicates on separate days. **Figure 3.26 A** shows the area of thrombus over 10 minutes with each embryo considered a single experimental unit (n=31-30/group). I then analysed the area under the curve of this data and in **Figure 3.26 B** this is expressed as mean value per replicate (n=3/group) and for **Figure 3.26 C** as individual embryos (n=31-30/group). As for miR-24, I did not detect any statistically significant effect of miR-126 knockdown on thrombosis.

It is important to note that the laser system used for the data obtained previously in this chapter was changed prior to investigation of the effect of miRNA knockdown. Therefore, there is a difference when comparing control thrombus area from the previous laser system to the laser system utilised for investigation of miRNA. However, it is equally important to state that this laser system remained unchanged throughout the investigation of miRNA effect, therefore miRNA results can be compared to each other.

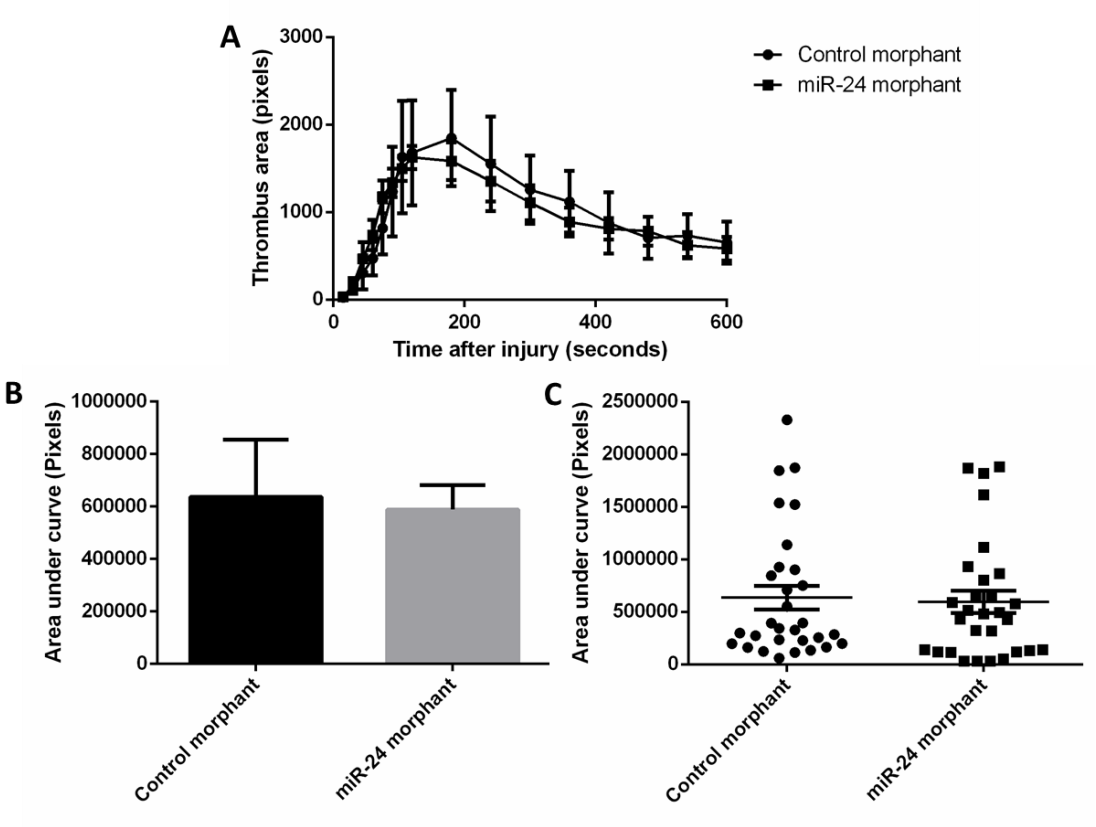

Figure 3.25 Effect of miR-24 knockdown on thrombosis response.

Groups of 9-10 miR-24 morphant or control embryos underwent laser induced aortic injury and thrombus area was quantified over 10 mins. Three replicate experiments were performed on different days. **A** shows a plot of thrombus area over 10 minutes following laser induced aortic injury, where every embryo has been considered as a separate experiment (n=30 control and n=29 miR-24 morphants). **B** shows the mean area under the curve in miR-24 or control morphants where data has been analysed by combining each experimental replicate into a single mean (n=3/group p=0.9). **C** shows a scatter graph with each individual embryo represented as an experimental unit (p=0.73). A Mann Whitney test was applied to both **B** and **C**, data is presented as mean ± SEM.

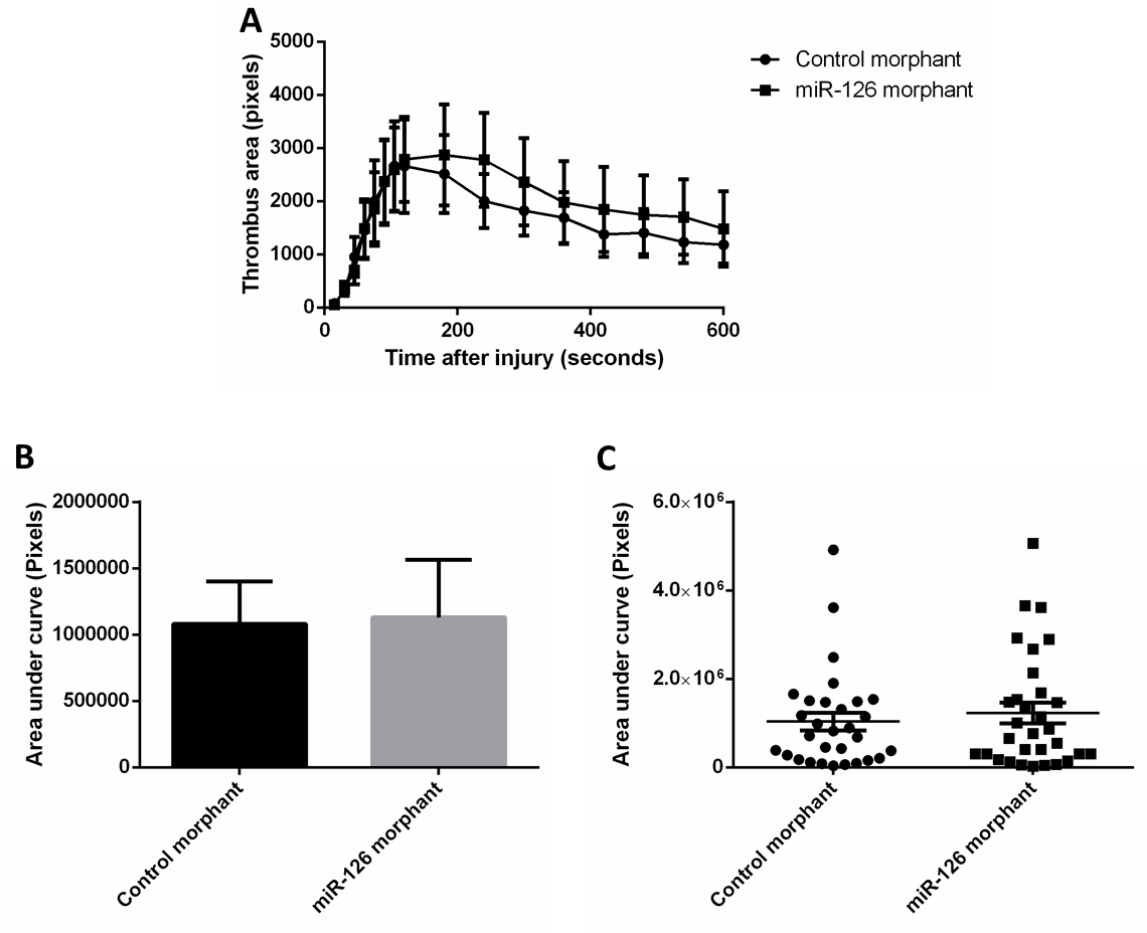

Figure 3.26 Effect of miR-126 knockdown on thrombosis response.

Groups of 10-11 miR-126 morphant or control embryos underwent laser induced aortic injury and thrombus area was quantified over 10 mins. Three replicate experiments were performed on different days. **A** shows a plot of thrombus area over 10 minutes following laser induced aortic injury, where every embryo has been considered as a separate experiment (n=31 control and n=30 miR-126 morphants). **B** shows the mean area under the curve in miR-126 or control morphants where data has been analysed by combining each experimental replicate into a single mean (n=3 p=0.9). **C** shows a scatter graph with each individual embryo represented as an experimental unit (p=0.77). A Mann Whitney test was applied to both **B** and **C**, data is presented as mean ± SEM.

3.1.5.4 Knockdown of miR-223 significantly increases thrombus area

The 3' UTR of *P2RY12* mRNA contains a miR-223 binding site, indicating that miR-223 may regulate P2y12 protein expression (Landry et al., 2009). miR-223 expression level is also inversely associated with MI risk (Zampetaki et al., 2012). Therefore, I hypothesised that miR-223 may play a role in thrombosis after vessel injury. I investigated the thrombosis response of both control and miR-223 morphants.

Figure 3.27 shows the effect of miR-223 knockdown on thrombus after laser injury. Three experimental replicates of n=8-10 embryos/group were performed. **Figure 3.25 A** shows the area of thrombus over 10 minutes following injury with each embryo considered as a single experiment (n=27-28/group). I analysed the area under the curve for the data shown in **Figure 3.27 A**, and expressed this as either the mean value per replicate experiment (n=3/group, **Figure 3.27 B**) or by individual embryo (n=30-31/group, **Figure 3.27 C**). Analysing the data by mean of each replicate showed a non-significant trend towards an increase in thrombus area in miR-223 morphants (**Figure 3.27 B** p=0.13). If each embryo is considered a separate experiment, then this difference becomes highly significant (**Figure 3.27 C** p=0.0013). These results suggest that knockdown of miR-233 may increase thrombus area and hence that miR-223 negatively regulates thrombus formation by some mechanism.

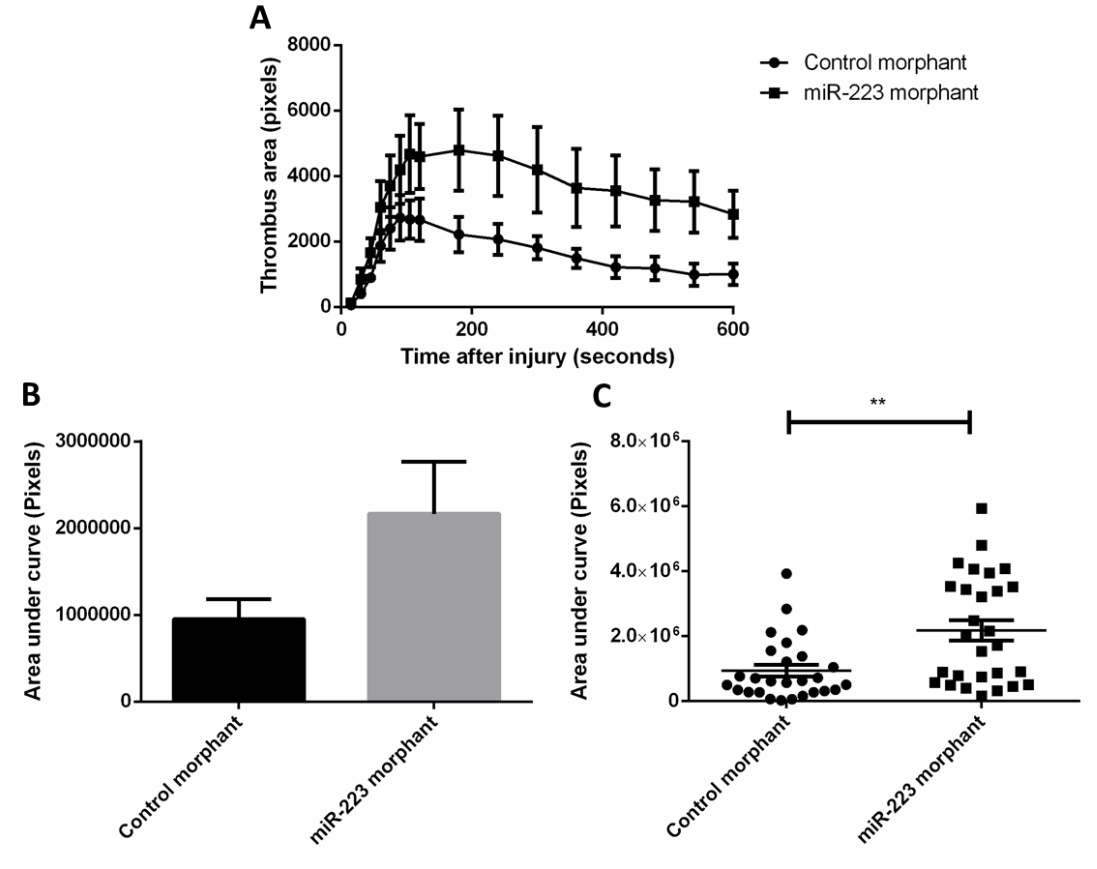

Figure 3.27 Effect of miR-223 knockdown on thrombosis response.

Groups of 8-10 miR-223 morphant or control embryos underwent laser induced aortic injury and thrombus area was quantified over 10 mins. Three replicate experiments were performed on different days. **A** shows a plot of thrombus area over 10 minutes following laser induced aortic injury, where every embryo has been considered as a separate experiment (n=27 control and n=28 miR-223 morphants). **B** shows the mean area under the curve in miR-223 or control morphants where data has been analysed by combining each experimental replicate into a single mean (n=3 p=0.2). **C** shows a scatter graph with each individual embryo represented as an experimental unit (p=0.002). A Mann Whitney test was applied to both **B** and **C**, data is presented as mean ± SEM.

3.2 Discussion

I have shown that *p2y12* is expressed in the zebrafish, at the mRNA level. The key residues involved in ligand binding in the human $P2Y_{12}$ receptor, such as Y^{105}, E^{188}, R^{256}, Y^{259} and K^{280}, are conserved in the zebrafish genome. The expression patterning for *p2y12* in the developing embryo via whole mount *in situ* hybridisation was consistent with what might be expected (**Figure 3.4**), corresponding to sites of both primitive haematopoiesis and definitive haematopoiesis. The expression pattern is similar to GFP positive cells in the CD41:GFP transgenic embryos, with clustering of GFP positive cells at 33-35 hpf in the AGM region before migrating to the CHT and thymus by 48 hpf (Kissa et al., 2008). The morphology and size of the expressing cells are consistent with thrombocytes, as they are larger than HSC and round, unlike macrophages. This, combined with the location of the staining, means it is likely that many of the cells expressing *p2y12* are thrombocytes. However, as sites of haematopoiesis also produce myeloid cells, and *P2RY12* is believed to be expressed on macrophages, it is possible that *p2y12* expressing cells include a subpopulation of macrophages. There are fewer stained cells in the *p2y12 in situ* when compared to an *in situ* for the leukocyte specific *L-plastin* (**Figure 3.5**), suggesting that *p2y12* is not present on both macrophages and neutrophils, however this will require further work to investigate whether there is co-localisation of *p2y12* and leukocytes. This would be possible by conducting an *in situ* for *p2y12* alongside an antibody stain against GFP in *mpo*:GFP or *mpeg*:GFP. It would also be possible to perform *in situ* hybridisation for $P2Y_{12}$ in an anaemic mutant line in which no thrombocytes were present and any staining would indicate the presence of *p2y12* on alternative cells to thrombocytes.

A *p2y12* specific ATG MO was utilised to knockdown expression of the $P2Y_{12}$ receptor. No significant differences in gross morphology or vessel development in *p2y12* morphants was observed (**Figures 3.6** and **3.7**), enabling this MO to be utilised for further investigation of the effect of *p2y12* knockdown. To investigate whether there was a loss of function of $P2Y_{12}$ in the morphants, a laser was utilised to injure the endothelium of the ventral wall of the dorsal aorta. This injury was

sufficient to induce thrombosis (although this was somewhat variable, necessitating large group sizes). This mechanism for inducing vessel damage activates the tissue factor pathway and leads to thrombin formation (Falati et al., 2002). Therefore, this assay encompasses many factors involved in thrombus development and required for accurate modelling of thrombosis response, such as thrombus development, stability and embolization. I found that knockdown of *p2y12* significantly reduced thrombus formation after laser-induced injury ($p<0.0001$) (**Figure 3.13**). In the *p2y12* morphants, some thrombi did form after injury (**Figure 3.14**) but there were significantly fewer than observed in control morphants ($p<0.0001$). These results are consistent with those seen in the *P2Y12 -/-* mouse, in which thrombus formation is reduced and bleeding times after tail transection are increased (Foster et al., 2001, Andre et al., 2003, Patil et al., 2010). Increased embolization of thrombi was also observed in *P2Y12 -/-* mice, corresponding to the results shown above in the *p2y12* morphants (Andre et al., 2003). My results suggest that P2Y12 receptor mediated amplification of thrombosis is conserved in the zebrafish and blocking of translation of *p2y12* by an ATG MO is sufficient to produce a loss of function phenotype in the 3 dpf embryo. The mechanisms for P2Y12 activation and the subsequent downstream signalling are yet to be elucidated in the zebrafish, and further work will be required to investigate whether the signalling pathways and mechanism in mammals are also conserved in the zebrafish.

The effects of splice modifying MO on target mRNA can be determined by RT-PCR to identify aberrant splicing. ATG start site MO, however, do not affect splicing of the gene therefore it is not possible to confirm the effect of the MO by RT-PCR. This presented a challenge to assess whether the *p2y12* MO was truly inducing a loss of function of P2Y12. One solution to this would be a western blot to determine presence of the P2y12 protein in the *p2y12* morphants. However, as shown in **Figure 3.15** and **Table 3.3**, although there are several commercial P2Y12 antibodies available, the epitopes targeted by these antibodies show a relatively low homology to the zebrafish. During the course of my work a p2y12::P2Y12-GFP transgenic became available (Sieger et al., 2012). Sieger et al. (2012) utilised the p2y12::P2Y12-GFP transgenic line to quantify fluorescence of *p2y12* expressing microglia in *p2y12*

and control morphants, showing a reduction in fluorescence in *p2y12* morphants. I obtained this transgenic, imaged both control and *p2y12* morphants, and also observed a reduction in GFP fluorescence in microglia in my *p2y12* morphants, (using my own morpholino, not the similar MO used by Sieger). In addition to this I sought to investigate whether thrombocytes expressed GFP in this transgenic. I imaged the CHT region of both control and *p2y12* morphants and observed an apparent reduction in fluorescence in *p2y12* morphants. Due to the low fluorescence of this transgenic, difference in fluorescence between control and *p2y12* morphants was not quantified, therefore this would require quantification to confirm whether translation of the P2y12 protein is reduced in the *p2y12* morphants. The GFP positive cells I observed in the CHT mostly corresponded to the thrombocytes seen in the same regions seen in the CD41:GFP transgenics. However, it is also possible that some of the p2y12::P2Y12-GFP positive cells are a subpopulation of macrophages, as $P2Y_{12}$ is proposed to be expressed on macrophages and this transgenic, as previously shown, has been utilised to visualise microglia. Therefore these results indicate that the morpholino generated for this thesis is indeed reducing, if not fully preventing, translation of $P2Y_{12}$.

In addition to using the p2y12::P2Y12-GFP transgenic to attempt to assess the effect of my *p2y12* morpholino, I also obtained the *p2y12* morpholino ($P2Y_{12}$mo2) published along with this transgenic (Sieger et al., 2012). I sought to investigate whether injection of $P2Y_{12}$mo2, which targets the 5' UTR region of *p2y12*, would have a similar effect on thrombosis after laser induced vessel injury. Knockdown with this morpholino showed a trend for reduced thrombus formation in P2Y12mo2 morphants, which was not statistically significant when analysed with a single mean for each experimental replicate ($p=0.1$). This reduction was statistically significant when analysed with each embryo representing a separate experiment ($p<0.0001$ **Figure 3.17 C**). Therefore, this would require further replication to allow firm conclusions to be drawn. However, taken together with my data from my other morpholino, these results suggest that morpholino knockdown of *p2y12* induces a loss of function of $P2Y_{12}$, leading to a reduction in thrombosis (Sieger et al., 2012).

Since morpholinos may induce off-target effects, I sought to confirm the specificity of the effect of the morpholino by attempting to rescue its effects by overexpression of *p2y12* mRNA engineered to be non-complementary to the morpholino sequence. To do this, I generated *p2y12* mRNA with alternate codons at the morpholino binding portion of the RNA, enabling the correct peptide to be translated, but preventing interaction of the co-injected mRNA with the morpholino. I found that co-injection of *p2y12* RNA with control and $P2Y_{12}$ morpholino may have diminished the reduction in thrombosis seen in *p2y12* morphants alone (**Figure 3.20**). It is important to note that global mRNA overexpression will overexpress the construct in a mosaic fashion throughout the embryo. *p2y12* mRNA overexpression did not increase thrombosis compared with controls; in fact there was a trend to reduced thrombosis. The observation that the *p2y12* mRNA blunted the effect of the *p2y12* morpholino suggests that, although co-injection with this altered *p2y12* RNA does not fully rescue the reduced thrombosis phenotype of *p2y12* morphants, it may induce a partial rescue of thrombosis response.

There are several potential reasons for *p2y12* mRNA not fully rescuing the anti-thrombotic phenotype of the *p2y12* morphants; when designing the mismatched portion of RNA, I changed 6 nucleotides since I matched alternate codons according to the prevalence of those codons (as per www.ZFIN.com). Therefore, it is possible that a change of 6 nucleotides, although evenly distributed throughout the morpholino target sequence, may still be sufficient for some binding with the morpholino. It is also possible that the *p2y12* mRNA has degraded by 3 dpf, and therefore was not able to exert sufficient effect. It would be possible to examine thrombosis at 2 dpf instead, as there is an increased chance that the RNA will be present, or to generate a GFP labelled construct to confirm expression at the time points of interest. However, I chose to examine 3 dpf embryos to be consistent with my previous studies and I did not have time to generate a labelled construct. It would be possible to use the thrombosis model at 2 dpf instead, as there is an increased chance that the RNA will be present.

MOs are known to induce non-specific toxicity of varying levels according to the MO sequence and dose, leading to a risk of attributing any subsequent MO off-target phenotypes to an effect of gene knockdown. Examples of this are delayed development, small heads and cardiac oedema. It is generally accepted that many of these off-target effects occur via activation of the p53 pathway (Robu et al., 2007). Therefore co-injection of the *p2y12* morpholino with a p53 morpholino would be another approach to determine whether the effects of the *p2y12* morpholino are specific. Due to recent improvements in generation of targeted mutations, it is possible to validate phenotypes observed after gene knockdown by comparison with a stable or transient mutant. In chapter 5, I detail my efforts to generate such a stable *p2y12* mutant.

My preliminary data on the effect of ticagrelor and prasugrel active metabolite contrasts with data obtained from mouse models, as preliminary data indicates that neither ticagrelor nor prasugrel active metabolite appeared to affect thrombosis in my studies. Data obtained from a single experiment showed exposure of embryos to 25 µM of ticagrelor, but not 20 µM, may reduce heart rate compared to the control group (**Figure 3.21** and **3.22**). This indicates the drug may have entered the circulation sufficiently to induce a physiological effect, as ticagrelor increases the incidence of bradycardia and bradyarrhythmia, such as ventricular pauses (Cannon et al., 2007). It is proposed that this effect may be due to off-target effects of ticagrelor on adenosine reuptake (Scirica et al., 2011). The implication of my preliminary findings is that ticagrelor may be reaching the circulation of the embryo but not exerting any effects on thrombus formation. However, caution should be taken when interpreting these results, as these data represents a single experimental replicate; it will require further investigation to discover if this antagonist is sufficiently active in zebrafish to induce off-target effects on adenosine re-uptake but is insufficient to induce targeted effects on thrombosis. This serves to highlight that there are differences between animal models, and that there is a possibility that although the key functions of the $P2Y_{12}$ receptor are conserved in the zebrafish, different mechanisms for activation may be present. Although the residues for the ADP binding site are conserved in zebrafish *p2y12,*

ticagrelor binds $P2Y_{12}$ at a site distinct from this, the location of which is not currently known; therefore we do not know whether these residues are conserved in the zebrafish. Biochemical and signalling studies would be required to investigate this further, which were outside the scope of my project. The mechanism for exposure of the embryos to these antagonists could also provide a reason for the lack of effect, as drugs were dissolved in DMSO and added to the media. The development of zebrafish embryos is affected if DMSO is above a 1% final concentration, therefore this was never exceeded. However, this concentration of DMSO may have been insufficient. Drugs are primarily taken up into circulation via entry through the skin and a lower concentration of DMSO may have impaired this (Rombough, 2002). It is an increasingly common practice to expose zebrafish embryos in this way for drug screening, therefore some agents are evidently reaching circulation for an effect to be seen. It remains to be seen whether any other $P2Y_{12}$ antagonists influence thrombosis in the zebrafish. The effect of clopidogrel on zebrafish embryos remains untested for several reasons. Firstly clopidogrel is insoluble in water requiring dissolution in DMSO. However, when I attempted to examine the effect of clopidogrel, the drug came out of solution upon addition to the embryo media. Also clopidogrel requires activation by liver P450 enzymes to be converted to its active metabolite which delays onset of function and these mechanisms are not well characterised in zebrafish (Savi et al., 1994). As part of my investigations the ATP analogue cangrelor was injected into the circulation of 3 dpf embryos and thrombosis was assessed in response to laser injury (data not shown). There were, however, technical challenges with this assay, as the short half-life of cangrelor (approximately 5 minutes) (Storey et al., 2001), required immediate injury of the embryos after injection. There was no significant difference on thrombosis induced by injection of cangrelor when compared to controls but the limitations of the assay may have masked any effect.

My preliminary results suggest that treatment of zebrafish with $P2Y_{12}$ antagonists may not recapitulate the effect seen in humans or mouse. The indication of a lack of effect of $P2Y_{12}$ antagonists on the zebrafish thrombosis response requires further investigation, and it would be beneficial to further explore the reasons why $P2Y_{12}$

antagonists may not be functional in zebrafish. However, it is important to note that these experiments did not contain a positive control to confirm whether these agents were entering the circulation. The apparent trend for reduced heart rate in the preliminary results obtained from the ticagrelor 25μM treated group indicates that perhaps, at this concentration, ticagrelor was indeed entering the embryo to some extent. Although there is increasing interest in the zebrafish as a platform for drug screening ((Mathias et al., 2012) for review), my results suggest caution as my assay would not have detected therapeutic activity with clinically proven antiplatelet agents.

Platelets are known to contain many miRNAs, some of which have been linked to a risk of MI in a study by Zampetaki et al (2012), however these have not been investigated for their roles in thrombosis (Zampetaki et al., 2012). I investigated the effect of knocking down three of these platelet miRNAs on laser induced thrombosis. miR-24 has previously been investigated in the zebrafish. Knockdown of the miR-24 targets PAK4 and GATA2 resulted in an abnormal vessel phenotype, similar to that seen after miR-24 overexpression (Fiedler et al., 2011). I found that knockdown of miR-24 resulted in no abnormal vascular phenotype (**Figure 3.24**). Therefore, this indicates that PAK4 and GATA2 are required for normal vessel development, (Fiedler et al., 2011) however miR-24 may not be. miR-126 has also previously been investigated in the zebrafish model. Fish et al (2008) and Nicoli et al. (2010) injected a miR-126 morpholino with the same sequence, except 6 bases longer than the morpholino used in my experiments, and found ectopic vascular branching and also haemorrhaging. In contrast to these data, I did not observe either phenotype during my investigations (**Figure 3.24**). This may be due to differences in morpholino dose or sequence. For example, Fish et al (2008) injected 4-8 ng and Nicoli et al. (2010) injected 7- 20 ng MO compared to a maximum of 4.22 ng in my investigations. These differences may explain the lack of vascular phenotype seen in my miR-126 morphants. Neither miR-24 nor miR-126 knockdown affected thrombosis in 3 dpf embryos after vessel injury (**Figure 3.25** and **3.26**).

miRNA-223 has not previously been examined in the zebrafish, however it is predicted to have a binding site in the 3'UTR region of *P2RY12* mRNA indicating

that miR-223 may regulate translation of *P2RY12* mRNA to protein, and therefore reduce $P2Y_{12}$ expression (Landry et al., 2009). My results in **Figure 3.27** showed that knockdown of miR-223 significantly increased thrombus area after vessel injury, when analysed considering each embryo as an individual experiment ($p=0.0013$). However, such analysis may be prone to confounding if embryos injected on the same day are not truly independent. When the means of each experimental replicate were analysed, this resulted in a similar trend, although this was non-significant ($p=0.13$) due to the reduction in statistical power. My data suggest that miR-223 may regulate thrombus generation, potentially via reducing expression of *p2y12*. These results are exciting since therapeutic modalities for modulating miR expression are already being clinically studied.

3.3 Conclusion

I used a *p2y12* ATG MO to knockdown receptor expression. This reduced fluorescence in a p2y12::P2Y12-GFP transgenic background, suggesting *p2y12* expression was truly reduced. $P2Y_{12}$ morphants had significantly reduced thrombus formation after laser injury of the aorta when compared to control embryos ($p=0.0005$), an effect also seen with a second, non-overlapping morpholino targeting the 5' UTR of *p2y12* ($p<0.0001$). My results are consistent with previous data obtained from the *$P2Y_{12}$ -/-* mouse, in which thrombus formation was significantly reduced in the $P2Y_{12}$ knockout mice (Foster et al., 2001, Andre et al., 2003). Therefore, I conclude that the *p2y12* MO successfully induces a loss of function of *p2y12* in 3 dpf zebrafish embryos. These results gave me sufficient confidence that I was able to modulate *p2y12* expression to go on to examine a less studied aspect of its function in the next chapter; the role of $P2Y_{12}$ on inflammation and the response to infection.

Chapter 4 : The role of P2Y$_{12}$ in inflammation and resistance to infection

The P2Y$_{12}$ receptor amplifies the release of α granule contents including a multitude of pro-inflammatory mediators and anti-microbial peptides (Zhang et al., 2011). I hypothesised that knockdown of the P2Y$_{12}$ receptor would affect inflammatory processes including leukocyte migration to sites of injury. In order to investigate this, I used a transgenic line with fluorescent reporters under the control of macrophage and neutrophil specific promoters to model an inflammatory response and enable the tracking of leukocytes to sites of injury. I utilised a *Staphylococcus aureus* inoculation model to investigate P2Y$_{12}$ morphants' resistance to systemic infection. *S. aureus* is a Gram-positive bacterium which is a common cause of sepsis (Fowler et al., 2005). Previous investigations have shown that P2Y$_{12}$ plays a key role in the amplification and release of PMP and platelet kinocidins after exposure to *S. aureus* (Trier et al., 2008). Therefore, I hypothesised that knockdown of *p2y12* would affect host resistance to infection.

4.1 Results

4.1.1 Investigating the effect of *p2y12* knockdown on leukocyte response

4.1.1.1 Does knockdown of *p2y12* affect total number of leukocytes?

I first assessed whether knockdown of *p2y12* affected total number of leukocytes in the developing embryo, as a difference in leukocyte number would affect interpretation of leukocyte numbers at the site of injury. I assessed total macrophage and neutrophil counts in the transgenic line *fmsgal4;*UNM*;mpo*GFP in control and *p2y12* morphant groups. **Figure 4.1 A** shows a representative 3 dpf embryo, with red labelled macrophages and green labelled neutrophils. I found no significant difference in either total macrophage number (**B,C**) or total neutrophil number (**D,E**), in the *p2y12* morphants compared to control.

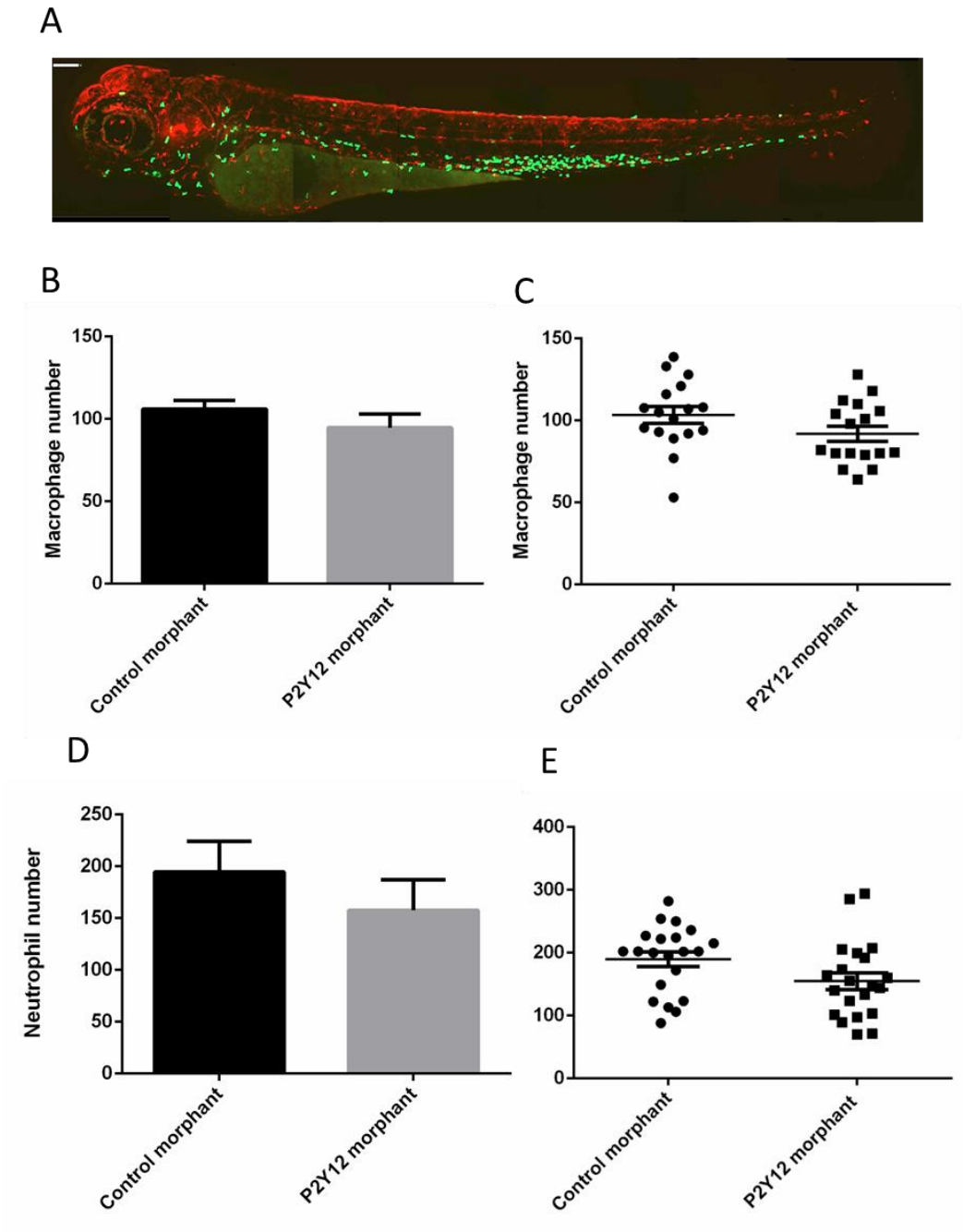

Figure 4.1 Total leukocyte number in 3 dpf control and *p2y12* morphant embryos.

Groups of 5-7 *p2y12* morphant or control embryos were assessed for total macrophage and neutrophil numbers. Three replicate experiments were performed on different days. **A** shows a 3 dpf *fmsgal4;UNM;mpo*GFP embryo, scale bar 160 µm. **B** shows a column plot of total macrophage number in both control and *p2y12* morphants, where data has been analysed by combining each experimental replicate into a single mean (n=3 p= 0.3), and **C** shows a scatter plot where every embryo has been considered as a separate experiment (n=17 p= 0.1). **D** shows a column plot of the total neutrophil number in control and *p2y12* morphants where data has been analysed by combining each experimental replicate into a single mean (n=3 p=0.42), and **E** a scatter plot where every embryo has been considered as a separate experiment (n=21 p=0.56). A Mann Whitney test was applied and data are presented as mean ± SEM.

4.1.1.2 Modelling of inflammatory response in zebrafish

I used three different models to investigate if knockdown of *p2y12* affected migration of leukocytes to sites of tissue injury (**Figure 4.2**); full transection of the tail fin (**A**), a small incision to the ventral fin (**B**) or laser induced vessel injury (**C**). The regions of interest in which numbers of macrophages and neutrophils were quantified, are highlighted in **Figure 4.2**. The two fin injury models were intended to induce inflammatory responses of different severities. A laser was used to injure the vessel endothelium and activate thrombocytes to model a vascular inflammatory response.

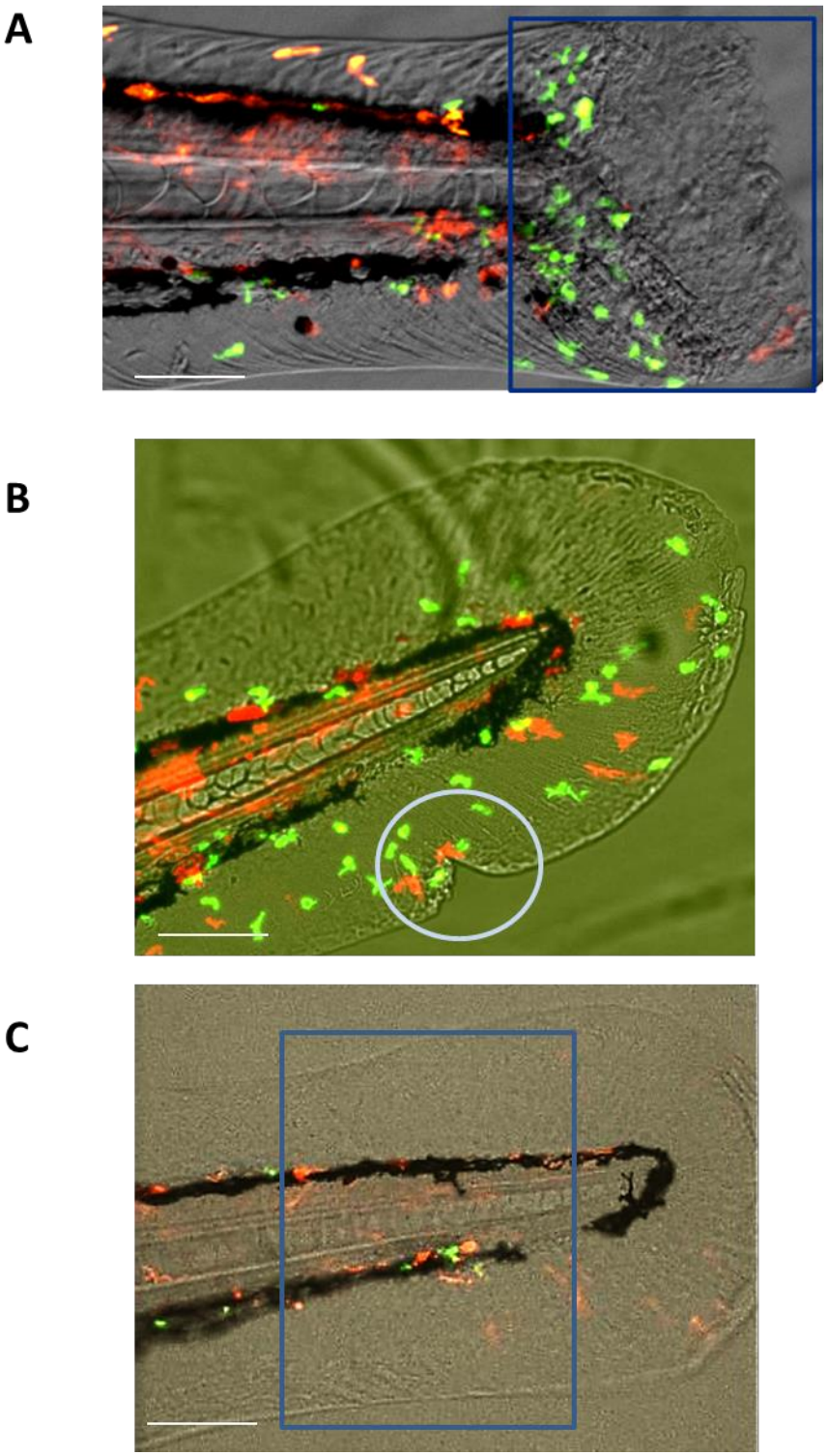

Figure 4.2 Models of inflammatory response in *fmsgal4;*UNM*;mpo*GFP.

A shows a full tail transection with the region of interest from the loop of circulation to the injury site highlighted by a blue box. **B** shows a small incision into the ventral tail fin, the region of interest is highlighted by a white circle. **C** shows the region of interest highlighted by a blue box after vessel injury. Scale bars represent 200 µm.

4.1.1.3 Does knockdown of *p2y12* affect leukocyte migration to site of tail fin transection?

The distal portion of the tail fin was transected with the region of interest spanning from the loop in circulation to the distal injury site. For each experimental replicate, groups of n=11-12 embryos were utilised, and three replicates were performed on separate days. Results for macrophage and neutrophil counts after full tail transection are shown in **Figure 4.3.** Data is presented either considering all embryos as independent experiments (control morphants n=35 *p2y12* morphants n=36, **A** and **C**), or as the mean of each experimental replicate (n=3, **B** and **D**). **A** and **B** show that macrophage recruitment to the site of injury increases until at least 8 hours, with no significant difference between the control and *p2y12* morphants. **C** and **D** show that neutrophil recruitment peaks at 4 hours post injury, with no significant difference in neutrophil numbers between control and *p2y12* morphants. These data reproduce previous research from our group which found that neutrophils respond and migrate to sites of injury more quickly than macrophages (Gray et al., 2011). My results indicate knockdown of *p2y12* does not significantly affect migration of neutrophils and macrophages to sites of fin transection within 8 hours after injury.

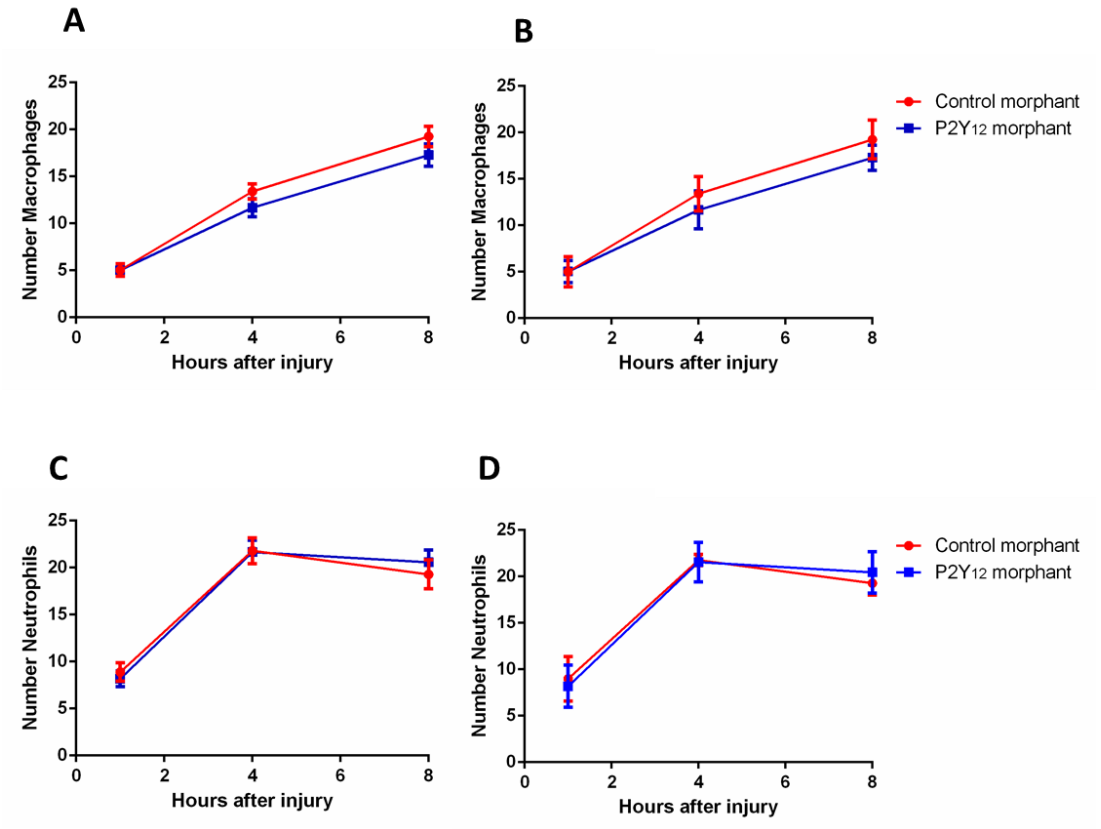

Figure 4.3 Number of leukocytes at site of tail transection over 8 hours post injury.

Tail fins of *p2y12* morphant or control embryos were transected, in groups of 11- 12, and leukocyte numbers were monitored at the injury site over 8 hours after injury. Three replicate experiments were performed on different days. **A** and **B** represents the number of macrophages at the site of injury after 8 hours with every embryo has been considered as a separate experiment (**A**, control n= 35 P2Y12 n=36), and where data has been analysed by combining each experimental replicate into a single mean (**B**, n=3). **C** and **D** represents the number of neutrophils at the site of injury after 8 hours, where every embryo has been considered as a separate experiment (**C**, control n= 35 P2Y12 n=36) and where data has been analysed by combining each experimental replicate into a single mean (**D**, n=3). A 2way ANOVA with Sidak's multiple comparison test was applied and data is presented as mean ± SEM.

4.1.1.4 Does knockdown of *p2y12* affect leukocyte migration to sites of ventral fin incision?

An incision into the ventral fin opposite the gap in pigmentation enabled the modelling of a less severe inflammatory response than complete tail fin transection. This injury induced fewer leukocytes migrating to the site of injury compared to tail fin transection. I quantified macrophage and neutrophil number in the injured region over 12 hours. **Figure 4.4** shows these data presented either considering all embryos as independent experiments (control morphants n=16 *p2y12* morphants n=14 **A** and **C**), or as the mean of each experimental replicate (n=2, **B** and **D**). There is a peak in both macrophages and neutrophils at 2 hours post injury, with a possible trend to a reduction in macrophage numbers at this time point in the *p2y12* morphants compared to control morphants (**A** and **B**). There also may be a reduction in neutrophil numbers in *p2y12* morphants at 8 hours post injury (**C** and **D**). However, it is not possible to fully interpret these results as they represent only 2 experimental replicates, with a great deal of variation, as shown by the wide and overlapping error bars. As these data were obtained from two experimental replicates preformed on different days, no statistical test was applied. This method of inducing an inflammatory response was too variable in terms of ensuring consistency of injury and the technical difficulty of mounting embryos after tail fin injury for successful confocal imaging. Therefore, no further replicates were performed.

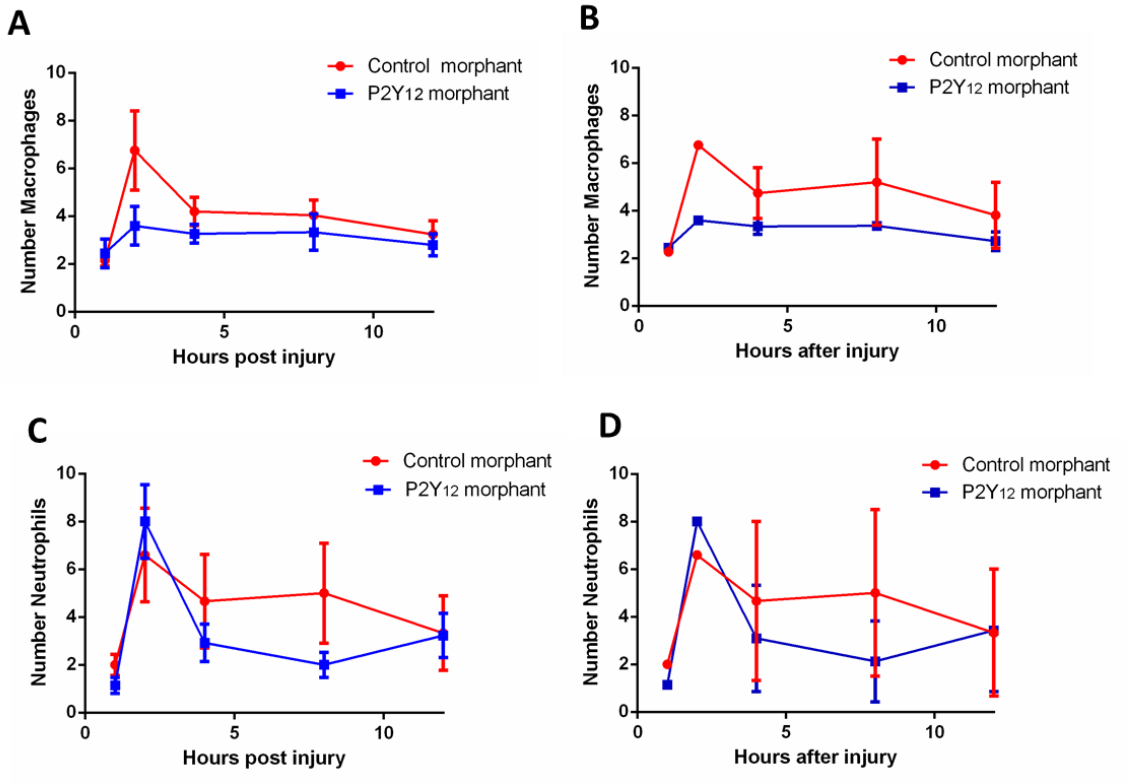

Figure 4.4 Leukocyte migration to site of ventral tail fin incision over 12 hours.

Groups of 7-8 *p2y12* morphant or control embryos underwent tail fin incisions and leukocyte numbers were monitored at the injury site over 12 hours after injury. Two replicate experiments were performed on different days. **A** and **B** represents the number of macrophages at the site of injury after 12 hours with every embryo has been considered as a separate experiment (**A**, control morphants n= 16, *p2y12* morphants n=14), and where data has been analysed by combining each experimental replicate into a single mean (**B**, n=2). **C** and **D** represents the number of neutrophils at the site of injury after 12 hours, where every embryo has been considered as a separate experiment (**C**, control n= 16 P2Y12 n=14) and where data has been analysed by combining each experimental replicate into a single mean (**D**, n=2). No statistical test was applied.

4.1.1.5 Does *p2y12* knockdown affect migration of leukocytes to sites of vessel injury?

As $P2Y_{12}$ is primarily present on platelets, I wished to examine a model of inflammation in which thrombocyte activation occurred. I used a laser to injure the endothelium at the site of the circulatory loop in the tail. I used an increased number of laser pulses than previously in the thrombosis model, to damage the endothelium such that it was sufficient to induce leukocyte migration. Injury to the endothelium induced leukocyte migration to the region of injury and this was quantified over 8 hours. This experiment was repeated on 3-4 different days. **Figure 4.5** shows the number of leukocytes in the region of interest over 8 hours post vessel injury. **A** and **C** show data considering all embryos as independent experiments (control morphants n=20-33 *p2y12* morphants n=20-34, **A** and **C**), and **B** and **D** show the mean of each experimental replicate (n=3 and n=4 respectively). There is no significant difference in macrophage or neutrophil number at the region of interest after vessel injury, between control and *p2y12* morphants. These leukocyte migration results encompassed a certain amount of variability, however the time consuming nature of these assays limited the number of experimental replicates. Therefore care should be taken in the interpretation of these results, however it appears *p2y12* knockdown did not significantly affect leukocyte migration to sites of tail fin or vessel injury.

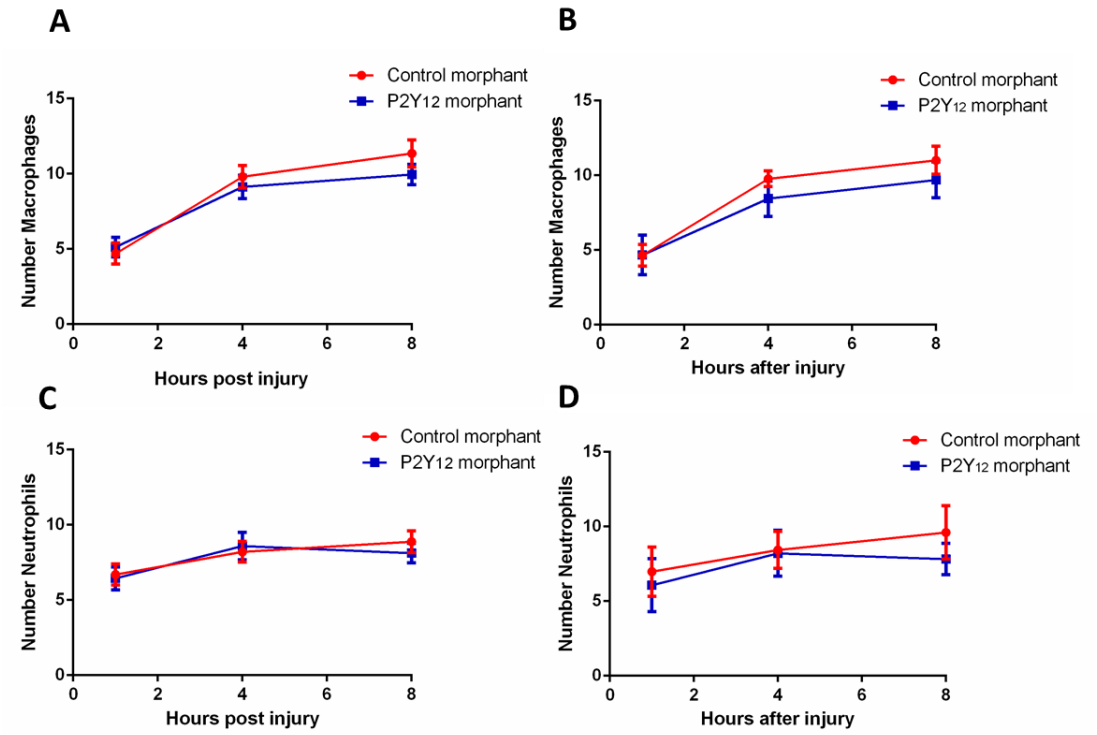

Figure 4.5 Leukocyte numbers at sites of vessel injury.

Groups of 6-8 *p2y12* morphant or control embryos had the endothelium in the tail loop damaged by a laser and leukocyte numbers were monitored at the injury site over 8 hours after injury. Three to four replicate experiments were performed on different days. **A** and **B** represents the number of macrophages at the site of injury after 8 hours where every embryo has been considered as a separate experiment (**A**, n= 20), and where data has been analysed by combining each experimental replicate into a single mean (**B**, n=3**). C** and **D** represents the number of neutrophils at the site of injury after 8 hours, where every embryo has been considered as a separate experiment (**C**, control morphant n= 33 *p2y12* morphant n=34) and where data has been analysed by combining each experimental replicate into a single mean (**D**, n=4). Data are presented as mean ± SEM. A 2way ANOVA with Sidak's multiple comparison test was applied.

4.1.2 Does adenosine exposure affect leukocyte migration to sites of injury?

Ticagrelor antagonises the $P2Y_{12}$ receptor, however it also blocks reuptake of adenosine. Adenosine is proposed to have differing roles in inflammation depending upon which receptor is activated. Activation of A_1 or A_3 enhances leukocyte chemotaxis and phagocytosis, whereas activation of A_{2A} or A_{2B} inhibits leukocyte degranulation and cytokine production (Cronstein et al., 1992, Chen et al., 2006, Nakav et al., 2008). I hypothesised that this excess of adenosine may induce benefits to survival after pulmonary infection and sepsis, potentially via the enhancement of leukocyte chemotaxis and activation (Storey et al., 2013). In order to investigate the effect of adenosine on leukocyte migration, 3 dpf embryos were exposed to a range of adenosine concentrations via addition to the media after fin transection, then macrophage and neutrophil numbers were assessed over 8 hours. Under normal physiological conditions levels of adenosine are in the nanomolar range, therefore I selected a range of concentrations from 1 mM to 100 nM. However, adenosine has a very short half-life being cleared from the plasma in approximately 1.5 seconds (Fredholm, 1997, Moser et al., 1989). **Figure 4.6** shows macrophage and neutrophil numbers over a time course of 8 hours after exposure to a range of adenosine concentrations. This was repeated on three different days for each adenosine concentration and on five different days for the control. **A** and **C** show data considering all embryos as independent experiments (control n=29, 1 mM n=18, 100 µM n=17, 10µM n=17, 100 nM n=18), and **B** and **D** shows the mean of each experimental replicate (n=3 for each adenosine concentration 100 nM-1mM and n=5 for control). There was no significant difference in number of macrophages or neutrophils migrating to sites of injury after exposure to adenosine at any of the tested concentrations when compared control, over 8 hours. However it is important to note that this experiment did not contain a positive control to ascertain whether adenosine was reaching the circulation, and was active. In light of the possible effects of ticagrelor on heart rate (**Figure 3.21**), it would have been interesting to assess heart rate in embryos exposed to adenosine as a possible indication whether adenosine was entering the blood stream however this was not recorded in this experiment.

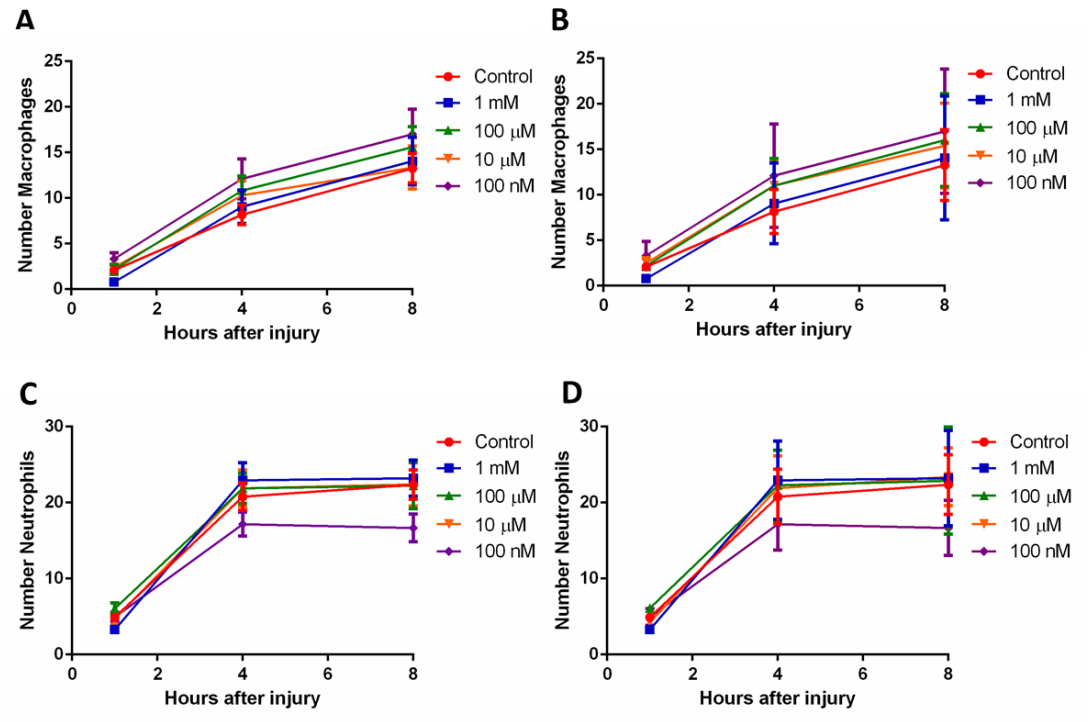

Figure 4.6 Leukocyte migration to tail transection after exposure to a range of adenosine concentrations.

Groups of 5-6 embryos had the tail fin transected and were then exposed to control or 100 nM-1 mM adenosine and leukocyte numbers were monitored at the injury site over 8 hours after injury. This was repeated on three on different days for each adenosine concentration and five for control. **A** and **B** represents the number of macrophages at the site of injury after 8 hours where every embryo has been considered as a separate experiment (**A**, control n=29, 1 mM n=18, 100 µM n=17, 10µM n=17, 100 nM n=18), and where data has been analysed by combining each experimental replicate into a single mean (**B**, adenosine 100 nM to 1 mM n=3 and control n=5**). C** and **D** represents the number of neutrophils at the site of injury after 8 hours, where every embryo has been considered as a separate experiment (**C**, control n=29, 1 mM n=18, 100 µM n=17, 10µM n=17, 100 nM n=18) and where data has been analysed by combining each experimental replicate into a single mean (**D**, adenosine 100 nM to 1 mM n=3 and control n=5). A 2way ANOVA with Tukey's multiple comparison post test was applied, data are presented as mean ± SEM.

4.1.3 Does *p2y12* knockdown affect resistance to *S. aureus* systemic infection?

I next assessed the resistance to *S. aureus* infection of control and *p2y12* morphants**.** 30 hpf embryos were inoculated with *S. aureus*, by microinjection directly into the circulation via the duct of Cuvier. In order to visualise bacterial expansion, I injected GFP labelled *S. aureus.* **Figure 4.7** shows both control and *p2y12* morphants 1 and 24 hours post infection (hpi). After 1 hpi, GFP labelled *S. aureus* is clearly visible in the cardiac region, at the site of entry and also in circulation. By 24 hpi *S. aureus* was no longer present in the circulation; however, it was in the yolk sac in both control and *p2y12* morphants. This indicates that *S. aureus* had either been cleared from the circulation by leukocytes or had exited the circulation. However the presence of *S. aureus* in the yolk sac indicated that the infection was spreading, as the yolk sac is an immune protected area with few leukocytes to combat infection. Within the yolk sac, bacteria are free to multiply until lesions form on the border with the heart, and the embryo is overwhelmed by the infection. **Figure 4.8** shows an example of the location of *S. aureus* injection at 30 hpf and a 30 hpi embryo with a developing lesion on the border of the heart and yolk sac, which represents the final stages of infection.

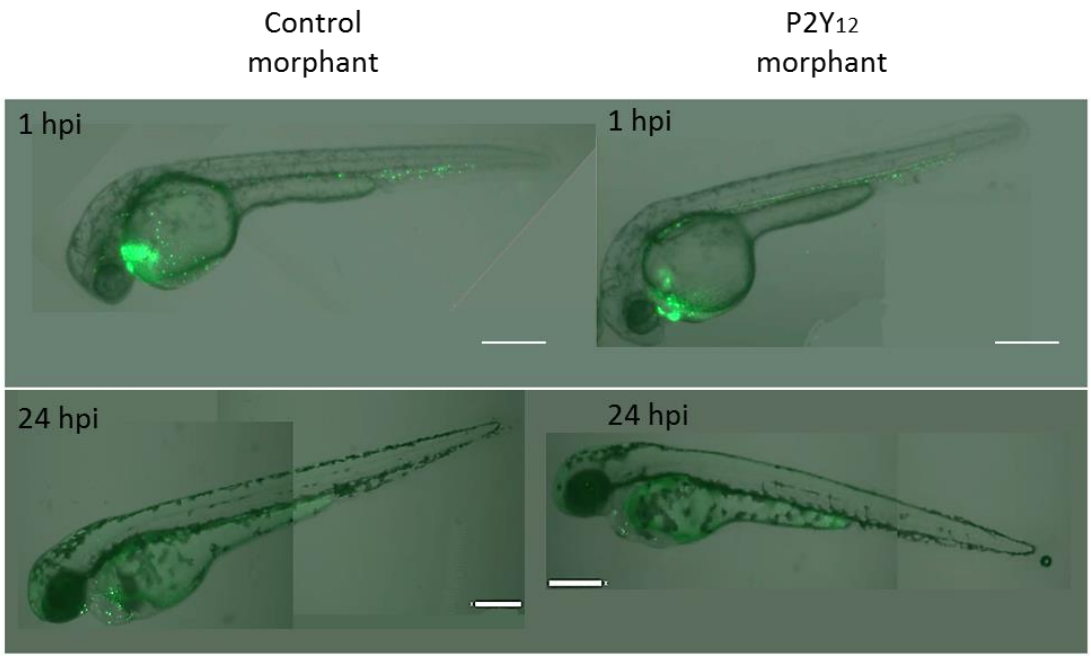

Figure 4.7 Control and *p2y12* morphants 1 and 24 hours after inoculation with GFP labelled *S. aureus.*

Fluorescent *S. aureus* is visible in the cardiac region and in the circulation in both control and P2Y12 morphants at 1 hpi. At 24 hpi GFP labelled *S. aureus* has exited the circulation and is contained within the yolk sac. White scale bars represent 200 µm.

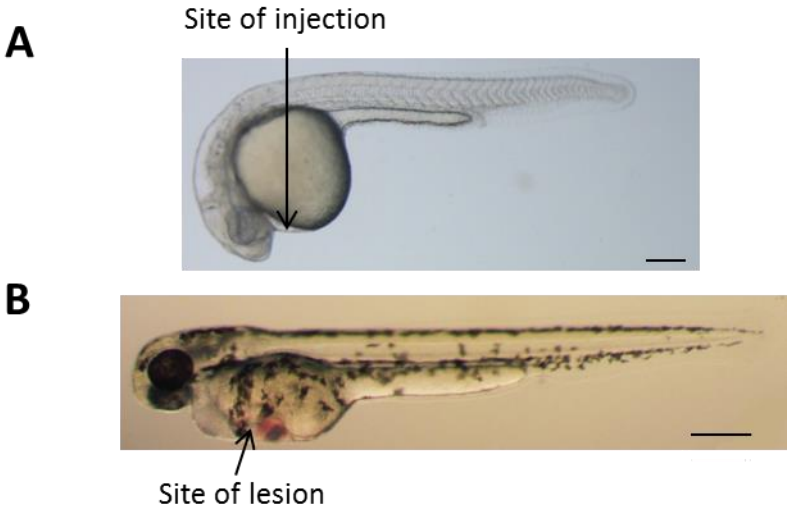

Figure 4.8 Site of injection and a developing *S. aureus* lesion in an embryo.

The site of injection of *S. aureus* is shown in **A** in a 30 hpf embryo. The arrow in **B** indicates the site of a developing lesion in an embryo 30 hpi with *S. aureus*. Scale bars indicate 200 µm.

I investigated whether there was a differential response in survival between control and *p2y12* morphants after the trauma caused by injection alone. **Figure 4.9 A** shows a Kaplan-Meier survival plot of both control and *p2y12* morphants after injection with sterile PBS. There was no significant difference in survival between the control and *p2y12* morphants, with minimal death subsequent to injection. **Figure 4.9 B** shows a Kaplan-Meier survival plot comparing control and *p2y12* morphants after inoculation with *S. aureus,* over a time course of approximately 90 hpi. I determined an appropriate bacterial colony forming units (CFU) concentration sufficient to cause 50% survival after approximately 90 hpi, in the control group. Control morphants were inoculated with a mean CFU count of 2176 and *p2y12* morphants were inoculated with a mean CFU count of 2244. There was a statistically significant reduction in the survival of *p2y12* morphants, compared to control morphants ($p<0.0001$). Therefore, these results demonstrate that *p2y12* morphants have an increased mortality when challenged with *S. aureus* infection.

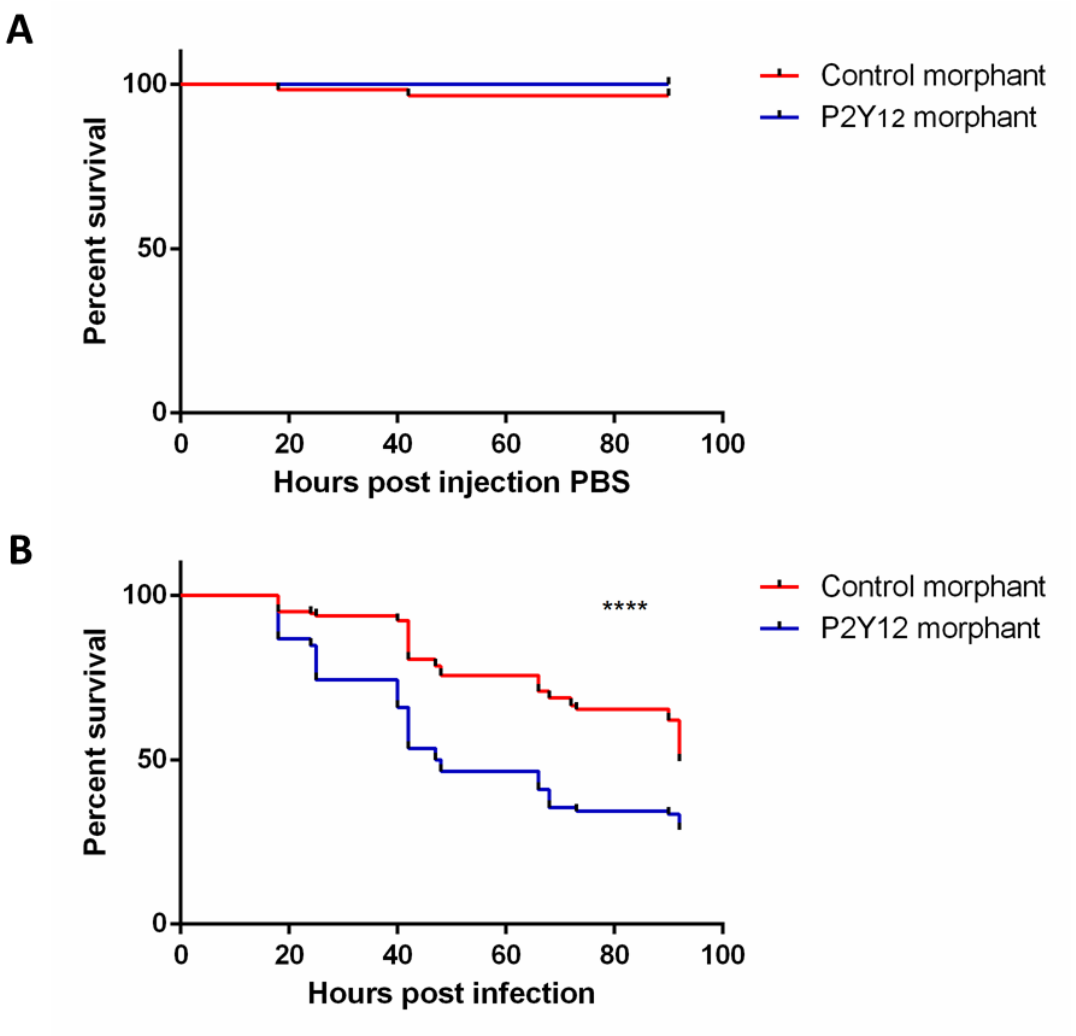

Figure 4.9 Survival of control and *p2y12* morphants inoculated with PBS and *S. aureus*.

A shows the survival of control and *p2y12* morphants after injection of a sterile PBS control containing no *S. aureus,* 59 embryos were utilised in each group, in 1 experimental replicate (n=59). Therefore no statistical test was applied to **A.** The survival of control and *p2y12* morphants after inoculation with *S. aureus* is shown in **B**. *p2y12* morphants have a statistically significant reduction in survival when compared to control morphants. There was a mean CFU count of 2176 for controls and 2244 for P2Y12 morphants. (144 embryos were utilised in each group where every embryo has been considered as a separate experiment n=144, $p<0.0001$ in 3 experimental replicates).

4.1.4 Does exposure to bacterially derived protein affect migration of leukocytes to sites of tail fin transection?

In order to investigate the possible mechanism behind the increased mortality of *p2y12* morphants when challenged by S aureus infection, I sought to investigate whether there was a reduced ability of *p2y12* morphant leukocytes to sense bacterial protein, thus impeding defence against bacterial pathogens. I first investigated whether exposure to bacterial proteins affected leukocyte migration to sites of injury. Lipopolysaccharide (LPS) is an endotoxin derived from the cell wall of the Gram-negative bacterium *E.coli.* 3 dpf embryos were exposed to LPS in the media directly after tail fin transection at a concentration of 1 µg/ml as per Taylor (2010). **Figure 4.10** shows macrophage and neutrophil numbers at the site of tail fin injury over 8 hours after exposure to a control solution or LPS, this was repeated on three different days. **A** and **C** show data considering all embryos as independent experiments (control n=21 LPS n=23,), and **B** and **D** show the mean of each experimental replicate (n=3). Macrophage numbers increase over 8 hours, whilst neutrophil numbers appear to plateau after 4 hours. Statistical analysis of these data shows that there was no significant difference in macrophage or neutrophil migration after exposure to this concentration of LPS.

I also exposed 3 dpf embryos to the bacterially derived protein N-formyl-methionyl-leucyl-phenylalanine (fMLP) via immersion of the scalpel blade in 200 nM fMLP immediately prior to transection of the tail fin. I monitored macrophage (**A** and **B**) and neutrophil (**C** and **D**) migration to the site of injury over 8 hours (**Figure 4.11**). **A** and **C** show data considering all embryos as independent experiments (control n=5 fMLP n=10 **A** and **C**), and **B** and **D** show the single mean (n=1). Preliminary data from this single experiment appeared to show no significant effect of fMLP exposure on leukocyte migration, although this data was not subjected to statistical analysis. Therefore, in these preliminary studies, I found no evidence for an effect on leukocyte migration of either LPS or fMLP, at the concentrations used.

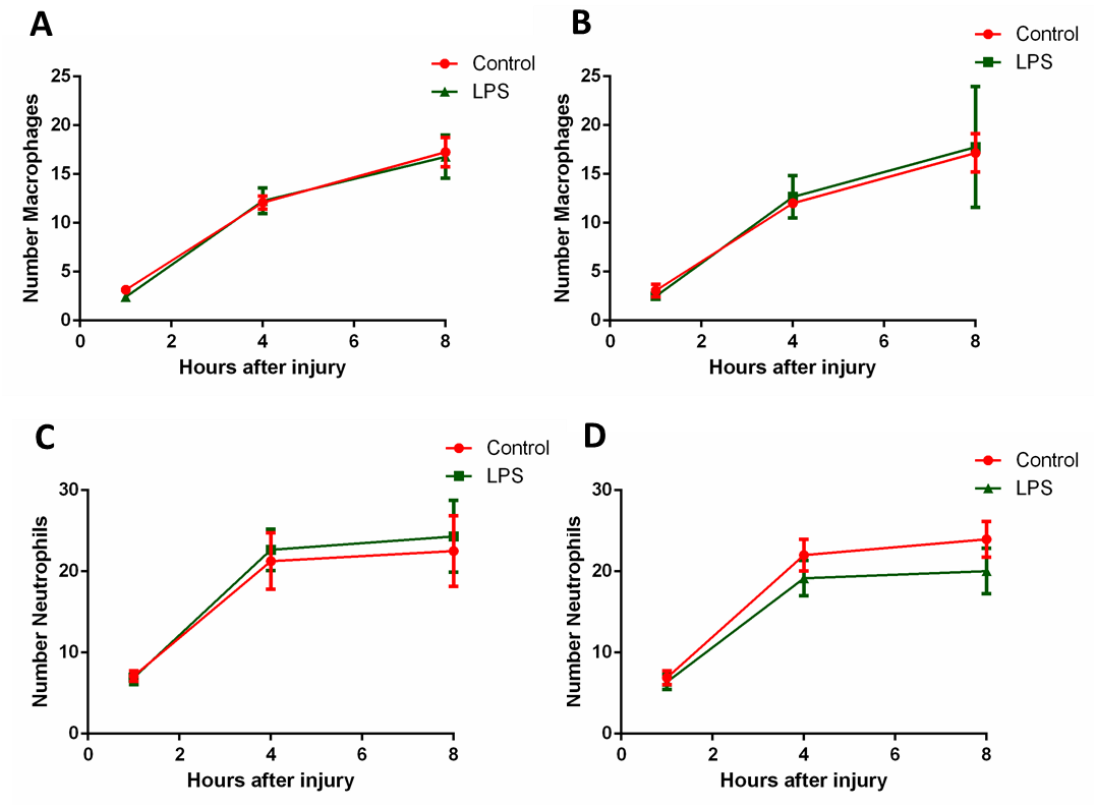

Figure 4.10 Leukocyte migration to the site of fin transection after LPS exposure.

Groups of 7-8 embryos underwent tail fin transection and were then exposed to either a control or 1 µg/ml LPS solution, this was repeated on three different days**. A** and **B** represents the number of macrophages at the site of injury after 8 hours where every embryo has been considered as a separate experiment (**A**, control n=21, LPS n=23) and where data has been analysed by combining each experimental replicate into a single mean (**B** n=3). **C** and **D** represents the number of neutrophils at the site of injury after 8 hours, where every embryo has been considered as a separate experiment (**C**, control n=21, LPS n=23) and where data has been analysed by combining each experimental replicate into a single mean (**D** n=3). Data are presented as mean ± SEM. A 2way ANOVA with Sidak's multiple comparison test was applied.

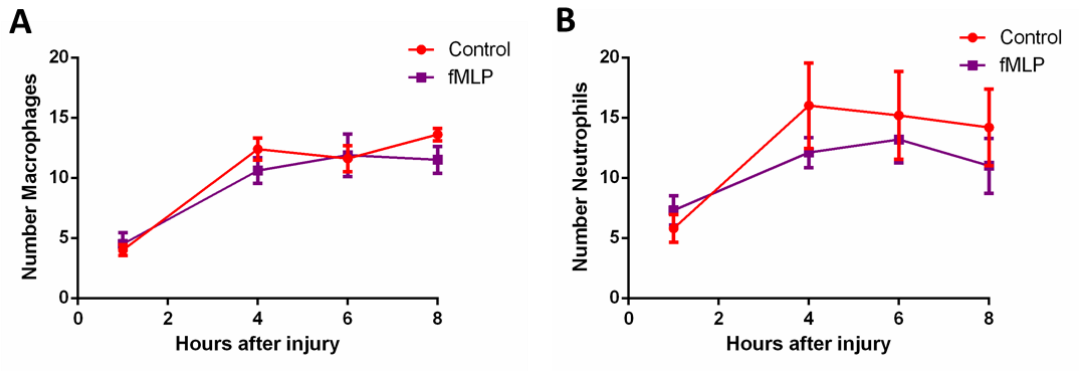

Figure 4.11 Leukocyte migration to the site of fin transection after fMLP exposure.

Groups of 5-10 embryos had their tail fins transected, either with a blade dipped in a control, or dipped in fMLP. Leukocyte numbers were monitored at the injury site over 8 hours after injury. The number of macrophages (**A**) and neutrophils (**B**) is shown at the site of injury with with every embryo has been considered as a separate experiment (control n= 5 fMLP n=10). This represents a single experiment, which was not repeated, therefore no statistical test was applied. Data are presented as mean ± SEM.

4.2 Discussion

The transgenic *fmsgal4;UNM;mpo*GFP was utilised for investigation of the inflammatory response of both control and *p2y12* morphants at 3 dpf. There was no significant difference in total macrophage and neutrophil number between the control and *p2y12* morphants, although there was a possible trend for reduction in neutrophil number, however this was not statistically significant (**Figure 4.1**).

Three different models of inflammation were used to investigate the effect of *p2y12* knockdown on inflammatory response: full tail fin transection, a small tail fin incision and laser induced vessel injury (**Figure 4.2**). Tail fin injury models for inflammation response are accepted techniques for investigation into leukocyte migration in the zebrafish (Lieschke et al., 2001, Renshaw et al., 2006, Mathias et al., 2006). I found that there was no significant difference in leukocyte migration to tail fin transection (**Figure 4.3**). I also investigated the inflammatory response to fin incision, preliminary results for this investigation appear to show no difference in leukocyte migration, however the technical challenges associated with mounting the embryos for confocal imaging after incision without further damaging the tail, limited the number of replicates for this experiment (**Figure 4.4**). As *p2y12* is particularly expressed on thrombocytes it was possible that an inflammatory model in which thrombocytes were directly activated would reveal a role of $P2Y_{12}$ in the inflammatory response. In order to damage the endothelium of the vessel loop in the tail, I used an increased number of laser pulses than used for the investigation of thrombosis response. Upon examination of macrophage and neutrophil response to these different stimuli, I found that there was no significant difference in leukocyte numbers migrating to these injury sites between control and *p2y12* morphants (**Figure 4.5**). Therefore I have not detected a role for $P2Y_{12}$ in leukocyte migration in these models. There was a certain amount of variation in these inflammation assays which made the results difficult to interpret with absolute confidence. I believe a proportion of this variability can be attributed to the challenge of standardising the extent of fin and vessel injury. An increase in experimental replicates would limit leukocyte number differences due to differing

severities of injury, and would enable interpretation of these results with greater confidence.

During the course of my studies I attempted to investigate whether the migratory behaviour of leukocytes was altered in *p2y12* morphants, by utilising cell tracking to a site of injury. Tracking software can measure cell velocity, distance and meandering index for directionality over time. Unfortunately I encountered challenges with the optimisation of this assay to track individual cells over time. It was possible to manually track each individual cell but this was very time consuming and resulted in an insufficient data set for accurate interpretation.

Ticagrelor antagonises the $P2Y_{12}$ receptor but also blocks reuptake of adenosine, which is proposed to have differential effects on leukocytes; this depends on which of the 4 receptors is activated, inducing either pro or anti-inflammatory properties (Fredholm, 2007). Storey et al. (2013) suggest that in the PLATO study ticagrelor reduced mortality related to pulmonary infection and sepsis in patients, compared to clopidogrel treatment (Storey et al., 2013). Therefore it was proposed that an excess of adenosine, rather than $P2Y_{12}$ antagonism, may contribute to a differential activation of leukocytes enabling an increased resistance to infection (Storey et al., 2013). I investigated leukocyte response to adenosine by exposure of 3 dpf *fmsgal4;UNM;mpo*GFP embryos to a range of concentrations from 1 mM to 100 nM, added to the media after tail fin transection. I found that there was no significant difference in macrophage or neutrophil migration to the site of injury (**Figure 4.6**). However it is possible that this method of exposure to adenosine is not suitable to enable an accurate interpretation of the possible effects of adenosine on leukocytes. Adenosine is labile and has a very short half-life, therefore this posed a challenge in terms of method of exposure. Embryos were exposed to adenosine via addition to the media at concentrations comparable to physiological levels (Fredholm, 1997). However no positive control for this experiment was included, therefore it is not possible to confirm that the adenosine used was active and indeed entering the circulation. A possible control for this may have been to assess the effect of adenosine exposure on heart rate, as previous data described in this thesis indicated that ticagrelor may affect heart rate, possibly through off-target

effects on adenosine re-uptake. However these data were not recorded for this experiment. It is possible that a higher adenosine concentration may be required to produce an effect on leukocyte migration. Further investigation into the effect of adenosine is warranted as this represents novel data in the zebrafish model; however a modification to the method of exposure, such as exposure exclusively at the site of injury, might be beneficial.

Figure 4.7 shows that GFP labelled *S. aureus* appears to clear from the circulation of infected control and *p2y12* morphants, however by 24 hpi this infection has infiltrated the yolk sac, with lesions forming near the heart. The use of time lapse monitoring of control and *p2y12* morphants would enable the monitoring of the dissemination of fluorescently labelled *S. aureus* from the circulation into the yolk sac. It would be interesting to assess the timescale of *S. aureus* exit from the circulation and the development of lesions, which represent the latter stages of infection.

The resistance of *p2y12* morphants to *S. aureus* infection was assessed and I found that *p2y12* morphants had significantly reduced survival compared to control morphants (**Figure 4.9** $p<0.0001$). This reduction in survival in the *p2y12* morphant group is seen after approximately 18 hours post infection (hpi), and is maintained throughout every subsequent time point. This is a novel finding which indicates that $P2Y_{12}$ may play a role in defence from systemic infection. This is an interesting result in light of current literature regarding a possible beneficial effect of ticagrelor on sepsis compared to clopidogrel (Varenhorst et al., 2012, Storey et al., 2013). A possible explanation for this might be that antagonism of $P2Y_{12}$ reduces resistance to infection, the effects of which may be negated by the off-target effect of ticagrelor blocking re-uptake of adenosine (Storey et al., 2013). As previously discussed, my results regarding the effect of adenosine on leukocyte migration showed no significant effect however this experiment would require further measures to confirm effective uptake of adenosine.

It was postulated that *p2y12* morphants may have a reduced leukocyte response to invading pathogens either through a reduced ability to recognise pathogens or

incapacity to dispose of them. I sought to investigate this via the addition of LPS which is derived from the Gram-negative bacteria *E. coli*. 3 dpf embryos which had undergone tail fin transection were exposed to 1 µg/ml of LPS in the media. Upon examination of leukocyte migration to the site of injury I found there was no significant difference in numbers of leukocytes (**Figure 4.10**). As embryos were exposed to LPS via addition to the media, LPS was not exclusively present at the site of injury. It would be interesting to utilise a different method for exposure to LPS such as a reservoir of media containing LPS delivered locally at the site of injury. This assay may also require a greater concentration of LPS, in order to assess *p2y12* morphant leukocyte response. I selected a concentration of 1 µg/ml as per Taylor (2010). However Novoa et al. (2009) used 50 µg/ml as a standard exposure concentration and showed that up to 150 µg/ml can be tolerated by 2 dpf embryos. I also exposed embryos to fMLP in order to induce an inflammatory response, however this preliminary data appeared to show no significant effect on leukocyte migration (**Figure 4.11**). It is, however, important to state that these data represent a single experimental replicate therefore further investigation, perhaps with an increased concentration of fMLP, would be required to ascertain whether there was an effect on leukocyte migration in response to exposure.

The CFU of each injection was monitored between control and *p2y12* morphants, to enable a careful matching of CFU for each experiment. However it would also be interesting to investigate the response of *p2y12* morphants to *S. aureus* CFU counts which in the control groups are not sufficient for mortality. This would demonstrate whether there is a reduced capability of the *p2y12* morphants to respond to moderate infection. There is no literature available discussing the function and interaction of zebrafish thrombocytes in defence against systemic infection, therefore this represents an area of research which requires considerable further study. However, mammalian platelets are known to participate in anti-microbial defence, they adhere to bacteria, activate and aggregate upon exposure to *S. aureus* pathogens in the blood stream (Bayer et al., 1995). Therefore, it is possible that the knockdown of $P2Y_{12}$ on zebrafish thrombocytes impedes host defence against systemic *S. aureus* infection. It was previously shown by Trier et al. (2008)

that antagonism of $P2Y_{12}$ abolished staphylocidal responses after exposure to *S. aureus* (Trier et al., 2008). Potentially a reduction in anti-microbial release from thrombocyte α granules could reduce the capacity to combat *S. aureus* infection in the first instance, thus allowing the infection to spread more rapidly than in controls. Trier et al. (2008) showed that reduced numbers of platelets increased susceptibility to infection. However, as shown in **Figure 3.8**, there was no significant difference in thrombocyte number in *p2y12* morphants at 3 dpf, which is the earliest time point available to assess thrombocyte number using the CD41:GFP transgenic. Embryos were inoculated with *S. aureus* at 30 hpf, at which time thrombocyte numbers have not been quantified, therefore it is possible that any delay in thrombocyte development or reduction in thrombocyte number, before 3 dpf, may account for a reduced defence against *S. aureus*. It may be thrombocytes themselves which participate in resistance to *S. aureus* infection via the release of PMPs and PKs. It would be interesting to examine whether anaemic mutants with reduced numbers of thrombocytes, have a similar resistance to infection as *p2y12* morphants. *S. aureus* induces aggregation of platelets therefore this is another avenue which could be further investigated in the zebrafish model (Bayer et al., 1995). The use of CD41:GFP labelled thrombocytes and fluorescently labelled *S. aureus* would enable visualisation of the interaction between these cell types after inoculation.

Macrophages are the primary cell which respond to, phagocytose and ultimately clear pathogens from the circulation of inoculated zebrafish embryos (Prajsnar et al., 2008). However, as $P2Y_{12}$ is believed to be expressed by macrophages, it is possible that *p2y12* knockdown may impair monocyte/macrophage interaction with pathogens. Therefore, further investigation is required to assess the involvement of $P2Y_{12}$ in the response to *S. aureus* infection and whether there is a reduced sensitivity of thrombocytes or leukocytes to bacterial pathogens in *p2y12* morphants. Any compromise to bacterial sensing may affect the ability to mount an effective response to prevent systemic infection. A model of localised infection in CD41:GFP or *fmsgal4;UNM;mpo*GFP, such as by injection of *S. aureus* into the otic vesicle, hind brain or somite in *p2y12* morphants, would enable the examination of

thrombocyte or leukocyte interaction with pathogens. It would also be interesting to investigate whether exposure of *S. aureus* inoculated embryos to an optimised concentration of adenosine would affect resistance to infection. As previously discussed, it has been suggested that excess adenosine may reduce susceptibility to infection in ticagrelor treated patients, therefore an investigation into the effect of both *p2y12* knockdown and adenosine exposure on inoculated embryos would serve to further elucidate a possible role for adenosine in resistance to infection (Storey et al., 2013).

It is important to emphasise that these results show the response of *p2y12* morphants after *S. aureus* infection alone. It would be beneficial, as previously discussed, to utilise other methods for bacterial, viral and fungal infection to further investigate whether a reduced resistance to systemic infection after *p2y12* knockdown is exclusive to *S. aureus* infection.

4.3 Conclusion

I investigated the effect of *p2y12* knockdown on leukocyte migration to sites of inflammation and resistance to *S. aureus* infection. I found that *p2y12* knockdown did not significantly affect leukocyte migration to sites of tail fin injury or vessel injury. However, *p2y12* morphants had significantly reduced survival after systemic infection with *S. aureus.* The results from this chapter indicate a possible role for the $P2Y_{12}$ receptor in resistance to infection. As previously discussed, the effect of morpholinos is limited to approximately 3 days and some can induce non-specific toxicity phenotypes. I therefore next sought to generate a stable *p2y12* mutant in order to further investigate thrombosis, inflammation and infection in a *p2y12* mutant, enabling assessment after 3 dpf. The next chapter details the process of generating such a mutant and the results of investigations into thrombosis and infection response.

Chapter 5 : Generating a *p2y12* mutant line

Recent improvements in site-directed mutagenesis have increased the efficiency for generating stable mutants with targeted mutations. A stable *p2y12* mutant would greatly add to my ability to assess the role of $P2Y_{12}$ in thrombosis, inflammation and infection. I therefore utilised two different methods to generate a mutation in the *p2y12* gene; CoDA ZFN and TALEN, both of which are discussed in this chapter.

5.1 Results

5.1.1 CoDA ZFN for the generation of a stable *p2y12* mutant

Zinc finger nucleases (ZFN) have been utilised for targeting genome editing and context dependent assembly (CoDA). CoDA ZFN utilises 2 custom designed ZF DNA binding proteins, a left and a right, which are fused to the FokI endonuclease cleavage domain. Each binding protein consists of 3 ZF motifs with each ZF motif binding 3 nucleotides. Each binding protein binds either side of a target region for mutagenesis, termed spacer region, of 5-7 nucleotides. Upon dimerization of the 2 binding proteins, the FokI nuclease domain cleaves DNA in the target region, inducing a double strand break (DSB) which is often erroneously repaired via non-homologous end joining (NHEJ), introducing insertions or deletions. Suitable ZFN cleavage sites are situated approximately every 500bp depending on DNA sequence (Sander et al., 2011).

5.1.1.1 Selection of a CoDA ZFN target site for mutagenesis

I chose two sites for mutagenesis; one site in the 3rd transmembrane (TM) domain, as this region is proposed to be important in ligand binding, and one in the 7th TM domain, a site which is linked to receptor recycling (shown in **Figure 5.1**). I will refer to them according to the spacer length; SP7 for the target in TM3 and SP5 for the target in TM7. Sites for mutagenesis are chosen in anticipation that frame shift mutations would result in a truncation of the protein at the target site.

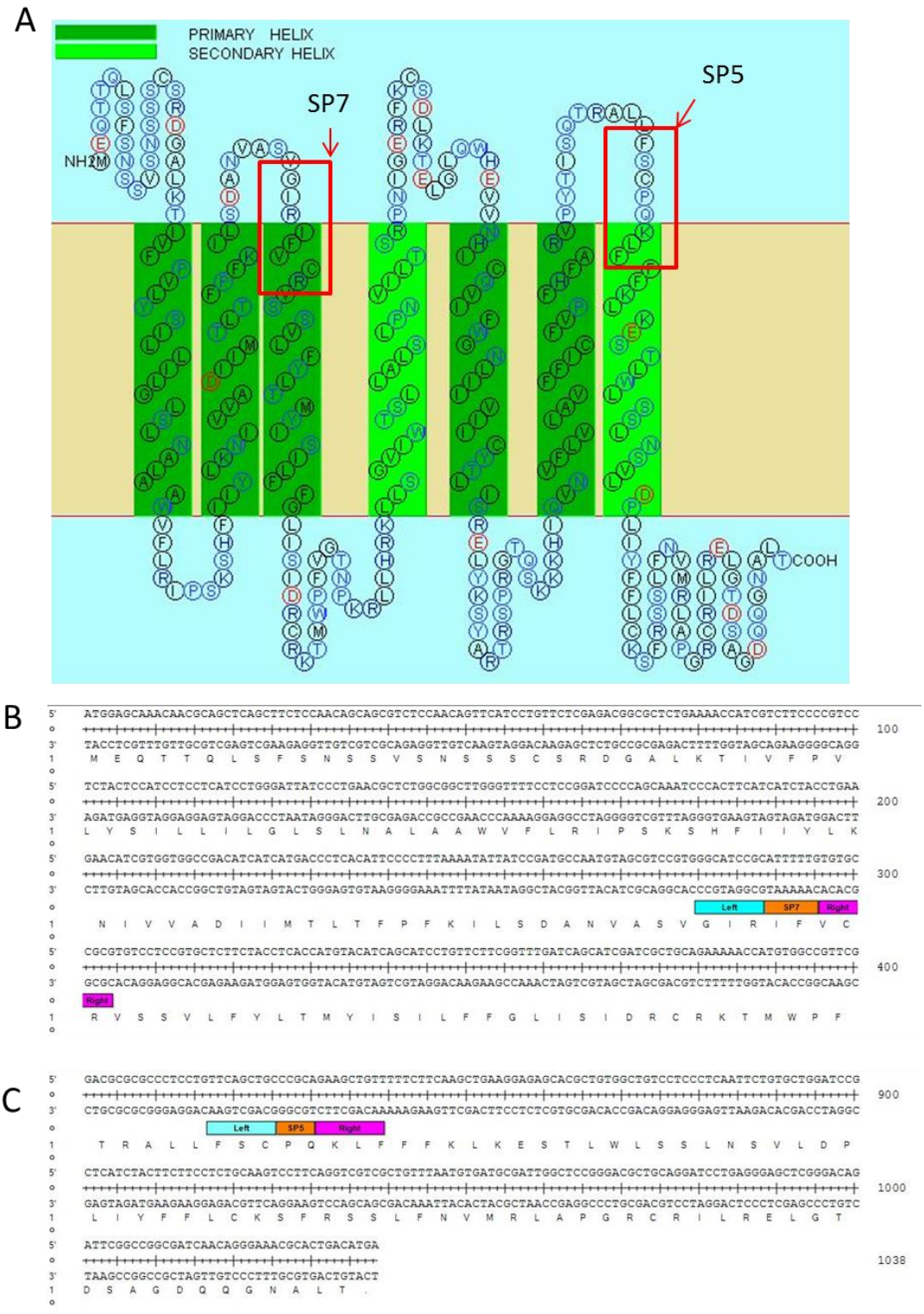

Figure 5.1 ZFN target sites in *p2y12.*

The predicted P2Y12 receptor is shown in **A** with both the ZFN target sites labelled. The position of SP7 ZFN target, proximal to the N-terminus is shown in **B** and **C** shows the position of SP5 proximal to the C- terminus. (P2Y12 prediction from Sosui).

5.1.1.2 ZFN assembly

ZFN are assembled in stages starting with the addition of zinc finger motifs to a generic plasmid backbone. The zinc finger motifs were added to the generic backbone via amplification of the custom designed ultramers with the Herculase enzyme. A digestion with NotI enzyme linearised the plasmids, which were then used to synthesise mRNA for injection. The gel electrophoresis for these stages are shown in **Figures 5.2** and **5.3**. mRNA was injected into 1 cell stage wildtype embryos at various concentrations. The optimum amount of SP7 mRNA for injection was titrated starting from the highest does of 1.3 ng to 0.52 ng (**Tables 5.1**). When optimizing the amount of mRNA for injection for mutagenesis, the accepted protocol in our department is to achieve approximately a 30% toxicity rate. Such that the mRNA is shown to have an effect with the majority of the embryos appearing morphologically normal, and with 30% showing some morphological signs of toxicity, such as small heads, delayed development or cardiac oedema. I calculated the toxicity rate for each mRNA amount I injected, this ranged from 100% with the highest amount to 30% with the lowest. Therefore, for SP7 0.52 ng was selected as a suitable amount of mRNA to induce toxic effects in a minority of embryos. I optimised the amount of SP5 mRNA for injection to 0.425 ng by injection of a range of mRNA amounts from 1.7 ng to 0.425 ng (**Table 5.2**). The toxicity rate ranged from 100% at the highest amount to 25% at the lowest, therefore 0.425 ng was selected as a suitable amount of mRNA to induce toxic effects in a minority of embryos. Embryos injected with the optimum concentration of ZFN mRNA were raised to adulthood then in-crossed. Genomic DNA from the F1 embryos was extracted and embryo gDNA from 3 pairs was pooled. Each pool of gDNA from 6 adults was assigned an MID tagged titanium primer, for tank identification. A PCR with this pooled gDNA was run with the MID primers and these products were then re-amplified with titanium primers to ensure a full length amplicon was available for 454 deep sequencing.

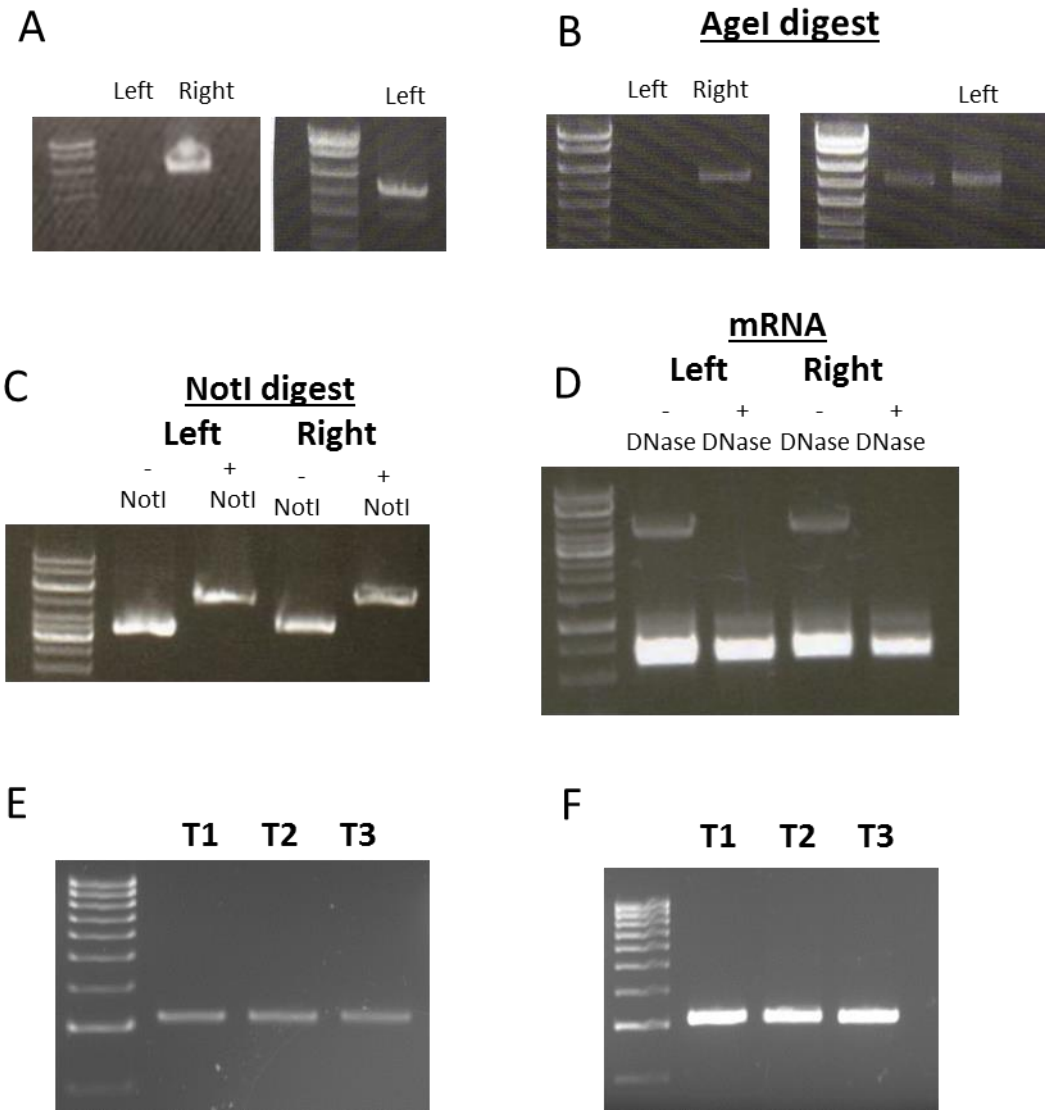

Figure 5.2 Assembly of SP 7 ZFN.

A shows the left and right amplicon at 5069bp, after addition of the zinc finger motifs. The left was re-amplified as initially there was no band. **B** shows the Age1 digest producing a 5059bp band. **C** shows the NotI unlinearised (NotI -) and linearized (NotI +) plasmid. This plasmid was then used to synthesise mRNA shown in **D**, before and after addition of DNAase, the second band showing that DNA contamination disappears after addition of DNAase (+ DNAase). **E** shows the PCR products from the 1st PCR with the MID tagged primers, T1 is tagged primer pair for the 1st tank of 6 fish, T2 is the tagged primer pair for the 2nd tanks and T3 is for primer pair for the 3rd tank of fish. **F** shows the PCR products after the second round of PCR with the titanium primers.

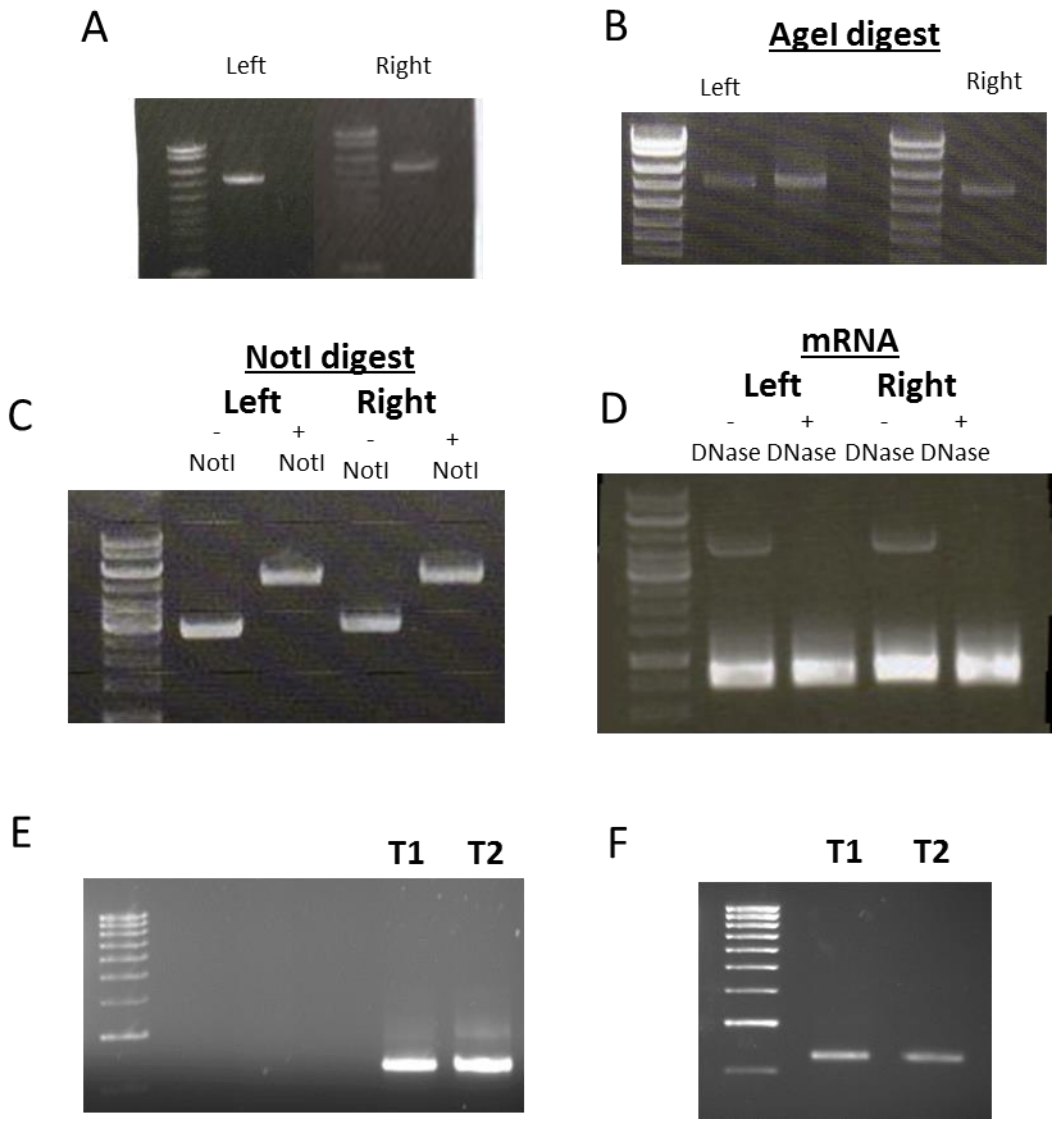

Figure 5.3 Assembly of SP5 ZFN.

A shows the left and right amplicon at 5069bp, after addition of the zinc finger motifs. **B** shows the Age1 digest producing a 5059bp band. **C** shows the NotI unlinearised (NotI -) and linearized (NotI +) plasmid. This plasmid was then used to synthesise mRNA shown in **D**, before and after addition of DNAase, the second band showing DNA contamination disappears after addition of DNAase (+ DNAase). **E** shows the PCR products from the 1st PCR with the MID tagged primers, T1 is tagged primer pair for the 1st tank of 6 fish, T2 is the tagged primer pair for the 2nd. **F** shows the PCR products after the second round of PCR with the titanium primers.

Table 5.1 Percentage rate of toxicity in embryos injected with varying concentrations of SP7 ZFN mRNA.

The optimum amount of mRNA for injection was titrated starting from the highest amount 1.3 ng to the lowest of 0.52 ng. Toxic phenotype were defined such as as small heads, delayed development and cardiac oedema. The percentage of toxic phenotype in injected embryos was calculated to determine the optimum amount of mRNA-such that it induced a toxic phenotype in approximately 30% of injected embryos. 0.52 ng of mRNA was selected as the optimised concentration to induce toxic phenotype in a minority of embryos, and these embryos were raised.

mRNA amount (ng)	Volume of mRNA injected (nl)	Number of embryos injected	Percentage with toxic phenotype (%)
1.3	1	60	67
1.04	1	60	35
0.65	0.5	80	55
0.52	0.5	296	30

Table 5.2 Percentage rate of toxicity in embryos injected with varying concentrations of SP5 ZFN mRNA.

The optimum amount of mRNA for injection was titrated starting from the highest amount 1.7 ng to the lowest of 0.425 ng. Toxic phenotype were defined such as as small heads, delayed development and cardiac oedema. The percentage of toxic phenotype in injected embryos was calculated to determine the optimum amount of mRNA-such that it induced a toxic phenotype in approximately 30% of injected embryos. 0.425 ng of mRNA was selected as the optimised concentration to induce toxic phenotype in a minority of embryos and these embryos were raised.

mRNA amount (ng)	Volume of mRNA injected (nl)	Number of embryos injected	Percentage with toxic phenotype (%)
1.7	1	50	100
1.36	1	65	91
0.85	1	51	60
0.85	0.5	58	66
0.68	0.5	70	43
0.425	0.5	50	25

5.1.1.3 ZFN mutagenesis quantification by deep sequencing

Deep sequencing was utilised to assess the mutation rate associated with each ZFN site. The mutation rate was defined as a percentage of all mutations found from the total number of sequences submitted; this was 3.4% for SP5 and 2.4% for SP7. The sequences containing mutations were assessed to investigate the number of bp deleted or inserted. However, it was difficult to determine whether mutations were genuine or possible errors in sequencing, for example I frequently saw a single A addition after a run of 3 or more As in the wildtype sequence, which can be an artifact of sequencing (Gilles et al., 2011). Therefore, I determined that this uncertainty combined with a relatively low mutation rate made screening of each potential founder by individual sequencing unfeasible. Therefore, I sought to generate a *p2y12* mutant via TALEN, a more recently described and more efficient method for mutagenesis.

5.1.2 TALEN for the generation of a stable *p2y12* mutant

Transcription activator-like effector nucleotides (TALEN) have been utilised for targeted mutation, as TAL effectors bind DNA and when fused to a FokI nuclease, enable cleavage at specific target regions. FokI is fused to the C-terminus and cleaves as a dimer, therefore a pair of TAL subunits are required; one for the sense strand and one for the antisense strand of DNA sequence, with the FokI domains dimerising at a spacer region between the two subunits, determined as the target site. As in CoDA ZFN, dimerisation of FokI induces a DSB in the DNA sequence, thus often introducing mutations or deletions. TAL effector sites occur approximately every 35bp, therefore there is often a large selection of possible TAL sites per gene (Cermak et al., 2011). A chosen target site encompasses a restriction enzyme recognition site, so mutation within this target region will prevent recognition at the enzyme site, thus preventing enzyme cleavage. This enables the use of a restriction enzyme digest as an efficient method for screening for mutants. These TALENs are generated by fusing an array of repeat-variable diresidues (RVDs) to generate a sequence specific DNA binding protein fused to FokI.

I generated 4 TALENs for *p2y12* with different target regions, however only one successfully produced mutations. The target region for each TALEN is shown in **Figure 5.4**, however only the successful TALEN is discussed in further detail in this chapter.

5.1.2.1 Selection of a target site for mutagenesis

The target site of the successful TALEN can be seen in **Figure 5.5**. I chose this region for mutagenesis as it is proximal to the N-terminus, therefore any frame shift mutation would be likely to truncate the receptor, potentially impairing its function. The target site is well conserved, however there is no known function for the chosen residues in terms of receptor signalling, so any point mutation at this site might also be of interest. During target selection, several criteria were required including the spacer length and the efficiency of the restriction enzyme to be used. A mutation will only be detected by this method if it occurs within the specific recognition sequence of the enzyme, so enzymes with wide spanning recognition sites such as MwoI (11bp) are more likely to detect any mutation within the spacer region, when compared to shorter spanning recognition sites. A short spacer length is proposed to increase efficiency of the TALEN (Christian et al., 2010), therefore I prioritised spacer length over the use of a wide spanning restriction enzyme. I chose a target with a 15bp spacer region containing a BamHI recognition site. BamHI is easily available and digests in a variety of buffers, although the recognition site is relatively short spanning (6bp).

Figure 5.4 Locations of the four TALEN target sites within *p2y12*.

Target sites selected for TALEN directed mutagenesis are shown in zebrafish *p2y12*. The first designed TALEN is shown in blue, 2nd in green, 3rd in pink and 4th in yellow. Out of these TALENs only TALEN 3 (pink) was successful in generating two mutations.

A

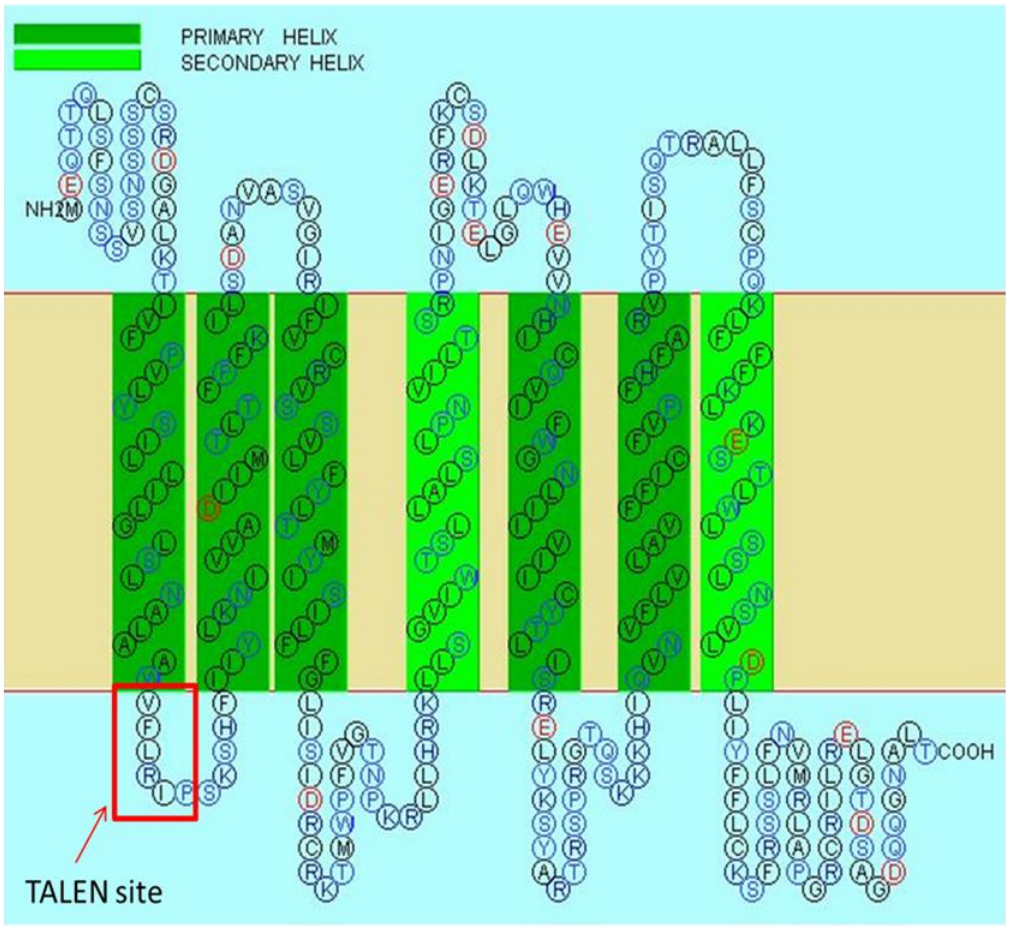

B

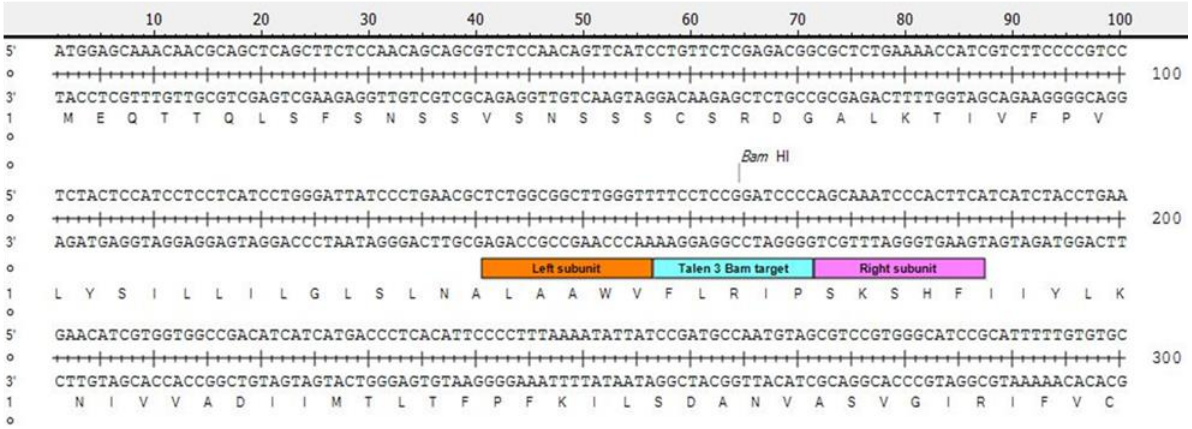

Figure 5.5 TALEN target sites in zebrafish *p2y12*.

A shows a predicted model of the zebrafish P2Y12 receptor, with the mutagenesis target region highlighted with a red box. **B** shows the position of the TALEN target region in *p2y12* proximal to the ATG start site, incorporating the BamHI restriction enzyme recognition site. (P2Y12 prediction model obtained from Sosui).

5.1.2.2 TALEN array assembly

Each subunit was constructed in two halves (A and B) in which individual RVDs were ligated together during a single golden gate reaction, using two different array plasmids for A and B respectively. An NheI and XbaI digest was utilised to verify the correct RVD plasmid sizes in the A and B plasmids (**Figure 5.6 A** and **B**). Subunit RB was partially digested; after the first digest this was repeated with halved concentration of product, resulting in a full digestion and confirmation of insertion of the correct RVD number. A and B subunits were then ligated into a full length array together with the last RVD unit in a second golden gate reaction, into the backbone vector containing the FokI domain. Sequencing for the left and right subunit confirmed correct insertion of RVD modules. The left and right subunits were then digested with BamHI and XbaI to test for the correct inclusion of subunits. A NotI reaction was then utilised to linearise the L and R constructs into the final construct. This final construct was synthesised into capped mRNA for injection. **Figure 5.6** shows the gel electrophoresis images of these stages of subunit assembly, verification and linearisation.

5.1.2.3 Screening of injected embryos for a somatic mutation

p2y12 TALEN mRNA concentration was optimised in order to limit toxic effects such as delayed development, small heads, cardiac oedema but to induce a reasonable mutation rate (**Table 5.3**). Genomic DNA was extracted from 3 dpf individual embryos to screen for partial digestion, and therefore possible mutation, via restriction enzyme digest (**Figure 5.7**). After confirmation of an ability to induce mutations, subsequently injected embryos were raised to adulthood. These F0 fish were in-crossed and their offspring genotyped to identify founders carrying mutations in their germ line.

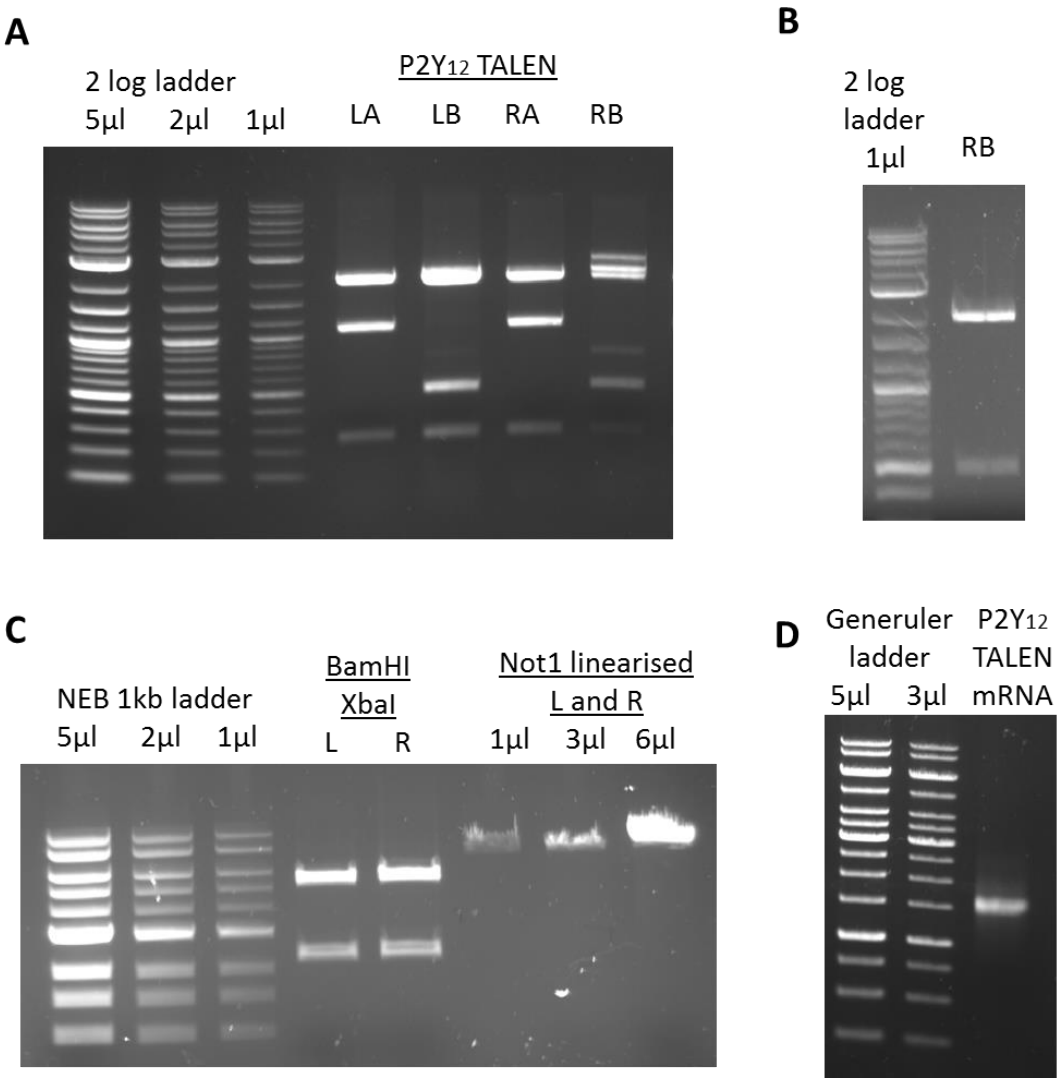

Figure 5.6 Assembly of *p2y12* TALEN RVDs and generation of mRNA for injection.

A shows the A and B parts for the left and right subunits, after the 1st golden gate reaction and transformation. LA, LB and RA have fully digested after the NheI and XbaI digest, however RB was partially digested. **B** shows a fully digested repeat reaction of RB with half the concentration of product. **C** shows the left and right subunits after the 2nd golden gate reaction to combine the A and B parts for the construct BamHI and XbaI digest, which were linearised with NotI. **D** shows the capped *p2y12* TALEN mRNA.

Table 5.3 Rate of toxicity of embryos injected with TALEN *p2y12* mRNA.

I injected a range of amounts of TALEN *p2y12* to optimise an amount of mRNA sufficient to produce toxic phenotype in a minority of embryos. 1.5 ng of TALEN *p2y12* mRNA was selected as an optimised amount, as the maximum volume of I injected into the yolk which resulted in a 19% toxicity phenotype, and these embryos were raised. I also raised embryos which were injected with 0.5 ng of TALEN *p2y12* mRNA which was injected directly into the cell resulting in a 35% toxicity phenotype, these amounts were selected as optimum concentrations to induce toxic phenotype, such as delayed development, small heads and cardiac oedema, in a minority of embryos.

mRNA amount (ng)	Volume of mRNA injected (nl)	Location of mRNA injection	Number of embryos Injected	Percentage of viable embryos (%)	Percentage of embryos with toxicity Phenotype (%)
1.5	3	Yolk	146	60	19
1.0	2	Yolk	33	84	9
0.5	1	Yolk	39	94	5
0.5	1	Cell	132	53	35

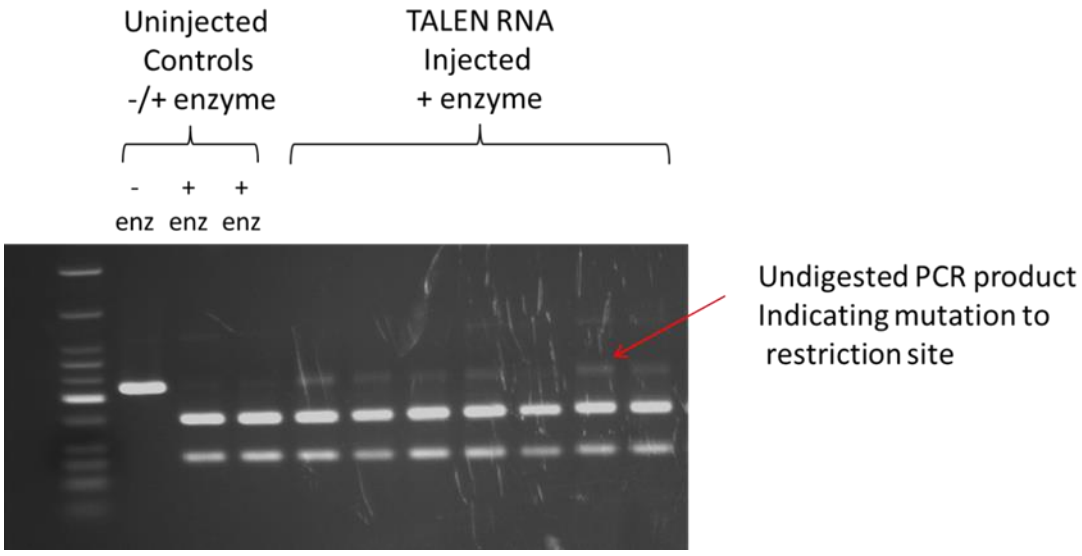

Figure 5.7 Screening gel for F0 TALEN RNA injected embryos.

The red arrow highlights the partial digest of TALEN RNA injected embryo gDNA PCR product after BamHI incubation (wells 4-10), which indicates a mutation. Low molecular weight ladder was used, the 1st well shows control gDNA PCR product without BamHI, wells 2 and 3 show control embryo gDNA PCR product after incubation with BamHI, both of which are fully digested.

5.1.3 Identification of two TALEN induced mutant alleles of *p2y12.*

5.1.3.1 Identification of *p2y12*^{sh338} and *p2y12*^{sh340} mutant alleles in F1 screen

Two founders were discovered upon screening of the F1 embryos from the in-cross of the F0 TALEN RNA injected fish. Each founder possessed a different mutation, and were from the group injected with 0.5 ng of RNA directly into the cell. This suggests that for a TALEN with low activity such as this, injection directly into the cell may be the most efficient way of inducing a mutation. Each mutation was in the target site and was detected by partial cleavage of PCR product after incubation with BamHI restriction enzyme. Sequencing of these mutations revealed one founder with a 6bp deletion (termed *p2y12*^{sh338}) and the other founder with a 10bp deletion (termed *p2y12*^{sh340}). In order to approximate a mutation rate for each allele, gDNA from 3 embryos was pooled for restriction enzyme digest, per reaction. I used 8 reactions, therefore screening a total of 24 embryos per founder. For *p2y12*^{sh338}, 2 of 8 pooled gDNA samples tested were partially digested, therefore out of 24 embryos approximately 2 embryos were carriers for the mutation indicating a somatic transmission rate of 8%. This 6bp deletion results in a deletion of an arginine (R^{55}) and isoleucine (I^{56}) (**Figure 5.8**). For *p2y12*^{sh340}, 6 out of 8 pooled gDNA samples showed partial digestion with a bright undigested band in sample 8, indicating the possibility of 2 out of the 3 embryos within that reaction being carriers for the mutation, therefore the approximate somatic transmission for this allele was 25%. This 10bp deletion is predicted to result in a frame shift and premature stop codon, 9 amino acids downstream of the target region (**Figure 5.9**).

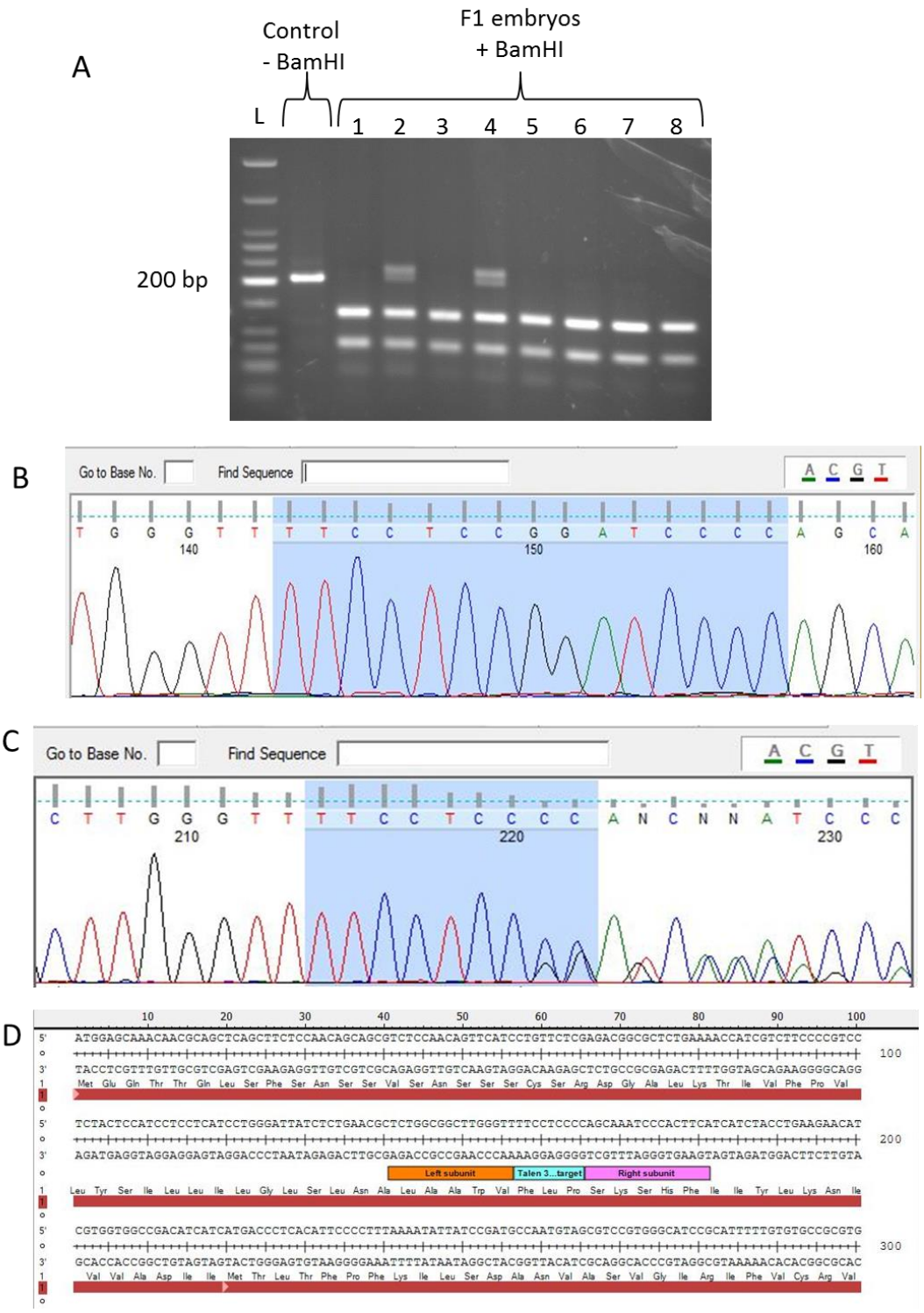

Figure 5.8 Identification of a TALEN induced 6bp deletion mutant of *p2y12* (*p2y12*^{sh338}).

A shows the screening restriction digest gel, in which each channel contains PCR product of 3 dpf genomic DNA pooled from 3 embryos. Both channels 2 and 4 show an undigested band at 200bp, indicating a mutation in one of the 3 embryos. **B** shows the wildtype sequence chromatogram, with the target site for TALEN mutagenesis highlighted blue. **C** shows the sequence chromatogram of a *p2y12*^{sh338} mutant showing a 6bp deletion within the blue highlighted target region. **D** shows the effect of the deletion of R^{55} and I^{56} on the peptide sequence.

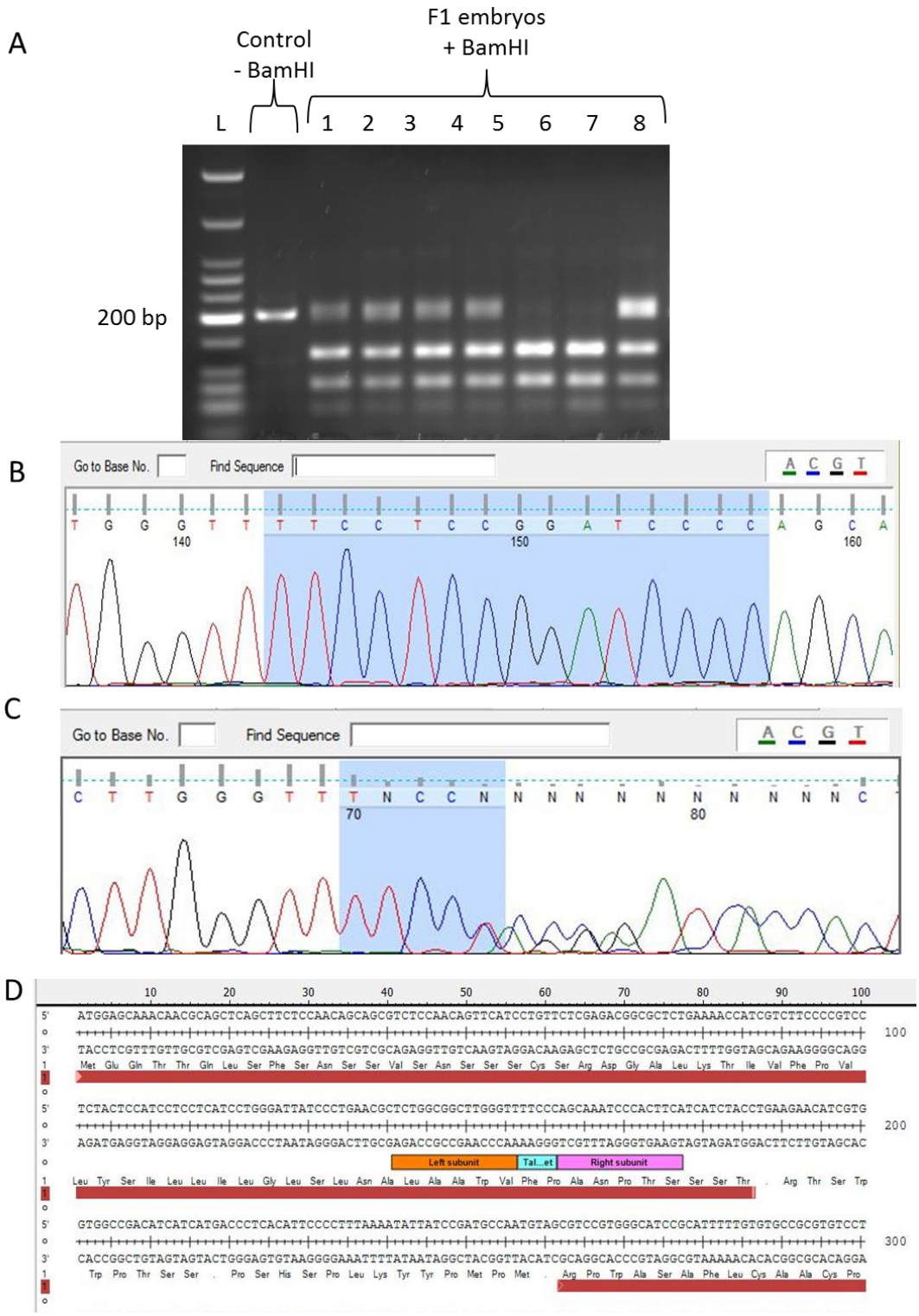

Figure 5.9 Identification of a TALEN induced 10bp deletion mutant of *p2y12* (*p2y12*^{sh340}).

A shows the screening restriction digest gel, in which each channel contains PCR product of 3 dpf genomic DNA pooled from 3 embryos. Channels 1, 2, 3, 4, 5 and 8 show an undigested band at 200bp, indicating a mutation. **B** shows the wildtype sequence chromatogram, with the target site for TALEN mutagenesis highlighted blue. **C** shows the sequence chromatogram of *p2y12*^{sh340} 10bp deletion. **D** shows the premature stop codon appearing downstream of the TALEN target site.

Both *p2y12*^{sh338} and *p2y12*^{sh340} F0 founders were out-crossed to *nacre* and the F1 progeny were raised then genotyped by fin clipping to identify heterozygotes, as shown in **Figure 5.10**. F1 heterozygotes for both alleles are viable and morphologically normal. F1 heterozygotes with the same mutation were in-crossed to produce approximate Mendelian ratios of 50% heterozygotes, 25% homozygotes and 25% wildtype F2 embryos. There was no gross morphological difference between wildtype, heterozygous and homozygous siblings, for either mutant allele (**Figure 5.11** and **5.12**). These embryos were utilised in the following investigations for thrombosis and resistance to infection.

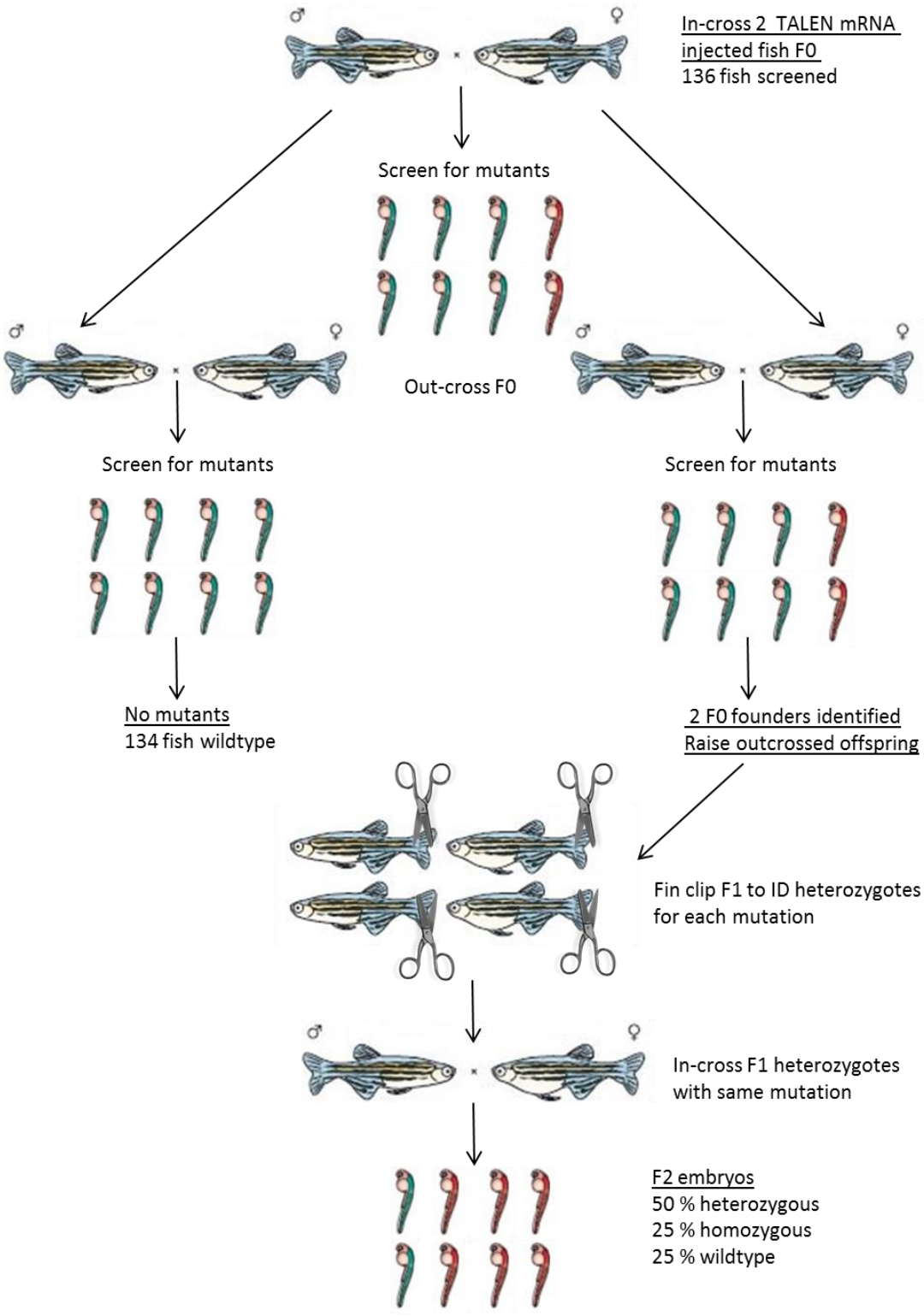

Figure 5.10 Schematic demonstrating the screening of TALEN generated mutants.

Embryos in red represent mutants, embryos in blue represent wildtypes. Approximately 156 embryos were raised after injection with TALEN RNA. The surviving 136 adult fish were screened for mutations in the target region of *p2y12*. 2 founders were discovered, one with a 6bp deletion (*p2y12*^{sh338}) and the other with a 10bp deletion (*p2y12*^{sh340}). The images in this figure are adapted, with permission, from (Lieschke and Currie, 2007).

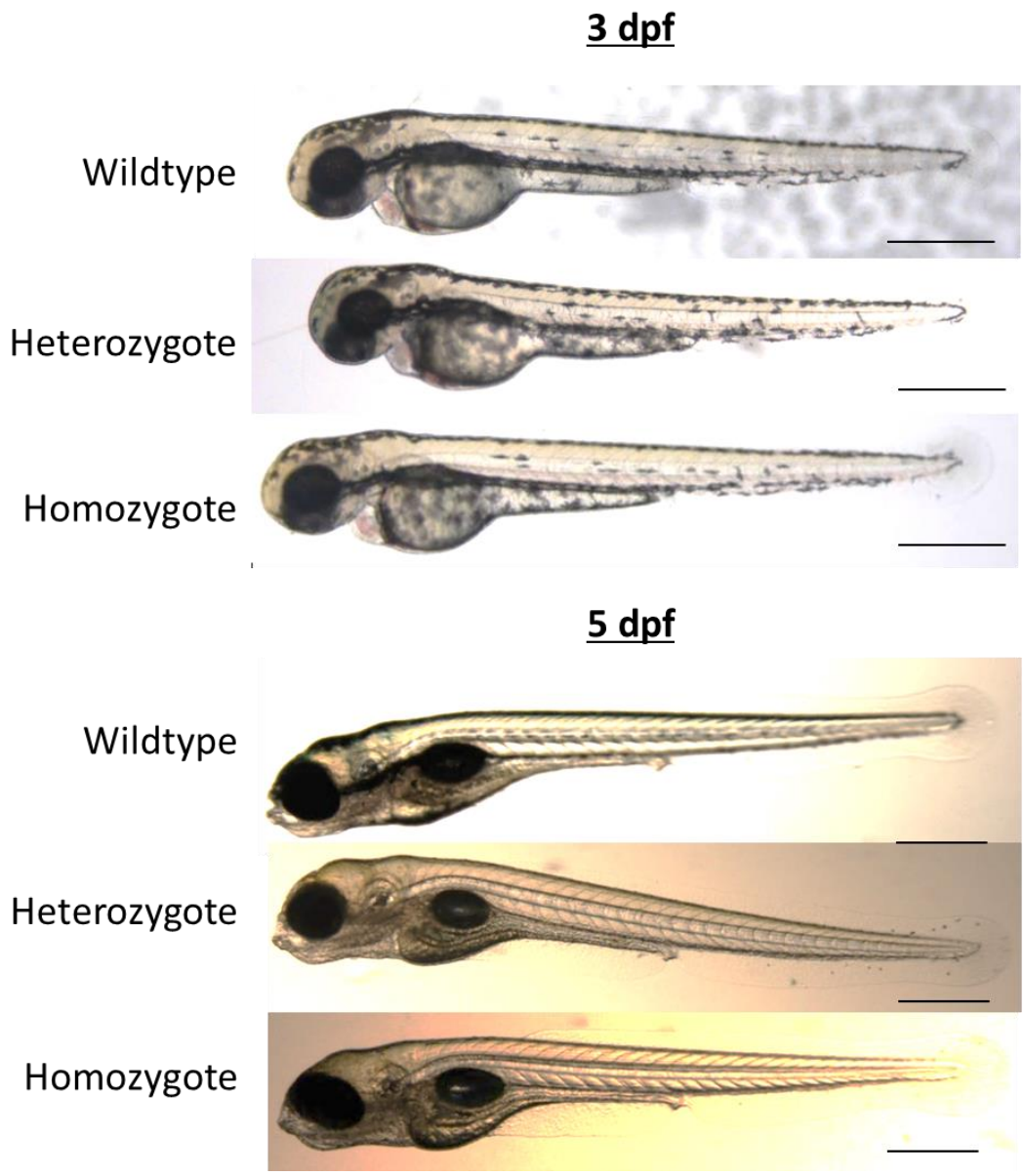

Figure 5.11 Morphology of 3 dpf and 5 dpf *p2y12*^{sh338} mutants.

Morphology of 3 dpf and 5 dpf *p2y12*^{sh338} mutants, there appears to be no significant morphological difference between wildtype, heterozygous and homozygous siblings. Scale bar shows 500 µm.

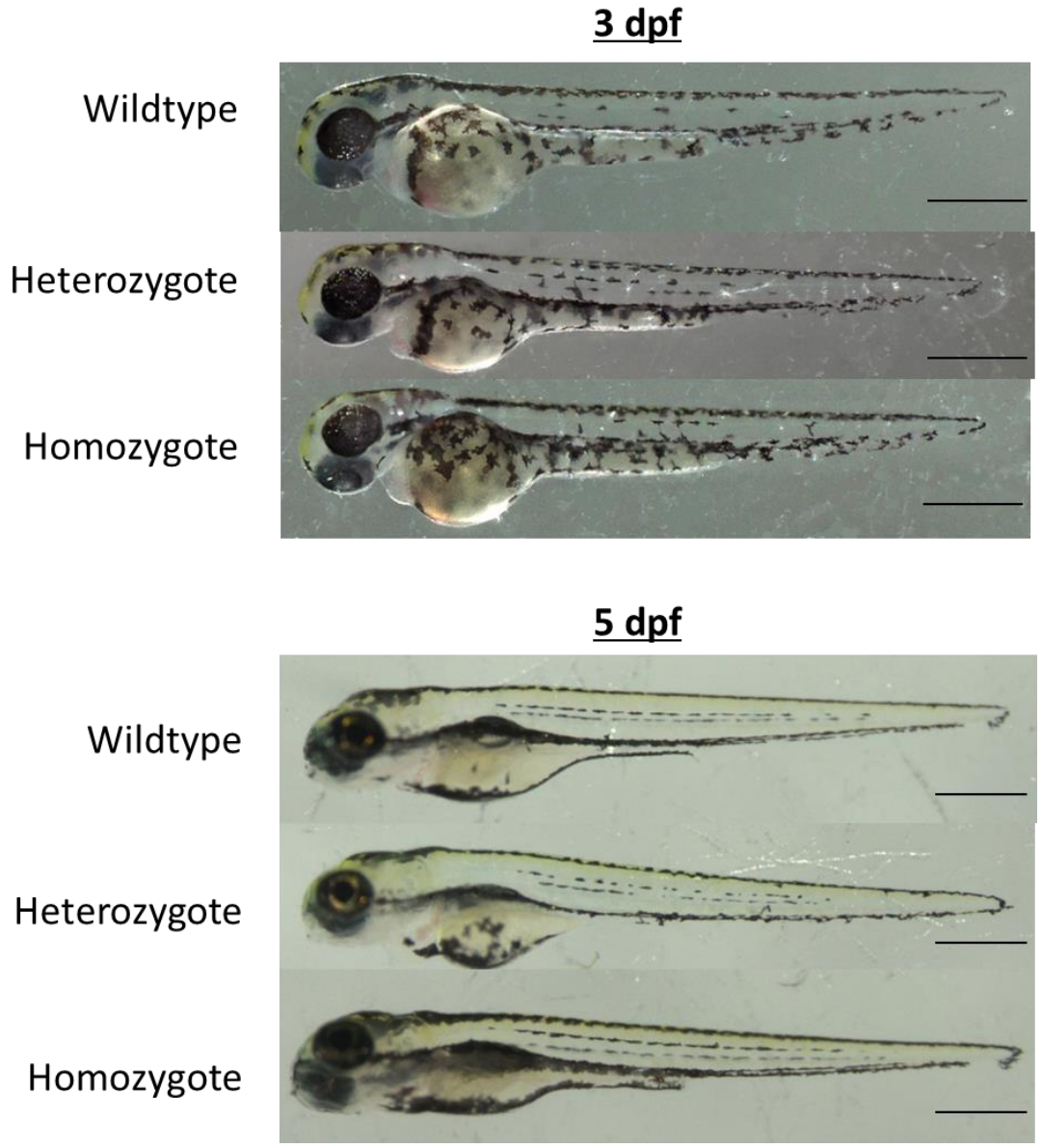

Figure 5.12 Morphology of 3 dpf and 5 dpf *p2y12*^{sh340} mutants.

Morphology of 3 dpf and 5 dpf *p2y12*^{sh340} mutants, there is appears to be no significant morphological difference between wildtype, heterozygous and homozygous siblings. Scale bar shows 500 µm.

5.1.3.2 Does a 6bp deletion of residues R^{55} and I^{56} affect thrombus formation?

I investigated the thrombosis response of 3 dpf embryos from a *p2y12*^{sh338} heterozygote in-cross. It is possible that this 6bp deletion may affect the receptor structure, however I hypothesised that this mutation would not affect thrombosis response, as the deletion did not result in a frame shift, and did not include residues known to be involved in $P2Y_{12}$ activation. Genomic DNA was extracted from each embryo subsequent to laser induced thrombosis and a PCR and restriction digest was used to genotype the embryos. The thrombosis response of 21-23 embryos of a wildtype, heterozygote or homozygote background was assessed by laser induced aortic injury, and the thrombus area was quantified over 10 minutes. The preliminary data for this investigation, consisting of 2 experimental replicates, performed on different days is shown in **Figure 5.13**. **A** shows a plot of thrombus area over 10 minutes after injury, where every embryo has been considered as a separate experiment (wildtype n=12, heterozygote n=26 and homozygote n=5). **B** shows the mean area under the curve of thrombus in wildtype, heterozygote and homozygotes where data has been analysed by combining each experimental replicate into a single mean (n=2). **C** shows a scatter graph with each individual embryo represented as a separate experiment (wildtype n=12, heterozygote n=26 and homozygote n=5). As this consists of 2 replicates the data was not subjected to statistical analysis. However, overlapping of the SEM error bars appears to indicate no difference in thrombosis response between wildtype, heterozygous and homozygous siblings. This mutation was not further investigated due to the prioritisation of investigating the second mutation consisting of a 10bp deletion.

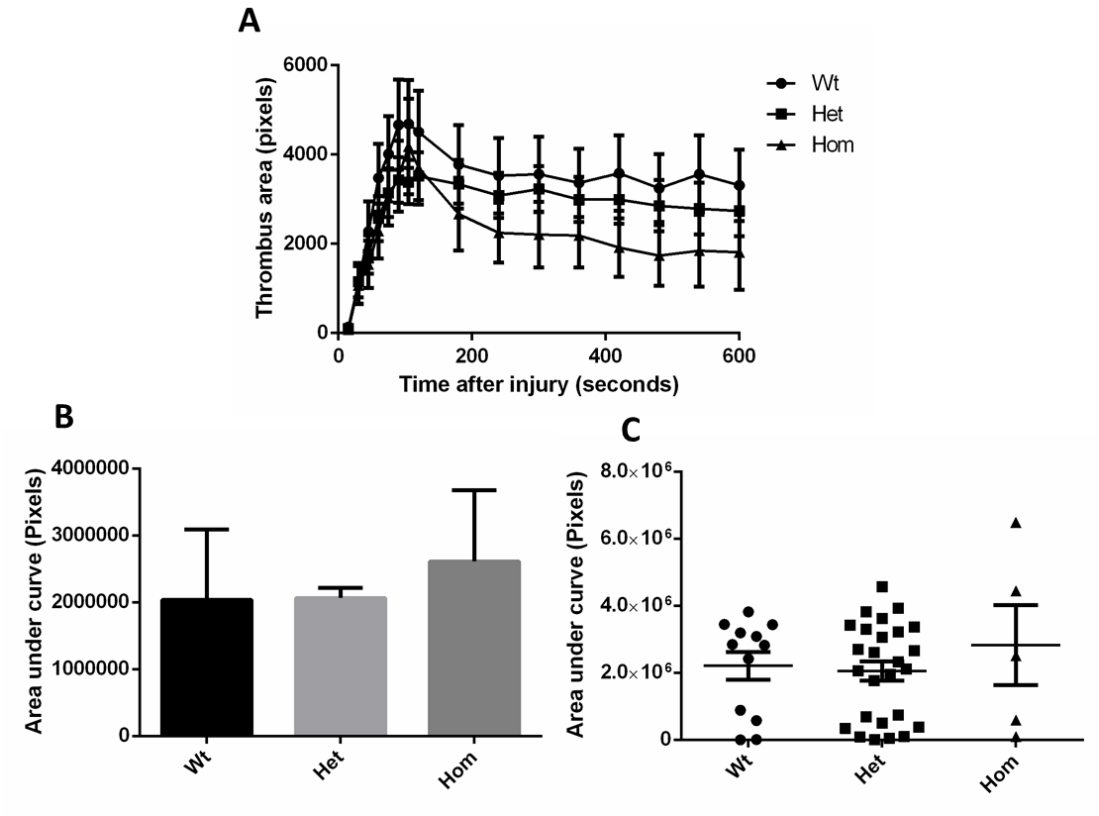

Figure 5.13 The effect of the 6bp *p2y12*^{sh338} mutation on thrombosis in 3dpf embryos.

21-23 embryos of a wildtype (wt), heterozygote (het) or homozygote (hom) background underwent laser induced aortic injury and thrombus area was quantified over 10 mins. The embryos were genotyped by PCR and restriction enzyme digest after completion of the thrombosis assay. Two replicate experiments were performed on different days. **A** shows a plot of thrombus area over 10 minutes following laser induced aortic injury, where every embryo has been considered as a separate experiment (wildtype n=12, heterozygote n=26 and homozygote n=5). **B** shows the mean area under the curve in wildtype, heterozygote and homozygotes where data has been analysed by combining each experimental replicate into a single mean (n=2). **C** shows a scatter graph with each individual embryo represented as an experimental unit. No statistical test was applied. Data are presented as mean ± SEM.

5.1.3.3 Does a 10bp deletion resulting in a premature stop codon affect thrombus formation?

I next investigated the thrombosis response of *p2y12*^{sh340} 3 dpf embryos obtained from a heterozygote in-cross. This 10bp deletion is predicted to induce a premature stop codon 9 amino acids downstream of the target region; homozygotes for this mutation should theoretically have a non-functional $P2Y_{12}$ receptor, therefore I hypothesised that this mutation would reduce thrombus area after laser injury, **Figure 5.14** show the results for this investigation. The thrombosis response of 20-22 embryos of wildtype, heterozygote or homozygote background was assessed by laser induced aortic injury, and quantification of the developing thrombus over 10 minutes. This was repeated 4 times on different days and the embryos were genotyped by PCR and restriction enzyme digest after completion of each experiment. **Figure 5.14 A** shows a plot of thrombus area over 10 minutes after injury with each embryo represented as a separate experiment (wildtype n=19, heterozygote n=46 and homozygote n=20). **B** shows the mean area under the curve of thrombus formation in wildtype, heterozygote and homozygote with each experimental replicate combined into a single mean (n=4). **C** shows the area under the curve data with each embryo represented as an individual experiment (wildtype n=19, heterozygote n=46 and homozygote n=20). I found that there was no significant difference in thrombus area between wildtype, heterozygote and homozygote siblings. This result was surprising, as it was expected that a frame shift and premature stop codon would result in a non-functional receptor. One possibility was that maternally contributed wildtype *p2y12* RNA present in the early embryo may be sufficient for a full thrombosis response.

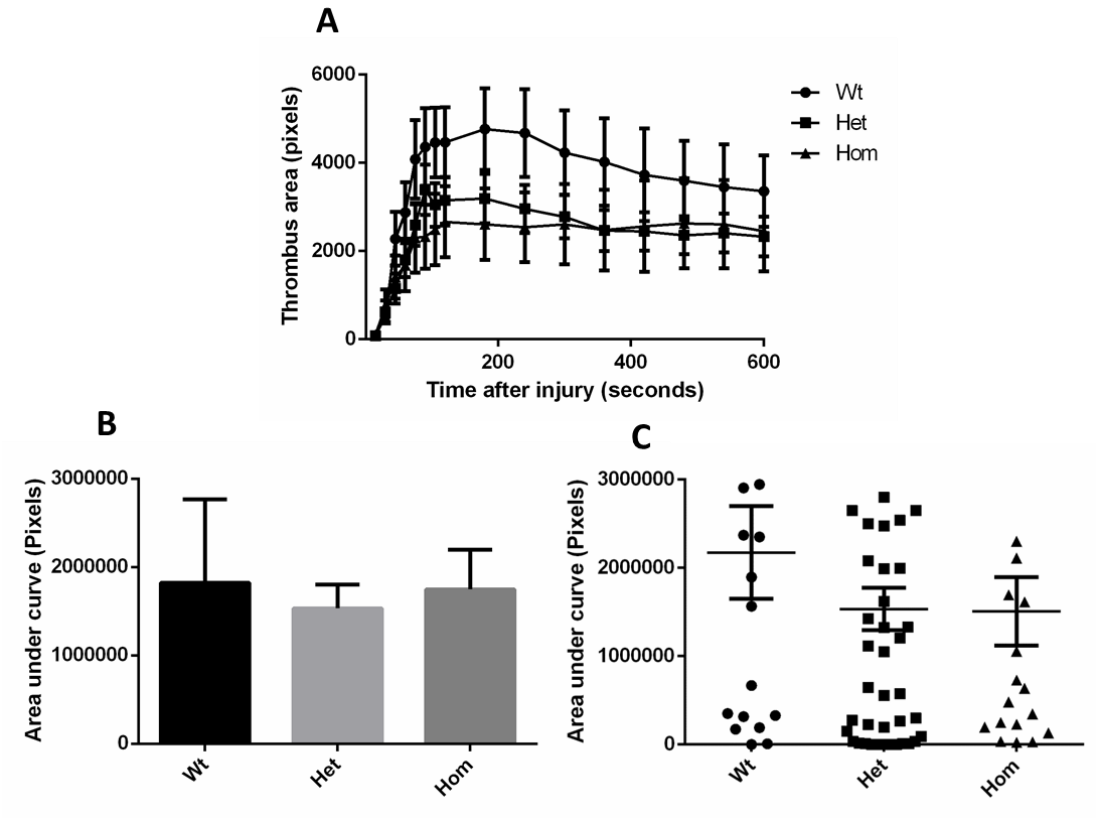

Figure 5.14 The effect of the 10bp *p2y12*^{sh340} mutation on thrombosis in 3dpf embryos.

Groups of 20-22 embryos of a wildtype (wt), heterozygote (het) or homozygote (hom) background underwent laser induced aortic injury and thrombus area was quantified over 10 mins. The embryos were genotyped by PCR and restriction enzyme digest after completion of the thrombosis assay. Four replicate experiments were performed on different days. **A** shows a plot of thrombus area over 10 minutes following laser induced aortic injury, where every embryo has been considered as a separate experiment (wildtype n=19, heterozygote n=46 and homozygote n=20). **B** shows the mean area under the curve in wildtype, heterozygote and homozygotes where data has been analysed by combining each experimental replicate into a single mean (n=4). **C** shows a scatter graph with each individual embryo represented as an experimental unit. A Kruskal-Wallis test was applied. Data are presented as mean ± SEM.

I next examined thrombosis in 5 dpf embryos, at which point maternally derived RNA should no longer be present. Due to the transient nature of MO, I have not previously utilised 5 dpf embryos in the examination of thrombosis response. **Figure 5.15** shows the results for the thrombosis response of 5 dpf embryos, after laser induced aortic injury of 12-13 embryos of a wildtype, heterozygote or homozygote background. The embryos were genotyped by PCR and restriction enzyme digest after completion of the thrombosis assay. Three replicate experiments were performed on different days. **A** shows a plot of thrombus area over 10 minutes after injury, where every embryo has been considered as a separate experiment (wildtype n=7, heterozygote n=24 and homozygote n=5). **B** shows the mean area under the curve of wildtype, heterozygote and homozygotes where data has been analysed by combining each experimental replicate into a single mean (n=3). **C** shows the thrombus area under the curve with each embryo considered as a separate experiment (wildtype n=7, heterozygote n=24 and homozygote n=5). I found that there was no significant difference in thrombosis response between wildtype, heterozygous and homozygous siblings.

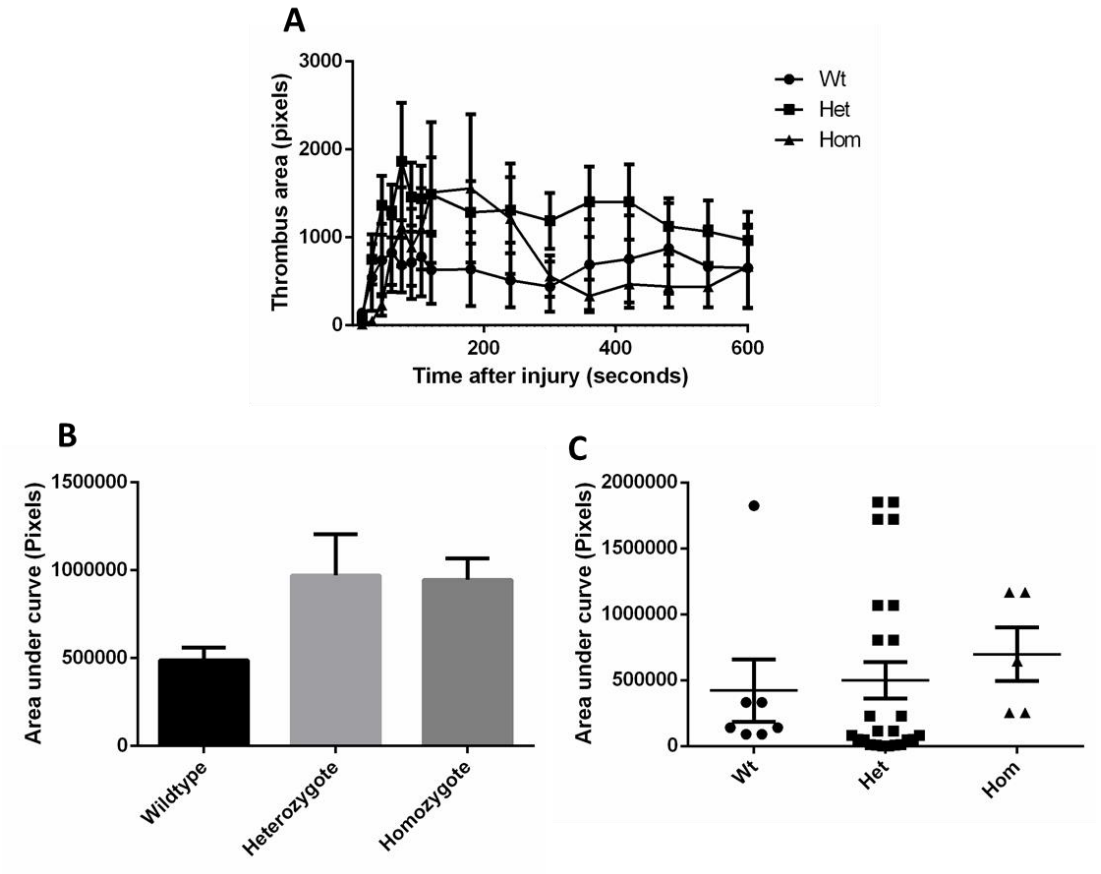

Figure 5.15 The effect of the 10bp *p2y12*^{sh340} mutation on thrombosis in 5 dpf embryos.

Groups of 12-13 embryos of a wildtype (wt), heterozygote (het) or homozygote (hom) background underwent laser induced aortic injury and thrombus area was quantified over 10 mins. The embryos were genotyped by PCR and restriction enzyme digest after completion of the thrombosis assay. Three replicate experiments were performed on different days. **A** shows a plot of thrombus area over 10 minutes following laser induced aortic injury, where every embryo has been considered as a separate experiment (wildtype n=7, heterozygote n=24 and homozygote n=5). **B** shows the mean area under the curve in wildtype, heterozygote and homozygotes where data has been analysed by combining each experimental replicate into a single mean (n=3). **C** shows a scatter graph with each individual embryo represented as an experimental unit. A Kruskal-Wallis test was applied, data are presented as mean ± SEM.

5.1.3.4 Is *p2y12* expressed in maternal RNA?

I investigated whether *p2y12* was expressed in maternally derived wildtype mRNA contributed from the heterozygous mother. RNA was extracted from unfertilised embryos and an RT-PCR reaction with $P2Y_{12}$ and GAPDH control primers was conducted. **Figure 5.16** shows that amplification with control GAPDH primers gives an amplified product in both the unfertilised cDNA and control cDNA well, whereas amplification with $P2Y_{12}$ primers shows amplified product in the control cDNA well exclusively therefore there has been no amplification of *p2y12* cDNA. This suggests that there is no significant maternal contribution of *p2y12* RNA.

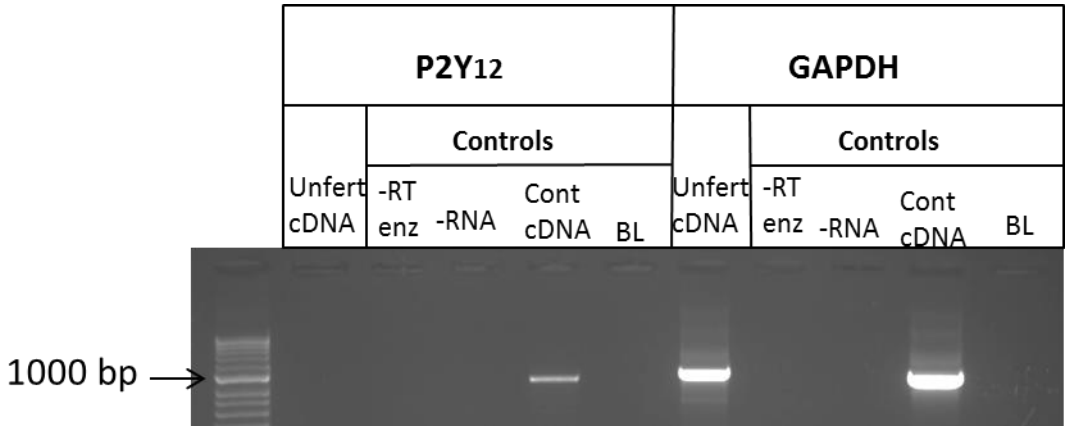

Figure 5.16 Assessment of maternally contributed *p2y12* expression.

P2Y12 and control GAPDH primers were utilised to assess whether there was maternally contributed *p2y12* RNA. RNA from unfertilised embryos was extracted and an RT- PCR with P2Y12 and GAPDH primers was conducted. There was no band in the lane for unfertilised cDNA with P2Y12 primers, however there was with GAPDH primers. There was a band in both control cDNA lanes with P2Y12 and GAPDH primer respectively. There are no bands in the controls; without reverse transcriptase enzyme (-RT enz), without RNA (-RNA) and the PCR blank (BL).

5.1.3.5 Does a 10bp deletion affect resistance to *S. aureus* infection?

I investigated the resistance to *S. aureus* infection of the *p2y12*^{sh340} mutants, to assess whether the mutants would reproduce the reduction in survival observed in the *p2y12* morphants. Embryos were inoculated with *S. aureus* directly into the circulation at 30 hpf, and survival was monitored over 90 hpi. Embryos which died during the experiment were genotyped within 12 hours of death, and all surviving embryos were genotyped at 90 hpi, at the conclusion of the experiment. This preliminary data representing 2 experimental replicates is shown in **Figure 5.17.** There appeared to be no difference in survival between the wildtype, heterozygotes and homozygote siblings. In order to assess whether the mortality shown in **A** was not due to trauma of injection alone, I injected the same volume of sterile PBS into *p2y12*^{sh340} mutants, **B** shows that there was minimal death subsequent to injection. As these data represents 2 experimental replicates, no statistical test was applied. However, these results do not appear to reproduce my previous data in which *p2y12* morphants showed significantly reduced survival after inoculation with a similar CFU of *S. aureus.*

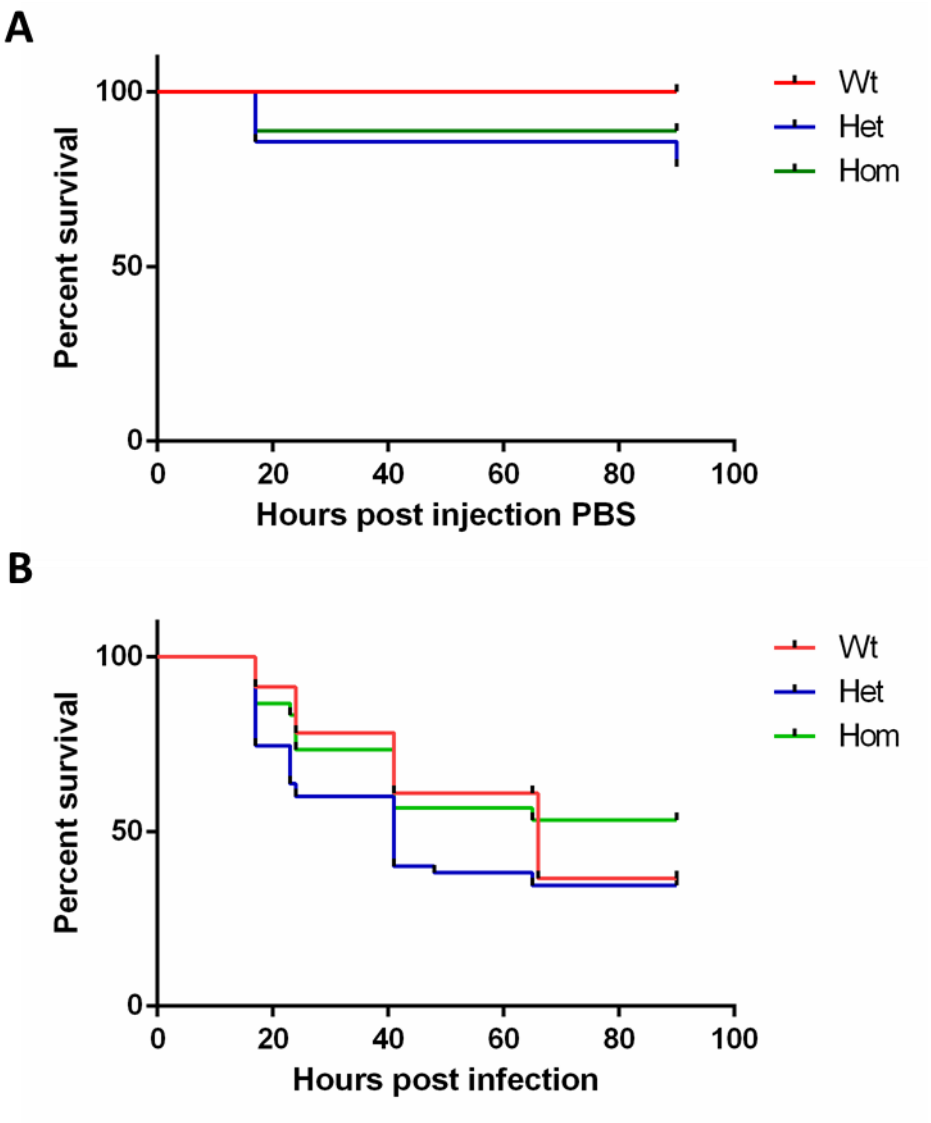

Figure 5.17 Survival of *p2y12*^{sh340} mutants after sterile PBS injection and *S. aureus* inoculation.

Wildtype (wt), heterozygotes (het) and homozygotes (hom) were injected with either a control of sterile PBS (**A**) or *S. aureus* (**B**), and their survival was monitored over 90 hours post injection. Embryos were genotyped either after death or after 90 hours post injection for surviving embryos. **A** shows the a Kaplan-Meier plot of survival of wt (n=4), het (n= 14) and hom (n=9) siblings after injection with a sterile PBS, in 2 experimental replicates on different days. **B** shows a Kaplan-Meier plot of survival after *S. aureus* infection of wt (n=23), het (n=55) and homs (n=30). A mean CFU count of 2201 was injected in 2 experimental replicates on different days. No statistical test was applied for analysis.

5.2 Discussion

ZFN mutagenesis was utilised in an attempt to generate a stable *p2y12* mutant, however the results of deep sequencing of pooled gDNA from F1 embryos showed a mutation rate (including all mutated alleles) of 2% for the SP5 and 3% for SP7. I considered these mutation frequencies too low to enable time and cost efficient screening for founders via sequencing. It was also difficult to confirm genuine mutations from pooled samples. A benefit of TALEN mutagenesis is the relative ease with which F0 fish can be screened for somatic mutations via the use of a restriction enzyme digest, as opposed to deep sequencing. This method for screening of TALEN F0 enabled the identification of 2 mutant alleles after the screening of approximately 100 fish. Therefore, although the mutation rate is similar for ZFN and this particular TALEN, the identification of founders is simpler and quicker. The TALEN mutant alleles were confirmed with sequencing and these mutants were selected for further investigation.

I identified both a 6bp deletion (*p2y12*^{sh338}) (**Figure 5.8**) and a 10bp deletion mutant allele (*p2y12*^{sh340}) (**Figure 5.9**). The 6bp deletion mutation resulted in a deletion of residues R^{55} and I^{56}. I investigated this mutant in terms of thrombus formation and found that there was no significant difference in thrombosis between wildtype siblings, heterozygotes and homozygotes (**Figure 5.13**). The 10bp deletion mutant allele was predicted to induce a frame shift and premature stop codon 9 amino acids downstream of the target site. I hypothesised that a homozygote with a frame shift and premature stop codon would have a reduced thrombosis response after vessel injury.

My thrombosis results indicate that a 10bp deletion, and subsequent premature stop codon within the first intracellular loop, does not significantly affect thrombus formation in 3 dpf embryos, after vessel injury (**Figure 5.14**). This was a surprising finding as I anticipated that the frame shift mutation proximal to the N-terminus would be sufficient to induce a loss of function phenotype that would reduce thrombosis. I also investigated the effect of this 10bp deletion on thrombosis in 5 dpf embryos, however once more there was no significant difference in thrombus area between the wildtype, heterozygote and homozygote (**Figure 5.15**). It is worth

noting the relatively low numbers of homozygotes and wildtypes in these assays when compared to heterozygotes, due to the in-cross of heterozygote F1s. The in-cross of F2 homozygotes would enable a high throughput approach to thrombosis assessment which was not available for my studies. This would be beneficial to investigate whether there is indeed a subtle difference in thrombosis response, as **Figure 5.14** suggests the possibility of a trend of reduction in thrombus area in the heterozygotes and homozygotes at 3 dpf, but was not statistically significant.

Several previously investigated mutations in the human *P2RY12* gene have shown a range of effects such as impaired ADP binding, reduced platelet secretion and limited cell surface expression of $P2Y_{12}$, resulting in extended bleeding times (Cattaneo et al., 2000) (Cattaneo et al., 2003, Patel et al., 2014, Daly et al., 2009). Fontana et al. (2009) suggest that a heterozygote with a *P2RY12* mutation resulting in a truncated protein is haploinsufficient and showed a bleeding phenotype with increased bleeding times compared to wildtype (Fontana et al., 2009). Considering this previous literature, it is interesting that there does not appear to be reduced thrombosis in *p2y12*^{sh340} mutants, neither heterozygotes nor homozygotes. There are several possible explanations for this; I largely excluded the possibility of a maternally derived contribution of wildtype *p2y12* RNA being sufficient for thrombosis response (**Figure 5.16**). It is possible that this thrombosis assay was not sufficient to determine a loss of function effect of $P2Y_{12}$, for example if too much vessel injury was sustained this may trigger various alternative platelet activation pathways, which could mask $P2Y_{12}$ effect. However, as this assay previously detected reduced thrombosis in *p2y12* morphants, this seems unlikely. Another possible explanation for the lack of effect on thrombosis is that, in the *p2y12* morphants, translation of *p2y12* mRNA is blocked, therefore there theoretically is no P2y12 protein produced and translocated to the cell surface, whereas in the mutant the truncated protein may retain some function. Anecdotal evidence presented by Nathan Lawson at the 'Zebrafish Disease Models Workshop 2013' suggests that a lack of phenotype in TALEN generated mutants is a relatively common occurrence.

The true mechanism is not currently known and this would require further investigation. It would be interesting to do a western blot on these mutants to ascertain whether protein is produced and of what length, however as previously discussed in chapter 3 there is no currently available antibody, suitable for this. As zebrafish have a genome duplication for many genes, there may be a transcript variant of *p2y12* which has not previously been described, which could rescue function of the receptor (Taylor et al., 2003), although it is hard to know why this redundancy would exist for mutants but not morphants. I have found no discrepancy with the Ensembl listed sequence for *p2y12*, except for the presence of several SNPs, and morpholinos designed against the ATG site of this gene produce the expected of reduction in thrombosis. The ATG MO I used for these studies also very closely resembles the ATG MO used by Sieger et al. (2012) which represents the first publication of *p2y12* knockdown in zebrafish and showed the same effect of reduction in GFP fluorescence in p2y12::P2Y12-GFP embryos as I observed. I also observed the reduced thrombosis phenotype with the P2Y12-mo2 published by Sieger et al. (2012). Therefore, this suggests that the Ensembl sequence for *p2y12* utilised in this thesis is consistent with the $P2Y_{12}$ receptor and that *p2y12* translation is being reduced in the morphants.

I investigated the resistance to infection of the $p2y12^{sh340}$ mutant siblings to ascertain whether the 10bp deletion in *p2y12* would affect the response to *S. aureus* infection. Previous data shown in this thesis documents that knockdown of *p2y12* significantly reduces resistance to *S. aureus* infection ($p<0.0001$). However, my preliminary data suggest that survival of neither $p2y12^{sh340}$ heterozygotes nor homozygotes differed to that of the wildtype sibling after *S. aureus* inoculation (**Figure 5.17**). Besides the mutation, there is a genetic difference between the mutant and morphant embryos as for the morphant experiments LWT line was utilised, however the genetic background of the TALEN fish is ABWT out-crossed to *nacre*. Therefore there may be some genetic difference in susceptibility which is not due to the *p2y12* mutation alone. Anecdotal evidence suggests that ABWT, may be more susceptible to *S. aureus* infection in this model, therefore this may partially explain the reduced survival of wildtypes when compared to previous control

morphants. This would require further work to fully investigate the infection response of *p2y12*^{sh340} in homozygotes from a homozygous in-cross.

Cattaneo et al. (2011) reviewed the different *p2y12* mutations found in patients with bleeding disorders; several of these patients had frame shifts in the open reading frame leading to a truncation of the protein (Cattaneo, 2011a). The effect of *P2RY12* truncation was analysed by the quantification of binding sites for 2MeS-ADP and platelet aggregation in response to ADP. Exposure of thrombocytes to ADP should induce a full and irreversible aggregation response, and *p2y12* deficiency would result in a reduced aggregation and reversible aggregation in response to ADP. Gregory and Jagadeeswaran (2002) selectively labelled thrombocytes in blood obtained from adult fish in order to assess the response of $P2Y_1$ to ADP. Therefore, this would be an interesting, if somewhat technically challenging, alternative to the thrombosis assay to interpret whether there is a loss of function of $P2Y_{12}$ in my mutants.

5.3 Conclusion

I generated two *p2y12* mutants via TALEN mutagenesis, resulting in a 6bp deletion (*p2y12*^{sh338}) and a 10bp deletion (*p2y12*^{sh340}). Upon assessment of these mutants I found that there was no significant difference in thrombosis response in either *p2y12*^{sh338} or *p2y12*^{sh340}. Resistance to infection was preliminarily examined in *p2y12*^{sh340} only, and I found that there appeared to be no difference in survival after inoculation with *S. aureus*. These findings conflict with my previous data generated with the use of an ATG MO targeting *p2y12.* Although I have found no significant thrombosis or infection phenotype during my investigations using my TALEN generated mutants, the functional effect of this mutation requires further examination. The assessment of whether there is a true loss of function of the receptor is vital. A western blot for P2y12 or an assessment of ADP binding capability of thrombocytes would give a good indication of the functional effect of the mutation.

Chapter 6 : General discussion, conclusion and future directions

6.1 General discussion

$P2Y_{12}$ has an established role in thrombosis with antagonists to this receptor frequently used as anti-thrombotic therapy for the treatment of acute coronary syndromes ((Mackman, 2008) for review). The aim of this thesis was to investigate whether $P2Y_{12}$ also plays a role in inflammation and resistance to infection. I initially utilised an ATG morpholino to induce knockdown of the zebrafish homologue *p2y12.* I then investigated the thrombosis response to endothelial injury of *p2y12* morphants and observed significantly reduced thrombus area compared to control morphants. This data is consistent with previous experimental work in the mouse model in which $P2Y_{12}$ knockout or treatment with $P2Y_{12}$ antagonists reduced thrombus formation and increased embolization (Foster et al., 2001, Andre et al., 2003, Patil et al., 2010). During the course of my project, Sieger et al. (2012) generated the p2y12::P2Y12-GFP transgenic line for investigation of the microglial response to injury, in addition they utilised a *p2y12* morpholino (P2Y12mo2) which targeted a different region to my morpholino. I utilised this line to investigate the effect of my *p2y12* morpholino on *p2y12* expression. I found my morpholino reduced GFP fluorescence of microglia, as previously reported in the experiment by Sieger et al. (2012) with P2Y12mo2. I also obtained this P2Y12mo2 morpholino and again found a significant reduction in thrombus area in *p2y12* morphants. To attempt to further ascertain the specificity of the effect of the morpholino studies, I generated a modified *p2y12* mRNA construct to which the *p2y12* morpholino would not bind. I co-injected this RNA with the *p2y12* morpholino and found that in the RNA co-injected morphants there was a suggestion that this ameliorated the effect of *p2y12* knockdown on thrombosis, although this was not statistically significant.

Therefore, taken together with studies of $P2Y_{12}$ in other species, it seems likely that the effect of the *p2y12* morpholino on thrombosis is truly due to *p2y12* knockdown rather than off-target or non-specific effects, although it is difficult to exclude these entirely.

After confirming that *p2y12* morpholino knockdown induced the expected effect on thrombosis. I moved on to assess the effect of *p2y12* knockdown on the inflammatory response. I first established that *p2y12* knockdown did not significantly affect total numbers of macrophages and neutrophils. I then found that *p2y12* knockdown did not significantly affect migration of either macrophages or neutrophils to sites of tail fin transection, tail fin incision or laser induced vessel damage in zebrafish embryos. Therefore, my data indicate that $P2Y_{12}$ does not play a role in leukocyte migration in these models of inflammatory response. This is an interesting negative result which indicates that $P2Y_{12}$ may not be directly involved in leukocyte migration to sites of injury. It is possible that the role of $P2Y_{12}$ in inflammation is related to the amplified release of pro-inflammatory mediators from α granules, rather than a more direct role in sensing of inflammatory cues. In which case, it is likely that the models of leukocyte migration for assessing inflammatory response used in this thesis may not be ideal for determining a more subtle inflammatory effect of thrombocyte releasates. It may be possible to develop a zebrafish assay for identification of pro-inflammatory mediator and chemokine release from activated thrombocytes, to enable assessment of leukocyte response. Another model for inflammation, for example chronic inflammation such as the atherosclerosis model in the *$P2Y_{12}$ -/-* mouse would allow good assessment of inflammatory response (Li et al., 2012a).

An off-target effect of ticagrelor is to block reuptake of adenosine, therefore I sought to investigate whether adenosine exposure affected leukocyte migration to sites of inflammation, however I found no significant difference in leukocyte migration in the concentrations of adenosine selected. This experiment lacked the necessary control to confirm that the adenosine was actively taken up into the blood stream of the embryos. The short half-life and labile nature of adenosine suggests that this would require further work to fully optimise an assay for investigation into the effect of adenosine.

I next investigated the resistance of *p2y12* morphants to *S. aureus* infection and even though I had found no effect of *p2y12* knockdown on inflammatory cell recruitment, I found that *p2y12* morphants suffered a statistically significant

increase in mortality after introduction of systemic infection. This finding indicates that the $P2Y_{12}$ receptor may play a role in defense against systemic *S. aureus* infection. My data may support work by Trier et al. (2008) showing reduced levels of platelet microbicidal proteins and kinocidins released from rabbit platelets, abolishing the staphylocidal capabilities, after exposure to both $P2X_1$ and $P2Y_{12}$ antagonists (Trier et al., 2008). It is possible that knockdown of *p2y12* reduces release of antimicrobial peptides from α granules, therefore impairing the defense against pathogens

It would be interesting to assess the functionality of α granules in the *p2y12* morphants, as a typical assessment of platelet activation is the detection of P-selectin release from α granules. An assessment of P-selectin release from *p2y12* morphant thrombocytes would indicate whether *p2y12* knockdown affects α granule release. However, human *P2RY12* is present on macrophages and although my *in situ* for zebrafish *p2y12* expression on macrophages was inconclusive, it is established to be present on microglia which arise from a phagocytic lineage shared by macrophages (Sieger et al., 2012). Therefore, it is possible that knockdown of *p2y12* impedes the response of macrophages to pathogens, and as macrophages are the primary cell responsible for combatting microbes this may explain the reduced survival of the *p2y12* morphants. It would be possible to utilise GFP labelled *S. aureus* and various transgenic lines, previously discussed, to investigate the interaction of thrombocytes, macrophages or neutrophils with *S. aureus in vivo*. Inoculating embryos with *S. aureus* after antagonism of the $P2Y_{12}$ receptor would indicate whether antagonism of the receptor, as opposed to knockdown, would be sufficient to increase susceptibility to *S. aureus*, as shown in *p2y12* morphants. However, during the course of my studies I have not observed anti-thrombotic effect of clinically used $P2Y_{12}$ antagonists on thrombus in the zebrafish model. This may be due to the challenges of delivering a sufficient systemic dose of drug by immersion, but also raises the possibility these antagonists may not be functional in zebrafish. Zebrafish are increasingly being used as a platform for drug screening, however my results suggest that clinically used $P2Y_{12}$ antagonists may not have been identified for an anti-thrombotic effect during a drug screen. Therefore,

further investigation and optimisation is required to determine whether $P2Y_{12}$ antagonists are functional in the zebrafish model and whether they can be used for the further investigation of inflammation and infective response in addition to thrombosis.

It would be interesting to assess the response of the *$P2Y_{12}$ -/-* mouse model to systemic *S. aureus* infection, in order to ascertain whether the results demonstrated in this thesis are reproduced in a mammalian model of *P2Y12* deficiency. Exposure of mice to $P2Y_{12}$ antagonists, such as ticagrelor, has resulted in a reduction in thrombosis, therefore this model would also enable the investigation of the effects of $P2Y_{12}$ antagonists on resistance to *S. aureus* infection (Patil et al., 2010). $P2Y_{12}$ antagonists are frequently used in anti-platelet therapy and *S. aureus* infection is a relatively common infection of hospitalized patients, therefore any possible reduction in defense against *S. aureus* would have implications for the current clinical use of $P2Y_{12}$ antagonists. This area requires further research to ascertain whether antagonism or deficiency of the $P2Y_{12}$ receptor increases susceptibility to *S. aureus* infection.

As previously discussed, the PLATO study showed a reduction in mortality associated with pulmonary infection and sepsis in ticagrelor treated patients compared to clopidogrel treated patients (Storey et al., 2013). Although this has caused some controversy it is an interesting finding. Recent unpublished data from our group has found that $P2Y_{12}$ antagonists reduce pro-inflammatory cytokines TNF and IL-6 release after systemic LPS administration in healthy volunteers, confirming that these drugs do indeed modulate the immune response in humans. The possible differential effect of ticagrelor and clopidogrel on susceptibility to infection remains unexplained, although it is possible that antagonism of $P2Y_{12}$ increases susceptibility to infection which, in the case of ticagrelor, is somewhat offset by other effects such as the action of adenosine on leukocytes. It would be interesting to examine whether adenosine was able to reduce mortality in *p2y12* morphant embryos after inoculation with *S. aureus* to address this question.

During the course of my studies I examined the effect of knockdown of miR-223, miR-126 and miR-24 on thrombosis after vessel injury. It is noteworthy that none of these morpholinos reduced thrombosis, implying that general off-target or non-specific effects of morpholinos are unlikely to explain the reduction in thrombosis seen in *p2y12* morphants. When I assessed thrombosis in miR-223 morphants, I found that knockdown of this microRNA significantly increases thrombus formation after vessel injury. This is novel data which offers an intriguing insight into the epigenetic regulation of thrombosis. It has been suggested that *P2RY12* can be regulated by miR-223 (Landry et al., 2009), providing a potential mechanism for my observation. Interestingly, recent work investigating thrombosis in the miR-223 null mouse has shown no significant effect on platelet activation and aggregation (Leierseder et al., 2013). This lack of effect on thrombosis in the mouse may be explained as there is currently no predicted miR-223 binding site in the 3' of mouse *P2Y12*, by www.mirBase.org. However, neither does www.mirBase.org predict a miR-223 binding site in zebrafish *p2y12*, therefore more investigation is required to determine whether miR-223 regulates *P2Y12* expression in species other than humans. miRNA research is a rapidly developing topic, however this contrasting data between different species serves to highlight the importance of a broad approach, encompassing different species, to investigate gene regulation by miRNAs.

In contrast to previously published investigations into knockdown of miR-126 in the zebrafish, I did not find ectopic vasculature or a haemorrhagic phenotype as described by Fish et al. (2008) and Nicoli (2010). This may be explained by either the difference in the morpholino used in my experiments, which was 6 nucleotides shorter, or the fact that I optimised 4.22 ng as the best morpholino amount to inject, as opposed to 4-8 ng by Fish et al (2008) and 7- 20 ng by Nicoli et al. (2010).

Morpholinos have been a mainstay for zebrafish research allowing for the knockdown of gene function in a relatively inexpensive and efficient manner. The use of either translation blocking or splice site morpholinos enable the knockdown of gene function until approximately 3 dpf. In the case of splice site blocking morpholinos, altered splicing such as intron inclusion or exon skipping can be

detected by RNA extraction and RT-PCR (although this does not confirm that any observed phenotype is due to specific effects on mRNA translation). However, the effect of translation blocking morpholinos cannot be detected by PCR. Ideally, this would require a western blot to prove a reduction in protein level, although this is rarely possible due to a lack of suitable antibodies. Morpholinos can induce non-specific toxicity which varies significantly depending on the gene target and morpholino design. Signs of non-specific toxicity in embryos include delayed development, cardiac oedema and small heads which can make interpretation of data generated in morpholino studies difficult. There is also a wide variation in injection volumes and amounts of morpholinos used in the literature, with up to 20 ng of morpholino injected, although for my studies the maximum amount of morpholino injected was 4.2 ng. Injection of large volumes or concentrations of morpholino is likely to increase the risk of non-specific effects which mask true effects of gene knockdown or produce a false positive result. It is clear therefore, that studies that rely entirely on morpholino knockdown are subject to technical considerations that make corroboration by other methods highly desirable.

Recent advances in mutagenesis have enabled the generation of mutants in a time and cost efficient manner. As well as reducing the chances of off-target effects being interpreted as the effect of gene knockdown, generation of stable mutants enables the study of stages of development later than is possible using morpholinos. The use of ZFN and TALEN mutagenesis techniques enable specific gene loci to be targeted for mutagenesis and the generation of different mutant alleles gives the possibility of assessing mutants with differing functional consequences. TALEN mutagenesis possesses advantages over ZFN mutagenesis as it is more time and cost efficient. There is an increased choice for target sites, with TAL sites occurring approximately every 35bp compared to 500bp for ZFN (Cermak et al., 2011, Sander et al., 2011). Screening for mutations in ZFN is primarily via sequencing rather than restriction digest, which increases the time and cost of confirming mutagenesis has been successful. The use of restriction enzyme digests for screening, which represents an advantage for TALEN mutagenesis, may be applied to ZFN mutagenesis. However the number of suitable ZF sites is considerably less

compared to TALEN, offering less chance of the target region coinciding with a suitable restriction enzyme digestion site. Both methods for generation of a mutant utilise the FokI cleavage domain to introduce a double strand break to introduce mutations via NHEJ. This technique appears to be a robust mechanism for introducing mutations. I generated 4 TALEN constructs and 2 ZFN constructs, however only one of the TALENs lines generated mutant alleles. Therefore, my results appear to show that there is a variation in levels of success depending on the method and positioning of the target region. This would require further investigation as to whether there is an optimum position of target sites for mutagenesis success, for example due to accessibility of the target region for mutagenesis.

My experience with TALEN mutagenesis suggests the possibility that injection of TALEN RNA directly into the cell as opposed to the yolk or cell/yolk border maximises the efficiency of mutagenesis of a TALEN with previously low efficiency. Both mutant alleles I discovered were raised from embryos injected with RNA directly into the cell, with no mutants found from injections of RNA into the yolk. Embryos were exclusively injected at 1 cell stage therefore, in the case of yolk injection, RNA should still be transported into the cell by cytoplasmic streaming. However, this is an interesting finding which highlights that mutagenesis may be more efficient when injected directly into the cell, which is an important consideration to increase efficiency of mutagenesis. It is also of note that the previous 3 TALENs and ZFNs were injected into the yolk, therefore it is possible that these TALEN and ZFN generated RNAs would also be successful if I changed my RNA injection method. However, others in our group have successfully induced stable mutants without needing repeated attempts using different TALEN or ZFN pairs, suggesting that *p2y12* truly is more challenging to mutate than other loci.

Due to the need for repeated attempts and the time required to raise potential founders for screening, successful generation of TALEN-induced *p2y12* mutants occupied a large amount of my time during this project. However, ultimately, I was able to identify two separate *p2y12* mutant alleles successfully generated by this approach, although by the time these were identified I only had limited time to

characterize their phenotype. The *p2y12*^{sh338} allele induced a six base pair deletion that would only cause a loss of two amino acids. This may have only minor or silent effects on the overall function of *p2y12*, and it was not surprising that no apparent effect on thrombosis was observed in these embryos. However, the *p2y12*^{sh340} allele that is predicted to induce an early stop codon was not associated with clear effects on thrombosis, which is surprising in the context of my morpholino data and the existing literature on the role of *p2y12* in this process.

The effects of mutations in *P2RY12* have been studied by a number of groups, many of which are reviewed by Cattaneo (2011)(Cattaneo, 2011b). A substitution mutation which affects the second extracellular loop of $P2Y_{12}$ was shown by Daly et al (2009) to impair ligand binding and result in a bleeding phenotype when in combination with a mild type 1 von Willibrand disease and a *VWF* defect (Daly et al., 2009). An individual homozygous for R122C substitution within the highly conserved DRY motif of *P2RY12* was shown to have impaired ADP stimulated aggregation and a reduction in $P2Y_{12}$ cell surface expression resulting in a bleeding disorder (Patel et al., 2014). Fontana et. al (2009) identified haploinsufficiency of *P2RY12*, in a heterozygote for a deletion downstream of the third transmembrane domain, resulting in a truncation of P2Y12 protein (Fontana et al., 2009, Conley 2001). This individual showed reduced platelet aggregation, reduced platelet secretion and a mild bleeding phenotype (Cattaneo et al., 2000). This study indicates that heterozygosity for a truncated protein is sufficient to result in a bleeding phenotype. Therefore, the absence of an effect on thrombosis in my *p2y12*^{sh340} homozygous mutant is all the more intriguing.

The reason for the failure of the *p2y12* mutants to reproduce the morphant phenotype with regard to either thrombosis or mortality after systemic infection remains unclear. There are several possible explanations. The wrong locus may have been mutated, but this is unlikely since these were confirmed by sequencing therefore they are present in the genome, in the coding region annotated as *p2y12*, and this is the gene which the morpholinos target. It is possible that there is a mechanism in the developing embryo which enables rescue of gene function perhaps via redundancy. Although zebrafish *p2y12* is currently listed on Ensembl

(www.ensembl.org) as a single orthologue of mammalian *P2Y12,* it is possible that, due to evolutionary genome duplication, there is an as yet unknown second orthologue of *p2y12* which can compensate for the mutation. Investigation into the thrombosis response of *P2Y$_{12}$ -/+* mice found that there was no significant difference in thrombotic response compared to wildtype, therefore in this model one functional copy of *P2Y12* appears to be sufficient for a normal thrombosis response (Patil et al., 2010). This is in contrast to the haploinsufficiency of human *P2RY12,* in which a single mutated allele (resulting in a truncated protein) caused impaired aggregation, secretion and reduced binding sites (Fontana et al., 2009).

However, the possibility of a second orthologue of *p2y12* does not explain why the *p2y12* morphants, in which the morpholino was designed according to the same cDNA sequence as my *p2y12* mutants, produces an effect on thrombosis consistent with previous mouse models of *P2Y12*. It is possible that the observed effect of the *p2y12* morpholino on thrombosis is caused not by specific *p2y12* knockdown but by other, off-target or non-specific effects. This would imply that zebrafish *p2y12* does not play a role in thrombosis. This is possible but it is noteworthy I have not seen a reduction in thrombosis induced by multiple other morpholinos, so an off-target effect would have to be specific to the sequences of both *p2y12* morpholinos that I examined, and this seems unlikely. If indeed loss of function of *p2y12* does not reduce thrombosis, this would indicate a very different function for *p2y12* in zebrafish than in any other species so far examined. This is again possible, although the previously demonstrated conservation of thrombotic pathways between zebrafish and mammals would make it surprising.

The explanation that best fits my data in the context of the known functions of *p2y12* is that the mutant alleles retain sufficient function to allow normal thrombosis. This might be expected for *p2y12*^{sh338}, but is a surprising finding for *p2y12*^{sh340}. To confirm this would require proteomic analysis in the zebrafish mutants to confirm the consequences of the mutation on protein primary structure (it is perhaps possible that the predicted stop codon does not cause a halt in translation). If indeed there is premature truncation of zebrafish *p2y12* in these mutants, then expression studies in cell culture would be interesting to assess the

functional consequences of the mutation. The *p2y12*^{sh340} mutation is predicted to produce a stop codon upstream of the key residues associated with activation of P2Y$_{12}$ such as Y^{105}, E^{188}, R^{256}, Y^{259} and ^{280} (which are conserved in the zebrafish) (Hoffmann et al., 2008, Ignatovica et al., 2012, Schmidt et al., 2013). There is also a partial conservation of the DRY motif, which is involved in trafficking and G protein interaction, downstream of the *p2y12*^{sh340} mutation (Nygaard et al., 2009). These sequence similarities indicates their functional importance in P2Y$_{12}$, therefore the disruption of these residues, for example as seen in the DRY motif mutation noted by Patel et al. (2014), could result in a bleeding phenotype (Patel et al., 2014), however no such effect was observed in *p2y12*^{sh340}.

There is an indication that that several TALEN generated mutants lack the phenotype associated with the morphants for that gene. This evidence, in addition to my data presented in this thesis, serves to highlight current difficulty in interpreting results obtained from morphants compared to mutants, in the zebrafish model.

6.2 Future directions

It would be interesting to further investigate the relationship between P2Y$_{12}$ and miR-223 in the zebrafish model of thrombosis. Overexpression studies of miR-223 would enable the investigation of the role of miR-223 in regulation of P2Y$_{12}$. As miR-223 may regulate translation of the *p2y12* mRNA to protein, overexpression of miR-223 would potentially produce the same phenotype as *p2y12* knockdown, which acts by sterically blocking translation of mRNA to protein. Co-injection of miR-223 MO with *p2y12* MO may rescue the reduction of thrombosis in the *p2y12* morphant and increase in thrombosis in the miR-223 morphant, respectively. It would be interesting to investigate whether co-injection of both of these MOs would cancel out each phenotype or whether *p2y12* MO would prevent overexpression due to blocking translation. It may be possible to quantify GFP fluorescence in the p2y12::P2Y12-GFP transgenic, after injection with the miR-223 MO, thus enabling the assessment of the role of miR-223 in regulation of *p2y12* translation.

There were time limitations impeding the investigation of the *p2y12* mutants. For example, it would be beneficial to assess the thrombosis, inflammation and infection response of embryos generated from a homozygous in-cross. This would enable high through put of investigations which were limited in this thesis by only being able to obtain the 25% Mendelian ratio of homozygotes from a heterozygous in-cross. Unfortunately I have conducted no investigation into the inflammatory response of the *p2y12*^{sh340}, as there was insufficient time to cross the mutant allele into the transgenic *mpo*:GFP or *fmsgal4;*UNM background. It would be possible to investigate migration of macrophages and neutrophils to sites of injury in *p2y12*^{sh340} mutants via the use of an *in situ* probe for *L-plastin* and an antibody for MPO. However, since the morpholino did not induce an effect and I consider it most likely that the *p2y12*^{sh340} allele does not induce loss of function of *p2y12* (despite its predicted effect on protein structure), I would expect not to detect a marked effect on inflammation in these mutants.

6.3 Conclusion

The involvement of P2Y$_{12}$ in thrombosis is well documented in many models, however, until this thesis, it has not to my knowledge, been investigated in the zebrafish. The results discussed in this thesis demonstrate that *p2y12* morphants show a statistically significant reduction in thrombus area after vessel injury when compared to control morphants. This is consistent with previous studies in which *P2Y$_{12}$ -/-* mice show reduced thrombosis response and increased embolization of thrombus when compared to wildtype mice (Andre et al., 2003, Foster et al., 2001) (Patil et al., 2010). This data also confirms that the function of P2Y$_{12}$ in thrombosis is conserved in the zebrafish. I found no significant difference in leukocyte migration to injury in the *p2y12* morphants, indicating that *p2y12* is not involved in leukocyte migration to sites of tail or vessel injury in this model. However I found that *p2y12* morphants had significantly reduced survival after inoculation with *S. aureus.* This is a novel finding which indicates that the P2Y$_{12}$ receptor may play a role in defence against systemic *S. aureus* infection via an unknown mechanism. I generated 2 TALEN *p2y12* mutants, however I found that neither the 6bp deletion nor 10bp deletion mutation phenocopied my morphant generated data, which I

consider likely to be due to the mutations not altering protein function sufficiently. During my investigations into the involvement of known platelet microRNAs in thrombosis, I discovered that knockdown of miR-223 significantly increases thrombus area after vessel injury. As miR-223 is proposed to regulate *P2RY12* (Landry et al., 2009), this is an important finding to begin to understand the role of miR-223 in thrombosis.

Chapter 7 : References

ALGAIER, I., JAKUBOWSKI, J. A., ASAI, F. & VON KUGELGEN, I. 2008. Interaction of the active metabolite of prasugrel, R-138727, with cysteine 97 and cysteine 175 of the human P2Y12 receptor. *J Thromb Haemost,* 6**,** 1908-14.

AMORES, A., FORCE, A., YAN, Y. L., JOLY, L., AMEMIYA, C., FRITZ, A., HO, R. K., LANGELAND, J., PRINCE, V., WANG, Y. L., WESTERFIELD, M., EKKER, M. & POSTLETHWAIT, J. H. 1998. Zebrafish hox clusters and vertebrate genome evolution. *Science,* 282**,** 1711-4.

ANDRE, P., DELANEY, S. M., LAROCCA, T., VINCENT, D., DEGUZMAN, F., JUREK, M., KOLLER, B., PHILLIPS, D. R. & CONLEY, P. B. 2003. P2Y(12) regulates platelet adhesion/activation, thrombus growth, and thrombus stability in injured arteries. *Journal of Clinical Investigation,* 112**,** 398-406.

ANGIOLILLO, D. J., CAPRANZANO, P., GOTO, S., ASLAM, M., DESAI, B., CHARLTON, R. K., SUZUKI, Y., BOX, L. C., SHOEMAKER, S. B., ZENNI, M. M., GUZMAN, L. A. & BASS, T. A. 2008. A randomized study assessing the impact of cilostazol on platelet function profiles in patients with diabetes mellitus and coronary artery disease on dual antiplatelet therapy: results of the OPTIMUS-2 study. *Eur Heart J,* 29**,** 2202-11.

ASSOIAN, R. K. & SPORN, M. B. 1986. Type beta transforming growth factor in human platelets: release during platelet degranulation and action on vascular smooth muscle cells. *J Cell Biol,* 102**,** 1217-23.

BARTEL, D. P. 2004. MicroRNAs: genomics, biogenesis, mechanism, and function. *Cell,* 116**,** 281-97.

BAYER, A. S., SULLAM, P. M., RAMOS, M., LI, C., CHEUNG, A. L. & YEAMAN, M. R. 1995. Staphylococcus aureus induces platelet aggregation via a fibrinogen-dependent mechanism which is independent of principal platelet glycoprotein IIb/IIIa fibrinogen-binding domains. *Infect Immun,* 63**,** 3634-41.

BENARD, E. L., VAN DER SAR, A. M., ELLETT, F., LIESCHKE, G. J., SPAINK, H. P. & MEIJER, A. H. 2012. Infection of zebrafish embryos with intracellular bacterial pathogens. *J Vis Exp*.

BENNETT, C. M., KANKI, J. P., RHODES, J., LIU, T. X., PAW, B. H., KIERAN, M. W., LANGENAU, D. M., DELAHAYE-BROWN, A., ZON, L. I., FLEMING, M. D. & LOOK, A. T. 2001. Myelopoiesis in the zebrafish, Danio rerio. *Blood,* 98**,** 643-51.

BERTRAND, J. Y., KIM, A. D., VIOLETTE, E. P., STACHURA, D. L., CISSON, J. L. & TRAVER, D. 2007. Definitive hematopoiesis initiates through a committed erythromyeloid progenitor in the zebrafish embryo. *Development,* 134**,** 4147-56.

BLASCO-COLMENARES, E., PERL, T. M., GUALLAR, E., BAUMGARTNER, W. A., CONTE, J. V., ALEJO, D., PASTOR-BARRIUSO, R., SHARRETT, A. R. & FARADAY, N. 2009. Aspirin Plus Clopidogrel and Risk of Infection After Coronary Artery Bypass Surgery. *Archives of Internal Medicine,* 169**,** 788-796.

BOEHLEN, F. & CLEMETSON, K. J. 2001. Platelet chemokines and their receptors: what is their relevance to platelet storage and transfusion practice? *Transfus Med,* 11**,** 403-17.

BOUDREAUX, M. K. & MARTIN, M. 2011. P2Y12 receptor gene mutation associated with postoperative hemorrhage in a Greater Swiss Mountain dog. *Vet Clin Pathol,* 40**,** 202-6.

BRANDT, J. T., CLOSE, S. L., ITURRIA, S. J., PAYNE, C. D., FARID, N. A., ERNEST, C. S., 2ND, LACHNO, D. R., SALAZAR, D. & WINTERS, K. J. 2007. Common polymorphisms of CYP2C19 and CYP2C9 affect the pharmacokinetic and pharmacodynamic response to clopidogrel but not prasugrel. *J Thromb Haemost,* 5**,** 2429-36.

BROTHERS, K. M., NEWMAN, Z. R. & WHEELER, R. T. 2011. Live imaging of disseminated candidiasis in zebrafish reveals role of phagocyte oxidase in limiting filamentous growth. *Eukaryot Cell,* 10**,** 932-44.

CANNON, C. P., HUSTED, S., HARRINGTON, R. A., SCIRICA, B. M., EMANUELSSON, H., PETERS, G., STOREY, R. F. & INVESTIGATORS, D.-. 2007. Safety, tolerability, and initial efficacy of AZD6140, the first reversible oral adenosine diphosphate receptor antagonist, compared with clopidogrel, in patients with non-ST-segment elevation acute coronary syndrome: primary results of the DISPERSE-2 trial. *J Am Coll Cardiol,* 50**,** 1844-51.

CARRILLO, M., KIM, S., RAJPUROHIT, S. K., KULKARNI, V. & JAGADEESWARAN, P. 2010. Zebrafish von Willebrand factor. *Blood Cells Mol Dis*.

CASTOR, C. W., MILLER, J. W. & WALZ, D. A. 1983. Structural and biological characteristics of connective tissue activating peptide (CTAP-III), a major human platelet-derived growth factor. *Proc Natl Acad Sci U S A,* 80**,** 765-9.

CATTANEO, M. 2011a. Molecular defects of the platelet P2 receptors. *Purinergic Signal,* 7**,** 333-9.

CATTANEO, M. 2011b. The platelet P2Y(1)(2) receptor for adenosine diphosphate: congenital and drug-induced defects. *Blood,* 117**,** 2102-12.

CATTANEO, M., LECCHI, A., LOMBARDI, R., GACHET, C. & ZIGHETTI, M. L. 2000. Platelets from a patient heterozygous for the defect of P2CYC receptors for ADP have a secretion defect despite normal thromboxane A2 production and normal granule stores: further evidence that some cases of platelet 'primary secretion defect' are heterozygous for a defect of P2CYC receptors. *Arterioscler Thromb Vasc Biol,* 20**,** E101-6.

CATTANEO, M., ZIGHETTI, M. L., LOMBARDI, R., MARTINEZ, C., LECCHI, A., CONLEY, P. B., WARE, J. & RUGGERI, Z. M. 2003. Molecular bases of defective signal transduction in the platelet P2Y12 receptor of a patient with congenital bleeding. *Proc Natl Acad Sci U S A,* 100**,** 1978-83.

CELI, A., PELLEGRINI, G., LORENZET, R., DEBLASI, A., READY, N., FURIE, B. C. & FURIE, B. 1994. P-SELECTIN INDUCES THE EXPRESSION OF TISSUE FACTOR ON MONOCYTES. *Proceedings of the National Academy of Sciences of the United States of America,* 91**,** 8767-8771.

CERMAK, T., DOYLE, E. L., CHRISTIAN, M., WANG, L., ZHANG, Y., SCHMIDT, C., BALLER, J. A., SOMIA, N. V., BOGDANOVE, A. J. & VOYTAS, D. F. 2011. Efficient design and assembly of custom TALEN and other TAL effector-based constructs for DNA targeting. *Nucleic Acids Res,* 39**,** e82.

CHAO, C. C., HSU, P. C., JEN, C. F., CHEN, I. H., WANG, C. H., CHAN, H. C., TSAI, P. W., TUNG, K. C., WANG, C. H., LAN, C. Y. & CHUANG, Y. J. 2010. Zebrafish as a model host for Candida albicans infection. *Infect Immun,* 78**,** 2512-21.

CHEN, A. T. & ZON, L. I. 2009. Zebrafish blood stem cells. *J Cell Biochem,* 108**,** 35-42.

CHEN, Y., CORRIDEN, R., INOUE, Y., YIP, L., HASHIGUCHI, N., ZINKERNAGEL, A., NIZET, V., INSEL, P. A. & JUNGER, W. G. 2006. ATP release guides neutrophil chemotaxis via P2Y2 and A3 receptors. *Science,* 314**,** 1792-5.

CHRISTIAN, M., CERMAK, T., DOYLE, E. L., SCHMIDT, C., ZHANG, F., HUMMEL, A., BOGDANOVE, A. J. & VOYTAS, D. F. 2010. Targeting DNA double-strand breaks with TAL effector nucleases. *Genetics,* 186**,** 757-61.

CLARKE, T. A. & WASKELL, L. A. 2003. The metabolism of clopidogrel is catalyzed by human cytochrome P450 3A and is inhibited by atorvastatin. *Drug Metab Dispos,* 31**,** 53-9.

COLUCCI-GUYON, E., TINEVEZ, J. Y., RENSHAW, S. A. & HERBOMEL, P. 2011. Strategies of professional phagocytes in vivo: unlike macrophages, neutrophils engulf only surface-associated microbes. *Journal of cell science,* 124**,** 3053-9.

CONLEY , P. B., JUREK, M.M., VINCENT, D., LECCHI, A. & CATTANEO, M. 2001. Unique mutations in the P2Y12 locus of patients with previously described defects in ADP-dependent aggregation. . *Blood,* 98**,** 43b

COPPINGER, J. A., CAGNEY, G., TOOMEY, S., KISLINGER, T., BELTON, O., MCREDMOND, J. P., CAHILL, D. J., EMILI, A., FITZGERALD, D. J. & MAGUIRE, P. B. 2004. Characterization of the proteins released from activated platelets leads to localization of novel platelet proteins in human atherosclerotic lesions. *Blood,* 103**,** 2096-104.

CRAMER, E. M., MEYER, D., LE MENN, R. & BRETON-GORIUS, J. 1985. Eccentric localization of von Willebrand factor in an internal structure of platelet alpha-granule resembling that of Weibel-Palade bodies. *Blood,* 66**,** 710-3.

CRONSTEIN, B. N., LEVIN, R. I., PHILIPS, M., HIRSCHHORN, R., ABRAMSON, S. B. & WEISSMANN, G. 1992. Neutrophil adherence to endothelium is enhanced via adenosine A1 receptors and inhibited via adenosine A2 receptors. *J Immunol,* 148**,** 2201-6.

DALY, M. E., DAWOOD, B. B., LESTER, W. A., PEAKE, I. R., RODEGHIERO, F., GOODEVE, A. C., MAKRIS, M., WILDE, J. T., MUMFORD, A. D., WATSON, S. P. & MUNDELL, S. J. 2009. Identification and characterization of a novel P2Y 12 variant in a patient diagnosed with type 1 von Willebrand disease in the European MCMDM-1VWD study. *Blood,* 113**,** 4110-3.

DANIEL, J. L., DANGELMAIER, C., JIN, J., ASHBY, B., SMITH, J. B. & KUNAPULI, S. P. 1998. Molecular basis for ADP-induced platelet activation. I. Evidence for three distinct ADP receptors on human platelets. *J Biol Chem,* 273**,** 2024-9.

DAVIDSON, A. J., ERNST, P., WANG, Y., DEKENS, M. P., KINGSLEY, P. D., PALIS, J., KORSMEYER, S. J., DALEY, G. Q. & ZON, L. I. 2003. cdx4 mutants fail to specify blood progenitors and can be rescued by multiple hox genes. *Nature,* 425**,** 300-6.

DAY, K., KRISHNEGOWDA, N. & JAGADEESWARAN, P. 2004. Knockdown of prothrombin in zebrafish. *Blood Cells Mol Dis,* 32**,** 191-8.

DETRICH, H. W., 3RD, KIERAN, M. W., CHAN, F. Y., BARONE, L. M., YEE, K., RUNDSTADLER, J. A., PRATT, S., RANSOM, D. & ZON, L. I. 1995. Intraembryonic hematopoietic cell migration during vertebrate development. *Proc Natl Acad Sci U S A,* 92**,** 10713-7.

DIEHL, P., OLIVIER, C., HALSCHEID, C., HELBING, T., BODE, C. & MOSER, M. 2010. Clopidogrel affects leukocyte dependent platelet aggregation by P2Y12 expressing leukocytes. *Basic Res Cardiol,* 105**,** 379-87.

DING, Z., KIM, S., DORSAM, R. T., JIN, J. & KUNAPULI, S. P. 2003. Inactivation of the human P2Y12 receptor by thiol reagents requires interaction with both extracellular cysteine residues, Cys17 and Cys270. *Blood,* 101**,** 3908-14.

DORSAM, R. T., TULUC, M. & KUNAPULI, S. P. 2004. Role of protease-activated and ADP receptor subtypes in thrombin generation on human platelets. *J Thromb Haemost,* 2**,** 804-12.

ECKLY, A., HECHLER, B., FREUND, M., ZERR, M., CAZENAVE, J. P., LANZA, F., MANGIN, P. H. & GACHET, C. 2011. Mechanisms underlying FeCl3-induced arterial thrombosis. *J Thromb Haemost,* 9**,** 779-89.

ELKS, P. M., VAN EEDEN, F. J., DIXON, G., WANG, X., REYES-ALDASORO, C. C., INGHAM, P. W., WHYTE, M. K., WALMSLEY, S. R. & RENSHAW, S. A. 2011. Activation of hypoxia-inducible factor-1alpha (Hif-1alpha) delays inflammation resolution by reducing neutrophil apoptosis and reverse migration in a zebrafish inflammation model. *Blood,* 118**,** 712-22.

ELLETT, F., PASE, L., HAYMAN, J. W., ANDRIANOPOULOS, A. & LIESCHKE, G. J. 2011. mpeg1 promoter transgenes direct macrophage-lineage expression in zebrafish. *Blood,* 117**,** e49-56.

EVANS, D. J., JACKMAN, L. E., CHAMBERLAIN, J., CROSDALE, D. J., JUDGE, H. M., JETHA, K., NORMAN, K. E., FRANCIS, S. E. & STOREY, R. F. 2009. Platelet P2Y(12) receptor influences the vessel wall response to arterial injury and thrombosis. *Circulation,* 119**,** 116-22.

FALATI, S., GROSS, P., MERRILL-SKOLOFF, G., FURIE, B. C. & FURIE, B. 2002. Real-time in vivo imaging of platelets, tissue factor and fibrin during arterial thrombus formation in the mouse. *Nat Med,* 8**,** 1175-81.

FAZI, F., ROSA, A., FATICA, A., GELMETTI, V., DE MARCHIS, M. L., NERVI, C. & BOZZONI, I. 2005. A minicircuitry comprised of microRNA-223 and transcription factors NFI-A and C/EBPalpha regulates human granulopoiesis. *Cell,* 123**,** 819-31.

FIEDLER, J., JAZBUTYTE, V., KIRCHMAIER, B. C., GUPTA, S. K., LORENZEN, J., HARTMANN, D., GALUPPO, P., KNEITZ, S., PENA, J. T., SOHN-LEE, C., LOYER, X., SOUTSCHEK, J., BRAND, T., TUSCHL, T., HEINEKE, J., MARTIN, U., SCHULTE-MERKER, S., ERTL, G., ENGELHARDT, S., BAUERSACHS, J. & THUM, T. 2011. MicroRNA-24 regulates vascularity after myocardial infarction. *Circulation,* 124**,** 720-30.

FISH, J. E., SANTORO, M. M., MORTON, S. U., YU, S., YEH, R. F., WYTHE, J. D., IVEY, K. N., BRUNEAU, B. G., STAINIER, D. Y. & SRIVASTAVA, D. 2008. miR-126 regulates angiogenic signaling and vascular integrity. *Dev Cell,* 15**,** 272-84.

FONTANA, G., WARE, J. & CATTANEO, M. 2009. Haploinsufficiency of the platelet P2Y12 gene in a family with congenital bleeding diathesis. *Haematologica,* 94**,** 581-4.

FONTANA, P., DUPONT, A., GANDRILLE, S., BACHELOT-LOZA, C., RENY, J. L., AIACH, M. & GAUSSEM, P. 2003. Adenosine diphosphate-induced platelet aggregation is associated with P2Y12 gene sequence variations in healthy subjects. *Circulation,* 108**,** 989-95.

FOSTER, C. J., PROSSER, D. M., AGANS, J. M., ZHAI, Y., SMITH, M. D., LACHOWICZ, J. E., ZHANG, F. L., GUSTAFSON, E., MONSMA, F. J., JR., WIEKOWSKI, M. T., ABBONDANZO, S. J., COOK, D. N., BAYNE, M. L., LIRA, S. A. & CHINTALA, M. S. 2001. Molecular identification and characterization of the platelet ADP receptor targeted by thienopyridine antithrombotic drugs. *J Clin Invest,* 107**,** 1591-8.

FOWLER, V. G., JR., MIRO, J. M., HOEN, B., CABELL, C. H., ABRUTYN, E., RUBINSTEIN, E., COREY, G. R., SPELMAN, D., BRADLEY, S. F., BARSIC, B., PAPPAS, P. A., ANSTROM, K. J., WRAY, D., FORTES, C. Q., ANGUERA, I., ATHAN, E., JONES, P., VAN DER MEER, J. T., ELLIOTT, T. S., LEVINE, D. P., BAYER, A. S. & INVESTIGATORS, I. C. E. 2005. Staphylococcus aureus endocarditis: a consequence of medical progress. *JAMA,* 293**,** 3012-21.

FREDHOLM, B. B. 1997. Purines and neutrophil leukocytes. *Gen Pharmacol,* 28**,** 345-50.

FREDHOLM, B. B. 2007. Adenosine, an endogenous distress signal, modulates tissue damage and repair. *Cell Death Differ,* 14**,** 1315-23.

GALLOWAY, J. L., WINGERT, R. A., THISSE, C., THISSE, B. & ZON, L. I. 2005. Loss of gata1 but not gata2 converts erythropoiesis to myelopoiesis in zebrafish embryos. *Dev Cell,* 8**,** 109-16.

GARCIA, A., KIM, S., BHAVARAJU, K., SCHOENWAELDER, S. M. & KUNAPULI, S. P. 2010. Role of phosphoinositide 3-kinase beta in platelet aggregation and thromboxane A2 generation mediated by Gi signalling pathways. *Biochem J,* 429**,** 369-77.

GEIGER, J., BRICH, J., HONIG-LIEDL, P., EIGENTHALER, M., SCHANZENBACHER, P., HERBERT, J. M. & WALTER, U. 1999. Specific impairment of human platelet P2Y(AC) ADP receptor-mediated signaling by the antiplatelet drug clopidogrel. *Arterioscler Thromb Vasc Biol,* 19**,** 2007-11.

GEORGE, J. N. 1978. Studies on platelet plasma membranes. IV. Quantitative analysis of platelet membrane glycoproteins by (125I)-diazotized diiodosulfanilic acid labeling and SDS-polyacrylamide gel electrophoresis. *J Lab Clin Med,* 92**,** 430-46.

GERRARD, J. M., PHILLIPS, D. R., RAO, G. H., PLOW, E. F., WALZ, D. A., ROSS, R., HARKER, L. A. & WHITE, J. G. 1980. Biochemical studies of two patients with the gray platelet syndrome. Selective deficiency of platelet alpha granules. *J Clin Invest,* 66**,** 102-9.

GILLES, A., MEGLECZ, E., PECH, N., FERREIRA, S., MALAUSA, T. & MARTIN, J. F. 2011. Accuracy and quality assessment of 454 GS-FLX Titanium pyrosequencing. *BMC Genomics,* 12**,** 245.

GONG, Y. F., XIANG, L. X. & SHAO, J. Z. 2009. CD154-CD40 interactions are essential for thymus-dependent antibody production in zebrafish: insights into the origin of costimulatory pathway in helper T cell-regulated adaptive immunity in early vertebrates. *J Immunol,* 182**,** 7749-62.

GRABHER, C., PAYNE, E. M., JOHNSTON, A. B., BOLLI, N., LECHMAN, E., DICK, J. E., KANKI, J. P. & LOOK, A. T. 2011. Zebrafish microRNA-126 determines hematopoietic cell fate through c-Myb. *Leukemia,* 25**,** 506-14.

GRAY, C., LOYNES, C. A., WHYTE, M. K., CROSSMAN, D. C., RENSHAW, S. A. & CHICO, T. J. 2011. Simultaneous intravital imaging of macrophage and neutrophil behaviour during inflammation using a novel transgenic zebrafish. *Thromb Haemost,* 105**,** 811-9.

GREGORY, M., HANUMANTHAIAH, R. & JAGADEESWARAN, P. 2002. Genetic analysis of hemostasis and thrombosis using vascular occlusion. *Blood Cells Mol Dis,* 29**,** 286-95.

GREGORY, M. & JAGADEESWARAN, P. 2002. Selective labeling of zebrafish thrombocytes: quantitation of thrombocyte function and detection during development. *Blood Cells Mol Dis,* 28**,** 418-27.

GURBEL, P. A., BLIDEN, K. P., BUTLER, K., TANTRY, U. S., GESHEFF, T., WEI, C., TENG, R. L., ANTONINO, M. J., PATIL, S. B., KARUNAKARAN, A., KEREIAKES, D. J., PARRIS, C., PURDY, D., WILSON, V., LEDLEY, G. S. & STOREY, R. F. 2009. Randomized Double-Blind Assessment of the ONSET and OFFSET of the Antiplatelet Effects of Ticagrelor Versus Clopidogrel in Patients With Stable Coronary Artery Disease The ONSET/OFFSET Study. *Circulation,* 120**,** 2577-U103.

HARKER, L. A. 1977. The kinetics of platelet production and destruction in man. *Clin Haematol,* 6**,** 671-93.

HAYNES, S. E., HOLLOPETER, G., YANG, G., KURPIUS, D., DAILEY, M. E., GAN, W. B. & JULIUS, D. 2006. The P2Y12 receptor regulates microglial activation by extracellular nucleotides. *Nat Neurosci,* 9**,** 1512-9.

HECHLER, B. & GACHET, C. 2011. P2 receptors and platelet function. *Purinergic Signal,* 7**,** 293-303.

HECHLER, B., LEON, C., VIAL, C., VIGNE, P., FRELIN, C., CAZENAVE, J. P. & GACHET, C. 1998. The P2Y1 receptor is necessary for adenosine 5'-diphosphate-induced platelet aggregation. *Blood,* 92**,** 152-9.

HENN, V., SLUPSKY, J. R., GRAFE, M., ANAGNOSTOPOULOS, I., FORSTER, R., MULLER-BERGHAUS, G. & KROCZEK, R. A. 1998. CD40 ligand on activated platelets triggers an inflammatory reaction of endothelial cells. *Nature,* 391**,** 591-594.

HERBOMEL, P., THISSE, B. & THISSE, C. 1999. Ontogeny and behaviour of early macrophages in the zebrafish embryo. *Development,* 126**,** 3735-3745.

HOFFMANN, K., SIXEL, U., DI PASQUALE, F. & VON KUGELGEN, I. 2008. Involvement of basic amino acid residues in transmembrane regions 6 and 7 in agonist and antagonist recognition of the human platelet P2Y(12)-receptor. *Biochem Pharmacol,* 76**,** 1201-13.

HOLLOPETER, G., JANTZEN, H. M., VINCENT, D., LI, G., ENGLAND, L., RAMAKRISHNAN, V., YANG, R. B., NURDEN, P., NURDEN, A., JULIUS, D. & CONLEY, P. B. 2001.

Identification of the platelet ADP receptor targeted by antithrombotic drugs. *Nature,* 409**,** 202-207.

HOLT, J. C., HARRIS, M. E., HOLT, A. M., LANGE, E., HENSCHEN, A. & NIEWIAROWSKI, S. 1986. Characterization of human platelet basic protein, a precursor form of low-affinity platelet factor 4 and beta-thromboglobulin. *Biochemistry,* 25**,** 1988-96.

HOWE, K., CLARK, M. D., TORROJA, C. F., TORRANCE, J., BERTHELOT, C., MUFFATO, M., COLLINS, J. E., HUMPHRAY, S., MCLAREN, K., MATTHEWS, L., MCLAREN, S., SEALY, I., CACCAMO, M., CHURCHER, C., SCOTT, C., BARRETT, J. C., KOCH, R., RAUCH, G. J., WHITE, S., CHOW, W., KILIAN, B., QUINTAIS, L. T., GUERRA-ASSUNCAO, J. A., ZHOU, Y., GU, Y., YEN, J., VOGEL, J. H., EYRE, T., REDMOND, S., BANERJEE, R., CHI, J., FU, B., LANGLEY, E., MAGUIRE, S. F., LAIRD, G. K., LLOYD, D., KENYON, E., DONALDSON, S., SEHRA, H., ALMEIDA-KING, J., LOVELAND, J., TREVANION, S., JONES, M., QUAIL, M., WILLEY, D., HUNT, A., BURTON, J., SIMS, S., MCLAY, K., PLUMB, B., DAVIS, J., CLEE, C., OLIVER, K., CLARK, R., RIDDLE, C., ELLIOT, D., THREADGOLD, G., HARDEN, G., WARE, D., MORTIMORE, B., KERRY, G., HEATH, P., PHILLIMORE, B., TRACEY, A., CORBY, N., DUNN, M., JOHNSON, C., WOOD, J., CLARK, S., PELAN, S., GRIFFITHS, G., SMITH, M., GLITHERO, R., HOWDEN, P., BARKER, N., STEVENS, C., HARLEY, J., HOLT, K., PANAGIOTIDIS, G., LOVELL, J., BEASLEY, H., HENDERSON, C., GORDON, D., AUGER, K., WRIGHT, D., COLLINS, J., RAISEN, C., DYER, L., LEUNG, K., ROBERTSON, L., AMBRIDGE, K., LEONGAMORNLERT, D., MCGUIRE, S., GILDERTHORP, R., GRIFFITHS, C., MANTHRAVADI, D., NICHOL, S., BARKER, G., WHITEHEAD, S., KAY, M., et al. 2013. The zebrafish reference genome sequence and its relationship to the human genome. *Nature,* 496**,** 498-503.

HUGHES, C. E., RADHAKRISHNAN, U. P., LORDKIPANIDZE, M., EGGINTON, S., DIJKSTRA, J. M., JAGADEESWARAN, P. & WATSON, S. P. 2012. G6f-like is an ITAM-containing collagen receptor in thrombocytes. *PLoS One,* 7**,** e52622.

HULOT, J. S., BURA, A., VILLARD, E., AZIZI, M., REMONES, V., GOYENVALLE, C., AIACH, M., LECHAT, P. & GAUSSEM, P. 2006. Cytochrome P450 2C19 loss-of-function polymorphism is a major determinant of clopidogrel responsiveness in healthy subjects. *Blood,* 108**,** 2244-7.

HURLBERT, S. H. 1984. Pseudoreplication and the Design of Ecological Field Experiments. *Ecological Monographs,* 54**,** 187-211.

IGNATOVICA, V., MEGNIS, K., LAPINS, M., SCHIOTH, H. B. & KLOVINS, J. 2012. Identification and analysis of functionally important amino acids in human purinergic 12 receptor using a Saccharomyces cerevisiae expression system. *FEBS J,* 279**,** 180-91.

ITALIANO, J. E., JR., RICHARDSON, J. L., PATEL-HETT, S., BATTINELLI, E., ZASLAVSKY, A., SHORT, S., RYEOM, S., FOLKMAN, J. & KLEMENT, G. L. 2008. Angiogenesis is regulated by a novel mechanism: pro- and antiangiogenic proteins are organized into separate platelet alpha granules and differentially released. *Blood,* 111**,** 1227-33.

JAGADEESWARAN, P. 2005. Zebrafish: a tool to study hemostasis and thrombosis. *Curr Opin Hematol,* 12**,** 149-52.

JAGADEESWARAN, P., SHEEHAN, J. P., CRAIG, F. E. & TROYER, D. 1999. Identification and characterization of zebrafish thrombocytes. *Br J Haematol,* 107**,** 731-8.

JIN, H., SOOD, R., XU, J., ZHEN, F., ENGLISH, M. A., LIU, P. P. & WEN, Z. 2009. Definitive hematopoietic stem/progenitor cells manifest distinct differentiation output in the zebrafish VDA and PBI. *Development,* 136**,** 647-54.

JIN, J. & KUNAPULI, S. P. 1998. Coactivation of two different G protein-coupled receptors is essential for ADP-induced platelet aggregation. *Proc Natl Acad Sci U S A,* 95**,** 8070-4.

JIN, J., QUINTON, T. M., ZHANG, J., RITTENHOUSE, S. E. & KUNAPULI, S. P. 2002. Adenosine diphosphate (ADP)-induced thromboxane A(2) generation in human platelets requires coordinated signaling through integrin alpha(IIb)beta(3) and ADP receptors. *Blood,* 99**,** 193-8.

JOHNNIDIS, J. B., HARRIS, M. H., WHEELER, R. T., STEHLING-SUN, S., LAM, M. H., KIRAK, O., BRUMMELKAMP, T. R., FLEMING, M. D. & CAMARGO, F. D. 2008. Regulation of progenitor cell proliferation and granulocyte function by microRNA-223. *Nature,* 451**,** 1125-9.

KAMAE, T., SHIRAGA, M., KASHIWAGI, H., KATO, H., TADOKORO, S., KURATA, Y., TOMIYAMA, Y. & KANAKURA, Y. 2006. Critical role of ADP interaction with P2Y12 receptor in the maintenance of alpha(IIb)beta3 activation: association with Rap1B activation. *J Thromb Haemost,* 4**,** 1379-87.

KAMYKOWSKI, J., CARLTON, P., SEHGAL, S. & STORRIE, B. 2011. Quantitative immunofluorescence mapping reveals little functional coclustering of proteins within platelet alpha-granules. *Blood,* 118**,** 1370-3.

KAUFFENSTEIN, G., BERGMEIER, W., ECKLY, A., OHLMANN, P., LEON, C., CAZENAVE, J. P., NIESWANDT, B. & GACHET, C. 2001. The P2Y(12) receptor induces platelet aggregation through weak activation of the alpha(IIb)beta(3) integrin--a phosphoinositide 3-kinase-dependent mechanism. *FEBS Lett,* 505**,** 281-90.

KIRCHHOFER, D., RIEDERER, M. A. & BAUMGARTNER, H. R. 1997. Specific accumulation of circulating monocytes and polymorphonuclear leukocytes on platelet thrombi in a vascular injury model. *Blood,* 89**,** 1270-8.

KISSA, K., MURAYAMA, E., ZAPATA, A., CORTES, A., PERRET, E., MACHU, C. & HERBOMEL, P. 2008. Live imaging of emerging hematopoietic stem cells and early thymus colonization. *Blood,* 111**,** 1147-56.

KLINGER, M. H., WILHELM, D., BUBEL, S., STICHERLING, M., SCHRODER, J. M. & KUHNEL, W. 1995. Immunocytochemical localization of the chemokines RANTES and MIP-1 alpha within human platelets and their release during storage. *Int Arch Allergy Immunol,* 107**,** 541-6.

KRONLAGE, M., SONG, J., SOROKIN, L., ISFORT, K., SCHWERDTLE, T., LEIPZIGER, J., ROBAYE, B., CONLEY, P. B., KIM, H. C., SARGIN, S., SCHON, P., SCHWAB, A. & HANLEY, P. J. 2010. Autocrine purinergic receptor signaling is essential for macrophage chemotaxis. *Sci Signal,* 3**,** ra55.

KUNAPULI, S. P., DORSAM, R. T., KIM, S. & QUINTON, T. M. 2003. Platelet purinergic receptors. *Curr Opin Pharmacol,* 3**,** 175-80.

KURZ, K. D., MAIN, B. W. & SANDUSKY, G. E. 1990. Rat model of arterial thrombosis induced by ferric chloride. *Thromb Res,* 60**,** 269-80.

LAM, S. H., CHUA, H. L., GONG, Z., LAM, T. J. & SIN, Y. M. 2004. Development and maturation of the immune system in zebrafish, Danio rerio: a gene expression profiling, in situ hybridization and immunological study. *Developmental and Comparative Immunology,* 28**,** 9-28.

LANDRY, P., PLANTE, I., OUELLET, D. L., PERRON, M. P., ROUSSEAU, G. & PROVOST, P. 2009. Existence of a microRNA pathway in anucleate platelets. *Nature structural & molecular biology,* 16**,** 961-6.

LAWSON, N. D. & WEINSTEIN, B. M. 2002. In vivo imaging of embryonic vascular development using transgenic zebrafish. *Dev Biol,* 248**,** 307-18.

LEIERSEDER, S., PETZOLD, T., ZHANG, L., LOYER, X., MASSBERG, S. & ENGELHARDT, S. 2013. MiR-223 is dispensable for platelet production and function in mice. *Thromb Haemost,* 110**,** 1207-14.

LI, D., WANG, Y., ZHANG, L., LUO, X., LI, J., CHEN, X., NIU, H., WANG, K., SUN, Y., WANG, X., YAN, Y., CHAI, W., GARTNER, T. K. & LIU, J. 2012a. Roles of purinergic receptor P2Y,

G protein-coupled 12 in the development of atherosclerosis in apolipoprotein E-deficient mice. *Arterioscler Thromb Vasc Biol,* 32**,** e81-9.

LI, L., YAN, B., SHI, Y. Q., ZHANG, W. Q. & WEN, Z. L. 2012b. Live imaging reveals differing roles of macrophages and neutrophils during zebrafish tail fin regeneration. *J Biol Chem,* 287**,** 25353-60.

LI, Z., ZHANG, G., LE BRETON, G. C., GAO, X., MALIK, A. B. & DU, X. 2003. Two waves of platelet secretion induced by thromboxane A2 receptor and a critical role for phosphoinositide 3-kinases. *J Biol Chem,* 278**,** 30725-31.

LI, Z., ZHANG, G., LIU, J., STOJANOVIC, A., RUAN, C., LOWELL, C. A. & DU, X. 2010. An important role of the SRC family kinase Lyn in stimulating platelet granule secretion. *J Biol Chem,* 285**,** 12559-70.

LIESCHKE, G. J. & CURRIE, P. D. 2007. Animal models of human disease: zebrafish swim into view. *Nature Reviews Genetics,* 8**,** 353-367.

LIESCHKE, G. J., OATES, A. C., CROWHURST, M. O., WARD, A. C. & LAYTON, J. E. 2001. Morphologic and functional characterization of granulocytes and macrophages in embryonic and adult zebrafish. *Blood,* 98**,** 3087-96.

LIESCHKE, G. J. & TREDE, N. S. 2009. Fish immunology. *Current Biology,* 19**,** R678-R682.

LIN, H. F., TRAVER, D., ZHU, H., DOOLEY, K., PAW, B. H., ZEN, L. I. & HANDIN, R. I. 2005. Analysis of thrombocyte development in CD41-GFP transgenic zebrafish. *Blood,* 106**,** 3803-3810.

LINDMARK, E., TENNO, T. & SIEGBAHN, A. 2000. Role of platelet P-selectin and CD40 ligand in the induction of monocytic tissue factor expression. *Arteriosclerosis Thrombosis and Vascular Biology,* 20**,** 2322-2328.

LISTER, J. A., ROBERTSON, C. P., LEPAGE, T., JOHNSON, S. L. & RAIBLE, D. W. 1999. nacre encodes a zebrafish microphthalmia-related protein that regulates neural-crest-derived pigment cell fate. *Development,* 126**,** 3757-67.

LOVA, P., PAGANINI, S., SINIGAGLIA, F., BALDUINI, C. & TORTI, M. 2002. A Gi-dependent pathway is required for activation of the small GTPase Rap1B in human platelets. *J Biol Chem,* 277**,** 12009-15.

LUDWIG, M., PALHA, N., TORHY, C., BRIOLAT, V., COLUCCI-GUYON, E., BREMONT, M., HERBOMEL, P., BOUDINOT, P. & LEVRAUD, J. P. 2011. Whole-body analysis of a viral infection: vascular endothelium is a primary target of infectious hematopoietic necrosis virus in zebrafish larvae. *PLoS Pathog,* 7**,** e1001269.

MA, D., ZHANG, J., LIN, H. F., ITALIANO, J. & HANDIN, R. I. 2011. The identification and characterization of zebrafish hematopoietic stem cells. *Blood,* 118**,** 289-97.

MA, L., ELLIOTT, S. N., CIRINO, G., BURET, A., IGNARRO, L. J. & WALLACE, J. L. 2001. Platelets modulate gastric ulcer healing: role of endostatin and vascular endothelial growth factor release. *Proc Natl Acad Sci U S A,* 98**,** 6470-5.

MACH, F., SCHONBECK, U., SUKHOVA, G. K., BOURCIER, T., BONNEFOY, J. Y., POBER, J. S. & LIBBY, P. 1997. Functional CD40 ligand is expressed on human vascular endothelial cells, smooth muscle cells, and macrophages: implications for CD40-CD40 ligand signaling in atherosclerosis. *Proc Natl Acad Sci U S A,* 94**,** 1931-6.

MACKMAN, N. 2008. Triggers, targets and treatments for thrombosis. *Nature,* 451**,** 914-8.

MARASCO, W. A., PHAN, S. H., KRUTZSCH, H., SHOWELL, H. J., FELTNER, D. E., NAIRN, R., BECKER, E. L. & WARD, P. A. 1984. Purification and identification of formyl-methionyl-leucyl-phenylalanine as the major peptide neutrophil chemotactic factor produced by Escherichia coli. *J Biol Chem,* 259**,** 5430-9.

MATHIAS, J. R., DODD, M. E., WALTERS, K. B., YOO, S. K., RANHEIM, E. A. & HUTTENLOCHER, A. 2009. Characterization of zebrafish larval inflammatory macrophages. *Developmental and Comparative Immunology,* 33**,** 1212-1217.

MATHIAS, J. R., PERRIN, B. J., LIU, T. X., KANKI, J., LOOK, A. T. & HUTTENLOCHER, A. 2006. Resolution of inflammation by retrograde chemotaxis of neutrophils in transgenic zebrafish. *Journal of Leukocyte Biology,* 80**,** 1281-1288.

MATHIAS, J. R., SAXENA, M. T. & MUMM, J. S. 2012. Advances in zebrafish chemical screening technologies. *Future Med Chem,* 4**,** 1811-22.

MCMORRAN, B. J., MARSHALL, V. M., DE GRAAF, C., DRYSDALE, K. E., SHABBAR, M., SMYTH, G. K., CORBIN, J. E., ALEXANDER, W. S. & FOOTE, S. J. 2009. Platelets Kill Intraerythrocytic Malarial Parasites and Mediate Survival to Infection. *Science,* 323**,** 797-800.

MEDEARIS, D. N., JR., CAMITTA, B. M. & HEATH, E. C. 1968. Cell wall composition and virulence in Escherichia coli. *J Exp Med,* 128**,** 399-414.

MILLS, D. C., ROBB, I. A. & ROBERTS, G. C. 1968. The release of nucleotides, 5-hydroxytryptamine and enzymes from human blood platelets during aggregation. *J Physiol,* 195**,** 715-29.

MOSER, G. H., SCHRADER, J. & DEUSSEN, A. 1989. Turnover of adenosine in plasma of human and dog blood. *Am J Physiol,* 256**,** C799-806.

MURAYAMA, E., KISSA, K., ZAPATA, A., MORDELET, E., BRIOLAT, V., LIN, H. F., HANDIN, R. I. & HERBOMEL, P. 2006. Tracing hematopoietic precursor migration to successive hematopoietic organs during zebrafish development. *Immunity,* 25**,** 963-75.

MUSSOLINO, C., MORBITZER, R., LUTGE, F., DANNEMANN, N., LAHAYE, T. & CATHOMEN, T. 2011. A novel TALE nuclease scaffold enables high genome editing activity in combination with low toxicity. *Nucleic Acids Res,* 39**,** 9283-93.

NAGALLA, S., SHAW, C., KONG, X., KONDKAR, A. A., EDELSTEIN, L. C., MA, L., CHEN, J., MCKNIGHT, G. S., LOPEZ, J. A., YANG, L., JIN, Y., BRAY, M. S., LEAL, S. M., DONG, J. F. & BRAY, P. F. 2011. Platelet microRNA-mRNA coexpression profiles correlate with platelet reactivity. *Blood,* 117**,** 5189-97.

NAKAV, S., CHAIMOVITZ, C., SUFARO, Y., LEWIS, E. C., SHAKED, G., CZEIGER, D., ZLOTNIK, M. & DOUVDEVANI, A. 2008. Anti-inflammatory preconditioning by agonists of adenosine A1 receptor. *PLoS One,* 3**,** e2107.

NEELY, M. N., PFEIFER, J. D. & CAPARON, M. 2002. Streptococcus-zebrafish model of bacterial pathogenesis. *Infection and Immunity,* 70**,** 3904-3914.

NERGIZ-UNAL, R., COSEMANS, J. M., FEIJGE, M. A., VAN DER MEIJDEN, P. E., STOREY, R. F., VAN GIEZEN, J. J., OUDE EGBRINK, M. G., HEEMSKERK, J. W. & KUIJPERS, M. J. 2010. Stabilizing role of platelet P2Y(12) receptors in shear-dependent thrombus formation on ruptured plaques. *PLoS One,* 5**,** e10130.

NICOLI, S., STANDLEY, C., WALKER, P., HURLSTONE, A., FOGARTY, K. E. & LAWSON, N. D. 2010. MicroRNA-mediated integration of haemodynamics and Vegf signalling during angiogenesis. *Nature,* 464**,** 1196-200.

NOVOA, B., BOWMAN, T. V., ZON, L. & FIGUERAS, A. 2009. LPS response and tolerance in the zebrafish (Danio rerio). *Fish Shellfish Immunol,* 26**,** 326-31.

NYGAARD, R., FRIMURER, T. M., HOLST, B., ROSENKILDE, M. M. & SCHWARTZ, T. W. 2009. Ligand binding and micro-switches in 7TM receptor structures. *Trends Pharmacol Sci,* 30**,** 249-59.

O'CONNOR, M. N., SALLES, II, CVEJIC, A., WATKINS, N. A., WALKER, A., GARNER, S. F., JONES, C. I., MACAULAY, I. C., STEWARD, M., ZWAGINGA, J. J., BRAY, S. L., DUDBRIDGE, F., DE BONO, B., GOODALL, A. H., DECKMYN, H., STEMPLE, D. L., OUWEHAND, W. H. & BLOODOMICS, C. 2009. Functional genomics in zebrafish permits rapid characterization of novel platelet membrane proteins. *Blood,* 113**,** 4754-4762.

O'CONNOR, S., MONTALESCOT, G. & COLLET, J. P. 2011. The P2Y(12) receptor as a target of antithrombotic drugs. *Purinergic signalling,* 7**,** 325-32.

OHMAN, E. M. & ROE, M. T. 2011. Explaining the unexpected: insights from the PLATelet inhibition and clinical Outcomes (PLATO) trial comparing ticagrelor and clopidogrel. Editorial on Serebruany "Viewpoint: Paradoxical excess mortality in the PLATO trial should be independently verified" (Thromb Haemost 2011; 105.5). *Thromb Haemost,* 105**,** 763-5.

OQUENDO, P., ALBERTA, J., WEN, D. Z., GRAYCAR, J. L., DERYNCK, R. & STILES, C. D. 1989. The platelet-derived growth factor-inducible KC gene encodes a secretory protein related to platelet alpha-granule proteins. *J Biol Chem,* 264**,** 4133-7.

PALABRICA, T., LOBB, R., FURIE, B. C., ARONOVITZ, M., BENJAMIN, C., HSU, Y. M., SAJER, S. A. & FURIE, B. 1992. Leukocyte accumulation promoting fibrin deposition is mediated in vivo by P-selectin on adherent platelets. *Nature,* 359**,** 848-51.

PATEL, Y. M., LORDKIPANIDZE, M., LOWE, G. C., NISAR, S. P., GARNER, K., STOCKLEY, J., DALY, M. E., MITCHELL, M., WATSON, S. P., AUSTIN, S. K. & MUNDELL, S. J. 2014. A novel mutation in the P2Y12 receptor and a function-reducing polymorphism in protease-activated receptor 1 in a patient with chronic bleeding. *J Thromb Haemost,* 12**,** 716-25.

PATIL, S. B., JACKMAN, L. E., FRANCIS, S. E., JUDGE, H. M., NYLANDER, S. & STOREY, R. F. 2010. Ticagrelor Effectively and Reversibly Blocks Murine Platelet P2Y(12)-Mediated Thrombosis and Demonstrates a Requirement for Sustained P2Y(12) Inhibition to Prevent Subsequent Neointima. *Arteriosclerosis Thrombosis and Vascular Biology,* 30**,** 2385-2391.

PICCARDONI, P., EVANGELISTA, V., PICCOLI, A., DE GAETANO, G., WALZ, A. & CERLETTI, C. 1996. Thrombin-activated human platelets release two NAP-2 variants that stimulate polymorphonuclear leukocytes. *Thromb Haemost,* 76**,** 780-5.

POWER, C. A., CLEMETSON, J. M., CLEMETSON, K. J. & WELLS, T. N. 1995. Chemokine and chemokine receptor mRNA expression in human platelets. *Cytokine,* 7**,** 479-82.

PRAJSNAR, T. K., CUNLIFFE, V. T., FOSTER, S. J. & RENSHAW, S. A. 2008. A novel vertebrate model of Staphylococcus aureus infection reveals phagocyte-dependent resistance of zebrafish to non-host specialized pathogens. *Cellular Microbiology,* 10**,** 2312-2325.

QIAN, L., VAN LAAKE, L. W., HUANG, Y., LIU, S., WENDLAND, M. F. & SRIVASTAVA, D. 2011. miR-24 inhibits apoptosis and represses Bim in mouse cardiomyocytes. *J Exp Med,* 208**,** 549-60.

QUAIFE, N., M.* & CHICO, T., J, A 2012. Blood flow is required for endothelial repair in a novel in vivo model using zebrafish embryos. *BCS 2012.* Heart.

QUINTON, T. M., MURUGAPPAN, S., KIM, S., JIN, J. & KUNAPULI, S. P. 2004. Different G protein-coupled signaling pathways are involved in alpha granule release from human platelets. *Journal of Thrombosis and Haemostasis,* 2**,** 978-984.

REMIJN, J. A., WU, Y. P., JENINGA, E. H., IJSSELDIJK, M. J. W., VAN WILLIGEN, G., DE GROOT, P. G., SIXMA, J. J., NURDEN, A. T. & NURDEN, P. 2002. Role of ADP receptor P2Y(12) in platelet adhesion and thrombus formation in flowing blood. *Arteriosclerosis Thrombosis and Vascular Biology,* 22**,** 686-691.

RENSHAW, S. A., LOYNES, C. A., TRUSHELL, D. M. I., ELWORTHY, S., INGHAM, P. W. & WHYTE, M. K. B. 2006. A transgenic zebrafish model of neutrophilic inflammation. *Blood,* 108**,** 3976-3978.

ROBU, M. E., LARSON, J. D., NASEVICIUS, A., BEIRAGHI, S., BRENNER, C., FARBER, S. A. & EKKER, S. C. 2007. p53 activation by knockdown technologies. *PLoS Genet,* 3**,** e78.

ROMBOUGH, P. 2002. Gills are needed for ionoregulation before they are needed for O(2) uptake in developing zebrafish, Danio rerio. *J Exp Biol,* 205**,** 1787-94.

ROQUE, M., FALLON, J. T., BADIMON, J. J., ZHANG, W. X., TAUBMAN, M. B. & REIS, E. D. 2000. Mouse model of femoral artery denudation injury associated with the rapid

accumulation of adhesion molecules on the luminal surface and recruitment of neutrophils. *Arterioscler Thromb Vasc Biol,* 20**,** 335-42.

ROSEN, E. D., RAYMOND, S., ZOLLMAN, A., NORIA, F., SANDOVAL-COOPER, M., SHULMAN, A., MERZ, J. L. & CASTELLINO, F. J. 2001. Laser-induced noninvasive vascular injury models in mice generate platelet- and coagulation-dependent thrombi. *Am J Pathol,* 158**,** 1613-22.

RUSSELL, W. M. S. A. B., R.L., 1959. *The Principles of Humane Experimental Technique,* London, Methuen.

SANDER, J. D., DAHLBORG, E. J., GOODWIN, M. J., CADE, L., ZHANG, F., CIFUENTES, D., CURTIN, S. J., BLACKBURN, J. S., THIBODEAU-BEGANNY, S., QI, Y., PIERICK, C. J., HOFFMAN, E., MAEDER, M. L., KHAYTER, C., REYON, D., DOBBS, D., LANGENAU, D. M., STUPAR, R. M., GIRALDEZ, A. J., VOYTAS, D. F., PETERSON, R. T., YEH, J. R. & JOUNG, J. K. 2011. Selection-free zinc-finger-nuclease engineering by context-dependent assembly (CoDA). *Nat Methods,* 8**,** 67-9.

SANTORO, M. M., PESCE, G. & STAINIER, D. Y. 2009. Characterization of vascular mural cells during zebrafish development. *Mech Dev,* 126**,** 638-49.

SASAKI, Y., HOSHI, M., AKAZAWA, C., NAKAMURA, Y., TSUZUKI, H., INOUE, K. & KOHSAKA, S. 2003. Selective expression of Gi/o-coupled ATP receptor P2Y12 in microglia in rat brain. *Glia,* 44**,** 242-50.

SAVI, P., COMBALBERT, J., GAICH, C., ROUCHON, M. C., MAFFRAND, J. P., BERGER, Y. & HERBERT, J. M. 1994. The antiaggregating activity of clopidogrel is due to a metabolic activation by the hepatic cytochrome P450-1A. *Thromb Haemost,* 72**,** 313-7.

SAVI, P., ZACHAYUS, J. L., DELESQUE-TOUCHARD, N., LABOURET, C., HERVE, C., UZABIAGA, M. F., PEREILLO, J. M., CULOUSCOU, J. M., BONO, F., FERRARA, P. & HERBERT, J. M. 2006. The active metabolite of Clopidogrel disrupts P2Y12 receptor oligomers and partitions them out of lipid rafts. *Proceedings of the National Academy of Sciences of the United States of America,* 103**,** 11069-74.

SCHAUFELBERGER, H. D., UHR, M. R., MCGUCKIN, C., LOGAN, R. P., MISIEWICZ, J. J., GORDON-SMITH, E. C. & BEGLINGER, C. 1994. Platelets in ulcerative colitis and Crohn's disease express functional interleukin-1 and interleukin-8 receptors. *Eur J Clin Invest,* 24**,** 656-63.

SCHMIDT, P., RITSCHER, L., DONG, E. N., HERMSDORF, T., COSTER, M., WITTKOPF, D., MEILER, J. & SCHONEBERG, T. 2013. Identification of determinants required for agonistic and inverse agonistic ligand properties at the ADP receptor P2Y12. *Mol Pharmacol,* 83**,** 256-66.

SCIRICA, B. M., CANNON, C. P., EMANUELSSON, H., MICHELSON, E. L., HARRINGTON, R. A., HUSTED, S., JAMES, S., KATUS, H., PAIS, P., RAEV, D., SPINAR, J., STEG, P. G., STOREY, R. F., WALLENTIN, L. & INVESTIGATORS, P. 2011. The incidence of bradyarrhythmias and clinical bradyarrhythmic events in patients with acute coronary syndromes treated with ticagrelor or clopidogrel in the PLATO (Platelet Inhibition and Patient Outcomes) trial: results of the continuous electrocardiographic assessment substudy. *J Am Coll Cardiol,* 57**,** 1908-16.

SEHGAL, S. & STORRIE, B. 2007. Evidence that differential packaging of the major platelet granule proteins von Willebrand factor and fibrinogen can support their differential release. *J Thromb Haemost,* 5**,** 2009-16.

SEIFFERT, D. & SCHLEEF, R. R. 1996. Two functionally distinct pools of vitronectin (Vn) in the blood circulation: identification of a heparin-binding competent population of Vn within platelet alpha-granules. *Blood,* 88**,** 552-60.

SENIOR, R. M., GRIFFIN, G. L., HUANG, J. S., WALZ, D. A. & DEUEL, T. F. 1983. Chemotactic activity of platelet alpha granule proteins for fibroblasts. *J Cell Biol,* 96**,** 382-5.

SEREBRUANY, V. L. 2011. Viewpoint: paradoxical excess mortality in the PLATO trial should be independently verified. *Thromb Haemost,* 105**,** 752-9.

SIEGER, D., MORITZ, C., ZIEGENHALS, T., PRYKHOZHIJ, S. & PERI, F. 2012. Long-range Ca2+ waves transmit brain-damage signals to microglia. *Dev Cell,* 22**,** 1138-48.

STEINHUBL, S. R., BADIMON, J. J., BHATT, D. L., HERBERT, J. M. & LUSCHER, T. F. 2007. Clinical evidence for anti-inflammatory effects of antiplatelet therapy in patients with atherothrombotic disease. *Vascular Medicine,* 12**,** 113-122.

STENBERG, P. E., MCEVER, R. P., SHUMAN, M. A., JACQUES, Y. V. & BAINTON, D. F. 1985. A platelet alpha-granule membrane protein (GMP-140) is expressed on the plasma membrane after activation. *J Cell Biol,* 101**,** 880-6.

STOREY, R., JAMES, S., SIEGBAHN, A., VARENHORST, C., HELD, C., YCAS, J., HUSTED, S., CANNON, C., BECKER, R., STEG, P., ASENBLAD, N. & WALLENTIN, L. 2013. Lower Mortality Following Pulmonary Adverse Events and Sepsis with Ticagrelor Compared to Clopidogrel in the PLATO Study. . *Platelets in press*.

STOREY, R. F. 2006. Biology and pharmacology of the platelet P2Y(12) receptor. *Current Pharmaceutical Design,* 12**,** 1255-1259.

STOREY, R. F., JUDGE, H. M., WILCOX, R. G. & HEPTINSTALL, S. 2002. Inhibition of ADP-induced P-selectin expression and platelet-leukocyte conjugate formation by clopidogrel and the P2Y12 receptor antagonist AR-C69931MX but not aspirin. *Thromb Haemost,* 88**,** 488-94.

STOREY, R. F., OLDROYD, K. G. & WILCOX, R. G. 2001. Open multicentre study of the P2T receptor antagonist AR-C69931MX assessing safety, tolerability and activity in patients with acute coronary syndromes. *Thromb Haemost,* 85**,** 401-7.

SULLIVAN, C. & KIM, C. H. 2008. Zebrafish as a model for infectious disease and immune function. *Fish & Shellfish Immunology,* 25**,** 341-350.

SUN, G., PAN, J., LIU, K., WANG, X. & WANG, S. 2010. Molecular Cloning and Expression Analysis of P-Selectin from Zebrafish (Danio rerio). *Int J Mol Sci,* 11**,** 4618-30.

TANG, Y. Q., YEAMAN, M. R. & SELSTED, M. E. 2002. Antimicrobial peptides from human plateletst. *Infection and Immunity,* 70**,** 6524-6533.

TAYLOR, H. B. 2010. *Functional analysis of zebrafish innate immune responses to inflammatory signals.* Thesis, The University of Edinburgh.

TAYLOR, J. S., BRAASCH, I., FRICKEY, T., MEYER, A. & VAN DE PEER, Y. 2003. Genome duplication, a trait shared by 22000 species of ray-finned fish. *Genome Res,* 13**,** 382-90.

THATTALIYATH, B., CYKOWSKI, M. & JAGADEESWARAN, P. 2005. Young thrombocytes initiate the formation of arterial thrombi in zebrafish. *Blood,* 106**,** 118-24.

THISSE, C., THISSE, B., SCHILLING, T. F. & POSTLETHWAIT, J. H. 1993. Structure of the zebrafish snail1 gene and its expression in wild-type, spadetail and no tail mutant embryos. *Development,* 119**,** 1203-15.

TOURNOIJ, E., WEBER, G. J., AKKERMAN, J. W. N., DE GROOT, P. G., ZON, L. I., MOLL, F. L. & SCHULTE-MERKER, S. 2010. Mlck1a is expressed in zebrafish thrombocytes and is an essential component of thrombus formation. *Journal of Thrombosis and Haemostasis,* 8**,** 588-595.

TRANZER, J. P., DA PRADA, M. & PLETSCHER, A. 1966. Ultrastructural localization of 5-hydroxytryptamine in blood platelets. *Nature,* 212**,** 1574-5.

TRAVER, D., PAW, B. H., POSS, K. D., PENBERTHY, W. T., LIN, S. & ZON, L. I. 2003. Transplantation and in vivo imaging of multilineage engraftment in zebrafish bloodless mutants. *Nat Immunol,* 4**,** 1238-46.

TRIER, D. A., GANK, K. D., KUPFERWASSER, D., YOUNT, N. Y., FRENCH, W. J., MICHELSON, A. D., KUPFERWASSER, L. I., XIONG, Y. Q., BAYER, A. S. & YEAMAN, M. R. 2008. Platelet

Antistaphylococcal Responses Occur through P2X(1) and P2Y(12) Receptor-Induced Activation and Kinocidin Release. *Infection and Immunity,* 76**,** 5706-5713.

URBICH, C., KUEHBACHER, A. & DIMMELER, S. 2008. Role of microRNAs in vascular diseases, inflammation, and angiogenesis. *Cardiovascular research,* 79**,** 581-8.

VAN DER SAR, A. M., MUSTERS, R. J. P., VAN EEDEN, F. J. M., APPELMELK, B. J., VANDENBROUCKE-GRAULS, C. & BITTER, W. 2003. Zebrafish embryos as a model host for the real time analysis of Salmonella typhimurium infections. *Cellular Microbiology,* 5**,** 601-611.

VAN GESTEL, M. A., HEEMSKERK, J. W. M., SLAAF, D. W., HEIJNEN, V. V. T., RENEMAN, R. S. & EGBRINK, M. 2003. In vivo blockade of platelet ADP receptor P2Y(12) reduces embolus and thrombus formation but not thrombus stability. *Arteriosclerosis Thrombosis and Vascular Biology,* 23**,** 518-523.

VAN GIEZEN, J. J., BERNTSSON, P., ZACHRISSON, H. & BJORKMAN, J. A. 2009. Comparison of ticagrelor and thienopyridine P2Y(12) binding characteristics and antithrombotic and bleeding effects in rat and dog models of thrombosis/hemostasis. *Thromb Res,* 124**,** 565-71.

VAN GIEZEN, J. J. J. 2008. Optimizing platelet inhibition. *European Heart Journal Supplements,* 10**,** D23-D29.

VAN NISPEN TOT PANNERDEN, H., DE HAAS, F., GEERTS, W., POSTHUMA, G., VAN DIJK, S. & HEIJNEN, H. F. 2010. The platelet interior revisited: electron tomography reveals tubular alpha-granule subtypes. *Blood,* 116**,** 1147-56.

VARENHORST, C., ALSTROM, U., SCIRICA, B. M., HOGUE, C. W., ASENBLAD, N., STOREY, R. F., STEG, P. G., HORROW, J., MAHAFFEY, K. W., BECKER, R. C., JAMES, S., CANNON, C. P., BRANDRUP-WOGNSEN, G., WALLENTIN, L. & HELD, C. 2012. Factors contributing to the lower mortality with ticagrelor compared with clopidogrel in patients undergoing coronary artery bypass surgery. *J Am Coll Cardiol,* 60**,** 1623-30.

VERGUNST, A. C., MEIJER, A. H., RENSHAW, S. A. & O'CALLAGHAN, D. 2010. Burkholderia cenocepacia creates an intramacrophage replication niche in zebrafish embryos, followed by bacterial dissemination and establishment of systemic infection. *Infect Immun,* 78**,** 1495-508.

VICIC, W. J., LAGES, B. & WEISS, H. J. 1980. Release of human platelet factor V activity is induced by both collagen and ADP and is inhibited by aspirin. *Blood,* 56**,** 448-55.

VON HUNDELSHAUSEN, P. & WEBER, C. 2007. Platelets as immune cells - Bridging inflammation and cardiovascular disease. *Circulation Research,* 100**,** 27-40.

VON KÜGELGEN, I. 2006. Pharmacological profiles of cloned mammalian P2Y-receptor subtypes. *Pharmacology and Therapeutics,* 110**,** 415-432.

WALLENTIN, L., BECKER, R. C., JAMES, S. K. & HARRINGTON, R. A. 2011. The PLATO trial reveals further opportunities to improve outcomes in patients with acute coronary syndrome. Editorial on Serebruany. "Viewpoint: Paradoxical excess mortality in the PLATO trial should be independently verified" (Thromb Haemost 2011; 105.5). *Thromb Haemost,* 105**,** 760-2.

WANG, S., AURORA, A. B., JOHNSON, B. A., QI, X., MCANALLY, J., HILL, J. A., RICHARDSON, J. A., BASSEL-DUBY, R. & OLSON, E. N. 2008. The endothelial-specific microRNA miR-126 governs vascular integrity and angiogenesis. *Dev Cell,* 15**,** 261-71.

WARGA, R. M., KANE, D. A. & HO, R. K. 2009. Fate mapping embryonic blood in zebrafish: multi- and unipotential lineages are segregated at gastrulation. *Dev Cell,* 16**,** 744-55.

WARTIOVAARA, U., SALVEN, P., MIKKOLA, H., LASSILA, R., KAUKONEN, J., JOUKOV, V., ORPANA, A., RISTIMAKI, A., HEIKINHEIMO, M., JOENSUU, H., ALITALO, K. & PALOTIE, A. 1998. Peripheral blood platelets express VEGF-C and VEGF which are released during platelet activation. *Thromb Haemost,* 80**,** 171-5.

WEST, L. E., STEINER, T., JUDGE, H. M., FRANCIS, S. E. & STOREY, R. F. 2014. Vessel wall, not platelet, P2Y12 potentiates early atherogenesis. *Cardiovasc Res*.

WIHLBORG, A. K., WANG, L., BRAUN, O. O., EYJOLFSSON, A., GUSTAFSSON, R., GUDBJARTSSON, T. & ERLINGE, D. 2004. ADP receptor P2Y12 is expressed in vascular smooth muscle cells and stimulates contraction in human blood vessels. *Arterioscler Thromb Vasc Biol,* 24**,** 1810-5.

WILLEIT, P., ZAMPETAKI, A., DUDEK, K., KAUDEWITZ, D., KING, A., KIRKBY, N. S., CROSBY-NWAOBI, R., PROKOPI, M., DROZDOV, I., LANGLEY, S. R., SIVAPRASAD, S., MARKUS, H. S., MITCHELL, J. A., WARNER, T. D., KIECHL, S. & MAYR, M. 2013. Circulating MicroRNAs as Novel Biomarkers for Platelet Activation. *Circ Res,* 112**,** 595-600.

WILLIAMS, C. M., FENG, Y., MARTIN, P. & POOLE, A. W. 2011. Protein kinase C alpha and beta are positive regulators of thrombus formation in vivo in a zebrafish (Danio rerio) model of thrombosis. *J Thromb Haemost,* 9**,** 2457-65.

WITTE, L. D., KAPLAN, K. L., NOSSEL, H. L., LAGES, B. A., WEISS, H. J. & GOODMAN, D. S. 1978. Studies of the release from human platelets of the growth factor for cultured human arterial smooth muscle cells. *Circ Res,* 42**,** 402-9.

WIVIOTT, S. D., BRAUNWALD, E., MCCABE, C. H., MONTALESCOT, G., RUZYLLO, W., GOTTLIEB, S., NEUMANN, F. J., ARDISSINO, D., DE SERVI, S., MURPHY, S. A., RIESMEYER, J., WEERAKKODY, G., GIBSON, C. M. & ANTMAN, E. M. 2007. Prasugrel versus clopidogrel in patients with acute coronary syndromes. *The New England journal of medicine,* 357**,** 2001-15.

WOULFE, D., JIANG, H., MORTENSEN, R., YANG, J. & BRASS, L. F. 2002. Activation of Rap1B by G(i) family members in platelets. *J Biol Chem,* 277**,** 23382-90.

YEAMAN, M. R. & BAYER, A. S. 1999. Antimicrobial peptides from platelets. *Drug Resistance Updates,* 2**,** 116-126.

YEAMAN, M. R., YOUNT, N. Y., WARING, A. J., GANK, K. D., KUPFERWASSER, D., WIESE, R., BAYER, A. S. & WELCH, W. H. 2007. Modular determinants of antimicrobial activity in platelet factor-4 family kinocidins. *Biochimica Et Biophysica Acta-Biomembranes,* 1768**,** 609-619.

YOUSSEFIAN, T., DROUIN, A., MASSE, J. M., GUICHARD, J. & CRAMER, E. M. 2002. Host defense role of platelets: engulfment of HIV and Staphylococcus aureus occurs in a specific subcellular compartment and is enhanced by platelet activation. *Blood,* 99**,** 4021-4029.

ZAMPETAKI, A., WILLEIT, P., TILLING, L., DROZDOV, I., PROKOPI, M., RENARD, J. M., MAYR, A., WEGER, S., SCHETT, G., SHAH, A., BOULANGER, C. M., WILLEIT, J., CHOWIENCZYK, P. J., KIECHL, S. & MAYR, M. 2012. Prospective study on circulating MicroRNAs and risk of myocardial infarction. *J Am Coll Cardiol,* 60**,** 290-9.

ZHANG, G., XIANG, B., YE, S., CHRZANOWSKA-WODNICKA, M., MORRIS, A. J., GARTNER, T. K., WHITEHEART, S. W., WHITE, G. C., 2ND, SMYTH, S. S. & LI, Z. 2011. Distinct roles for Rap1b protein in platelet secretion and integrin alphaIIbbeta3 outside-in signaling. *J Biol Chem,* 286**,** 39466-77.